2020

Regulation of Murine Physiology and Metabolism by the Adipocyte Circadian Clock through Sphingosine Kinase 1

Andrea Kelsey Anderson
Medical University of South Carolina

Regulation of Murine Physiology and Metabolism by the Adipocyte Circadian Clock through Sphingosine Kinase 1

Andrea Kelsey Anderson

A Dissertation Submitted to:

The Medical University of South Carolina

Charleston, South Carolina, United States of America

To the Faculty of:

The Department of Biochemistry and Molecular Biology

In Partial Fulfillment for the Degree of:

Doctor of Philosophy

In the Year:

2020

Approved by:

L. Ashley Cowart, Chair, Advisory Committee _____

Committee Members

Joe B. Blumer _____

Samar M. Hammad _____

David T. Long _____

Martin E. Young _____

ABSTRACT

ANDREA KELSEY ANDERSON. Regulation of Murine Physiology and Metabolism by the Adipocyte Circadian Clock through Sphingosine Kinase 1. (Under the direction of LAUREN ASHLEY COWART).

The adipocyte, widely known for its large lipid droplets, is a crucial signaling cell at the crux of metabolism. Programs within the adipocyte itself may have massive impacts upon the body. For example, the internal cell-autonomous circadian clock within the adipocyte regulates such lipid droplet-associated processes as lipolysis (triacylglycerol breakdown) and lipogenesis (lipid uptake, triacylglycerol synthesis), which influence circulating lipids, thus impacting other organs. Circadian rhythms (molecular, metabolic, and behavioral patterning over a day) and lipid droplets are both highly evolutionarily conserved biological phenomena that also happen to be intertwined in the system about which we care today, the global human obesity pandemic. Excessive adiposity is a hallmark of obesity, and humans live in an extraordinarily artificially-lit world, which serves to disrupt circadian clocks, thereby disrupting metabolism.

Characterized by their unique sphingosine backbone, sphingolipids, which may derive, in part, from the excess of adiposity and lipid free fatty acids, are well known to affect metabolic disease phenotypes. As the Cowart lab has shown in the past, and as shown in this work, sphingosine kinase 1 (SPHK1) and its enzymatic product sphingosine-1-phosphate (S1P) affect cellular signaling pathways that directly influence metabolism. SPHK1 is a lipid kinase which phosphorylates sphingosine (an *N*-acylated amino alcohol) to S1P, a bioactive autocrine and

paracrine signaling lipid, to influence various processes including cellular survival, angiogenesis, endothelial permeability, immune cell trafficking, and oncogenesis. Since SPHK1 is highly involved in metabolism, such as glucose metabolism, and since metabolism is a circadian-governed process, we hypothesized that SPHK1 is involved in the regulation of the adipocyte circadian clock, which may impact circulating metabolites, such as glucose, fatty acids, and adipokines, thereby affecting weight gain and glucose tolerance. Using a wide variety of techniques and methodologies including RNA sequencing, mass spectrometry coupled with lipidomics and proteomics, chromatin immunoprecipitation (ChIP), protein co-immunoprecipitation, microscopy, gene and protein expression analysis, we conclude that novel properties of SPHK1 and S1P elicit changes in nuclear chromatin remodeling events, leading to circadian clock disruption and subsequent impairment of key metabolic physiological parameters in the mouse. To our knowledge, his is the first report of a lipid metabolite directly affecting the circadian clock.

Table of Contents

ACKNOWLEDGEMENTS……..vii

ABSTRACT……...ix

LIST OF FIGURES……..……xii

LIST OF TABLES……..xiv

NOMENCLATURE……..xv

PREFACE……....…xxiv

CHAPTER 1: …….....

BACKGROUND AND INTRODUCTION……...1

1.1 Sphingolipid Biochemistry…….2

1.2 Importance and Significance of Sphingolipids……7

1.3 Adipose Tissue……..……9

1.4 Sphingolipids in Adipose Tissue……..…….12

1.5 Circadian Rhythm……...14

1.6 Sphingosine Kinase 1/S1P Regulation…….30

CHAPTER 2: ……..

SPHINGOLIPIDS IN ADIPOSE TISSUE: WHAT'S TIPPING THE SCALE? (ANDERSON and Lambert et al., 2018, *Advances in Biological Regulation*)……..……40

CHAPTER 3: ……..

DEPLETION OF ADIPOCYTE SPHINGOSINE KINASE 1 LEADS TO CELL HYPERTROPHY, IMPAIRED LIPOLYSIS, AND NON-ALCOHOLIC FATTY LIVER DISEASE (ANDERSON, et al., 2020, *Journal of Lipid Research*)……..……..…72

CHAPTER 4: ……...

ADIPOCYTE SPHINGOSINE KINASE 1 REGULATES HISTONE MODIFIERS TO DISRUPT CIRCADIAN FUNCTION (ANDERSON, et al., 2020)……115

CHAPTER 5: ……...

SUMMARY AND PERSPECTIVE…….163

CHAPTER 6: ……...

SOLUTIONS TO BE FOUND……..167

CHAPTER 7: ……...

MATERIALS AND METHODS……177

CHAPTER 8: ……

REFERENCES……..…198

ACKNOWLEDGEMENTS

I would like to acknowledge the scientific team that oversaw my scientific development over this time: my mentor, Dr. Cowart (Ashley), and my committee of Dr. Young (Martin), Dr. Blumer (Joe), Dr. Hammad (Samar), and Dr. Long (David). We also had former MUSC committee members Drs. Kelley Argraves and J. Alan Diehl who provided invaluable insight for the work.

I want to acknowledge the gracious gifts of science I have been given, not just in the way of supplies and support, but also the incredible traveling opportunities to share not just my science but my passion for interprofessionalism across the broader healthcare enterprise.

I want to thank Dr. Steve Kubalak for his unwavering support from the beginning of my studies.

I want to thank Drs. Mary Mauldin and Jennifer Bailey for being wonderful interprofessional advisors.

I would like to acknowledge my support network at VCU, Drs. Sarah Spiegel, Chris D. Green, Cynthia Weigel, Jason Newton, Santiago Lima, Tomek Kordula, Binks Wattenberg, and Carmen Sato-Bigbee.

I would like to acknowledge all the folks that help make the daily activities we undertake in the lab possible, namely the facilities and security personnel that watch after the premises.

The support in Richmond from my dear Ditu, Theo, Kathy, and Jason has been a gift. The support from my classmates and friends that sojourned the same road with a knowing heart, Shardai, Tucker, Clarisse, Whitney, Pallavi, Elyse, Alex, Dan, Alice, Dany, Meg. I'd like to heavily acknowledge the shoulders of giants upon which I stood to make this work possible!

Last, but certainly my absolute greatest, my mom and brother A.J. for their enduring, unwavering, unparalleled, down-in-the-trenches love and support. I am honored to have you two in my life and so grateful. I thank you for always being there for me. And thanks to my sweet fur and feather babies for their love.

ABSTRACT

The adipocyte, widely known for its large lipid droplets, is a crucial signaling cell at the crux of metabolism. Programs within the adipocyte itself may have massive impacts upon the body. For example, the internal cell-autonomous circadian clock within the adipocyte regulates such lipid droplet-associated processes as lipolysis (triacylglycerol breakdown) and lipogenesis (lipid uptake, triacylglycerol synthesis), which influence circulating lipids, thus impacting other organs. Circadian rhythms (molecular, metabolic, and behavioral patterning over a day) and lipid droplets are both highly evolutionarily conserved biological phenomena that also happen to be intertwined in the system about which we care today, the global human obesity pandemic. Excessive adiposity is a hallmark of obesity, and humans live in an extraordinarily artificially-lit world, which serves to disrupt circadian clocks, thereby disrupting metabolism.

Characterized by their unique sphingosine backbone, sphingolipids, which may derive, in part, from the excess of adiposity and lipid free fatty acids, are well known to affect metabolic disease phenotypes. As the Cowart lab has shown in the past, and as shown in this work, sphingosine kinase 1 (SPHK1) and its enzymatic product sphingosine-1-phosphate (S1P) affect cellular signaling pathways that directly influence metabolism. SPHK1 is a lipid kinase which phosphorylates sphingosine (an *N*-acylated amino alcohol) to S1P, a bioactive autocrine and paracrine signaling lipid, to influence various processes including cellular survival, angiogenesis, endothelial permeability, immune cell trafficking, and oncogenesis. Since SPHK1 is highly involved in metabolism, such as glucose metabolism, and since metabolism is a circadian-governed process, we hypothesized that SPHK1 is

involved in the regulation of the adipocyte circadian clock, which may impact circulating metabolites, such as glucose, fatty acids, and adipokines, thereby affecting weight gain and glucose tolerance. Using a wide variety of techniques and methodologies including RNA sequencing, mass spectrometry coupled with lipidomics and proteomics, chromatin immunoprecipitation (ChIP), protein co-immunoprecipitation, microscopy, gene and protein expression analysis, we conclude that novel properties of SPHK1 and S1P elicit changes in nuclear chromatin remodeling events, leading to circadian clock disruption and subsequent impairment of key metabolic physiological parameters in the mouse. To our knowledge, this is the first report of a lipid metabolite directly affecting the circadian clock.

Key Words

Adipocyte | Circadian Rhythm | Sphingosine Kinase 1 | Sphingosine 1 Phosphate

Subject Areas

Biochemistry | Molecular Biology | Physiology

LIST OF FIGURES

(chapter shown in parentheses)

(1.1.) Figure 1. S1P synthesis, degradation, and utilization.

(1.2.) Figure 2. The molecular circadian clock.

(2.1.) Figure 3. Sphingolipid biosynthesis pathway. (Lambert, J.M., Anderson, A.K., Cowart, L.A. (2018) Sphingolipids in Adipose Tissue: What's Tipping the Scale? Advances in Biological Regulation 70: 19-30.)

(2.2.) Figure 4. Healthy versus unhealthy adipose tissue. (Lambert, J.M., Anderson, A.K., Cowart, L.A. (2018) Sphingolipids in Adipose Tissue: What's Tipping the Scale? Advances in Biological Regulation 70: 19-30.)

(3.1.) Supplemental Figure 1. *Sphk1* knockout in the adipocyte and effects on *Sphk2* and insulin.

(3.2.) Figure 5. High fat diet-induced weight gain and systemic glucose intolerance.

(3.3.) Figure 6. Adipocyte hypertrophy in $SK1^{fatKO}$ gWAT.

(3.4.) Supplemental Figure 2. Adipokine crosstalk with liver sphingolipid metabolism.

(3.5.) Figure 7. Inflammation within the adipose tissue.

(3.6.) Supplemental Figure 3. High fat fed $SK1^{fatKO}$ gonadal fat pads have fewer infiltrating neutrophils.

(3.7.) Figure 8. Fasting serum non-esterified fatty acids, basal glycerol release, and lipolytic proteins are reduced in $SK1^{fatKO}$ mice.

(3.8.) Figure 9. Serum triacylglycerol, liver lipid accumulation, and lipogenesis.

(4.1.) Figure 10. *Sphk1* is a circadian gene in adipocytes.

(4.2.) Supplemental Figure 4. $SK1^{fatKO}$ gWAT mRNA Sequencing analysis.

(4.3.) Supplemental Figure 5. *Sphk1* oscillates in 3T3 cells and murine lung tissue.

(4.4.) Figure 11. SPHK1$^{-/-}$ adipocytes have a dysfunctional circadian clock.

(4.5.) Figure 12. Loss of actively transcribing chromatin and CLOCK occupancy in SPHK1$^{-/-}$ adipocytes and disruption of chromatin modifiers.

(4.6.) Figure 13. Energy homeostasis and liver metabolism are perturbed in SK1^{fatKO}.

(4.7.) Figure 14. Proposed model of SPHK1/S1P regulation of adipocyte circadian rhythm.

(6.1.) Figure 15. Matured primary adipocytes in culture.

LIST OF TABLES

(*as they appear*)

(2.1.) Table 1. Sphingolipid knockout models and their adipose tissue phenotypes. (Lambert, J.M., Anderson, A.K., Cowart, L.A. (2018) Sphingolipids in Adipose Tissue: What's Tipping the Scale? Advances in Biological Regulation 70: 19-30.)

(2.2.) Table 1. (*re-printed in text for convenience*) Sphingolipid knockout models and their adipose tissue phenotypes. (Lambert, J.M., Anderson, A.K., Cowart, L.A. (2018) Sphingolipids in Adipose Tissue: What's Tipping the Scale? Advances in Biological Regulation 70: 19-30.)

(3.1) Supplemental Table 1. Densitometry values calculated by ImageJ for Western blots and graphs shown in Figure 8C, D.

NOMENCLATURE

ABC = ATP-binding cassette transporter

ABC294640 = SPHK2 pharmacological inhibitor

ABHD5 = abhydrolase domain containing 5, also known as CGI-58

aCDase = acid ceramidase

Adipoq = adiponectin

ADSC = adipose-derived stem cell

alkCDase = alkaline ceramidase

AMP-DNM = N-5-(adamantane-1-yl-methoxy)-pentyl-1-deoxynojirimycin

AMPK = 5’ adenosine monophosphate-activated protein kinase

ApoM = apolipoprotein M

Arg1 = arginase 1

ARNT = aryl hydrocarbon receptor nuclear translocator

AU = arbitrary units

ATGL = adipose triglyceride lipase

AUC = area under curve

β3-AR = beta 3 adrenergic receptor

BAT = brown adipose tissue

BCA = bicinchoninic acid

BMAL1 = brain and muscle ARNT-like protein 1

cAMP = cyclic adenosine monophosphate

Cbxypa = carboxypeptidase A

Ccl2 = C-C motif chemokine ligand 2

Ccrn4l = carbon catabolite repression 4-like, also known as nocturnin

CD = control diet

CD36 = cluster of differentiation 36

C/EBP = CCAAT/enhancer-binding protein

Cebpα = CCAAT/enhancer-binding protein alpha

CerS1 = ceramide synthase 1

CerS2 = ceramide synthase 2

CerS3 = ceramide synthase 3

CerS4 = ceramide synthase 4

CerS5 = ceramide synthase 5

CerS6 = ceramide synthase 6

CGI-58 = lipid droplet binding protein, also known as ABHD5

ChIP = chromatin immunoprecipitation

CLOCK = circadian locomotor output cycles kaput

CLS = crown-like structure

Col1a1 = collagen type I alpha 1 chain

C_q = quantitation cycle

Cry1 = cryptochrome 1

Cry2 = cryptochrome 2

C_t = cycle threshold

CT = circadian time

DAG = diacylglycerol

Dbp = D-site of albumin promoter binding protein

DEGS1 = sphingolipid delta(4)-desaturase

Dgat2 = diacylglycerol transferase 2

dhCERS = dihydroceramide synthase

DMEM = Dulbecco's modified eagle medium

DPPC = dipalmitoylphosphatidylcholine

DSG = disuccinimidyl glutarate

Emr1 = EGF-like module-containing mucin-like hormone receptor-like 1

ER = endoplasmic reticulum

EtOH = ethanol

F4/80 = murine macrophage marker, also known as Emr1

FAF = fatty acid-free

FABP4 = fatty acid binding protein 4

Fasn = fatty acid synthase

FBS = fetal bovine serum

FSP27 = fat-specific protein 27

G0S2 = G0/G1 switch 2

GLUT4 = glucose transporter type 4

GM3 = monosialodihexosylganglioside

GSK3β = glycogen synthase kinase 3 beta

gWAT = gonadal white adipose tissue

HAT = histone acetyl transferase

H&E = hematoxylin and eosin

H3K9ac = histone 3 acetylated lysine 9

H3K27ac = histone 3 acetylated lysine 27

HDAC1 = histone deacetylase 1

HDAC2 = histone deacetylase 2

HDAC3 = histone deacetylase 3

HDL = high density lipoprotein

HFD = high fat diet

HILPDA = hypoxia inducible lipid droplet associated protein

Hmbs1 = hydroxymethylbilane synthase 1

HOMA-IR = Homeostatic Model Assessment of Insulin Resistance

Hr = hour

HRP = horseradish peroxidase

HSL = hormone sensitive lipase

IKK = IκB kinase

IL-1β = interleukin 1 beta

IL-6 = interleukin 6

IL-10 = interleukin 10

iNOS = inducible nitric oxide synthase

IR = insulin resistance

K1 = sphingosine kinase 1

K2 = sphingosine kinase 2

KO = knockout

KCl = potassium chloride

KOH = potassium hydroxide

LINC = linker of nucleoskeleton and cytoskeleton

Lipe = gene symbol for HSL

LPL = lipoprotein lipase

LPS = lipopolysaccharide

MAG = monoacylglycerol

MAPK = mitogen-activated protein kinase

Mcp1 = monocyte chemoattractant protein 1

MEF = mouse embryonic fibroblast

MESOR = midline estimating statistic of rhythm

$MgCl_2$ = magnesium chloride

MKRN1 = Makorin Ring Finger Protein 1

MNE = mean normalized expression

MPO = myeloperoxidase

mTOR = mechanistic target of Rapamycin

mTORC1 = mTOR complex 1

NAFLD = nonalcoholic fatty liver disease

NASH = nonalcoholic steatohepatitis

nCDase = neutral ceramidase

NCoR = nuclear corepressor

NEFA = non-esterified fatty acid

NFκB = nuclear factor kappa light-chain enhancer of activated B cells

NLR = Nucleotide-binding oligomerization domain (NOD), Leucine rich Repeat (LRR)

NLRP3 = NLR family, pyrin domain containing 3

NPAS2 = neuronal PAS domain protein 2

Nr1d1 = nuclear receptor subfamily 1, Group D, member 1

NUP98 = nuclear pore complex protein 98

ORMDL = orosomucoid 10-like

ORO = Oil Red O

PBS = phosphate-buffered saline

PDE3B = phosphodiesterase 3B

Per1 = period 1

Per2 = period 2

Per3 = period 3

PGC1α = peroxisome proliferator-activated receptor gamma coactivator 1 alpha

PI3K = phosphoinositide 3-kinase

PIP3 = phosphatidylinositol (3,4,5)-triphosphate

PKA = protein kinase A

PLC = phospholipase C

PLIN1 = perilipin 1

PMA = phorbol 12-myristate 13-acetate

PMSF = phenylmethylsulfonyl fluoride

PNPLA3 = patatin-like phospholipase domain-containing protein 3

PP2A = protein phosphatase 2A

PPARγ = peroxisome proliferator activated receptor gamma

Ppia = peptidylprolyl isomerase A

PRDM16 = PR domain containing 16

PREF1 = preadipocyte factor 1

Ptgds = prostaglandin D2 synthase

RAE1 = ribonucleic acid export 1

RanBP3 = ran-binding protein 3

RER = respiratory exchange ratio

Rev-Erbα = reverse of c-Erb alpha; nuclear receptor subfamily 1, Group D, member 1 (Nr1d1)

Rev-Erbβ = reverse of c-Erb beta; nuclear receptor subfamily 1, Group D, member 2 (Nr1d2)

RIN = RNA integrity number

RIPA = radioimmunoprecipitation assay

RIP1 = receptor-interacting serine/threonine-protein kinase 1

Rorα = retinoic acid receptor-related orphan receptor alpha

Rorβ = retinoic acid receptor-related orphan receptor beta

Rorγ = retinoic acid receptor-related orphan receptor gamma

S1P = sphingosine-1-phosphate

S1Pr1 = sphingosine-1-phosphate receptor 1

S1Pr2 = sphingosine-1-phospate receptor 2

S1Pr3 = sphingosine-1-phospate receptor 3

S1Pr4 = sphingosine-1-phosphate receptor 4

S1Pr5 = sphingosine-1-phosphate receptor 5

SCD1 = stearoyl CoA desaturase 1

SEM = standard error of the mean

SGPL = sphingosine-1-phosphate lyase

SGPP1 = sphingosine-1-phosphate phosphatase 1

SGPP2 = sphingosine-1-phosphate phosphatase 2

SK = sphingosine kinase (also known as SPHK)

$SK1^{fatKO}$ = adipocyte-specific SK1 knockout

SK1-I = (2R,3S,4E)-N-methyl-5-(4'-pentylphenyl)-2-aminopent-4-ene-1,3-diol . HCl (pharmacologically inhibits SPHK1)

SKI-II = 4-[[4-(4-chlorophenyl)-2-thiazoyl]amino]phenol (pharmacologically inhibits both SPHK1 and SPHK2)

Slc9a3 = solute carrier family 9 member A3

SMS1 = sphingomyelin synthase

SPHK1 = sphingosine kinase 1

SPHK2 = sphingosine kinase 2

$SPHK1^{-/-}$ = sphingosine kinase 1 knockout (“whole-body,” “constitutive”)

Spns2 = spinster 2

SPTLC1 = serine palmitoyltransferase, long chain base subunit 1

SPTLC2 = serine palmitoyltransferase, long chain base subunit 2

SPTLC3 = serine palmitoyltransferase, long chain base subunit 3

Sptss1a = serine palmitoyltransferase, small subunit 1a

Sptss1b = serine palmitoyltransferase, small subunit 1b

SubQ = subcutaneous

SVF = stromal vascular fraction

sWAT = subcutaneous adipose tissue

T3 = triiodothyronine

T4 = thyroxine

TAG = triacylglycerol

Tbp = TATA box binding protein

TERT = telomerase reverse transcriptase

Tgf-β1 = transforming growth factor-beta 1

TNFα = tumor necrosis factor alpha

TRAF2 = TNF receptor associated factor 2

TSH = thyroid-stimulating hormone

TSS = transcription start site

Ub = ubiquitin

WAT = white adipose tissue

WT = wildtype

ZT = Zeitgeber time

PREFACE

This project began with the generation of the adipocyte-specific sphingosine kinase 1-null mice due to interest from previous work in the Cowart lab showing protection from systemic inflammation yet drastically increased weight gain on high fat diet in mice lacking sphingosine kinase 1 (SPHK1) constitutively. During the course of the adipocyte-specific SPHK1 knockout ($SK1^{fatKO}$) diet-induced obesity study, we discovered through unbiased messenger RNA sequencing of gonadal white adipose tissue that these mice had disrupted circadian clocks, as measured by fold change of key clock regulatory genes. The text herein describes the intertwined nature of adipocyte metabolism and the clock and how sphingolipids are poised to perturb homeostasis in both of those systems. The overall hypothesis of the project is that SPHK1, a sphingolipid biosynthesis enzyme, participates in the regulation of the adipocyte circadian clock molecular machinery, which manifests in metabolic disturbances, such as aberrant circulating lipids and adipokines, and this impacts the overall metabolic phenotype, such as glucose tolerance and weight gain.

The first specific aim of the project was to determine if *Sphk1* is a clock-controlled gene in adipocytes, and if it is directly controlled by the clock transcriptional machinery, or by indirect mechanism(s). To further answer whether SPHK1 may be involved in a novel feedback regulatory loop with the clock, we developed the next aim. The second specific aim was to determine the extent to which SPHK1 may participate in the regulation of the core molecular components of the circadian clock. Finally, we sought to determine a potential role for adipocyte SPHK1 in the maintenance of whole-body metabolic homeostasis of carbohydrates and lipids using an *in vivo* mammalian model system.

It should be noted that the work described in Chapter 3 reflects *in vivo* and *ex vivo* work utilizing only the $SK1^{fatKO}$ mouse that we generated for the first time. The work in Chapter 4, however, is mostly *in vitro* work derived from primary adipocytes from wildtype or $SPHK1^{-/-}$ constitutive knockout mice, for a culture free of SPHK1. The emphasis here is to show that Chapter 3 is the overall metabolic characterization of the conditional knockout mouse along with a role for adipocyte SPHK1 in the metabolic perturbations observed when challenged with a high fat diet. For Chapter 4, the $SK1^{fatKO}$ mouse is described further, specifically in the context of circadian rhythm with minimal panels of *in vivo* data, which is not a part of Chapter 3. In addition, Chapter 4 is largely based on tissue culture data, in which we assessed the role of SPHK1 in circadian rhythm in adipocytes in a dish. At the Cowart lab's disposal, which is not always typical, was the constitutive SPHK1 knockout ($SPHK1^{-/-}$) mouse, so we therefore assessed roles for SPHK1 largely utilizing a model of constitutive genetic deletion of SPHK1 compared to wildtype controls.

The reason to also make the distinction between the usage of a constitutive knockout for tissue culture versus conditional knockout for physiological characterization clear is because conducting the primary tissue culture protocol for matured adipocytes derived from the adipose stromal vascular fraction from the Cowart lab's novel $SK1^{fatKO}$ mice was not suitable for drawing conclusions on SPHK1 loss, as the tissue culture system would be contaminated with SPHK1-expressing cells. As the reader will find later, the adipose tissue is described as a highly heterogenous milieu of cell types, and the $SK1^{fatKO}$ is generated only in cells expressing adiponectin, which are presumably the mature adipocytes, but not the remainder of the adipose tissue (preadipocytes, immune cells, stem cells, etc.). Therefore, it was noted that any experiments performed in a dish in which we compared SPHK1 genetic ablation with a control, we solely utilized cells from $SPHK1^{-}$

$^{/-}$ mice, which lack SPHK1 in all cells, rather than just those cells that express adiponectin (the *Cre* driver in the SK1^{fatKO}). To conclude, the tissue culture experiments were always performed in conditions in which the growth-arrested mature adipocytes comprised ≥85% of the visible culture under a light microscope. That is to say, the tissue culture is not entirely pure, although it is highly enriched for adipogenic stem cells that had successfully undergone an adipocyte differentiation protocol. Despite all of these nuances, be assured that the protocol for obtaining these fresh cells (for single-passage use) was highly successful, performed on a weekly basis or more frequently, and adhered to the most accepted protocols in use today for the study of primary matured adipocytes in culture. The writer is compelled to qualify these details to preemptively declare that cellular roles for SPHK1 were delineated in this project by the use of the SPHK1$^{-/-}$ mouse primary cells rather than the use of 1) the novel SK1^{fatKO} mouse primary cells, 2) transfection, or 3) viral infection silencing strategies.

CHAPTER 1

BACKGROUND AND INTRODUCTION

1.1. Sphingolipid Biochemistry

Sphingolipids were discovered by Johann Thudichum in the late 19th century (Kleuser, 2018; Thudichum, 1962.) He was a neurochemist; and he was extracting brain tissue in organic solvent (ethanol) to discover what he thought to be enigmatically-behaving lipids, which he named in honor of the riddle of the Greek sphinx (Breathnach, 2001). Sphingolipids are formed through three prominent pathways within the sphingolipid biosynthetic pathway (Merrill, et al., 1988; Castillo, et al., 2016). The *de novo* sphingolipid pathway begins at the top with the condensation of a fatty acyl CoA and an amino acid (Merrill Jr., et al., 2002, Hannun and Obeid, 2002). In most cases in mammalian sphingolipid biosynthesis, the pathway is initiated with palmitic acid and serine, however, the enzyme responsible for this condensation may preferentially utilize other species, such as myristic acid, and alanine or glycine (Merrill Jr., et al., 2002). This is mediated by the specific subunits comprising this enzyme, serine palmitoyltransferase, which has a long chain base subunit (SPTLC1, 2, 3) as well as a short chain subunit (Sptss1a, 1b) and other regulatory components, such as the ORMDL proteins and other non-protein constituents, and the manner by which they heteromultimerize determines the substrate preference and the unique backbone chemistry of the subsequently formed sphingolipid (Gable, et al., 2010; Han, et al., 2009; Hornemann, et al., 2009).

Further down the sphingolipid biosynthetic pathway is described in Chapter 2. In short, through a series of condensation, reduction, and dehydrogenation reactions, ceramide is generated *de novo* (the first of three pathways) and can be interconverted to more complex glycosylceramide species, sphingomyelin, or sphingosine. A careful balance emerges among several metabolites at this juncture (traditionally, chiefly ceramide); and the second pathway, the sphingomyelinase pathway, serves to

reconstitute the ceramide pool by the action of the eponymous enzyme, and thirdly, the salvage pathway within the lysosome contributes to sphingosine conversion by ceramide synthases to ceramide (Kitatani, et al., 2008; Zelnik, et al., 2020). On the other hand, cytotoxic sphingosine can be phosphorylated by either of two known kinase isoenzymes, sphingosine kinase (SPHK) 1 and 2, which are further discussed later. The emphasis of this dissertation is SPHK1, a cytosolic enzyme, and its bioactive product sphingosine-1-phosphate, S1P for shorthand (Figure 1). SPHK2 is mainly thought to be a nuclear protein (Igarashi, et al., 2003; Qin, et al., 2018). S1P may be dephosphorylated by either of two sphingosine phosphatase enzymes or irreversibly cleaved by the sphingosine-1-phosphate lyase enzyme to generate myristaldehyde and phosphoethanolamine. Moreover, other lipid phosphatases (such as lipid phosphate phosphatase 3) and ectophosphatases are thought to act on S1P in tissue and certainly in the circulation *in vivo* (Bréart, et al., 2011; Kharel, et al., 2020; López-Juárez, et al., 2011; Tang, et al., 2015).

S1P is known to signal through extracellular G-protein coupled receptors (S1Pr1-5) (Figure 1). Moreover, S1P may be transported between extracellular and cytosolic compartments by Spinster 2 (Spns2) or ATP-binding cassette (ABC) transporters, such as ABCC1 (Ihlefeld, et al., 2015; Nagahashi, et al., 2013; Nieuwenhuis, et al., 2009; Spiegel, et al., 2019). More roles and insights continue to be uncovered about S1P metabolism and dynamics with each passing year.

Figure 1.

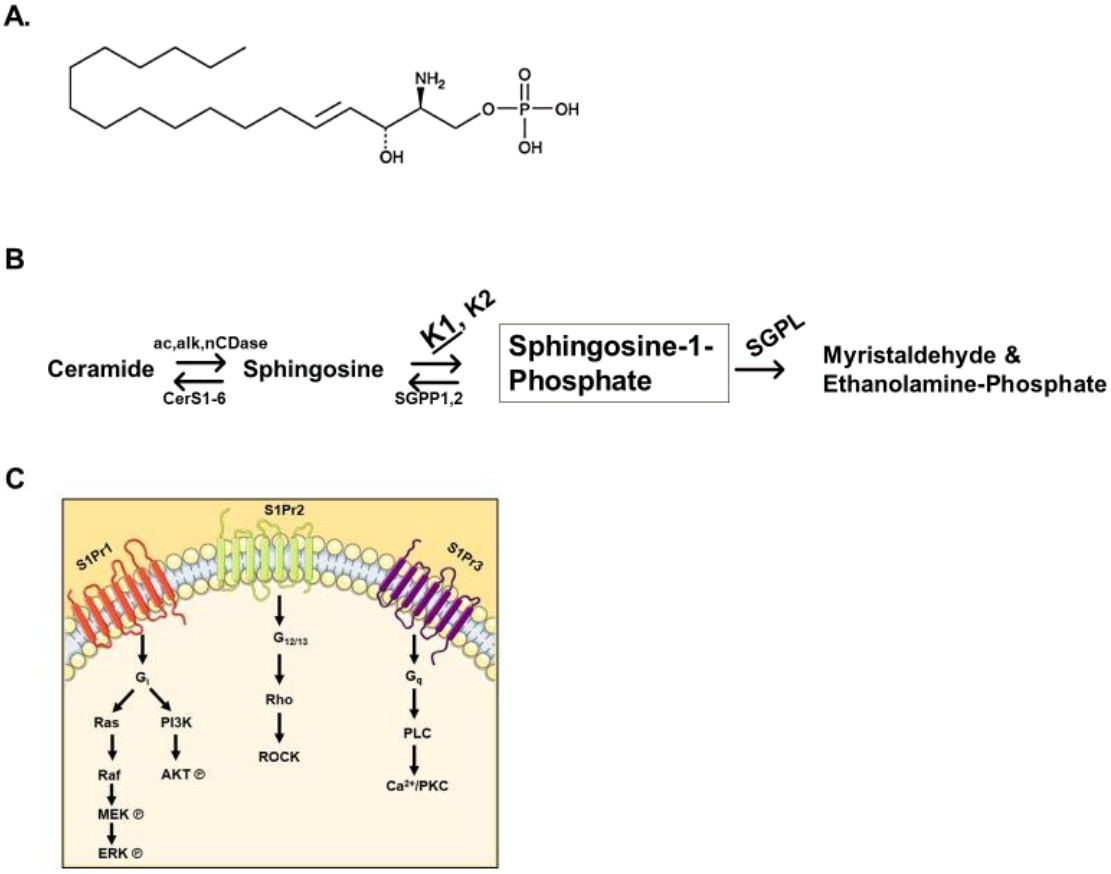

Figure 1. S1P synthesis, degradation, and utilization. A. The most typically studied mammalian S1P chemical species is 2S-amino-4E-octadecene-1,3R-diol 1-(dihydrogen phosphate). This is also referred to as d18:1 sphingosine-1-phosphate. This molecule is a phosphorylated *N*-acylated amino alcohol, typically with the 18-carbon acyl chain generating the sphingoid backbone. The acyl moiety to the left is hydrophobic while the alcohol and phosphate groups lend to hydrophilicity and a negative charge at physiological pH. **B.** There are two distinct breakdown pathways for S1P, and only one synthetic pathway for S1P. Ceramides can be broken down by ceramidases in different cellular locations to generate sphingosine, which can then be phosphorylated by SPHK1

(Figure 1 legend, continued.)

or SPHK2 to generate S1P. S1P can be broken down reversibly by either of the two S1P phosphatases to regenerate sphingosine. If S1P is broken down by S1P lyase, this is irreversible, and it marks the exit from the sphingolipid biosynthetic pathway. Myristaldehyde may be utilized post-processing as a fatty acid in a variety of synthetic pathways, including sphingolipid synthesis. Phosphoethanolamine is primarily associated with the plasma membrane. **C.** S1P may signal through one of 5 G-protein coupled receptors to generate a variety of cellular responses. S1PR1-3 are the best-characterized S1P receptors, signaling through Ras, phosphoinositide 3-kinase (PI3K), Rho, or phospholipase C. *acCDase, acid ceramidase; alkCDase, alkaline ceramidase; nCDase, neutral ceramidase; CerS 1-6, ceramide synthase 1, 2, 3, 4, 5, 6; PLC, phospholipase C; PI3K, phosphoinositide-3-kinase; K1, sphingosine kinase 1; K2, sphingosine kinase 2; SgpP1-2, sphingosine-1-phosphate phosphatase 1, 2; SgpL, sphingosine 1 phosphate lyase; S1Pr1-3, sphingosine-1-phosphate receptor 1-3*.

Of important mention, sphingosine kinases and their product S1P are enigmatic (Spiegel and Milstien, 2003). It was found in human skin fibroblasts that SPHK1$^{-/-}$ cells had increased sphingosine levels, compared to baseline (as expected), however, S1P levels were also increased in SPHK1$^{-/-}$ fibroblasts compared to wildtype fibroblasts (Qin, et al., 2018). On the other hand, SPHK2$^{-/-}$ fibroblasts showed somewhat of a decrease in cellular S1P (Qin, et al., 2018). In contrast, Samad and colleagues showed that SPHK1$^{-/-}$ mice had decreased S1P (as would be expected) but sphingosine was unchanged in null animals compared to controls (Wang, et al., 2014). Strangely, SPHK2$^{-/-}$ mice also have much higher circulating levels of S1P compared to wildtype counterparts (Kharel, et al., 2012 and 2020; Sensken, et al., 2010). Moreover, SPHK2, but not SPHK1, is generally considered the kinase responsible for phosphorylation of the FDA-approved multiple sclerosis drug FTY-720 *in vivo* (Billich, et al., 2003; Saba and Hla, 2004; Sanchez, et al., 2003).

1.2. Importance and Significance of Sphingolipids

Although not related to the project described here, a major FDA-approved treatment on the market for multiple sclerosis is fingolimod, which is an S1P receptor 1 (S1PR1) modulator (Pelletier and Hafler, 2012). S1PR1 is critically important for immune cell function and trafficking (Adada, et al., 2013; Liu, et al., 2000). In fact, the circadian (24-hour cycle) oscillation of S1PR1 within immune cells is crucial for their variation in circulatory egress versus lymph node and organ homing (Druzd, et al., 2017). Knockout of S1PR1 in mice is embryonically lethal, with impaired vasculogenesis and severe hemorrhaging (Liu, et al., 2000). Moreover, knockout of both sphingosine kinases results in an embryonically lethal phenotype (Mizugishi, et al., 2005). Much of this is attributable to early angiogenic and endothelial developmental perturbations, and hemorrhaging within the embryo is visible to the naked eye (Mizugishi, et al., 2005).

Sphingolipids are also present throughout cellular membranes, meaning not just the plasma membrane but organellar membranes. Sphingolipids are generally thought to reside in special domains of the plasma membrane lipid bilayer called “lipid rafts,” and it is within these specialized domains that protein complexes may anchor to create signaling platforms (Brugger, et al., 2004; Gulbins and Kolesnick, 2003). Thus, sphingolipids contribute to the membrane heterogeneity that is necessary for curvature as well as specialized membrane locations with varying docking affinity for protein signaling complexes (Sonnino, et al., 2006).

Sphingolipids are also appreciated as bioactive signaling molecules, with ceramide and S1P at the forefront. Typically, ceramide is thought to be pro-apoptotic while S1P is thought to be pro-survival, and the balance of these two species is highly dependent on sphingosine kinases (Mathias and Kolesnick, 1993; Ruvolo, et al., 2002; Van Brocklyn, et

al., 2012). These pathways have been exploited for treatment strategies in cancer (Lewis, et al., 2018; Ponnusamy, et al., 2010). However, for this project the study of SPHK1 and its significance in metabolism were studied since the Cowart lab focuses on metabolic disease. Indeed, roles for sphingolipids and sphingolipid enzymes in metabolic disease have been established in the literature over the last few decades. In short, many changes in sphingolipids are context- and tissue-specific, lending to the varying degrees of metabolic perturbations observed in response to sphingolipid alterations. In general, ceramides tend to increase with obesity (Holland, et al., 2007). Even more fascinating, the ratio of particular acyl-chain length ceramide species found in the circulation may provide better prognostic information than circulating cholesterol-laden lipoproteins for cardiovascular disease, one of the major hallmarks of the metabolic syndrome (Laaksonen, et al., 2016; Peterson, et al., 2018; Turpin, et al., 2014).

1.3. Adipose Tissue

Adipose tissue was underappreciated for a long time as an inert energy storage depot. The discovery of leptin, which is nicknamed the obesity gene, is what set ablaze the field of adipose endocrinology, physiology, and metabolism. In the 1950's, a subset of mice at the Jackson Laboratories had a recessive mutation leading to an overweight phenotype, and in the early 90's, the gene responsible for this phenotype was cloned and named leptin (Zhang, et al., 1994; Halaas, et al., 1995). Today, the adipose tissue is understood to be a master secretory organ, as it releases adipokines that signal receptors in distant tissues (Scherer, 2006). Moreover, the adipose tissue-intrinsic processes of lipolysis and lipogenesis plant this tissue at the center of metabolic regulation within the organism. Its extreme plasticity in comparison to other organs also contributes to its function and effects upon the rest of the body; and this plasticity arises from the processes of adipocyte hyperplasia and hypertrophy, which are defined as expansion in cell number and cell size, respectively (Jo, et al., 2009; Muir, et al., 2016).

Adipose tissue that is hyperplastic tends to be healthier adipose compared to the fat pad that selectively undergoes hypertrophy of the residing adipocytes (Samocha-Bonet, et al., 2014; Vishvanath and Gupta, 2019). Hyperplastic adipose is thought to be more adipogenic, thus allowing the tissue to expand healthily in the face of excess energy (Muir, et al., 2016). On the other hand, hypertrophic adipocytes suggest various mechanistic issues including overactive lipogenesis, underactive lipolysis, and underachieving adipogenesis. As the adipose tissue expands via hypertrophy, resident immune cells begin to infiltrate, thus propagating a state of chronic low-grade inflammation (Berg and Scherer, 2005; Crewe, et al., 2017). Moreover, rapid expansion of the adipocyte squelches nearby capillaries, and the immediate surrounding tissue becomes hypoxic due

to loss of oxygen and nutrients as angiogenesis programs must inc to support the tissue (Hosogai, et al., 2007). All of the processes mentioned are subjects of intense study.

At basal regulation of both lipolysis and lipogenesis in the adipocyte, key enzymes are responsible for the ebb and flow of these processes, including ATGL, HSL, stearoyl-CoA desaturase-1 (SCD1), and lipoprotein lipase (LPL) (Paschos, et al., 2012; Shostak, et al., 2013). ATGL is rate-limiting for hydrolysis of the lipid droplet, as it is the first enzyme to cleave a fatty acyl group from the triacylglycerol (TAG) glycerol backbone (Duncan, et al., 2010). LPL is important at the cell surface for breaking down circulating TAG so that individual fatty acyl and glycerol components can be utilized within the cell to re-esterify the glycerol backbone for storage inside the lipid droplet (Maggio and Greenwood, 1982). SCD-1 is the rate-limiting enzyme for synthesizing monounsaturated fatty acids from saturated fatty acids, and it is important for the lipogenic capacity of the adipocyte (Ntambi, et al., 2002; Thiede and Strittmatter, 1985).

Moreover, the basal lipolysis state also shows itself to be redundant in the face of lipase deficiency. For example, HSL-deficient mice still have detectable circulating levels of fatty acids and glycerol at baseline, and they also have significant increases of both of these plasma species in the presence of an isoproterenol (a pharmacological lipolysis inducer) injection, although it is severely blunted, of course (Osuga, et al., 2000). In agreement with these, ATGL-deficient mice also maintain a comparable level of secreted fatty acids and glycerol without lipolytic stimulation. However, adipose explants from *Atgl*$^{-/-}$ mice fail to mount a lipolytic burst of free fatty acids and glycerol with isoproterenol stimulation (Langin, et al, 2005).

In contrast to basal homeostatic lipid control, catecholamines (epinephrine, isoproterenol) initiate β-3 adrenergic receptor (β-3AR) agonism through $G\alpha_S$ to stimulate

cyclic AMP and ultimately PKA, to stimulate HSL (hormone sensitive lipase) and PLIN1 (perilipin 1) in a sequential cascade (Bezaire, et al., 2009). Treatment with these compounds is typical for stimulating lipolysis, although it must always be qualified as β-3AR-mediated when reported. Lipolytic bursts flood the circulation with fatty acids and glycerol to be used as energy substrates during a fight-or-flight response (Geerling, et al., 2014). Insulin opposes lipolysis by signaling through the insulin receptor to activate the PI3K pathway; then PIP3 activates AKT to lead to the activation of phosphodiesterase 3B (PDE3B); PDE3B works against cAMP accumulation by converting cAMP into 5'-AMP. Hence, insulin decreases cAMP. Thus, insulin can stop the action of catecholamine-mediated lipolysis (Morigny, et al., 2016).

1.4. Sphingolipids in Adipose Tissue

Roles for sphingolipids other than S1P and its kinases (isomers SPHK1 and SPHK2) have been described in adipose tissue. A complete review of sphingolipids and their function in adipose tissue was written in 2018 and the contents of which are laid out in Chapter 2.

Since the contents of Chapter 2 went to press, it was published that the other isoform of SPHK1, SPHK2, was involved in metabolic homeostasis governed by glucose absorption (Ravichandran, et al., 2018). SPHK2-null mice were found to be protected from aging-related obesity, as well as more glucose tolerant with lower levels of circulating leptin and insulin when compared to control animals (Ravichandran, et al., 2018). Importantly, this study did not subject the SPHK2$^{-/-}$ mice to a high fat diet regimen, so it is unknown how the genetic depletion of *Sphk2* orchestrates metabolic parameters, such as liver and adipose lipids (triglycerides, sphingolipids, fatty acids), and circulating glucose, insulin, and adipokines (Ravichandran, et al., 2018). On the other hand, no notable differences were observed between SPHK1$^{-/-}$ and WT mice on control diet, but high fat fed SPHK1$^{-/-}$ mice gained more weight than their WT counterparts; notwithstanding mutants were protected from obesity-induced IL-6 expression in the plasma and skeletal muscle (Ross, et al., 2013). In another report, Samad and colleagues showed that SPHK1$^{-/-}$ mice weighed the same as WT mice when fed a high fat diet, but had better metabolic profiles compared to WT matches, such as lower plasma insulin and better glucose tolerance (Wang, et al., 2014).

Due to the nuanced findings of SPHKs and weight gain by the Cowart lab and others, it seemed reasonable to further assess the role for SPHK1 in obesity by ablating it specifically in the adipocyte, a crucial cell type involved in the onset, progression, and

maintenance of obesity. Thus, the project for adipocyte-specific Cre-recombinase-mediated deletion of *Sphk1* with dietary intervention and the subsequent findings are laid out in Chapter 3. This is the first report utilizing a mouse model with an adipocyte-specific ablation of *Sphk1*. Importantly, the mechanisms underlying the metabolic abnormalities described in Chapter 3 are still open for debate. Thus, forthcoming publications further describing roles for adipocyte SPHK1 are set to be released that would underlie and provide explanation for the Chapter 3 findings. Hence, Chapter 4 uncovers a novel role for adipocyte SPHK1 and the maintenance of the circadian clock and its epigenetics. Other efforts have been aimed at clarifying mechanisms for SPHK1 in adipogenesis and in brown adipose mitochondrial biogenesis, which both (adipogenesis and mitochondrial biogenesis) contribute to obesity-associated pathological outcomes (Lambert, *data not shown*; Valentine, *data not shown*).

1.5. Circadian Rhythm

To begin this section, it is important to acknowledge that the Nobel Prize in Medicine or Physiology during the course of this Ph.D. dissertation was awarded to three circadian researchers in 2017. I had the privilege of attending two circadian rhythm conferences where I interacted with the likes of Drs. Michael Rosbash, Mike Young, Joe Takahashi, Carrie Partch, Katja Lamia, Gad Asher, Satchin Panda, Charna Dibner, Luciano DiTacchio, Chuck Weitz, and other impressive scientists. This added immeasurable value to my degree work, and I am so grateful.

1.5.i. The Molecular Circadian Clock

The molecular circadian clock is composed of the primary positive and negative feedback loops, in which BMAL1 and CLOCK (or their paralogs BMAL2 and NPAS2, respectively) are the positive limb transcription factors that regulate the expression of the negative limb composed of PERs and CRYs (Figure 2).

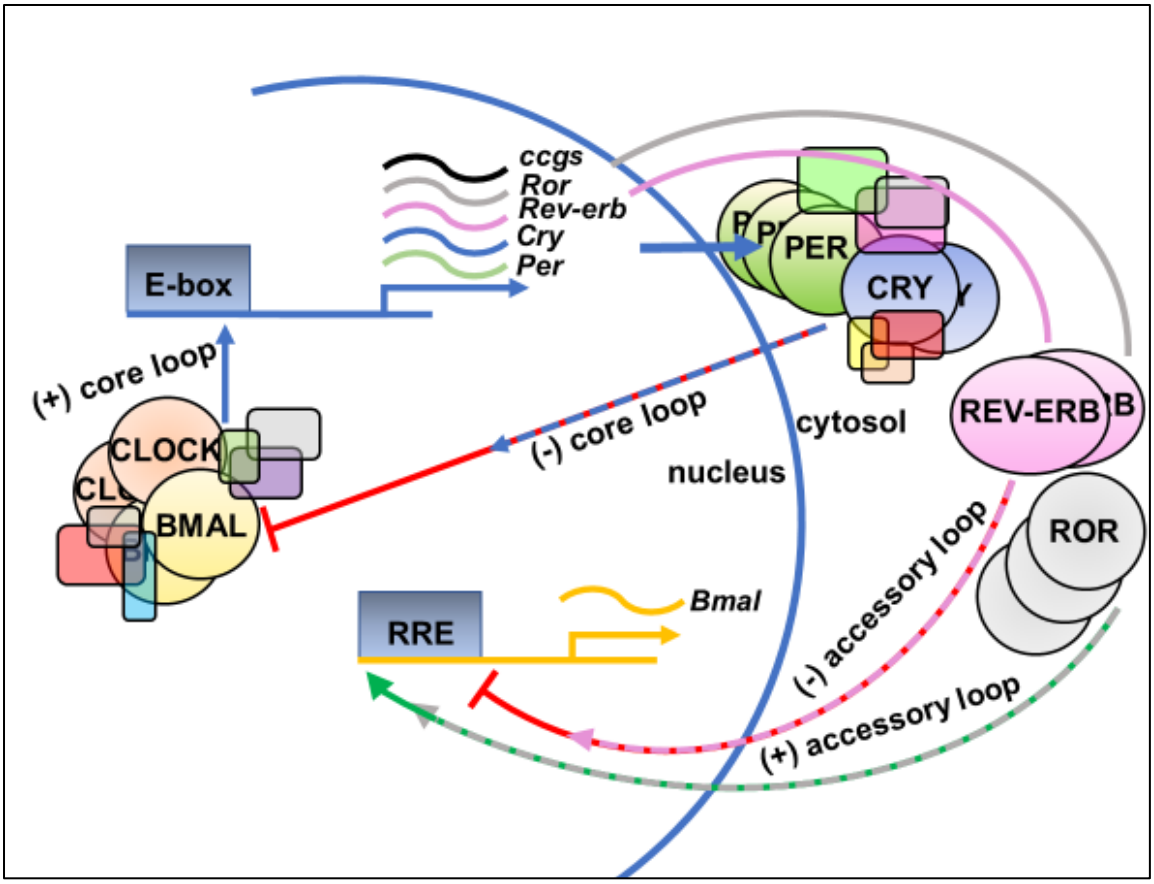

Figure 2. The molecular circadian clock. The transcriptional translational feedback loop undergoes a 24-hour round of positive and negative regulation upon itself. BMAL1 and CLOCK transcription factors heterodimerize to form a transcriptional activation complex which elicits transcription of its targets through E-box elements in the target promoters. Targets of BMAL1:CLOCK include *Per*s and *Cry*s as well as the nuclear hormone receptors *Ror*s and *Reverb*s. Comprising the core negative loop, PERs and CRYs are translated in the cytosol following transcription, and they translocate back to the nucleus as a large complex to inhibit BMAL:CLOCK activity. In so doing, PERs and CRYs repress their own expression while at the same time undergo temporally controlled degradation.

(Figure 2 legend, continued.)

Eventually, this PER:CRY brake is released on BMAL:CLOCK so that BMAL:CLOCK may resume once again another round of transcription. Accessory to this core regulation is REVERB or ROR which respectively add negative or positive transcriptional control upon *Bmal1* expression through a ROR-response element in the *Bmal1* promoter. Additional depicted square and circular shapes indicate and emphasize the existence of paralogs as well as other proteins within these large activator and repressor complexes. *Bmal1, brain and muscle ARNT-like protein 1; ccgs, core clock genes; CLOCK, circadian locomotor output cycles kaput; Cry, cryptochrome; Per, period; REVERB, reverse orientation c-erb; ROR, retinoic acid receptor related orphan receptor; RRE, ROR response element.*

The accessory positive and negative loops primarily affect *Bmal1* gene expression through ROR response elements, in which REVERBα or its paralog REVERBβ repress *Bmal1* expression. The positive accessory regulators are the RORs- α,β,γ; through the same promoter motif, these regulators may enhance transcription of *Bmal1* (Figure 2).

The negative core constituents, the PERs, are regulated tightly by a sequential phosphorylation cascade that is mediated by casein kinases 1δ and ε. This mechanism has been elucidated by Partch and coworkers (Hunt, et al., 2017). The other major player in the complex, the CRYPTOCHROMES, under AMPK-mediated phosphorylation, will degrade with circadian rhythmicity (Lamia, et al., 2009) (Figure 2). Importantly, this highlighted a mode by which glucose depletion directly impacts the clock in an AMPK-dependent manner (Lamia, et al., 2009).

Not only do PERs and CRYs undergo a vast array of modifications and translocations about the cell, these proteins also reside in intricately complex heteromultimeric protein conglomerates that are typically heavier than twenty megadaltons (Aryal, et al., 2017). Considering the dependability of the clock, it seems that this feat of moving such large complexes about the cell would require certain superhighways that are consistently tracked, from day to night. This is where the interest in the linker of cytoskeleton and nucleoskeleton LINC complex arose. Several proteins involved in the LINC were found bound to BMAL1 in a differential manner in SPHK1$^{-/-}$ adipocytes compared to control adipocytes by mass spectrometry proteomics analysis (Anderson and Tomaino, *data not shown*).

1.5.ii. Evolution and the Philosophy of the Clock

Circadian rhythm evolved due to the rotation of the Earth, which gives rise to day and night. Due to the axis of the Earth and the location in space with respect to the sun as it revolves around the sun, further patterning is driven into the molecular gears of our being. With day and night come other changes, including such fluctuations in temperature, animal and human activity, the humidity, availability of resources. Naturally, these phenomena drive the fitness of species to exploit the contrasting fruits that night and day separately may bring to bear.

Thus, such processes like photosynthesis obviously occur during the hours at which the sun shines above (Dodd, et al., 2005; Hennessy and Field, 1991). Due to the finite availability of the sun hours, plants have evolved to make best use of their necessary resource. Other less sun-trinsic and -dependent processes can be put off until the time it is dark.

In a human, many processes have a fluctuation with the day and night. For example, body temperature fluctuates throughout the day, with the body decreasing temperature in the evening (Clark, et al., 1939; Morrison, et al., 2014; Tabarean, et al., 2010; Zhao, et al., 2017). Moreover, immune cell egress and homing are circadian, with the immune cell surveillance making their presence known throughout the lymph and bloodstream during the day and at night returning to the lymph nodes, thymus, and other homes to undergo repair, selection, etc. (Druzd, et al., 2017). Moreover, skeletal muscle strength, heart contractility and output, lung respirometry, vascular tone, gastrointestinal motility all are governed by the pattern of day and night (Atkinson and Reilly, 1996; Conroy and O'Brien, 1974; Davidson, et al., 2005; Durgan and Young, 2010; Gifford, 1987; Konturek, et al., 2011; Layer, et al., 1987; Panza, et al., 1991; Spengler and Shea, 2000).

Amazingly and stunningly, the circadian clock, which is present in virtually all cell types, undergoes one entire round of its transcriptional translational feedback loop in approximately 24 hours. That is, the cell autonomous molecular time tracker has a free-running period of ~24 hours. Without a light pulse, a growth factor, feeding or starvation pulse, a temperature pulse, a hypoxic pulse, an acidic pulse, or pressure loading, the molecular clock maintains its 24-hour periodicity (Adamovich, et al., 2016; Ranieri, et al., 2015; Rensing and Ruoff, 2002; Walton, et al., 2018). This periodicity fluctuates slightly from organism to organism with some being sub 24 and some being supra 24 hours, but this usually does not vary by more than 60 minutes. This truly highlights the biology of Earth, and that this particular pervasive mechanism ceases its utility on another planet or in a different solar system.

Because of the Earth's axis, some areas on Earth lack the typical equatorial day and night. For instance, the Scandinavian peninsula, near the North Pole, has periods of the year in which the day is shrouded in perpetual darkness and other periods of the year in which blackout curtains are necessary for a decent night's sleep. Considering that the climate gets harsher and more extreme towards the poles of the Earth, it is reasonable to presume that the circadian molecular clock evolved from beings living in the more constant, temperate environments within the vicinity of the Equator, in the tropics.

This wieldy 24-clock makes itself readily apparent in instances of daylight savings time in which the change of just one hour markedly induces physiological changes in the human (Manfredini, et al., 2019; Roenneberg, et al., 2019). What's more, humans voluntarily undergo jetlag when they fly from one region of the Earth to another. Moreover, humans (who are a diurnal species) suffer, physiologically speaking, when undertaking a shift-work occupation to make a living (Esquirol, et al., 2009; Karlsson, et al., 2009; Ramin,

et al., 2015). Interestingly, these several phenomena described here most likely would never apply to any other animal, but only happens to humans due to our artificial means of living with airplanes and lightbulbs. This undoubtedly highlights the discordance between the industrialized society we know today and the unfathomable age of the Earth that has been undergoing its 24-hour day, day-in and day-out, for its existence. Thus, approximately 2 centuries' worth of man-made upending to this Earthly day and night rhythm would certainly and unmistakably lead to deleteriously existential outcomes, namely health consequences (Karlsson, et al., 2001; Zimmet, et al., 2019).

The circadian clock accomplishes and executes its functions day after day with almost certainty. We may not know if tomorrow will come but our circadian clock anticipates it to be so, and thus rolls on, cycle after cycle. This is orchestrated by a series of transcriptional and translational events, as well as posttranslational and epigenetic events, as well as localization/location/geography of the cell. Beautiful strides in circadian research have been made for some decades, but many advances have seen their glory since the nineties to the present. Much of this has culminated to the coveted Nobel Prize in Medicine and Physiology to three extraordinary circadian science researchers. As of the writing of this dissertation there is yet to be discovered the true reason for why humans need sleep. The actual identities of molecules that build up to cause sleep pressure are still waiting to be uncovered and fully defined. Some even speculate that another Nobel Prize stands to be won for the true meaning and understanding of human sleep. It is important to note that sleep and wake activities constitute a type of circadian rhythm, but circadian rhythm itself describes any natural processes that follow a cyclical pattern of behavior, activity, expression, etc., that occur on "about-a-day's" time, or from Latin, "*circa dia*." Although circadian rhythm and sleep are closely related, they are different entities. It

is worth saying, however, that if a human suffers from a sleep disorder, such as insomnia or sleep apnea, they are intrinsically going to disrupt their circadian rhythm as well. This could lead to other downstream maladies pertaining to processes (*e.g.*, metabolism) that would rather rely on a robust behavioral circadian pattern than a disrupted, disjointed one.

For example, the thyroid is a target of disrupted circadian rhythm, since the thyroid-stimulating hormone (TSH) is secreted from the pituitary gland in a circadian manner to ultimately stimulate the production of hormones thyroxine (T4) and triiodothyronine (T3) (Brabant, et al., 1990; Ikegami, et al., 2019; Konlouri, et al., 2013; Leso, et al., 2020). In an experiment in which healthy human subjects were directed to sleep only 4 hours per night for 6 night to simulate an accumulation of sleep debt, the authors found that the plasma of these subjects at the end of the experiment had no rhythmic production of thyrotropin (upstream of TSH) and strikingly that T4 was strongly elevated at all times of the day compared to normal sleep conditions (Spiegel, et al., 1999). The increase in thyroid hormones was also corroborated by an analysis showing that nightshift workers had markedly high levels of circulating TSH (Leso, et al., 2020). In addition, at the cellular level, T3 is required for the function of brown adipose tissue and temperature regulation, which is a circadian-governed process (Giralt, et al., 1990; Hernández & Obregón, 2000; Obregón, et al., 1987, 2008; Wyatt, et al., 1999). T3, retinoic acid, transferrin, and insulin are some constituents of serum-free cell culture media necessary to maintain mesenchymal cell viability. Interestingly, T3 hormones also interact with retinoic acid binding proteins, which have opposing dual roles in adipocyte differentiation whereby T3 promotes chromatin re-ordering for mesenchymal stem cell differentiation, but once the cell is committed to an adipocyte lineage, T3 is involved in repression of several genes (Wei, 2012). Coincidentally, the promoter region for the cellular retinoic acid binding

protein (CRABPI) has a dihydrosphingosine- and ethanol-responsive promoter (Wei, 2012). This is important because the circadian clock mechanism is composed of the retinoic acid-related orphan receptors, RORs and REVERBs, which could have potential interplay in this context of ligand binding.

On the other hand, circadian rhythm disorders, which, in humans, have been linked genetically to the *Per*s and casein kinases, seem to elicit, quite predominantly, disordered sleep phenotypes, such as advanced sleep phase syndrome (Parsons, et al., 2014; Toh, et al., 2001; Xu, et al., 2005; Xu, et al., 2007). Thus, it may seem semantical and overly nuanced to dissociate and define the uniqueness of circadian rhythm and sleep/wake cycles, but the distinction is valid and important. When speaking about circadian rhythm at large, it usually is quite rare that the same circadian researcher is also an expert in the five human electroencephalographic wave patterns of human sleep in the brain.

With regard to the circadian clock, the systems are essentially mirror images of one another, but from kingdom to kingdom, the proteins and genes are named differently. The system studied for the work herein was the mouse circadian clock in the white adipose tissue. Thus, implications for human disease and other outcomes are speculative. Regardless, work from animal (mouse) studies, such as these, provide insight and targets for future work.

1.5.iii. Circadian Protein Dynamics

Nuclear import and export are also essential functions of the molecular clock, and these would appear to be implicated in LINC-associated biological processes. One group of authors studied the interaction of BMAL1:CLOCK heterodimer with ribonucleic acid export 1 (RAE1) and nucleoporin protein NUP98, of the nucleoporin complex and mRNA export machinery (Zheng, et al., 2019). Knockdown of RAE1 results in the increase of BMAL1 and CLOCK expression, due to decreased ubiquitination, with concomitant increased transcriptional luciferase reporter activity from *Per* and *Cry* loci (Figure 2). RAE1 promotes BMAL1 shuttling and regulates degradation and activity of CLOCK:BMAL1 heterodimer. While the BMAL1 and CLOCK expression were high in RAE1 knockdown conditions, PER2 and CRY1 proteins failed to reach control amplitudes in expression; in other words, the protein expression was rather low in the knockdown cells compared to control. The ultimate conclusion from this study was that the shuttling of the BMAL1:CLOCK heterodimer is much related to its activity as a transcription factor and to its protein stability (Zheng, et al., 2019). It seems when nuclear shuttling is disrupted, there is an increase in the positive limb proteins, but this does not necessarily translate to a constitutively high output marker expression. Paradoxically, the data showed that the *Per* and *Cry* mRNA transcript expression was high, but that the protein expression was not, in the absence of RAE1 and nuclear shuttling (Zheng, et al., 2019).

The commanding work by Lee and colleagues demonstrates unintuitive and paradoxical patterns in the BMAL1 and CLOCK heterodimer, with one of the most striking being that BMAL1-mediated transcriptional activation occurs with a concomitant degradative action on BMAL1, thus especially depleting nuclear levels (Kwon, et al., 2006). Furthermore, the nuclear export and localization sequences are key for the

shuttling of BMAL1 between the nucleus and cytoplasm and for mediating CLOCK degradation. That is, if BMAL1 does not shuttle, CLOCK protein does not degrade. Overexpression of tagged BMAL1 or CLOCK resulted in the lower expression of the other (Kwon, et al., 2006). Interestingly, CLOCK overexpression partitions it to the cytoplasm in a strong manner. On the other hand, overexpression of both CLOCK and BMAL1 together abolishes the cytoplasmic expression of CLOCK (Kwon, et al., 2006). It is well-established too, that in order for the BMAL1:CLOCK transactivator to function, there must be reciprocal histone marks that promote the work of these activators in a temporal fashion (Zhu, et al., 2020; Takahashi, 2017).

BMAL1 stability is in part mediated by GSK3β phosphorylation action on Ser17 and Thr21. After phosphorylation occurs, BMAL1 is primed for ubiquitylation. It is noted that BMAL1 is a phosphoprotein targeted by various kinases (Sahar, et al., 2010).

It is important to note that posttranslational modifications have a strong impact on the transcriptional outputs of BMAL1, meaning that targets' period lengths may depend on the posttranslational modification status of BMAL1. MAPK phosphorylates BMAL1 at Ser527, Thr534, Ser599. It was found that phosphorylated MAPK is able to phosphorylate BMAL1 and affect downstream transcriptional programs, although protein dynamics regulating BMAL1 stability were not described (Sanada, et al., 2002). The sites for MAPK action are conserved among many vertebrate species for BMAL1, but these sites are <u>not</u> present in BMAL2 (Sanada, et al., 2002). Casein kinase 2α phosphorylates BMAL1 (Tamaru, et al., 2009). Tamura *et al.* showed that S90 was a necessary phosphorylation site for nuclear translocation (Tamaru, et al., 2009). CLOCK has been shown to possess histone acetyltransferase properties and can acetylate BMAL1 at a highly conserved residue, Lys537 (Hirayama, et al., 2007). Dimerization is necessary for the acetylation of

BMAL1 by CLOCK (Hirayama, et al., 2007). This acetylation in complex helps the recruitment of CRY1 to the complex (Hirayama, et al., 2007). CLOCK, and not PER or CRY, is necessary for proper BMAL1 sumoylation. Lysine 259 is the conserved residue at which sumoylation occurs (Cardone, et al., 2005).

The group of Gruissem has done stunning work in an Arabidopsis model, in which they characterize light-responsive and time-dependent gene expression and correlate this with histone posttranslational modifications (Baerenfaller, et al., 2016). For example, the genes that peaked in the end of the day also had the strongest acetylated histone signal at K9 and K27 on genes that peak at the end of the day. In accordance with high expression and high acetylation in a small subset, ChIP-sequencing across the entire genome showed the acetylation signature at histone 3 lysines 9 and 27 was strongest at loci of genes expressed highly at the end of the night when assessed at the end of the night. Moreover, the acetylation signal is absent in the respective opposite time of the day genetic loci in both cases presented here, thus showing that the acetylated histone has a positive effect on its transcriptional targets, whether they peak in the day or the night (Baerenfaller, et al., 2016). Essentially, permissive and repressive states of chromatin are governed by posttranslational modifications, and these occur with day/night rhythmicity.

The group of Naef found that distal enhancer sites and respective transcription start sites for certain genes displayed, pairwise, that H3K27ac marks oscillated at more than 1000 of these pairs, which are hypersensitive to DNAse I treatment, also suggestive that these marks would lead to transcription without latency (Sobel, et al., 2017). Moreover, the phase of H3K27ac chromatin occupancy over 24 hours was significantly correlated with the phase of RNA Polymerase II chromatin occupancy.

In an effort to dissociate diurnal feeding and fasting cycles from the circadian cycle, Sobel and coworkers also found that transcription at E-boxes was positively correlated with CREB and D-box motifs and negatively correlated with elements that bind REVERBα, RORs, SREBP, and FOX (Sobel, et al., 2017) (Figure 2). In *Bmal1*$^{-/-}$ mice, the ablated circadian rhythm, generated by BMAL1 and CLOCK, is somewhat compensated peripherally by other cues, like feeding and fasting, that impinge on regulatory elements associated with CREB, FOX, and SREBP, truly demonstrating the robust nature of nutrient-sensing and its potential to synchronize oscillating transcripts (Sobel, et al., 2017).

Using ChIP-Sequencing, Feng and colleagues showed that HDAC3 is recruited to its genetic targets in a circadian manner in a mouse liver model (Feng, et al., 2011). HDAC3 is known to be part of the REV-ERBα repressor complex, which also includes NCoR (nuclear corepressor) (Feng, et al., 2011). HDAC3 was found to be bound to chromatin strongly in the inactive period *in vivo*, at ZT10. Moreover, the acetylation signal at H3K9 was decreased comparatively to the active period. Thus, the HDAC was performing deacetylase enzymatic activity. Unintuitively, however, the genetic loci at these epigenetic occurrences were undergoing active transcription. This further affects RNA Polymerase II binding, as the HDAC3 repressor complex kicks it off. The authors go on to describe the system by pointing out that HDAC3 protein levels did not fluctuate over a circadian time course *in vivo*. What's more, NCoR, which helps to impart the repressive activities of the REV-ERBα and HDAC3 complex, also binds at its targets with diurnal rhythmicity. To conclude the study, Feng *et al.* determined a physiological role for the circadian recruitment of HDAC3 to liver transcriptomic targets. They found that the most significantly affected cellular program was lipid metabolism, and they concluded that depletion of REV-ERBα and/or HDAC3 led to a fatty liver phenotype. When qualifying

these results, it is important to remember the other isoforms of proteins involved in these complexes (Feng, et al., 2011).

Moreover, Hong and coworkers here showed the circadian occupancy of HDAC3 at circadian genes in mouse skeletal muscle (Hong, et al., 2017). Another intriguing aspect to Hong's story was that skeletal muscle-specific HDAC3-knockout mice had worse glucose utilization, were apparently insulin resistant (HOMA-IR), but they had better muscle endurance. The authors made a point to discuss this paradoxical finding and that apparent contradictions to the logically-thinking scientist do exist (Hong, et al., 2017).

1.5.iv. Concluding Remarks about Circadian Rhythm

To conclude, the molecular circadian clock is an evolutionary cycle-generator that evolved to anticipate and align biochemical/behavioral/physiological processes with the Earthly day and night (Gerhart-Hines and Lazar, 2015). Almost all cells have this autonomous ticking clock, which highlights the pervasive ubiquity of circadian rhythm (Mohawk, et al., 2012; Takahashi, 2017). Thus, cells are poised to be affected by alterations in the clock. Moreover, tissue specificity arises for circadian rhythmicity in genes, based on the nature of the organ (Qu, et al., 2018; Storch, et al., 2002; Zhang, et al., 2014). Aside from the molecular core clock (Figure 2), other aspects have circadian rhythmicity and directly contribute to top-level circadian manifestations in physiology, with some examples including: posttranslational modifications, epigenetic modifications, and temporal spatial positioning of cellular synthesis and degradation hubs (Aguilar-Arnal and Sassone-Corsi, 2015; Aviram, et al., 2016; Dyar and Eckel-Mahan, 2017; Kim, et al., 2013; Ryzhikov, et al., 2019; 2019a).

1.6. Sphingosine Kinase 1/S1P Regulation

1.6.i. S1P as an aPKC Ligand

The intracellular actions of S1P are far less understood than the paracrine/autocrine actions it exerts through its GPCRs at the cellular surface. For example, Kajimoto and colleagues demonstrated the utilization of S1P as a second messenger by atypical protein kinase C (aPKC) isoenzyme zeta within the catalytic domain to stimulate kinase activity (Kajimoto, et al., 2019). Despite the newness in this thinking, S1P is shown to act still in its canonical pro-growth (through an anti-apoptotic mechanism) manner (Kajimoto, et al., 2019).

PKC's are long known to be stimulated by calcium and diacylglycerol, a well-known second messenger (Huang, 1989). After that, the atypical PKC's were then discovered to be stimulated by phosphatidylserine (Orr and Newton, 1992). And as recently as 2019, it is now recognized that aPKC isozymes can be stimulated by S1P, a simple yet potent signaling bioactive lipid (Kajimoto, et al., 2019).

Basic residues Arg375 and Lys399 are part of the PKC substrate binding pocket, interacting with the negatively charged phosphate group in S1P; Arg375 was shown to be critical for the S1P-induced kinase action (Kajimoto, et al., 2019). Asparagine, glutamine, and valine seem to line the path touching the nonpolar part acyl chain of S1P (Kajimoto, et al., 2019). These are hydrophobic and negatively charged. Glycine and cysteine seem to react with the amino group of the S1P molecule (Kajimoto, et al., 2019). Many of these observed effects occurred in conditions of non-serum-containing media as well as micromolar concentrations of S1P, usually around 30 μM to 100 μM, which is highly unusual for the study of S1P signaling through receptors, which all have K_d's around 20 nM (Kajimoto, et al. 2019).

1.6.ii. S1P as an Enhancing Cofactor for TRAF2

Lys-63-linked polyubiquitination occurs on the protein RIP1 as a result of TNFα treatment. Typically, this particular residue linkage results in a signaling cascade associated with ubiquitination rather than the typically thought of K48-linked ubiquitin, which sends many proteins to the proteasome for degradation (Alvarez, et al., 2010).

TNFα treatment stimulates the phosphorylation of IκBα, and this is shown to be dependent on SPHK1, and it was shown in a few cells types. Moreover, TNFα treatment can stimulate the production of S1P within the cell as well as secretion into the cell culture media. A positive control used for SPHK1 activation was phorbol myristate acetate and ionomycin (Alvarez, et al., 2010). I have avoided this in my work due to the off-target effects of PMA. It tends to activate other kinases besides SPHK1. VPC23019, which antagonizes S1P receptors 1 and 3 was shown to have no effect on the phosphorylation status of IκBα when treated in conjunction with S1P, implicating that the ensuing cellular response upon S1P treatment was due to actions distinctly inside the cell. Stunningly, these effects were observed at 100 nM concentrations of S1P, which is thought to be an acceptable dosing range for extracellular receptor signaling, however, this cascade is side-stepped while S1P acts in concert with TNFα and its associated factors.

While TNFα potently phosphorylates IκBα and SPHK1 at Ser225, it does not affect ERK phosphorylation. On the other hand, S1P treatment stimulates ERK1/2 phosphorylation while failing to stimulate any IκBα phosphorylation at 100 nM. Counter to that, 10 μM, a whopping high concentration of S1P, was able to mimic the effects of TNFα (10 ng/mL) treatment. Moreover, the downstream transcription factor NFκB activity was measured through a reporter assay indicating that S1P and TNFα, when treated together and at the high concentration, markedly induce the expression of the reporter. This

solidifies a role for S1P to mediate a transcriptional program. Typical pathways stimulated by the NFκB pathway tend to steer toward survival, proliferation, lymphogenesis, and inflammation. These are all very well-accepted broad-stroke roles of S1P.

> "Molecular modeling of S1P into the RING domain of the crystal structure of TRAF2 24 revealed that it docked remarkably well in a 16 Å long binding cavity consisting of a hydrophobic region (F45, L58, A59, L62, A90, F91 and F92) and positively charged region (R43 and R97), which may stabilize the phosphate group of S1P." (Alvarez, et al., 2010)

RIP1 undergoes K-63-linked polyubiquitination to serve as part of a scaffold for signaling events at the plasma membrane transducing through second messengers to reach the IKK complex, which ultimately induces NFκB activation. RIP1 polyubiquitination was shown by Alvarez and colleagues to be dependent on S1P, when induced by the TNFα E3 ubiquitin ligase TRAF2 (TNFα receptor-associated factor) (Alvarez, et al., 2010). Moreover, they demonstrated that TRAF2 has the ability to directly bind S1P, and that TRAF2 co-immunoprecipitates with RIP1. What's more, they confirmed that this binding was specific for TRAF2, and that, remarkably, S1P could not detectably bind RIP1 *in vitro* (Alvarez, et al., 2010).

1.6.iii. S1P as a TERT Stabilizer

With regard for a noncanonical role of S1P, Ogretmen, Selvam, and coworkers show that SPHK2 is the isozyme majorly responsible for the observed effect through use of the SPHK2 inhibitor, ABC294640 in which telomerase reverse transcriptase (TERT) protein decreases within 8 hours of ABC treatment (Selvam, et al., 2015). TERT overexpression resulted in the abundant increase of ^{17}C-S1P (d17:1 sphingoid backbone) generation upon ^{17}C-sphingosine feeding. Asp684 is identified as an integral residue responsible for the interaction between S1P and TERT (Selvam, et al., 2015). They used, interestingly, a biotin-conjugated S1P to pull-down avidin, which revealed binding of TERT. Oddly, ubiquitination of TERT is stimulated upon SPHK2 inhibition with the ABC compound, thus implicating that decreasing the S1P would result in heavy ubiquitination (Selvam, et al., 2015). On the other hand, the S1P effects on TRAF2 do the opposite, in which lots of S1P around helps to ubiquitinate the target (Alvarez, et al., 2010). In the case of TERT, however, the lysine ubiquitination is K48, which leads to proteasomal degradation, whereas the TRAF2 ubiquitination cascade results in signaling scaffold maintenance and formation.

Overall, TERT stability is decreased when SPHK2 is ablated. Thus, lack of S1P is promoting ubiquitin mediated proteasome degradation. S1P saves TERT stability by decreasing binding of its respective E3 ubiquitin ligase partner MKRN1 (Selvam, et al., 2015). This is made possible by S1P binding the Asp684 residue within an TERT quadruplex of α helices, and this results in a dissociation of MKRN1 from TERT (Selvam, et al., 2015). Serines 921 and 992 also contribute to the binding of S1P within the TERT α helical loops (Selvam, et al., 2015).

1.6.iv. S1P as a Class I HDAC Inhibitor

The Spiegel lab identified SPHK2-generated S1P in the nucleus had effects on histone deacetylases 1 and 2 (HDAC) (Hait, et al., 2009). Isolated nuclei were subjected to lipidomics and indicated that overexpressed *Sphk2* resulted in significant accumulation of S1P in the nucleus. Moreover, western blotting of fractionated cells, down to the chromatin, showed that histone H3 and SPHK2 proteins resided solely in the chromatin post-nuclear fraction (Hait, et al., 2009). Moreover, histone H3 protein was found to co-immunoprecipitate with sphingosine kinase 2. The signal for H3K9 acetylation more than doubled compared to control, when cells were transfected with an overexpression vector for *Sphk2* (Hait, et al., 2009). In the converse experiment in which siRNA was utilized to knockdown each of the isozymes of SPHK, they observed a disappearance of the band for acetylated H3K9. It is important to note that acetylated histone 3 lysine residue 9 is typically associated with transcriptional activation when tested in the lab (Gates, et al., 2017; Heintzman, et al., 2007). 5-minute treatment with 1 μM S1P and dhS1P also induced the acetylation of H3K9. Although not central to their story, Hait and coworkers found that knockdown of SPHK1 significantly depleted the cytoplasmic proportion of S1P, while eliciting no effect on the nuclear content of S1P nor dhS1P. SPHK2 knockdown, on the other hand, had no effect on cytoplasmic S1P concentrations, but it did significantly decrease nuclear S1P and dhS1P signal. S1P-conjugated beads were shown to co-immunoprecipitate HDAC1 as well as HDAC2 (Hait, et al., 2009). S1P and dhS1P treatments decreased recombinant HDAC1 activity. Overexpressing SPHK2 and also overexpressing SPHK2 in the presence of PMA, an activator of SPHK, the H3K9ac pulldown yielded a strong qPCR signal at chromatin promoter loci for p21 and c-fos. P21 is important in inducing cell cycle arrest, but at the same time it inhibits apoptosis, a

function consistent with the signaling qualities of S1P (Harper, et al., 1993; Harper, et al., 1995). Moreover, *c-fos* is an early transcription gene, and it generally indicates a cell is active in its transcription, which is also supported by the pro-mitogenicity of S1P (Hait, et al., 2009; Morgan and Curran, 1989).

1.6.v. Overall Remarks about S1P

Overall, the work of Hait, Alvarez, Selvam, and Kajimoto have propelled S1P into the intracellular signaling space intellectually, through mechanisms not heretofore described in the more typical extracellular signaling mode that many understand (via the 5 S1P GPCRs). From Alvarez and coworkers, we do not find whether SPHK1 or SPHK2 specifically contributes to the effects elicited by S1P, but nevertheless, the effects are strikingly differential and particular compared to Shan's work in the Ogretmen lab (Selvam, et al., 2015). Alvarez found that S1P binds cytosolic TRAF2, an E3 ubiquitin ligase, to promote its polyubiquitin chain-making on RIP1, an important scaffolding protein in IKK and NFκB signaling and transcription mediation (Alvarez, et al., 2010). Interestingly, this ubiquitin modification on K63 does not promote proteasomal degradation, but it promotes the formation of the signaling scaffold to transduce signals from the TNFα receptor and TRAF2 through to the IKK complex (Alvarez, et al., 2010). In a different context, Ogretmen's group showed that S1P promoted TERT stability in the nucleus, by binding within its α helices to disrupt TERT's cognate E3 ubiquitin ligase, MKRN1, to thus prevent K48 polyubiquitination and subsequent proteasomal degradation (Selvam, et al., 2015). Interestingly, S1P acts to promote one E3 Ub ligase and in the other case acts to disrupt an E3 Ub ligase. Despite this, the target proteins in both cases remain more stable. Moreover, S1P directly binds TRAF2 E3 ubiquitin ligase in the cytosol, while S1P directly binds the ligase's target, TERT in the nucleus. For the TRAF2 binding in the cytoplasm, an arginine residue was essential for grabbing the phosphate on the S1P molecule to obtain ligase activity (Alvarez, et al., 2010). Serine was also noted to be essential in stabilizing the negatively charged phosphate of S1P in this pocket (Alvarez, et al., 2010).

Leucine and phenylalanine residues also line the TRAF2 RING domain pocket with contacts in the nonpolar sphingoid backbone of S1P (Alvarez, et al. 2010).

1.6.vi. New Roles for Nuclear S1P

Seo and coworkers demonstrated a role for sphingosine kinase 1 inside the cell at the level of nuclear viral replication and nuclear export within a host. It was found that viral infection induces the expression of SPHK1 protein as well as its phosphorylated form within 24 hours. Inhibition of SPHK1 with SKI-II dose-dependently reduces the viral titer in human lung cells (Seo, et al., 2013). Inhibition with the same drug similarly decreased the expression of several viral proteins, such as matrix, nonstructural, and nucleoprotein. Phospho p65 signal is weakened post viral infection in the presence of SKI-II compared to control, which indicated that components of the NFκB pathway, stimulated by viral infection, lose their signaling capacity in the absence of SPHK1 action (Seo, et al., 2013). Dimethylsphingosine, as a sphingosine kinase 1 inhibitor, was used in the presence of influenza infection to block phosphorylation of RanBP3, which is critical for the transport of the viral particles out of the nucleus (Lindsay, et al., 2001). ERK and AKT inhibitors were shown to decrease phosphorylation of the same during conditions of flu infection (Seo, et al., 2013). These results were recapitulated with SKI-II on pAKT and pERK, and pRanBP3, all showing less phosphorylation (Seo, et al., 2013). This study did not differentiate between the two kinases except in the beginning in which they specifically used siRNA against *Sphk1* to show dependent decreases in viral protein expression. None of the experiments showed the converse, in which exogenous S1P treatment was utilized or overexpression constructs or pharmacological upregulation of the kinase. Seo and colleagues showed in an earlier study that exogenously applied S1P did not affect flu replication (Seo, et al., 2010). SKI-II seemed to have more potent suppressive effects on viral proteins than did SK1-I. Moreover, SKI-II specifically decreased the cytosolic viral

protein, but not the nuclear viral protein. They quantified this by relative cytosolic to nuclear expression of viral nucleoprotein (Seo, et al., 2013).

In another interesting work, Hait and colleagues demonstrate a role for SPHK2-derived S1P as a positive modulator of HIF1α (Hait, et al., 2020). Strikingly, they suggest and show that S1P has the ability to bind HIF1α within its PAS B pocket (Hait, et al., 2020). What is even more curious is that HIF1α belongs to the same group of basic helix-loop-helix transcriptions as BMAL1, CLOCK, and the PERIOD proteins, to name some. Moreover, three separate works described roles for crosstalk of hypoxia and the clock (Adamovich, et al., 2016; Peek, et al., 2017; Wu, et al., 2017).

Measurements of sphingolipids in epithelial cells show that sphingosine, dihydrosphingosine, and ceramide are present in both the cytoplasm and nucleus, with a greater constituent present in the nucleus (Fu, et al., 2018). Meanwhile, S1P is also detectable in both cell fractions, but both pools are at equal concentrations, thus begging the question as to how nuclear S1P, confined to such a smaller space, is affecting nuclear programs in the cell. The Pynes and their coworkers demonstrated a role for SPHK1 and S1P localized at the nucleus as a biomarker of survivability in breast cancer (Ohotski, et al., 2013). Importantly, only sphingosine kinase 1 can utilize dihydrosphingosine to make dihydrosphingosine-1-phosphate, and only sphingosine kinase 2 can utilize FTY-720 to generate phosphorylated FTY-720 (Fu, et al., 2018).

CHAPTER 2

SPHINGOLIPIDS IN ADIPOSE TISSUE: WHAT'S TIPPING THE SCALE?

(ANDERSON*, Lambert*, Cowart, 2018)

Review Manuscript

*(*co-first-authorship)*

2.1. Introduction

2.1.i. Sphingolipids are Bioactive Lipids Linked to Obesity

In addition to their roles as structural membrane components, sphingolipids including ceramides and sphingosine-1-phosphate (S1P), regulate many signaling pathways related to the development of obesity and the metabolic syndrome. The aberrant production of these bioactive lipids has been linked to insulin resistance andβ-cell dysfunction, low grade inflammation, ectopic lipid deposition, cardiovascular disease and non-alcoholic fatty liver disease (NAFLD) (Cantrell Stanford, et al., 2012; Meikle and Summers, 2017; Montefusco, et al., 2018). In addition to potential intracellular mechanistic roles played by sphingolipids in these processes, obesity is associated with elevated circulating levels of several sphingolipid species in rodents and humans (Blachnio-Zabielska, et al., 2012a; Samad, et al., 2006). Therefore, many mouse models have been developed to target distinct aspects of the sphingolipid metabolic pathway and these have revealed various roles of sphingolipids in obesity-associated disease processes (Table 1). As much of the pathophysiology associated with obesity may arise from adipose tissue dysfunction, mechanisms for sphingolipids in adipose tissue homeostasis is a growing focus of sphingolipid research in the context of obesity and related pathology. This review will focus on the current understanding of sphingolipids in adipose tissue.

Table 1. Sphingolipid knockout models and adipose tissue phenotypes.

Mouse Strain	Adipose Tissue Phenotype	References
Adipocyte-specific deletion of *Sptlc1*	-Reduced adipose tissue -Increased pro-inflammatory gene expression -Increased adipocyte size -Increased fibrosis -Increased cell death	(Alexaki, et al., 2017)
Adipocyte-specific deletion of *Sptlc2*	-Reduced WAT and BAT -Smaller adipocytes -Increased expression of thermogenic genes in WAT -Increased browning of WAT -Reduced adipogenic and lipolytic gene expression in BAT -Increased lipid oxidation -Increased adipose inflammation	(Chaurasia, et al., 2016a; Lee, et al., 2017)
Myeloid deletion of *Sptlc2*	-No effect on HFD induced adipose inflammation, IR	(Camell, et al., 2015)
Inducible acid ceramidase overexpression in adipose tissue	-Redistribution of adipose tissue on HFD (more gonadal, less mesenteric adipose tissue) -Reduced fibrosis -Reduced immune cell infiltration/pro-inflammatory gene expression -Increased glucose uptake	(Xia, et al., 2015)
Constitutive *Cers2* haploinsufficiency	-Increased adiposity	(Raichur, et al., 2014)
Constitutive *Cers5* knockout	-Reduced adipose tissue mass on HFD -Protection from hypertrophy on HFD -Protection from insulin resistance -Reduced pro-inflammatory cytokines -Up-regulation of both lipolytic and lipogenic genes	(Gosejacob, et al., 2016)

Constitutive *Cers6* knockout	-Reduced adiposity -Reduced adipocyte size -Reduced adipose inflammatory markers -Reduced BAT lipid droplet size	(Turpin, et al., 2014)
Brown adipose tissue-specific *Cers6* knockout	-Reduced adiposity -Reduced energy expenditure	(Turpin, et al., 2014)
Constitutive *Sphk1* knockout	-Reduced adipose inflammation -Increased adipose tissue mass -Decreased adipocyte size -Enhanced insulin signaling	(Ross, et al., 2013; Wang, et al., 2014)
Constitutive S1P lyase knockout	-Reduced adipose tissue mass	(Bektas, et al., 2010)
Constitutive sphingomyelin synthase 1 knockout	-Reduced adipose tissue mass with age -Reduced adipocyte size -Increased oxidative stress	(Yano, et al., 2013)
Constitutive sphingomyelin synthase 2 knockout	-Reduced adipose tissue mass on HFD -Protection from PPARγ and CD36 increase on HFD	(Mitsutake, et al., 2011)
GM3 synthase knockout	-Reduced gWAT and sWAT mass on control diet -Reduced Mesenteric and subcutaneous adipose tissue mass on HFD -Reduced TNFα on HFD -Increased IL-10 and Adiponectin on HFD	(Nagafuku, et al., 2015)

Table 1. Sphingolipid knockout models and adipose tissue phenotypes. (Lambert, J.M., Anderson, A.K., Cowart, L.A. (2018) Sphingolipids in Adipose Tissue: What's Tipping the Scale? Advances in Biological Regulation 70: 19-30.)

2.1.ii. Adipose Tissue Biology

Adipose tissue is in constant metabolic flux as it must respond to ever-changing energy requirements. It is distributed throughout the body in distinct depots, which vary in size, function, and gene/protein expression. The primary function of adipose tissue is storage of energy as triglyceride, which is regulated by triacylglycerol anabolic and catabolic pathways, lipogenesis and lipolysis, respectively. Adipose tissue also serves as an endocrine organ via the secretion of many hormones and cytokines, also referred to as adipokines. Adipokines elicit a multitude of effects on the adipose tissue itself and also overall metabolic physiology by direct and indirect mechanisms. Two major adipokines include adiponectin, which mediates glucose homeostasis and fatty acid catabolism, and leptin, which regulates satiety. Altered levels of adipokines including these are implicated in many disease states, including obesity (Sulaieva, et al., 2018). Additionally, the thermogenic function of adipose tissue has emerged as a topic of major interest in recent years. Brown and beige adipocytes are rich in mitochondria and Uncoupling Protein 1, which allows for generation of heat. Activation of brown adipose tissue in rodents garners protection from obesity by increasing energy expenditure, though whether this is paradigmatically similar in adult humans remains controversial. Thus, a focus on conversion of white adipocytes to oxidative brown adipocytes has been an attractive area of therapeutic interest (Cannon and Nedergaard, 2004). While most of the mass of the tissue comes from the adipocytes, a variety of other cell types are present including stem cells, preadipocytes, vascular endothelial cells and immune cells. However, adipose tissue mass is modulated primarily at the level of the adipocyte largely through either hyperplasia or hypertrophy, as well as cell death. For example, both white and brown adipocytes are generated via hyperplasia, where stem cells residing in the adipose tissue undergo

differentiation. This is referred to as adipogenesis. Impairments in this process are thought to compromise adipose tissue function and contribute to obesity-related pathologies. In contrast, adipocyte hypertrophy occurs under conditions that necessitate the existing adipocytes to take on a larger lipid load, including impaired adipogenesis and diet induced obesity. Moreover, mounting evidence suggests that adipogenesis/hyperplasia maybe beneficial; adipose tissue expansion by hypertrophy is in fact deleterious, as it promotes adipose tissue inflammation and adipocyte cell death. Importantly, sphingolipids have been implicated in many of these diverse processes and functions of adipose tissue (Berry, et al., 2016; Rosen and Spiegelman, 2014; Tang and Lane, 2012).

2.2. Sphingolipid Synthesis and Metabolism

Discovered at the turn of the twentieth century, sphingolipids were an “enigma” just like the Greek sphinx, as neurochemist Thudichum, who first described them, opined. Some of the first sphingolipids discovered were in the brain, thus giving rise to such names as sphingomyelin and cerebrosides (Merrill, et al., 1997). Even so, it is now appreciated that sphingolipids are ubiquitous in eukaryotic cells as critical components of cell membranes (Levy and Futerman, 2010; Pruett, et al., 2008). Although their role is long-established as structural membrane lipids, research from the late 1980's and 1990's provided unequivocal evidence that they function as vital signaling molecules (Hannun, 1996). This notion also gains support from studies that demonstrate mice lacking certain enzymes in the sphingolipid biosynthesis pathway die *in utero* (Hojjati, et al., 2005; Ishii, et al., 2002; Li, et al., 2002; Liu, et al., 2000; Yamashita, et al., 2002). Sphingolipids are defined by the sphingosine backbone, a long chain amino alcohol. *De novo* synthesis in the cytoplasmic face of the endoplasmic reticulum (ER) begins with the condensation of a saturated fatty acid (usually palmitate) and serine (Figure 3). This is catalyzed by the sphingolipid biosynthetic rate-limiting enzyme, serine palmitoyltransferase (SPT), to form 3-ketosphinganine. Next, 3-ketosphinganine is reduced to dihydrosphingosine by the action of 3-ketosphinganine reductase. A fatty acyl group is then added to dihydrosphingosine to form dihydroceramide through the actions of 1 of 6 (dihydro)ceramide synthase enzymes (dhCERS1-6). This fatty acyl group can vary in chain length, and this is dictated by the specificity of certain CERS isoforms for the utilization of particular acyl CoA species. Dihydroceramide is then desaturated to form ceramide. From this point, ceramide can be interconverted into a number of different metabolites, including sphingomyelin, ceramide-1-phosphate, glucosylceramide,

galactosylceramide, and sphingosine. Indeed, ceramide can be reformed through recycling by re-acylation of sphingosine or breakdown of sphingomyelin. Sphingosine can then be phosphorylated by either isoform of sphingosine kinase (SPHK1, 2) to form S1P, which is the final step in the biosynthetic pathway before exiting via the S1P lyase as hexadecenal and phosphoethanolamine, which may be used for the synthesis of glycerophospholipids. Importantly, while ceramides and S1P are the subject of most studies addressing sphingolipid signaling, the “complex sphingolipids,” *e.g.*, sphingomyelin, glucosylceramides, and their derivatives are orders of magnitude more abundant.

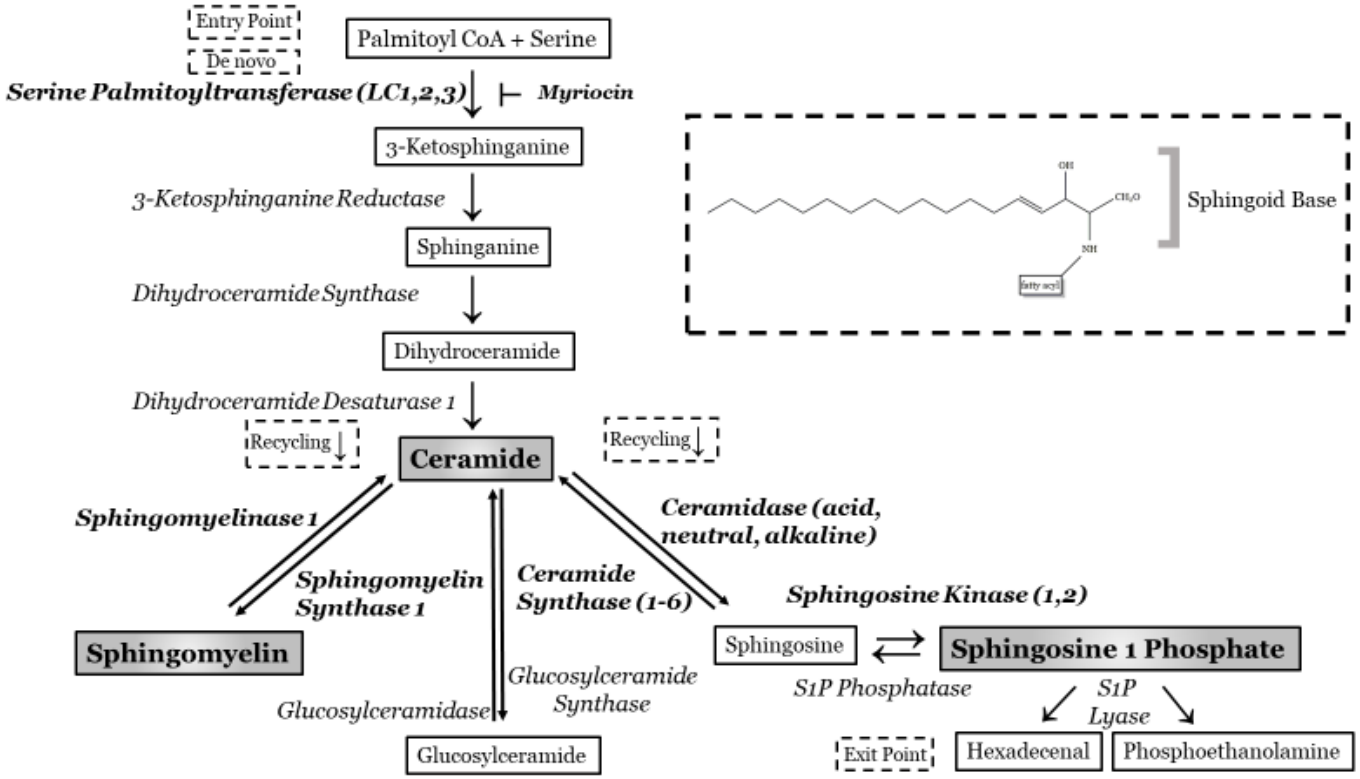

Figure 3. Sphingolipid biosynthesis pathway.

(Lambert, J.M., Anderson, A.K., Cowart, L.A. (2018) Sphingolipids in Adipose Tissue: What's Tipping the Scale? Advances in Biological Regulation 70: 19-30.)

LC, long chain.

While ceramides are synthesized *de novo* largely in the ER, they are also generated by hydrolysis of sphingomyelin (mediated by sphingomyelinase). Furthermore, ceramides undergo catabolism in lysosomes by acid ceramidase. This not only produces sphingosine, the key substrate for sphingosine kinases (discussed below) but allows generation of ceramides via what is termed the “salvage” pathway in which ceramide is hydrolyzed and the resulting sphingosine is re-acylated back to ceramide. This process, which seems to serve fundamental roles in remodeling the acyl chain composition of the intracellular ceramide pool, is localized to the late endosome or lysosome (Levy and Futerman, 2010). While S1P is a key signaling molecule, its modes of biosynthesis, degradation, and signaling are paradigmatically distinct from those of ceramide. Sphingosine kinases occur as two isoforms, Sphingosine Kinases 1 and 2. (SPHK1 and 2, respectively). These enzymes have numerous locations. They are cytosolic but can translocate to the plasma membrane upon phosphorylation. The isoforms share partially distinct intracellular localization, as SPHK2 has been found in the nucleus, and SPHK1 may be found in the ER (Pitson, et al., 2005; Siow, et al., 2011; Wattenberg, 2010). S1P is generated at the plasma membrane through the hydrolysis of ceramide, generating sphingosine, the substrate for SPHK. Phosphorylation of sphingosine yields S1P, which signals in part through one of its five G-protein coupled receptors. Export of S1P occurs via transporters such as SPNS2 and ABC transporters and enables paracrine and endocrine signaling. While export of S1P may also be required for autocrine S1P signaling, structural information on the S1P receptor suggests that S1P formed at the plasma membrane might undergo lateral diffusion through membrane lipid to bind the receptor, whose active site is accessible to the plasma membrane bilayer (Donoviel, et al., 2015; Fukuhara, et al., 2012; Hisano, et al., 2011; Parrill, et al., 2012; Pyne and Pyne, 2017;

Takabe, et al., 2008; van Meer, et al., 2006; Yamada, et al., 2018). There are reports that S1P receptors are internalized through endocytic vesicles and can thus be found intracellularly. However, it is not known whether signaling occurs through these endocytic S1P receptors (Spiegel and Milstien, 2003). Mounting evidence suggests that S1P originating from a certain cell type or from within or outside the cell may have differential signaling capacities. Thus, more work is needed to delineate the roles of S1P in specific cell types, but also to assess the downstream effects on paracrine/endocrine effector cells.

The balance among sphingomyelin, ceramide, and S1P is mediated by the action of sphingomyelin synthase/sphingomyelinase, ceramide synthases/ceramidases as well as SPHKs, the S1P lyase, and the S1P phosphatase. Extracellular stimuli cause dynamic flux between these pools and therefore sphingolipids comprise a “rheostat,” where ceramide levels promote differentiation, senescence, autophagy, and apoptosis, while its downstream metabolite, S1P tends to promote cell division and migration. Therefore, cells, by modification of sphingolipid metabolism, drastically alter their processes. Accordingly, the careful and intricate balance of these metabolites is critical for cell homeostasis and function. Interconversion between these distinct lipid species is orchestrated not just by transcriptional regulation of the anabolic or catabolic processes, but also in some cases by the availability of substrate (Johnson, et al., 2002; Lee, et al., 2008; Pitson, 2011; Ross, et al., 2013).

The sphingolipid pathway is highly relevant in the context of metabolic disease, because it is known to be driven at least in part by the oversupply of saturated fatty acids (required for *de novo* biosynthesis), as occurs in dyslipidemia associated with obesity. Although the adipocyte is specialized to store large quantities of lipid, there comes a tipping point at which lipids can no longer be transported into the adipocyte, and they

consequently spill out into circulation for deposition in peripheral tissues not equipped to take on such a burden. Ectopic lipid deposition indeed is another hallmark of obesity and is one of the theorized causes for the downstream pathologies associated with obesity and the metabolic syndrome (Kraegen, et al., 2001; Ross, et al., 2014). For example, in skeletal muscle and liver, ceramides have been implicated in insulin resistance of these tissues. This process, which is often referred to under the general term “lipotoxicity,” ensues as hepatic steatosis develops, pancreatic β-cells die, skeletal muscle becomes insulin resistant, and atherosclerosis is instigated. Sphingolipids play major roles in the etiologies of these pathologies. Only recently, studies have begun to address the potential impact of sphingolipids on the biology of the adipocyte in order to comprehend the underlying causes of obesity and the metabolic syndrome.

2.3. Sphingolipids in Adipogenesis

While excess adipose tissue is generally recognized as deleterious to health, expansion of adipose tissue is necessary for storage of lipids and is therefore critical to health. In this regard, subcutaneous adipose tissue expansion is understood to be more metabolically favorable than expansion of the visceral/abdominal depots (mesenteric/epididymal depots in rodents). Additionally, as mentioned above, expansion of adipose tissue mass is most healthfully accomplished via adipocyte hyperplasia, which occurs through adipo-genesis. This process is mediated by a tightly regulated transcription factor cascade in which stem cells undergo a metabolic and structural transformation into lipid droplet-containing adipocytes. It is often described in two phases. First, stem cells become preadipocytes committed to the adipocyte lineage defined by expression of preadipocyte factor 1 (PREF1) and C/EBPs, then undergo maturation, which is marked by extracellular matrix remodeling, unilocular lipid droplet formation, and expression of peroxisome proliferator-activated receptor gamma (PPARγ), adiponectin, fatty acid binding protein 4 (FABP4), leptin, and others (Cawthorn, et al., 2012; Hudak and Sul, 2013; Tang and Lane, 2012). Evidence for a role of sphingolipids in this process is emerging, including from studies demonstrating that several mouse models targeting sphingolipid genes display phenotypes involving impaired adipogenesis (Table 1).

Table 1. Sphingolipid knockout models and adipose tissue phenotypes.

Mouse Strain	Adipose Tissue Phenotype	References
Adipocyte-specific deletion of *Sptlc1*	-Reduced adipose tissue -increased pro-inflammatory gene expression -increased adipocyte size -Increased fibrosis -increased cell death	(Alexaki, et al., 2017)
Adipocyte-specific deletion of *Sptlc2*	-Reduced WAT and BAT -Smaller adipocytes -Increased expression of thermogenic genes in WAT -Increased browning of WAT -Reduced adipogenic and lipolytic gene expression in BAT -Increased lipid oxidation -Increased adipose inflammation	(Chaurasia, et al., 2016a; Lee, et al., 2017)
Myeloid deletion of *Sptlc2*	-No effect on HFD induced adipose inflammation, IR	(Camell, et al., 2015)
Inducible acid ceramidase overexpression in adipose tissue	-Redistribution of adipose tissue on HFD (more gonadal, less mesenteric adipose tissue) -Reduced fibrosis -Reduced immune cell infiltration/pro-inflammatory gene expression -increased glucose uptake	(Xia, et al., 2015)
Constitutive *Cers2* haploinsufficiency	-Increased adiposity	(Raichur, et al., 2014)
Constitutive *Cers5* knockout	-Reduced adipose tissue mass on HFD -Protection from hypertrophy on HFD -Protection from insulin resistance -Reduced pro-inflammatory cytokines - Up-regulation of both lipolytic and lipogenic genes	(Gosejacob, et al., 2016)

Constitutive *Cers6* knockout	-Reduced adiposity -Reduced adipocyte size -Reduced adipose inflammatory markers -Reduced BAT lipid droplet size	(Turpin, et al., 2014)
Brown adipose tissue-specific *Cers6* knockout	-Reduced adiposity -Reduced energy expenditure	(Turpin, et al., 2014)
Constitutive *Sphk1* knockout	-Reduced adipose inflammation -Increased adipose tissue mass -Decreased adipocyte size -Enhanced insulin signaling	(Ross, et al., 2013; Wang, et al., 2014)
Constitutive S1P lyase knockout	-Reduced adipose tissue mass	(Bektas, et al., 2010)
Constitutive sphingomyelin synthase 1 knockout	-Reduced adipose tissue mass with age -Reduced adipocyte size -Increased oxidative stress	(Yano, et al., 2013)
Constitutive sphingomyelin synthase 2 knockout	-Reduced adipose tissue mass on HFD -Protection from PPARγ and CD36 increase on HFD	(Mitsutake, et al., 2011)
GM3 synthase knockout	-Reduced gWAT and sWAT mass on control diet -Reduced Mesenteric and subcutaneous adipose tissue mass on HFD -Reduced TNFα on HFD -Increased IL-10 and Adiponectin on HFD	(Nagafuku, et al., 2015)

Table 1 (*reprinted*). Sphingolipid knockout models and their adipose tissue phenotypes. (Lambert, J.M., Anderson, A.K., Cowart, L.A. (2018) Sphingolipids in Adipose Tissue: What's Tipping the Scale? Advances in Biological Regulation 70: 19-30.)

Sphingolipid delta (4)-desaturase (DEGS1) catalyzes the final step in the *de novo* synthesis of ceramides and is decreased in obesity. This leads to accumulation of ceramide precursors, the dihydroceramides. While ceramides per se are a focus of abundant research, few specific roles for the dihydroceramides have been discovered. Interestingly, however, pharmacological inhibition of DEGS1 in both mice and 3T3-L1 preadipocytes and genetic knockdown *in vitro* impaired both adipogenesis and lipogenesis. Similarly, treatment of 3T3-L1 cells with dihydroceramide, concomitant with the induction of adipogenesis led to impaired differentiation and reduced expression of PPARγ, the master regulator of adipogenesis. Cells with depletion of DEGS1 via siRNA-mediated knockdown, maintained high levels of mRNA encoding PREF1, a preadipocyte marker, suggesting they do not leave the preadipocyte stage. These findings suggest that conversion of dihydroceramide to ceramide may be important during early events of adipogenesis (Barbarroja, et al., 2014).

Sphingolipid biosynthesis is initiated by a multimeric enzyme, serine palmitoyltransferase, of which the catalytic subunit is SPTLC1. Deletion of *Sptlc1* specifically in adipose tissue in mice led to cell death. These mice showed normal development of adipose tissue early in life, but increased cell death and inflammation as they aged (Alexaki, et al., 2017). Similar results were observed in constitutive knockout of sphingomyelin synthase 1 (SMS1) (Yano, et al., 2013), which generates sphingomyelin and thus reduces intracellular ceramide via the consumption of ceramide as substrate. Because SMS1 and DEGS1 decrease versus increase ceramide, respectively, the similarity in phenotypes that were observed may arise not from absolute ceramide content but rather alterations in the ratio between ceramides and precursors or downstream metabolites. Or other metabolites altogether may underlie these phenotypes. For

example, mice bearing adipocyte-specific deletion of *Sptlc2* demonstrated significantly reduced adipose tissue mass and also hepatic steatosis. Coinciding with this, alterations in the expression of genes involved in adipogenesis (*Pparγ*, *Fabp4*, *Cebpα*, and *Srebp1c*) were observed concomitant with reduced S1P and S1PR1 in the *Sptlc2* knockout (Lee, et al., 2017).

S1P has been shown to be both pro- (Hashimoto, et al., 2009; Mastrandrea, 2013) and anti-adipogenic (Hashimoto, et al., 2015; Jeong, et al., 2015). Constitutive deletion of SPHK1 led to increased adipose tissue mass and a corresponding increased expression of pro-adipogenic genes upon high fat feeding. Strikingly, despite increased adiposity, these mice were metabolically healthy, suggesting that SPHK1 deletion encouraged adipose tissue expansion. FTY720, a structural analog of sphingosine, acts as a functional antagonist of S1PR1 when phosphorylated by causing internalization of the receptor. Treatment of 3T3-L1 cells with phosphorylated FTY720 decreased adipogenesis. Additionally, FTY720 injection of mice on a high fat diet reduced adiposity (Moon et al., 2012). Though more information on mechanisms will be important, ceramide, sphingosine and SPHK levels decrease throughout adipogenesis and inversely correlate with lipid droplet content (Choi, et al., 2011; Mastrandrea, 2013). This suggests that their down-regulation may be important for adipocyte maturation.

While ceramides and S1P have received by far the most attention, data show that GM3 ganglioside is the most abundant ganglioside in adipose tissue and is elevated in adipose tissue from obese mice. Tissue GM3 may not arise from adipocytes, per se, as adipose tissue macrophages produce sphingolipids such as GM3, and macrophage depletion improved adipogenesis *in vitro* in mesenteric stromal vascular cells. Constitutive knockout of GM3 synthase also improved adipogenesis of mouse embryonic fibroblasts

(MEFs). Consistent with this, GM3 knockout mice displayed reduced epididymal and subcutaneous adipose tissue mass on a standard chow diet, and decreased mesenteric and subcutaneous adipose tissue mass, combined with less inflammation, on a high fat diet (Nagafuku, et al., 2015). Similarly, pharmacological inhibition of glycosphingolipid synthesis by treatment with N-(5-adamantane-1-yl-methoxy)-pentyl-1-deoxynojirimycin (AMP-DNM) improved adipogenesis, leading to metabolically healthy adipose tissue expansion in mice fed a high fat diet (van Eijk, et al., 2009). These findings provide a hint that pharmacological targeting of these pathways may eventually serve as a therapeutic strategy.

An important caveat to these experimental approaches is that manipulation of anabolic and/or catabolic pathways through genetic or pharmacological means affects metabolite pools both upstream and downstream of the intended target. Therefore, it is important to interpret data keeping in mind these potential mechanisms. However, from these studies it is clear that disrupting the sphingolipid balance has a negative impact on adipogenesis. More research will be required to understand the mechanistic basis for changes in these genes, enzymes, and subsequently their metabolites in pathological contexts.

2.4. Sphingolipids in Adipocyte Metabolism

Depending on the needs of the animal, adipocyte metabolism switches between lipolysis and lipogenesis, which are opposing metabolic processes. This ability to switch requires coordination of the regulation of many players in these molecular pathways. The adipocyte must properly coordinate these pathways to adapt to the differing energy demands and caloric consumption of sleeping and waking phases in diurnal animals. Sleeping necessitates adipocyte lipolysis, in which lipid droplet neutral triglycerides are catabolized to their constituents, fatty acid and glycerol, by a series of sequential enzymes that are tightly regulated and specific for triacylglycerol, diacylglycerol, monoacylglycerol (TAG, DAG, and MAG respectively). Lipolysis tends to increase when the activity of AMPK increases (Daval, et al., 2006). Moreover, when AMPK is activated, this generally lowers glucose concentration in the circulation (Jordan and Lamia, 2014).

In the fed state, energy storage is the metabolic priority. This occurs via lipogenesis, the process by which fatty acids and/or triglycerides are taken up from the circulation by adipocytes to be esterified into the lipid droplet for later use as energy when the organism is in need. Other than these hallmark processes which are abundantly studied, the adipocyte must make choices among other metabolic pathways including glycolysis, β-oxidation, glyceroneogenesis, and sphingolipid synthesis (Chavez and Summers, 2003; Duncan, et al., 2007; Ferreira, et al., 2017; Franckhauser, et al., 2002; Hodson, et al., 2013; Kersten, 2001; Krycer, et al., 2017; Larsen and Tennagels, 2014; Miller, et al., 2015; Romero, et al., 2015; Rotondo, et al., 2017).

Data support numerous roles of sphingolipids in adipocyte metabolism. One key finding is the observation that lipolysis-driven inflammation required SPHK1 (Wang, et al., 2014). Isoproterenol, which agonizes β-3 adrenergic receptors, is a commonly-used

reagent for studying lipolysis due to the inherent receptor mechanism of catecholamine-induced increases in cAMP and PKA, which stimulate the activity of lipolytic enzymes (Greenberg, et al., 2001). In both mouse gonadal adipose tissue and 3T3-L1 adipocytes, isoproterenol induced the expression of *Sphk1* mRNA. Also, depletion of SPHK1 abrogated the lipolysis-mediated production of interleukin 6 (IL-6) (Wang, et al., 2014). In support of a role for S1P in lipolysis was the observation that glycerol release was increased by S1P treatment in a dose-dependent fashion (Jun, et al., 2006). Thus, the lipolysis metabolic pathway is affected by the SPHK axis. More studies will be needed to determine the role of S1P as the effector or the affected in this scheme.

It is widely accepted that stimulation of lipolytic pathways occurs via cAMP. Interestingly, adenylyl cyclase, the enzyme responsible for cAMP production, is typically found at the membrane localized to lipid rafts, which are known to contain higher concentrations of sphingolipids and cholesterol than the surrounding plasma membrane. Considering this interplay, the membrane dynamics of the adipocyte and its relationship with sphingolipids poses intriguing questions for scientific inquiry. Furthermore, cAMP is not only important for lipolysis, but it is one of the major effectors of early adipogenesis (Cooper, 2003). In addition, elevated cAMP is typically associated with decreased leptin, which intuitively suggests that these opposing characters (leptin, lipolytic mediators) must work in temporally discrete modes. Lipolysis occurs when circulating insulin and glucose are low, which indicates the organism is in an energy deficient state. Thus, fatty stores can be liberated through lipolysis to be provided to other organs for energetic support. On the other hand, if an organism is fed, adipocyte-derived leptin levels should increase, thus signaling to the hypothalamus the state of satiety and suppression of hunger.

A recently emerging concept in adipocyte metabolic biology is the role of the intrinsic adipocyte circadian clock as a key player in regulation of adipocyte metabolism. Major effectors of lipolysis, such as ATGL and HSL, and other effectors of lipogenesis, such as PPARγ, are under the control of the circadian transcription program. The adipocyte is specialized to communicate with the rest of the body with its immense secretion of numerous adipokines as well as lipids. The liver, one of its well-appreciated crosstalk partners, has a robust circadian clock that can mediate feeding and fasting rhythms. The role of sphingolipids in circadian rhythm is still largely unexplored, despite the fact that circulating lipids are known to fluctuate with 24-h rhythmicity. Adiponectin and leptin also rise and fall according to circadian patterns (Shostak, et al., 2013, 2013a; Unger, et al., 2013). Studies examining the effect of time of day on feeding and the downstream consequences have revealed numerous intriguing mechanisms. For example, mice fed a high fat diet restricted only to the waking portion of the day completely recovered from metabolic aberrancies, such as insulin resistance, compared to ad libitum fed controls (Chaix, et al., 2019; Hatori, et al., 2012). Considering that the adipocyte is at the crux of whole-body metabolic regulation, and that the circadian system is intertwined with metabolism, one would be amiss to disregard these important details. At the very least, researchers may consider aligning media changes and experimental initiation, or time restricted feeding in addition to high fat diet feeding.

One of these circadian regulated adipokines, adiponectin is associated with improved insulin sensitivity. Treatment of mice and MEFs with adiponectin reduces ceramide content by enhancing ceramidase activity and leads to increased production of the metabolite S1P. Additionally, deletion of adiponectin receptors led to reduced ceramidase activity, and elevation in ceramide content. These results suggest that the

protective effects of adiponectin against the development of insulin resistance may be in part due to degradation of ceramides (Holland, et al., 2011). The Holland group also found that inducible adiponectin deletion during the final two weeks of a six-week high fat feeding regimen, resulted in elevated ceramides, reduced sphingosine, S1P, and sphinganine-1-phosphate, and a variety of metabolic abnormalities (Xia, et al., 2018). Aside from major findings in lipolysis and adiponectin, the role of sphingolipids in other facets of adipocyte metabolism are worth further investigation.

2.5. Sphingolipids in Adipose Tissue Inflammation and Insulin Resistance

Pathological obesity is often associated with low grade inflammation within the adipose tissue. In addition to lipotoxicity, inflammation and glucocorticoid excess are the major mechanisms of insulin resistance. Infiltration of pro-inflammatory immune cells such as macrophages, paired with increased expression of inflammatory cytokines, including tumor necrosis factorα (TNFα), IL-6, interleukin 1β (IL-1β), monocyte chemoattractant protein (MCP1) and inducible nitric oxide synthase (iNOS) and reduced expression of anti-inflammatory interleukin 10 (IL-10) and adiponectin are indicators of adipose inflammation. As inflammation progresses, infiltrating macrophages accumulate around dying adipocytes, forming what are referred to as crown like structures. Inflammation, in addition to lipotoxicity, impairs adipose function, including glucose uptake (reduced GLUT4 translocation to the plasma membrane) and lipogenesis, which contribute to insulin resistance, locally within adipose tissue and systemically. Studies investigating the role of sphingolipids in insulin resistance have primarily focused on liver, skeletal muscle, and pancreas, however there is evidence that sphingolipids generated within the adipose tissue are effectors of systemic and localized insulin signaling. Treatment of 3T3-L1 cells with sphingolipids induces pro-inflammatory gene expression; for example, treatment with soluble ceramide analogues induced TNFα, MCP1, and IL-6. TNFα was also induced by sphingosine and S1P. MCP1 was induced by sphingosine, and IL-6 was induced by sphingosine and S1P. Consistent with this, inhibition of *de novo* ceramide synthesis with myriocin increased expression of anti-inflammatory M2 macrophage genes. This occurred with increase in IL-10 (anti-inflammatory) and decrease in IL-6, MCP1, and TNFα (pro-inflammatory). Together these results suggest that *de novo* ceramide synthesis promotes inflammation (Samad, et al., 2006).

There is a well-established role for ceramide in promoting insulin resistance. One mechanism by which ceramide affects insulin signaling in adipocytes is through inhibition of the AKT/PKB signaling pathway via ceramide-mediated stimulation of PP2A, which antagonizes phosphorylation of AKT in response to insulin receptor-mediated signaling (Zhang, et al., 2012). Inhibition of the AKT pathway then reduces GLUT4 translocation to the plasma membrane, which reduces glucose uptake. Experimental evidence for this includes the observation that raising ceramide levels in 3T3-L1 cells by addition of ceramide or ceramide activators including saturated fatty acids prevented insulin activation of the AKT pathway (Stratford, et al., 2004; Summers, et al., 1998). This activity of ceramide has been observed in many other cell types (Salinas, et al., 2000; Schubert, et al., 2000).

Another mechanism of insulin resistance is through inflammatory pathways, which are activated in both immune cells and adipocytes resulting in the production of pro-inflammatory cytokines. Ceramide has been shown to induce the NLRP3 inflammasome, which activates caspase-1 and IL-1β secretion, both of which impair insulin signaling through caspase-1 upregulation. Palmitate also induces IL-1β, however myriocin does not inhibit this upregulation suggesting that *de novo* ceramide synthesis is not required for its induction. To determine if de novo ceramide synthesis in macrophages is responsible for adipose tissue inflammation and insulin resistance in diet induced obesity, a myeloid-specific Sptlc2 knockout mouse was generated. This had no effect on adipose tissue inflammation or insulin resistance suggesting that *de novo* ceramide synthesis in macrophages is not required for these pathologies (Camell, et al., 2015). Another activator of ceramide synthesis is the mTOR pathway. Deletion of mTORC1 from adipose tissue was shown to increase *de novo* ceramide synthesis, leading to increased adipose tissue

inflammation, despite reduced adiposity. Treatment with myriocin prevented this inflammation (Chimin, et al., 2017).

Glucosylceramides have also been implicated in the development of adipose tissue inflammation and insulin resistance. GM3 ganglioside is elevated in obesity and abundant in adipose tissue. TNFα treatment of 3T3-L1 adipocytes induced GM3 expression in addition to insulin resistance. GM3 treatment also induced insulin resistance. Treatment with an inhibitor of glucosylceramide synthase reversed the impaired insulin signaling (Tagami, et al., 2002). These effects have also been observed in vivo. Ob/ob mice treated with glucosylceramide synthase inhibitor AMP-DNM reduced levels of GM3 and reversed their insulin resistant phenotype, in addition to reducing adipose tissue inflammation (van Eijk, et al., 2009). Additionally, genetic ablation of GM3 prevented systemic insulin resistance due to high fat diet (Nagafuku, et al., 2015; Yamashita, et al., 2003). GM3 localizes at caveolae in the plasma membrane of adipocytes where it regulates insulin receptor localization. GM3 forms a complex with the insulin receptor and mobilizes it away from caveolae which prevents insulin signaling (Kabayama, et al., 2007).

SPHK and S1P have also been studied with regards to their impact on adipose tissue inflammation and insulin resistance. Both palmitate and LPS treatment have been shown to stimulate SPHK activity *in vitro* in many experimental systems including rat primary adipocytes. This occurred concomitant with an increase in pro-inflammatory cytokines. This increase in pro-inflammatory gene expression was suppressed by treatment with SPHK1 inhibitor (SK1-I), indicating that there is an SPHK1 dependent mechanism for adipose inflammation (Tous, et al., 2014). Additionally, SPHK1 expression and activity has been shown to be induced in macrophages in genetic and diet induced

obesity. This has been recapitulated *in vitro* with palmitate treatment of RAW264.7 macrophage-like cells which also induced SPHK1 expression and activity, along with S1P levels. SPHK2 was unchanged with palmitate treatment. Palmitate treatment in the presence of SK1-I was associated with decreased cell survival, indicating that SPHK1 activity and the S1P it produces protects macrophages from lipotoxicity induced cell death (Gabriel, et al., 2017), which has previously been reported in the context of TNFα and LPS using RAW264.7 cells (Hammad, et al., 2008). Another group used macrophages lacking both SPHK isoforms to demonstrate that SPHK is not necessary for inducing inflammation in macrophages but leads to elevated autophagy (Xiong, et al., 2013). Alternatively, constitutive knockout of SPHK1 in mice has been shown to be protective against pro-inflammatory gene ex-pression and recruitment of adipose tissue macrophages in diet induced obesity. This occurred concomitantly with improved insulin signaling in adipose tissue and protection from systemic insulin resistance. Pharmacological inhibition of SPHK1 in obese mice reversed adipose inflammation and impairments in insulin signaling (Wang, et al., 2014). These studies highlight the overall importance of sphingolipids in adipose insulin signaling and inflammatory pathways.

2.6. Sphingolipids in Brown Adipose Tissue

Brown adipose tissue is thought to be the metabolic panacea of obesity due to its literal fat burning potential. The high mitochondrial content of this depot distinguishes it in color and function from the white adipose, as it uncouples fat oxidation from ATP production to generate heat. S1P was explored in the functioning of brown adipose tissue. S1P is known to be carried in the bloodstream on apolipoprotein M (ApoM) on HDL particles, as well as albumin (Christensen, et al., 2016; Christoffersen, et al., 2011). In the brown adipose tissue, it is known that lipoproteins interact with lipoprotein lipase as well as the fatty acid transporter CD36 at the interface of the brown adipocytes and the endothelium. An ApoM knockout mouse has been used to assess its function in adipose tissue with some striking findings in brown adipose tissue. For example, histological analysis of brown adipose tissue revealed a dramatic decrease in lipid droplets with a concomitant increase in mitochondria. This finding was coupled with increased *Glut4* mRNA expression, implicating a potential role for S1P in GLUT4 translocation and insulin signaling. Also intriguing was the differential activity in the $ApoM^{-/-}$ brown adipose tissue, in which uptake of radiolabeled oleic acid was increased in the brown adipose tissue relative to control mice. These findings highlight the specificity of fatty acids utilized by the adipocyte in response to a change in sphingolipid dynamics (Christoffersen, et al., 2018). The Summers group has also published widely in the field of brown adipocyte biology. They have found, in the context of high fat diet, myriocin induced browning markers, such as Peroxisome proliferator-activated receptor gamma coactivator 1-alpha (PGC1α) and PR domain containing 16 (PRDM16) in subcutaneous adipose tissues. This was associated with increased circulating adiponectin (Chaurasia, et al., 2016). They also found that cold exposure decreased ceramide levels in both gonadal and subcutaneous

adipose depots. Cold exposure, a common experimental method to assess browning activity, upregulated miR-144-3p in brown adipose tissue of mice. Indeed, through miRNA sequencing and pathway analyses, it was shown that modulation of miR-144-3p was concomitant with increased expression of *Sphk2* mRNA brown adipose tissue (Tao, et al., 2015). In light of these intriguing findings, a mechanism linking SPHK and browning is open for investigation, as the benefits of browning existent white fat could be used therapeutically to combat obesity and its associated pathologies.

2.7. Human Data and Relevance

As described above, rodent studies have provided insight into the various roles of sphingolipids in adipose tissue. Many groups have demonstrated that sphingolipids levels are elevated in the plasma and tissues of obese, insulin resistant humans (Adams, et al., 2004; Blachnio-Zabielska, et al., 2012a; Kowalski, et al., 2013). Furthermore, weight loss through bariatric surgery, is associated with decreases in plasma ceramides that correlate with a reduction in plasma TNFα and improvements in insulin sensitivity (Huang, et al., 2011). However, relatively few studies have looked at sphingolipids specifically in human adipose tissue. They have been measured by a few groups in the context of obesity, type 2 diabetes, and fatty liver disease. Adipose tissue from obese subjects has been associated with higher ceramide (Blachnio-Zabielska, et al., 2012a; Candi et al., 2018; Turpin et al., 2014), dihydroceramide (Blachnio-Zabielska, et al., 2012), sphingosine (Blachnio-Zabielska, et al., 2012a), dihydrosphingosine (Blachnio-Zabielska, et al., 2012a), S1P (Blachnio-Zabielska, et al., 2012a), and sphingomyelin (Turpin, et al., 2014) content. Additionally, expression of enzymes involved in the *de novo* synthesis of ceramides (Spt1, Spt2, ceramidase, sphingomyelinase) was elevated in obesity and exacerbated by insulin resistance (Blachnio-Zabielska, et al., 2012). Of the ceramide synthases, only CERS6 was found to correlate with BMI and blood glucose levels (Turpin et al., 2014). Similarly, C16 ceramide, produced preferentially by CERS5 and CERS6, was shown to negatively correlate with adiponectin (Blachnio-Zabielska, et al., 2012a). A study of subjects with or without type 2 diabetes revealed higher sphingolipid content (ceramides, dihydroceramides, dihexosylceramides and sphingomyelins) in the subcutaneous but not visceral adipose tissue of those with type 2 diabetes (Chaurasia, et al., 2016). Additionally, individuals with fatty liver were shown to have higher levels of

adipose ceramides, sphingomyelin and inflammation (Kolak, et al., 2007). Sphingomyelinase expression was elevated, but genes involved in *de novo* ceramide synthesis were not, suggesting that ceramides are generated through the breakdown of sphingomyelins in this context (Kolak, et al., 2012). In general, these results suggest that elevated adipose tissue sphingolipids are associated with less favorable metabolic outcomes. It is important to consider that differences in adipose depot sampling, dietary intake, and variations in lipidomics methods likely contribute to experimental outcomes

2.8. Conclusions

Increasing evidence implicates sphingolipids at the crossroads of obesity and adipose tissue dysfunction (summarized in Figure 4). Dyslipidemia, a hallmark of obesity and its associated comorbidities, perturbs sphingolipid synthesis and metabolism. More research is needed to elucidate the molecular mechanisms by which sphingolipids regulate adipose function. The structural diversity of the sphingolipid class of lipids and their abundance in adipose tissue alludes to an exciting future in the discovery of their functions, and contribution to adipose tissue homeostasis.

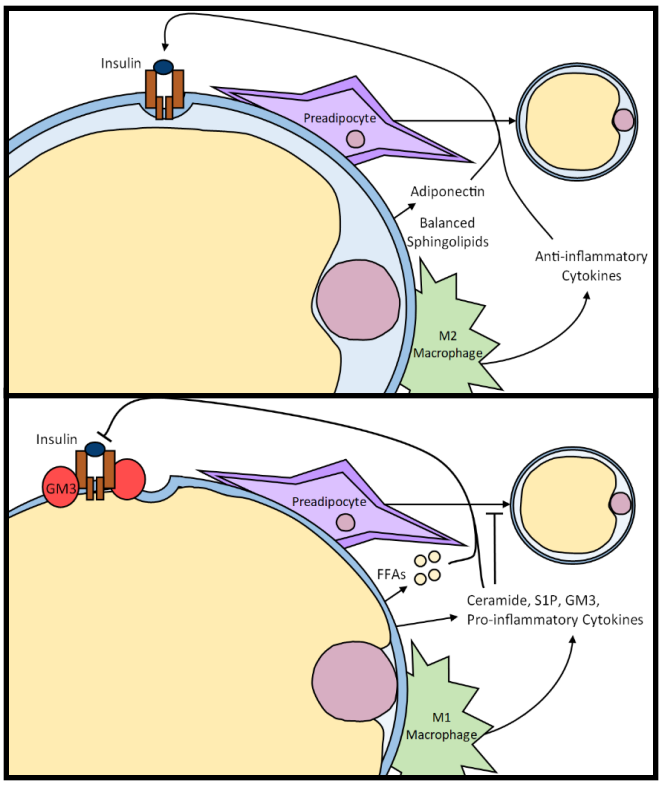

Figure 4. Healthy (top) versus unhealthy (bottom) adipose tissue. Healthy adipose tissue requires functional insulin signaling, adipogenesis, and lipid storage. It is marked by balanced production of sphingolipids, high adiponectin production, and release of anti-inflammatory cytokines from resident M2 macrophages. In the pathological state, elevated levels of sphingolipids are released, in addition to excess free fatty acids (FFAs), and pro-inflammatory cytokines from M1 macrophages. GM3 interferes with insulin receptor localization to caveolae, while elevated ceramides and pro-inflammatory cytokines interfere with downstream signaling aspects of insulin signaling. Aberrant sphingolipid synthesis, inflammation, and excess FFAs also interfere with adipogenesis and lipogenesis. (Lambert, J.M., Anderson, A.K., Cowart, L.A. (2018) Sphingolipids in Adipose Tissue: What's Tipping the Scale? Advances in Biological Regulation 70: 19-30.)

CHAPTER 3

DEPLETION OF ADIPOCYTE SPHINGOSINE KINASE 1 LEADS TO CELL HYPERTROPHY, IMPAIRED LIPOLYSIS, AND NON-ALCOHOLIC FATTY LIVER DISEASE

(ANDERSON, et al., 2020)

Primary Research Manuscript

3.1. Introduction

Obesity precipitates a variety of conditions including type 2 diabetes, cardiovascular pathology, non-alcoholic fatty liver disease, and others (Dal Canto, et al., 2019; Aguilar-Salinas and Viveros-Ruiz, 2019). The molecular mechanisms connecting obesity to its downstream pathologies are not fully understood and are likely multi-faceted, however, data support major contributions from alterations in bioactive lipid metabolism and signaling. Among these, metabolism of sphingolipids including ceramide and sphingosine-1-phosphate is altered in obese humans and in mouse models of obesity and contribute to obesity-induced pathology (Choi and Snider, 2015; Geng, et al., 2015; Hannun and Obeid, 2018; Wang, et al., 2014). Indeed, it is well-established that ceramide, a principal signaling sphingolipid, plays a role in insulin resistance (Chavez, et al., 2003; Chavez and Summers, 2012; Cowart, 2009). On the other hand, ceramide can be interconverted to sphingosine-1-phosphate (S1P) through the action of ceramidases and sphingosine kinases (SK), SPHK1 and SPHK2. SPHK1 and its product S1P have also been identified as contributors to metabolic disease at least in part due to the well-documented pro-inflammatory signaling pathways through the S1P G protein-coupled receptors and downstream activation of NFκB signaling and other pathways of inflammation (Japtok, et al., 2015; Lee, et al., 2015; Wang, et al., 2014).

The Cowart lab and others have shown that SPHK1 and its product S1P are increased in several tissues in obese humans and mice including liver, skeletal muscle, and adipose tissue (Geng, et al., 2015; Ross, et al., 2013). The Cowart group also showed that SPHK1 is induced by saturated fatty acids, which are elevated in the circulation of individuals with metabolic disease (Geng, et al., 2015; Ross, et al., 2013). Therefore, because S1P is generally a pro-inflammatory lipid mediator, and because outcomes of

obesity include systemic inflammation, a pathway dependent upon SPHK1/S1P could serve as a primary mechanism by which lipid excess contributes to pathology. Supporting the link between SPHK1 and obesity, a previous study provided evidence that SPHK1 deficiency in mice was associated with enhanced insulin sensitivity and reduced pro-inflammatory signaling in adipose tissue of animals fed obesogenic diets (Ross, et al., 2013). As adipose tissue inflammation is thought to be a key driver of obesity-related pathophysiology (Gustafson, et al., 2007; Scherer, 2006), we speculated that SPHK1 expression in adipose tissue may mediate pro-inflammatory signaling, thereby promoting metabolic disease.

In this study, we generated a mouse strain lacking SPHK1 in adipose tissue ($SK1^{fatKO}$). These animals were challenged with high fat diet feeding for 18 weeks to assess the contribution of adipocyte SPHK1 to metabolic homeostasis, adipose tissue function, inflammation, and systemic glucose tolerance. In contrast to expected findings, mice exhibited components of metabolic phenotypes even on control diet, and outcomes of high fat feeding were exacerbated in these mice including increased weight gain, impaired glucose clearance, and adipocyte hypertrophy. Adipocytes and adipose explants showed impaired lipolysis and dysregulation of lipolytic machinery. Moreover, the livers of these mice displayed NAFLD pathophysiology. Thus, SPHK1 serves a previously unidentified essential homeostatic role in adipocytes that protects from obesity-associated pathology. These data may have implications for pharmacological targeting of the SPHK1/S1P signaling axis.

3.2. Results

Previous studies demonstrated that sphingosine kinase 1 (SPHK1) increased in adipose tissue of type 2 diabetic humans and in diet-induced obesity in mice (Wang, et al., 2014). Moreover, in that study, global depletion of SPHK1 protected mice from high fat diet-induced insulin resistance and systemic inflammation. Because adipose tissue is a central regulator of metabolic homeostasis, and adipocyte dysfunction is thought to underlie much of the downstream pathophysiology of obesity including insulin resistance and inflammation (Kusminski, et al., 2016; Scherer, 2006), we sought to test the role of SPHK1 intrinsic to the adipocyte in these processes. To this end, mice with an adipocyte-specific deletion of SPHK1 ($SK1^{fatKO}$) were generated using mice harboring a *Sphk1* allele with Loxp sites flanking exons 3-6. These mice were crossed with mice carrying a transgenic Cre recombinase enzyme driven by the adiponectin promoter (Allende, et al., 2004). We confirmed gene depletion in the adipose tissue genomic DNA by PCR using an upstream primer 5' to exon 1 and a downstream primer 3' to exon 6, which should produce a 600-bp product only in the modified *Sphk1* gene. This product was indeed amplified and visualized by agarose gel (Supplemental Figure 1A, B), confirming gene depletion. Because SPHK1 depletion can be compensated by upregulation of SPHK2, mRNA for *Sphk2* was measured in gonadal white adipose (gWAT) homogenates of these mice (Supplemental Figure 1C). No upregulation of *SphK2* was observed, indicating this was not a confounding factor for data interpretation in these studies (Supplemental Figure 1C).

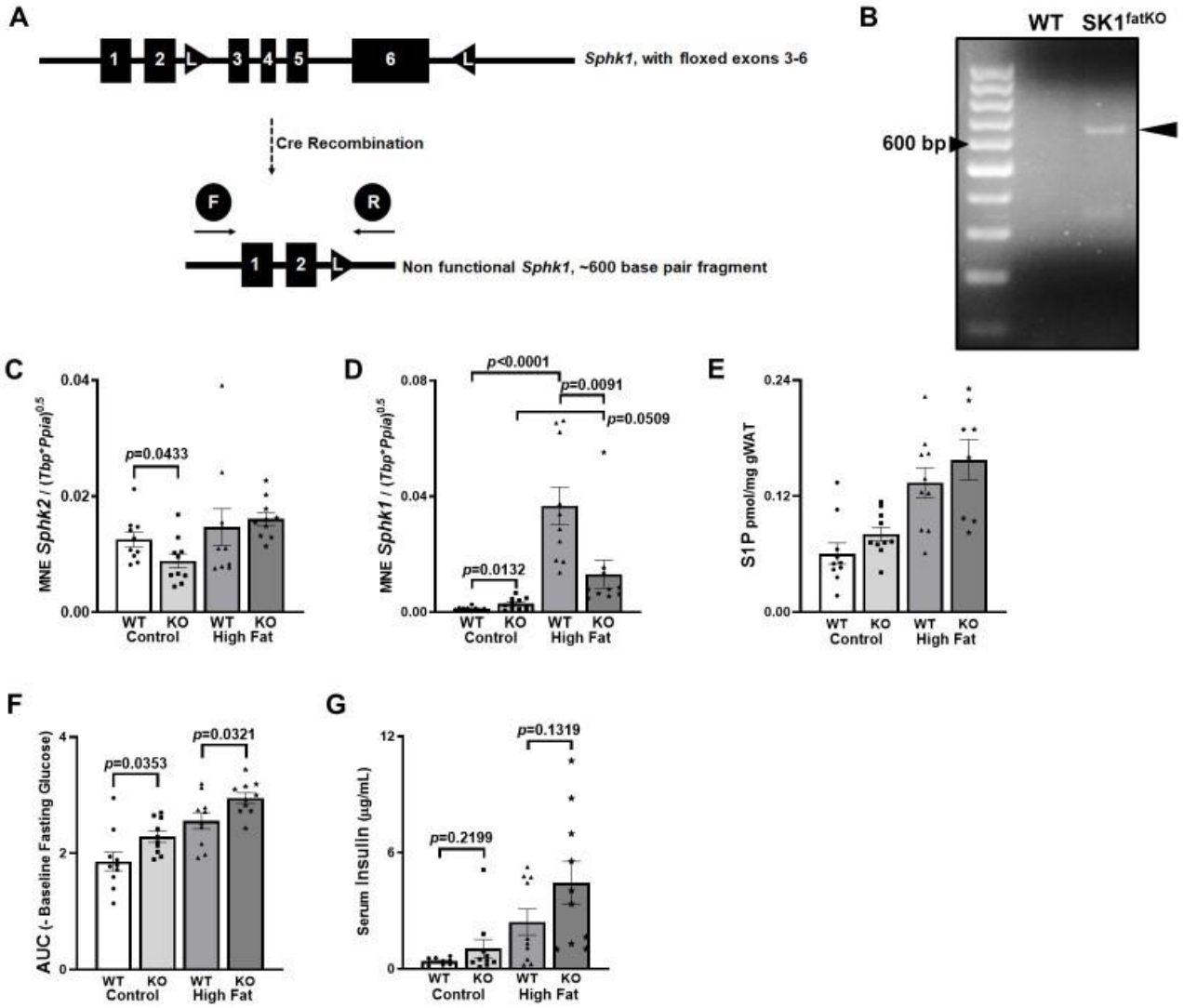

Supplemental Figure 1. *Sphk1* knockout in the adipocyte and effects on *Sphk2* and insulin. **A.** Schematic floxed *Sphk1* gene construct, with *loxP* sites surrounding exons 3 through 6. Cre expression, under the control of the adiponectin promoter, generates a ~600 base pair fragment upon excision. **B.** Representative agarose electropherogram indicating the excised 600-base pair amplicon in the mutant and not the control. Flox primer pairs forward and reverse 2 were used to generate this band. **C.** *Sphk2* message was not concomitantly upregulated in the SK1^{fatKO} gonadal adipose tissue due

to loss of *Sphk1*. **D.** Induction of *Sphk1* mRNA in gonadal adipose tissue homogenates in response to high-fat feeding. **E.** S1P levels determined by LC:MS/MS lipidomics in gonadal adipose tissue homogenates. **F.** AUC assessment of ipGTT, calculated differently from Fig. 5E, by first normalizing to the differences in baseline fasting glucose. **G.** Fasting serum insulin.

To test effects of adipocyte-specific depletion of SPHK1 in pathophysiology in diet-induced obesity, $SK1^{fatKO}$ mice and their adiponectin-CRE:$SK1^{+/+}$ control counterparts were subjected to either a high fat diet (HFD) or a control low glycemic isocaloric diet (CD) for 18 weeks. Mice on control diet exhibited low levels of *Sphk1* mRNA (Supplemental Figure 1D). Adipose tissue homogenates from $SK1^{fatKO}$ mice exhibited some basal elevation of *Sphk1*, however, this is likely due to expression in other adipose tissue cell types. Similar to previous findings, HFD feeding robustly induced *Sphk1* mRNA in gWAT homogenates from control mice, and this was significantly attenuated in $SK1^{fatKO}$ mice, again, with residual message likely resulting from other adipose tissue cell types (*e.g.*, immune cells, fibroblasts, vascular endothelial cells, etc.) (Supplemental Figure 1D). S1P, the enzymatic product of SPHK1 was also very low in gWAT in control diet feeding but robustly induced by HFD feeding (Supplemental Figure 1E). While adipose tissue homogenates showed similar S1P levels in $SK1^{fatKO}$ and WT mice, S1P is found in μM amounts in plasma and even higher amounts in whole blood from erythrocytes (Allende, et al., 2004; Kharel, et al., 2020; Yatomi, et al., 1997), and therefore it is likely that these high levels obscured the differences in tissue S1P that would be expected based on reduced mRNA in the HFD-fed $SK1^{fatKO}$ mice. These data also suggest that SPHK1 in adipocytes does not contribute to circulating levels of S1P, but rather acts in a localized fashion within the tissue.

Previous studies indicated that, though *Sphk1*-null mice were protected from insulin resistance and inflammation induced by high fat feeding, weight gain was comparable to that of control mice (Wang, et al., 2014). In contrast, while HFD-feeding increased weights of both $SK1^{fatKO}$ mice and control mice steadily over the first 8 weeks, by 8-10 weeks of the feeding course, $SK1^{fatKO}$ began to gain notably more weight on HFD

compared to control (Figure 5A). Indeed, by the end of the feeding course, the percent weight gain on CD and HFD was significantly greater in the $SK1^{fatKO}$ compared to controls (Figure 5B). Further analyses suggested that weight gain arose from expansion of both the gonadal (gWAT) and subcutaneous inguinal (iWAT) white adipose depots (Figure 5C). On the other hand, retroperitoneal white adipose tissue (retroWAT) and intrascapular brown adipose tissue (BAT) depots did not exhibit such wet weight differences as gWAT and iWAT between genotypes (Figure 5C). Remaining differences in weight between genotypes were most likely due to remaining subcutaneous fat (axial, gluteal, and other compartments beneath the skin) throughout the animal which we observed in mutant animals upon dissection (*data not shown*). Therefore, in contrast to whole-body depletion of *Sphk1*, adipocyte-specific depletion exacerbated diet-induced obesity, suggesting a distinct role for adipocyte SPHK1 in inhibiting diet-induced obesity.

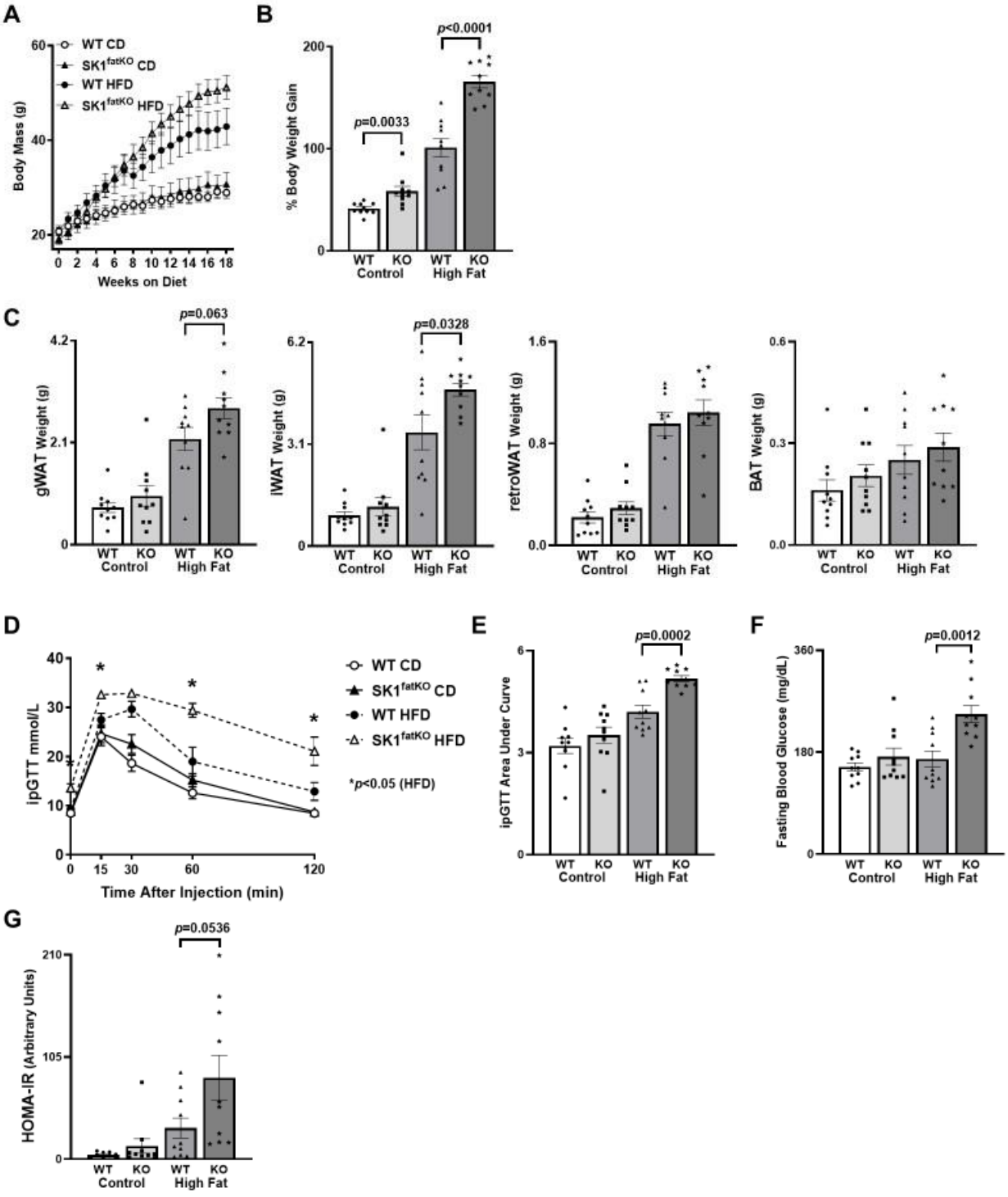

Figure 5. High fat diet-induced weight gain and systemic glucose intolerance. A. Mouse body weights over 18-week high fat diet study. **B.** Percent weight

(*Figure 5 legend continued.*)

gain between final weight at sacrifice and initial starting weight at diet commencement. **C.** rom left to right, gonadal (gWAT), subcutaneous (inguinal) fat pad (iWAT), retroperitoneal (retroWAT) fat pad, and brown adipose (BAT) weights at sacrifice. **D.** After 18 weeks of high fat feeding, an intraperitoneal glucose tolerance test (ipGTT) was administered over 2 hours, at the same time in the afternoon for each animal, following a 6-hour fast. **E.** The corresponding area under the curve analysis for ipGTT. **F.** Baseline fasting glucose shown as mg/dL as measured from whole tail blood droplets. **G.** HOMA-IR calculated from fasting blood glucose concentration and fasting blood insulin concentration.

Though SK1^{fatKO} mice were more obese than their control counterparts, obesity does not always coincide with metabolic disease (Samocha-Bonet, et al., 2014), indicating a possibility for SK1^{fatKO}, despite their increased adiposity, to be protected from deleterious metabolic outcomes of obesity including impaired glucose clearing, a marker of insulin resistance. To test this, we performed glucose tolerance tests (GTT). As expected, high fat feeding impaired glucose clearing in control mice; however, these tests showed exacerbation of impaired glucose clearance in HFD-fed SK1^{fatKO} mice compared to controls, both in kinetics of clearance and area under the curve assessments (Figure 5D, E). Fasting glucose was also elevated (Figure 5F), and normalization of blood glucose in the GTT to basal glucose also demonstrated a significant elevation of area under the curve in CD- and HFD-fed SK1fatKO mice relative to control mice (Supplemental Figure 1F). Averaged fasting serum insulin trended strongly to increase in HFD-fed mutant mice relative to controls, and, though statistical significance was not reached (p = 0.1319, Supplemental Figure 1G), pairing fasting glucose with fasting insulin for each individual revealed a marked and significant increase in HOMA-IR in the HFD-fed SK1^{fatKO} relative to controls (Figure 5G). Together, these data support a role for adipocyte SPHK1 in suppressing HFD-induced obesity and subsequent deficiencies in glucose clearance.

Increased fat mass can arise from either adipocyte hypertrophy (increase in cell size) and/or hyperplasia (increase in adipocyte number). While adipocyte hyperplasia may underlie the phenomenon of 'healthy obesity,' *i.e.*, WAT expansion with numerous smaller adipocytes and little inflammation or fibrosis, hypertrophic adipocytes more closely correlate to insulin resistance (Vishvanath and Gupta, 2019). Because the obese, insulin resistant phenotype was exacerbated in SK1^{fatKO} mice, we hypothesized they would show greater hypertrophy with high fat feeding than controls. Upon histological examination, we

found that the gonadal adipocytes in SK1^{fatKO} mice were markedly larger than those of control mice even with CD feeding, and this was further increased with HFD feeding (Figure 6A, B). Quantification of mean area showed an approximately 2-fold larger size in SK1^{fatKO} on HFD relative to controls (Figure 6C).

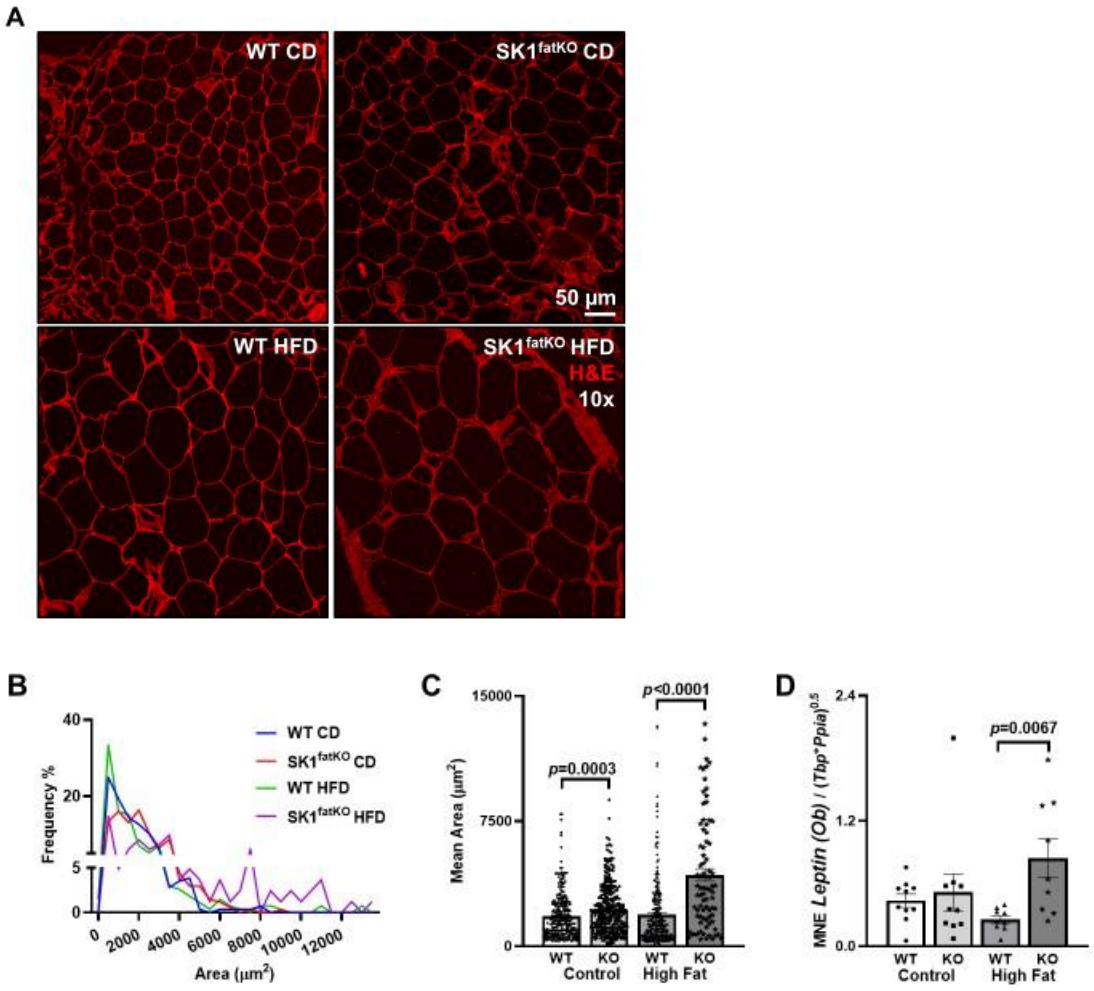

Figure 6. Adipocyte hypertrophy in SK1^{fatKO} gWAT. A. Confocal microscopy of representative sections of gWAT shown by H&E staining. **B.** Quantification of gWAT adipocyte size, as shown by a frequency distribution. **C.** Adipocyte size displayed as the mean ± S.E.M. **D.** Pro-inflammatory adipokine leptin (*Ob*) mRNA expression.

The hypertrophic adipocyte phenotype is generally considered more closely linked with overall metabolic perturbations and adipocyte dysfunction, and therefore the larger adipocytes observed in SK1^{fatKO} mice suggested there could be a general disruption of key adipocyte functions (Jo, et al., 2009; Muir, et al., 2016). The endocrine function of adipose tissue is essential for metabolic homeostasis, and aberrant adipokine production and signaling is a key feature of obesity-induced metabolic disease and closely associated with adipocyte size (Scherer, 2006). For example, hyperleptinemia and leptin resistance occur in human obesity and mouse models, and leptin secretion by human adipocytes correlated directly with adipocyte size (Skurk, et al., 2007). Consistent with this, HFD increased leptin mRNA in SK1^{fatKO} to a greater extent than in control mice (Figure 6D). Serum leptin trended modestly higher in SK1^{fatKO} mice upon HFD feeding, however, this did not meet criteria for statistical significance (Supplemental Figure 2A). Adiponectin, produced by adipocytes, is a protective factor in the context of metabolic disease and acts on multiple cell types and tissues for anti-atherogenic and anti-diabetic effects.

Adiponectin production is decreased in obesity and inversely correlated with adipocyte hypertrophy. Adiponectin mRNA from adipose tissue homogenates was modestly reduced in SK1^{fatKO} mice on CD, consistent with larger basal adipocytes; however, no differences were observed between SK1^{fatKO} and control mice on HFD (Supplemental Figure 2B). In mouse sera, adiponectin levels were higher in female mice generally, but showed no differences by diet or genotype. In males, however, high fat feeding reduced circulating adiponectin by 50% (Supplemental Figure 2C). Notwithstanding, significant sex differences were not observed in other measures, suggesting decreased adiponectin could not explain the robust exacerbation in insulin resistance observed in both male and female SK1^{fatKO} mice. Adiponectin receptors (highly

expressed in the liver) are thought to have intrinsic ceramidase activity (Holland, et al., 2011). Liver ceramides and hexosylceramides were measured among groups, which indicated that, while no major effects were observed in the high fat diet-fed condition, low glycemic control diet-fed $SK1^{fatKO}$ mice had increased C22:0 and C:24 ceramides, and decreased C18:0 and C22:0 hexosylceramides in their livers (Supplemental Figure 2D, E).

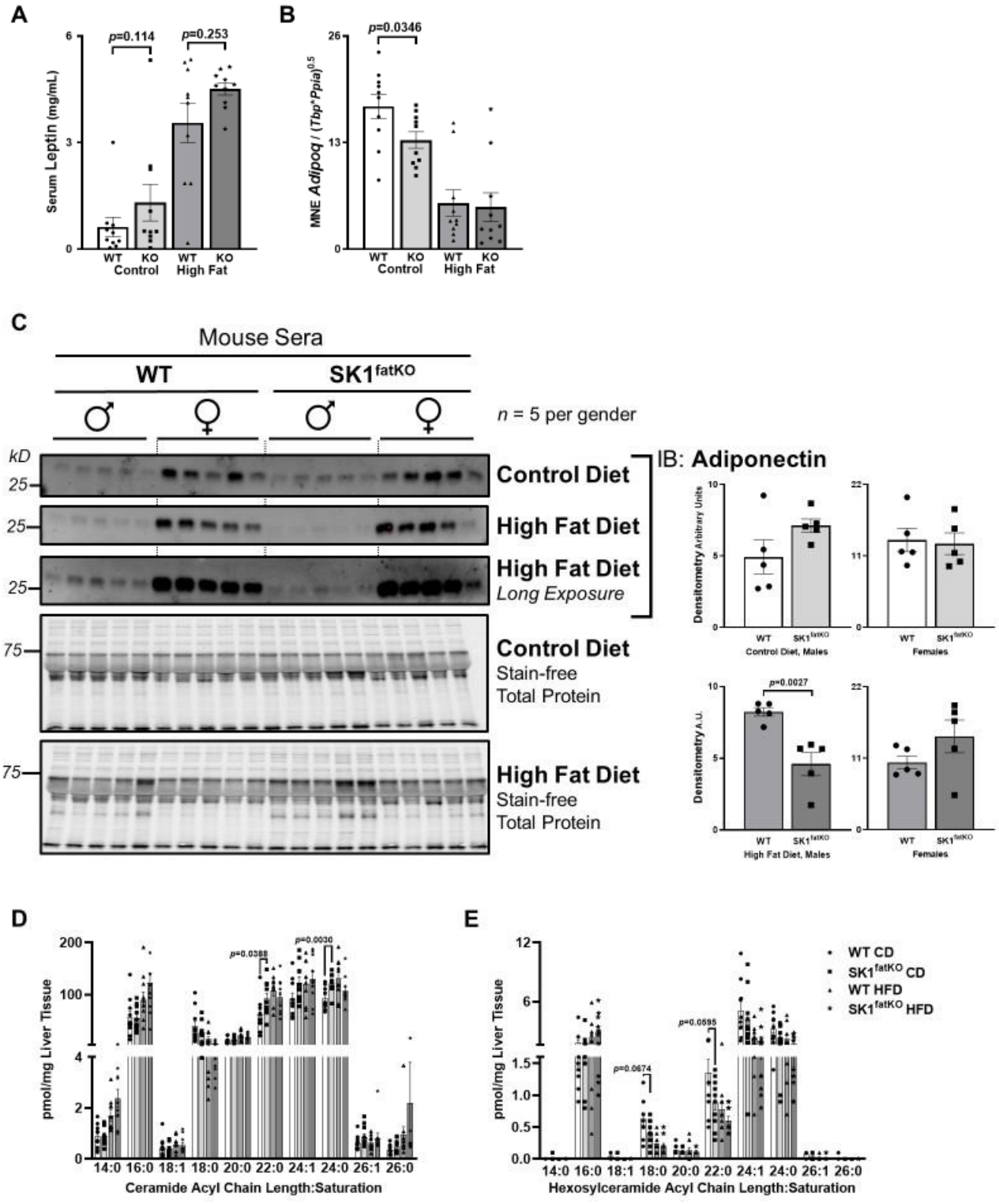
A
Serum Leptin (mg/mL)
p=0.114
p=0.253
WT KO WT KO
Control High Fat
B
MNE Adipoq / (Tbp*Ppia)^0.5
p=0.0346
WT KO WT KO
Control High Fat
C
Mouse Sera
WT
SK1fatKO
n = 5 per gender
kD
25
Control Diet
High Fat Diet
High Fat Diet
Long Exposure
75
Control Diet
Stain-free
Total Protein
High Fat Diet
Stain-free
Total Protein
IB: Adiponectin
Densitometry Arbitrary Units
WT SK1fatKO
Control Diet, Males
Females
p=0.0027
Densitometry A.U.
High Fat Diet, Males
D
pmol/mg Liver Tissue
p=0.0388
p=0.0030
14:0 16:0 18:1 18:0 20:0 22:0 24:1 24:0 26:1 26:0
Ceramide Acyl Chain Length:Saturation
E
pmol/mg Liver Tissue
p=0.0674
p=0.0595
WT CD
SK1fatKO CD
WT HFD
SK1fatKO HFD
14:0 16:0 18:1 18:0 20:0 22:0 24:1 24:0 26:1 26:0
Hexosylceramide Acyl Chain Length:Saturation

Supplemental Figure 2. Adipokine crosstalk with liver sphingolipid metabolism. **A.** Fasting serum leptin. **B.** Gonadal white adipose tissue adiponectin mRNA expression. **C.** Serum adiponectin as shown by Western blot. Quantification shown at right per respective membrane, separated by sex. **D.** Liver ceramides determined by LC:MS/MS lipidomics. **E.** Liver hexosylceramides determined by LC:MS/MS lipidomics.

Inflammation in gWAT is closely associated with adipocyte hypertrophy and is thought to couple obesity to insulin resistance (Andersson, et al., 2008; Gustafson, et al., 2007, 2009; Hardy, et al., 2012). Moreover, a previous study showed that *Sphk1*-null mice were protected from inflammation upon high fat feeding (Wang, et al., 2014). Inflammation in gWAT was assessed by several markers. First, mRNA of macrophage marker *F4/80* was measured, and data showed that expression was similar in both wildtype and $SK1^{fatKO}$ mice on CD though there was a trend to increase in HFD-fed mutant mice relative to control mice on HFD. (Figure 7A). Consistent with this, the macrophage chemoattractant protein marker *Mcp1* increased by HFD-feeding in both strains but was not significantly different between strains (Figure 7B). Crown-like structures (CLSs) in gWAT were identified, and negligible differences in numbers were found between genotypes, although CLSs tended to be less frequent in females compared to males (Figure 7C, and *data not shown*). Partially consistent with previous work showing protection from pro-inflammatory cytokine expression in obesity in SPHK1-null mice, HFD-fed $SK1^{fatKO}$ mice showed strong trends toward decreased *Il-6* and *Tnfα* levels, though these did not reach statistical significance (Figure 7D, E). As F4/80 does not necessarily indicate macrophage polarization status (*e.g.*, M1 vs. M2), M2 macrophage markers were also assessed. *Arg1* showed no changes (Figure 7F); however, there was a pronounced increase of *Tgf-β1* in $SK1^{fatKO}$ on HFD (Figure 7G). Assessment of neutrophil infiltration by myeloperoxidase puncta visualization and quantification showed little if any difference between wildtype and $SK1^{fatKO}$ mice (Supplemental Figure 3A, B). In summary, relative to HFD-fed control mice, $SK1^{fatKO}$ mice showed more fat mass, exacerbated glucose intolerance, and basal adipocyte hypertrophy, which was exaggerated upon high fat feeding. However, while adipocyte hypertrophy is linked to inflammation and impaired adipokine production,

increases in these measures in the gWAT of SK1^{fatKO} relative to control mice were modest, at best, and largely negligible, suggesting other links between adipocyte-specific depletion of SPHK1, obesity, and impaired glucose clearance.

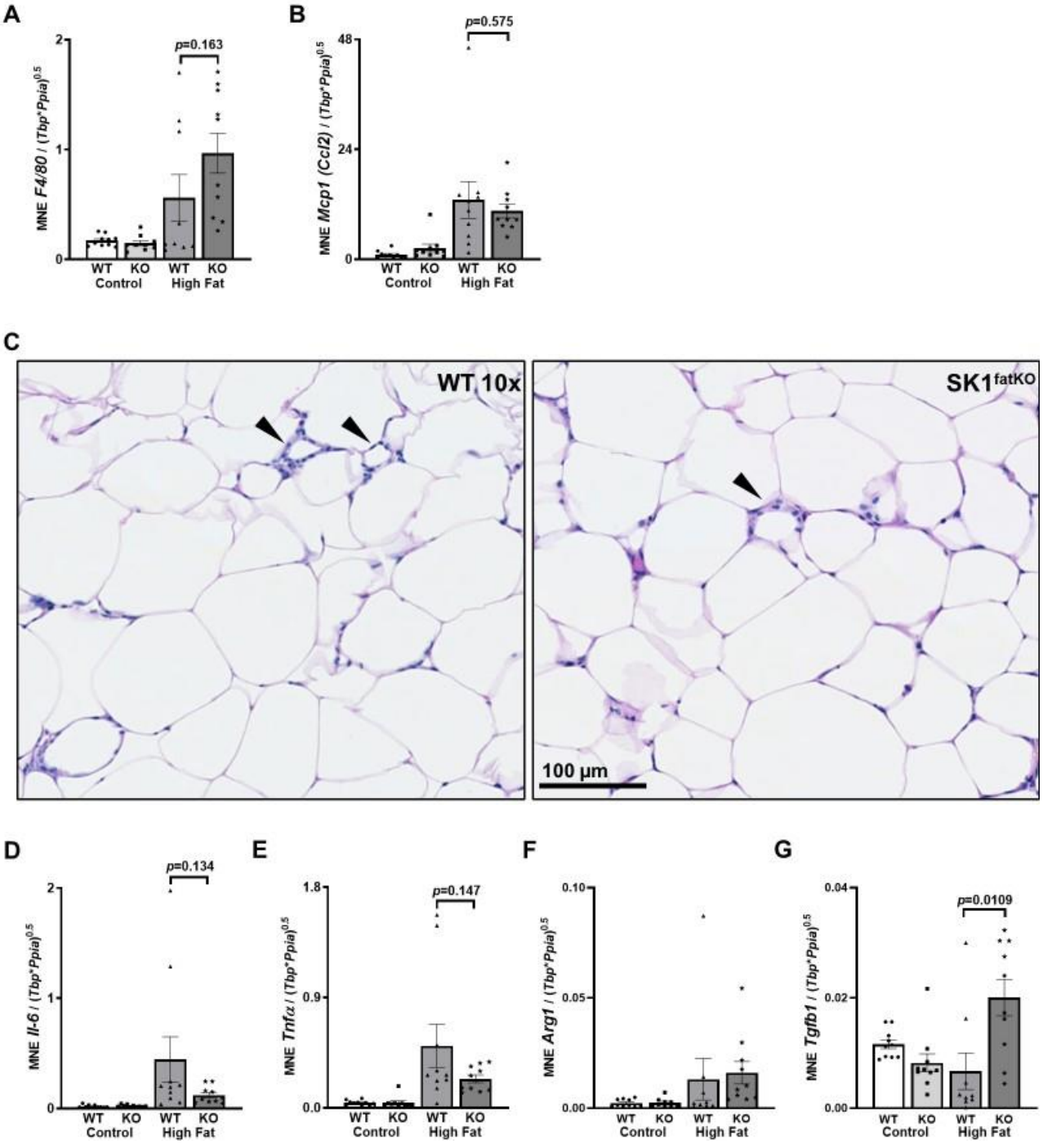

Figure 7. Inflammation within the adipose tissue. mRNA was isolated from gWAT homogenates from mice of both genotypes on both diets. After cDNA preparation,

(*Figure 7 legend continued.*)

real-time PCR was used to measure message for the indicated proteins **A.** Inflammatory adipocytokine *F4/80* (*Emr1*). **B.** Pro-inflammatory M1 macrophage *Mcp1* (*Ccl2*). **C.** Representative crown-like structures shown by brightfield H&E in gWAT from high fat-fed mice. **D.** Pro-inflammatory *Il-6* transcript. **E.** Pro-inflammatory *Tnfα* transcript. **F.** M2 macrophage marker *Arg1*. **G.** M2 macrophage marker *Tgf-β1*.

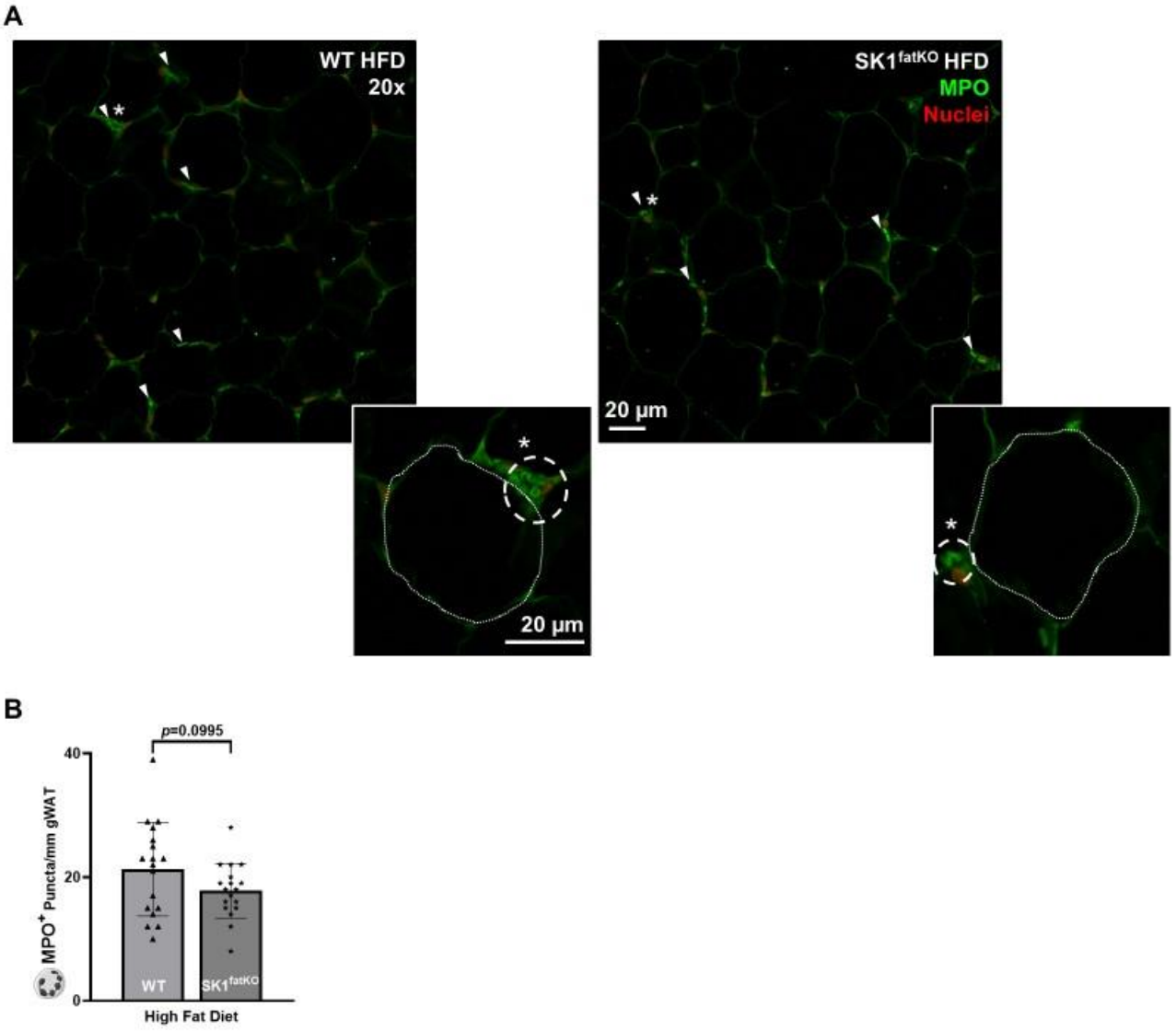

Supplemental Figure 3. High fat fed SK1^{fatKO} gonadal fat pads have fewer infiltrating neutrophils. **A.** Myeloperoxidase, strongly associated with pro-inflammatory neutrophil oxidant activities, expression in gWAT. Insets show an adipocyte outlined by a fine dotted line and clusters of neutrophils with the classical horseshoe-shaped nuclei are denoted by the heavy dashed circles as well as asterisks. **B.** Quantification of myeloperoxidase puncta.

Other than endocrine function, adipocytes perform lipogenesis and lipolysis to contribute to metabolic homeostasis. Therefore, we hypothesized that SPHK1 may play a role in regulating these processes. Lipolysis increases with fasting to release FFA into circulation where they can be distributed to peripheral organs and tissues for energy production in the context of low glucose (Frubeck, et al., 2014). To test whether lipolysis may be impaired in $SK1^{fatKO}$ mice, we assessed serum NEFA in fasted HFD-fed mice. These data demonstrated a 20-25% reduction in serum NEFA in HFD-fed $SK1^{fatKO}$ mice (Figure 8A). To test whether this was due to deficient adipose tissue lipolysis, glycerol release of explants of gWAT from $SK1^{fatKO}$ mice was measured. Consistent with decreased fasting NEFA observed *in vivo*, explants from mutant mice released only ~50% of the glycerol released by explants of control mice (Figure 8B). These differences were only observed in basal lipolysis, as isoproterenol-stimulated lipolysis showed no differences between wildtype and mutant explants (*data not shown*). Consistent with this, critical mediators of adipocyte lipolysis including adipose triacylglycerol lipase (ATGL), CGI-58, and FABP4 (fatty acid binding protein 4) were all lower in $SK1^{fatKO}$ mice at basal and/or HFD-fed conditions (Figure 8C, D). In general, levels of these proteins were lower in mutant mice, with females showing statistically significant differences and males mirroring this trend (Figure 8D, densitometry values shown in Supplemental Table 1). Therefore, adipocyte SPHK1 plays a role in basal lipolysis and likely contributes to fasting circulating NEFA.

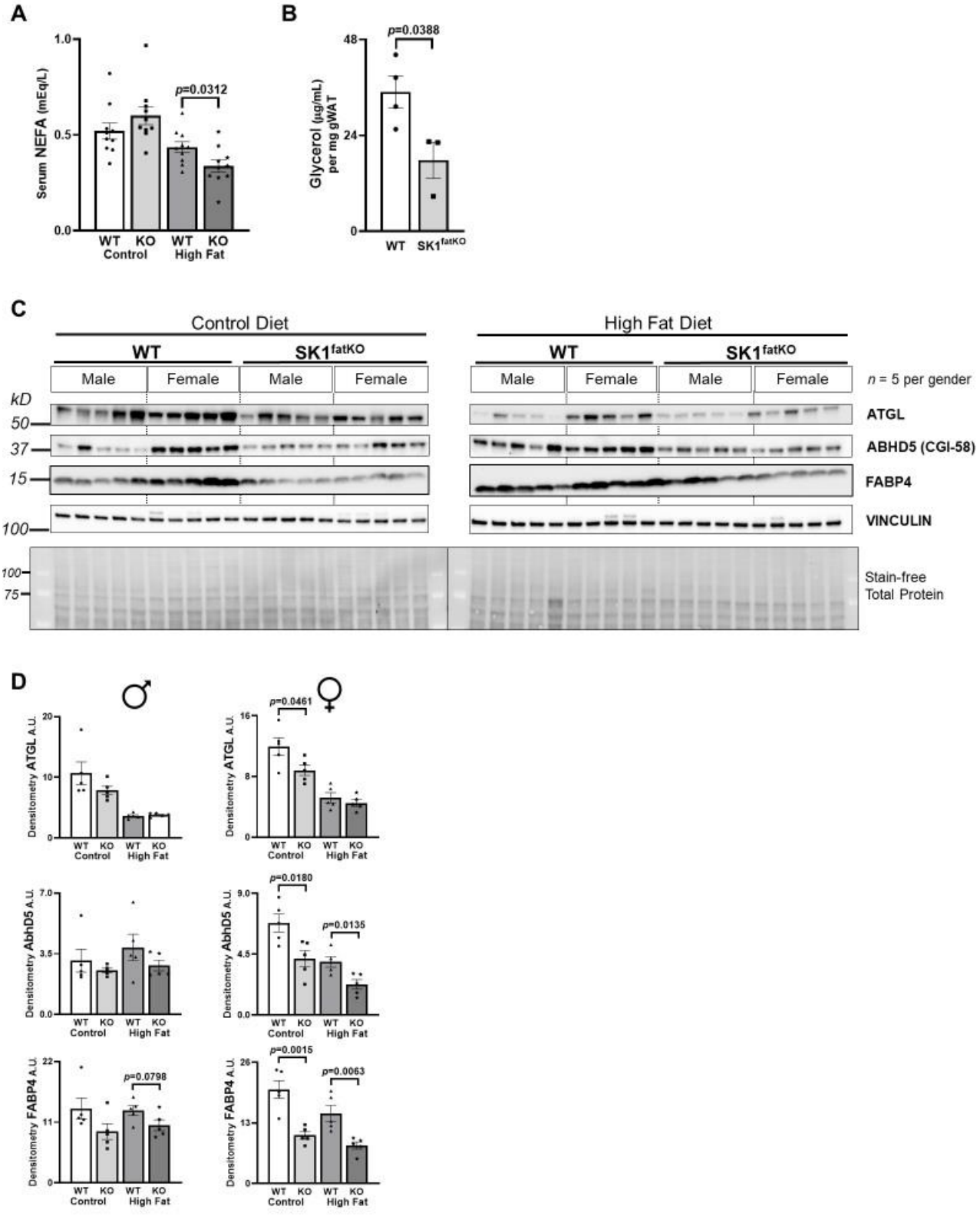
A
Serum NEFA (mEq/L)
1.0
0.5
0.0
p=0.0312
WT KO WT KO
Control High Fat
B
Glycerol (µg/mL) per mg gWAT
48
24
0
p=0.0388
WT SK1fatKO
C
Control Diet
High Fat Diet
WT
SK1fatKO
Male Female Male Female
n = 5 per gender
kD
50
37
15
100
ATGL
ABHD5 (CGI-58)
FABP4
VINCULIN
100
75
Stain-free Total Protein
D
♂
♀
Densitometry ATGL A.U.
p=0.0461
Densitometry AbhD5 A.U.
p=0.0180
p=0.0135
Densitometry FABP4 A.U.
p=0.0798
p=0.0015
p=0.0063
WT KO WT KO
Control High Fat

Figure 8. Fasting serum NEFA, basal glycerol release, and lipolytic proteins are reduced in SK1^{fatKO} mice. **A.** Serum non-esterified fatty acids were measured from mice fasted for 6 hours. **B.** Gonadal white adipose tissue explants were incubated in fatty acid-free media for 48 hours and media glycerol was measured. Media glycerol was normalized to the weight of tissue utilized in each well. **C.** Western blot protein analysis of lipolytic proteins (ATGL, CGI-58, FABP4) from gonadal white adipose tissue. Protein loading was normalized by stain-free total loading, as well as vinculin. **D.** Band intensities were quantified by densitometry using ImageJ and graphed separately as males (*left*) and females (*right*).

Densitometry	WT	WT	WT	WT	WT	WT	WT	WT	WT	WT	fatKO	fatKO	fatKO	fatKO	fatKO	fatKO	fatKO	fatKO	fatKO	fatKO
	M	M	M	M	M	F	F	F	F	F	M	M	M	M	M	F	F	F	F	F
ATGL CD	7.89	7.84	9.07	10.72	17.86	8.49	12.33	12.68	10.88	15.47	6.22	10.17	7.53	6.85	8.39	10.84	7.69	7.07	9.73	8.82
ATGL HFD	3.11	4.31	3.46	3.61	3.72	4.40	7.16	4.59	3.61	6.40	3.82	3.68	4.06	4.02	3.32	5.01	3.27	5.89	4.35	4.10
ABHD5 CD	2.86	5.71	2.49	2.16	2.30	5.73	8.73	6.81	5.11	7.77	2.19	2.53	2.92	2.39	2.67	3.41	2.28	5.44	5.33	4.48
ABHD5 HFD	3.32	3.42	4.27	1.87	6.49	2.98	3.92	3.36	4.18	5.21	2.28	3.62	2.35	3.52	2.34	1.29	1.65	3.02	3.08	2.34
FABP4 CD	12.38	11.48	11.78	10.79	20.97	13.93	19.66	18.92	24.40	24.06	14.54	9.47	6.23	7.41	8.85	11.61	8.11	9.77	12.64	9.67
FABP4 HFD	13.48	15.56	12.59	13.87	10.10	13.35	18.46	11.30	12.43	19.89	9.80	13.74	11.50	8.91	8.31	9.78	5.35	9.23	7.99	8.56

Supplemental Table 1. Densitometry values calculated by ImageJ for Western blots and graphs shown in Figure 8C, D. *F*, female; *M*, male.

Adipocyte hypertrophy and impaired function arise when adipocytes reach their capacity for lipid storage, at which point ectopic lipid deposition occurs in other organs and tissues including liver (Haczeyni, et al., 2018). Thus, livers in SK1^{fatKO} mice were tested for pathology consistent with non-alcoholic fatty liver disease. HFD-fed SK1^{fatKO} mice showed over 2-fold increase in liver TAG relative to control mice fed HFD (Figure 9A), and this was consistent with Oil Red O staining of neutral lipid, which showed increased lipid and also that both male and female mice exhibited macrosteatosis (Figure 9B). Liver steatosis can arise from several mechanisms including increased lipid uptake, decreased lipid secretion, or increased lipogenesis. Because serum NEFA were lower in SK1^{fatKO}, increased uptake seemed an unlikely mechanism. However, lipogenic machinery *Dgat2* and *Fasn* mRNA were significantly elevated on control and/or HFD (Figure 9C, D). In addition to steatosis, further evidence of progression of non-alcoholic fatty liver disease (NAFLD) included *Mcp1* and *Tnfα* increase in HFD-fed SK1^{fatKO} (Figure 9E, F). Fibrogenic activity was suggested by elevated *Col1a1* mRNA, which increased in male mutant mice (Figure 9G). Data were separated by sex to illustrate that male mice more strongly exhibit the effects of liver fibrosis than female mice, who showed no significant increase. This is consistent with data showing that females of reproductive age exhibit less fibrosis in NAFLD (Ballestri, et al., 2017).

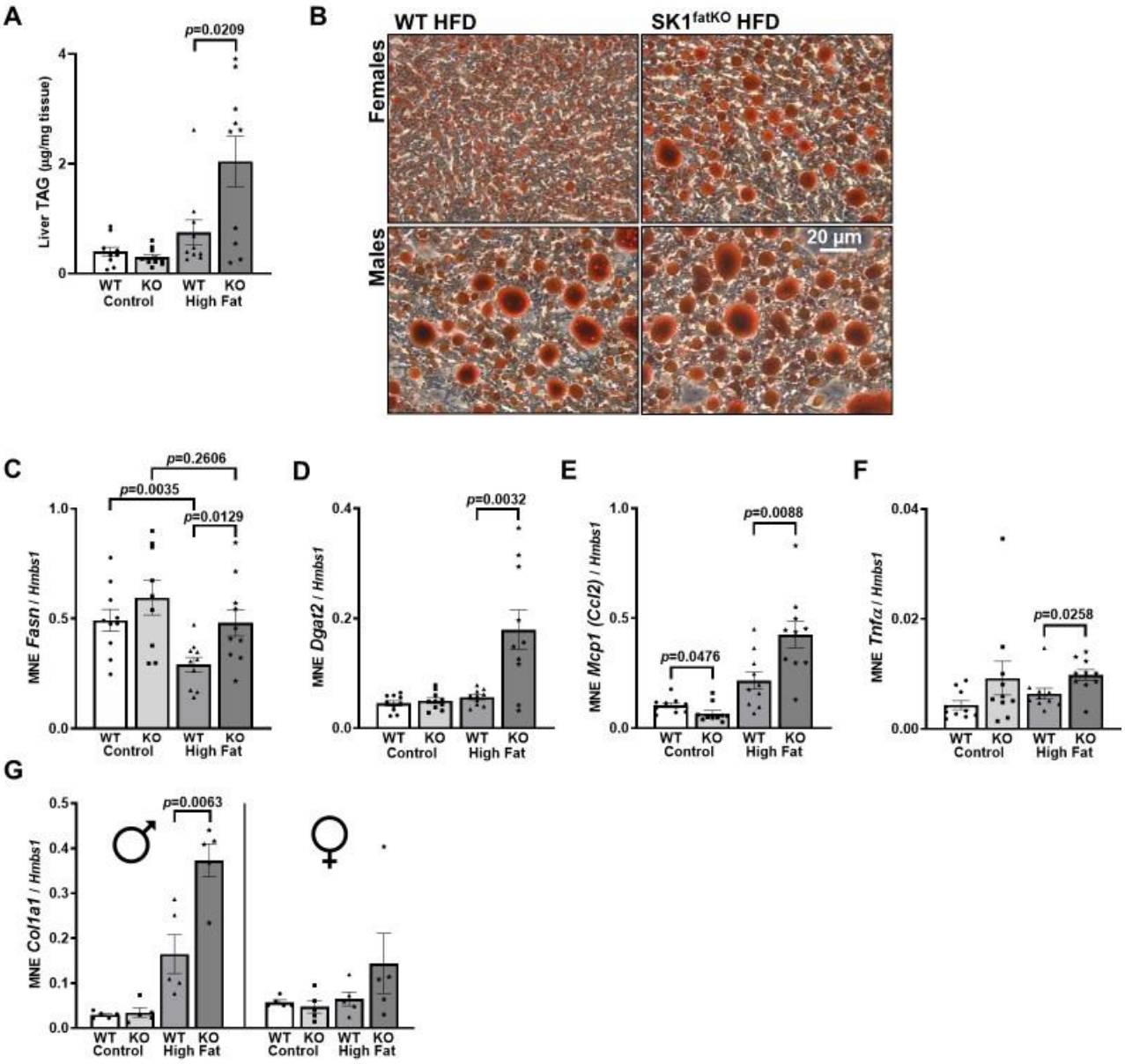

Figure 9. Serum triacylglycerol, liver lipid accumulation, and lipogenesis. **A.** Total liver triacylglycerols. **B.** Oil Red O-stained sections of HFD condition, separated by sex. **C.** Liver lipogenic gene expression of *Fasn*. **D.** Liver lipogenic gene expression of *Dgat2*. **E.** Liver pro-inflammatory cytokine marker *Mcp1I* mRNA

(*Figure 9 legend continued.*)

expression. **F.** Liver pro-inflammatory cytokine marker *Tnfα* mRNA expression. **G.** Liver pro-fibrogenic expression of *Col1a1*, separated by sex, males on left, females on right.

3.3. Discussion

Previous data from the Cowart lab and others indicated that sphingosine kinase 1 was involved in pathological mechanisms related to metabolism in various tissues, including adipose, muscle, liver, and pancreas (Aguilar-Salinas and Viveros-Ruiz, 2019; Geng, et al., 2015; Qi, et al., 2013; Ross, et al., 2013). Furthermore, previous studies have shown that constitutive deletion of SPHK1 elicits protection from high fat diet-induced diabetes and inflammation (Wang, et al., 2014). Given the importance of adipose tissue function on whole-body metabolism and its role in the development of the metabolic syndrome, the goal in this study was to determine whether adipocyte SPHK1/S1P plays a specific role in pathophysiology associated with obesity. Specifically, as S1P is largely a pro-inflammatory lipid mediator, and adipose tissue inflammation occurs in obesity and is thought to underlie maladaptive responses to obesity, we hypothesized that depletion of adipocyte *Sphk1* would be protective in the obese context. Surprisingly, however, physiological characterization of $SK1^{fatKO}$ mice revealed that SPHK1 depletion from adipocytes exacerbated outcomes of diet-induced obesity in mice. Specifically, $SK1^{fatKO}$ mice gained more weight, had hypertrophic adipocytes, and had decreased glucose tolerance relative to controls, and they exhibited liver steatosis and inflammation indicative of a NASH phenotype. These findings suggest that adipocyte SPHK1 is required for normal systemic metabolic homeostasis and also can at least partially attenuate some negative outcomes of obesity.

As the product of SPHK1, sphingosine-1-phosphate, is an established immune cell chemoattractant, we were surprised to see little impact of SPHK1 depletion on adipose tissue inflammatory markers in HFD-fed mice. Though two key indicators of an inflammatory phenotype, Tnfα and IL-6, showed a trend toward decrease in $SK1^{fatKO}$ on

HFD relative to controls on HFD, these measures did not reach statistical significance. Additionally, neutrophil infiltration, previously shown to be influenced by the S1P signaling axis in liver (Allende, et al., 2011), was not notably different in adipose tissue between genotypes in this study. As yet undiscovered outcomes of SPHK1 depletion in adipocytes therefore must outweigh the potential protection from inflammation. This is intriguing, as adipose tissue inflammation is thought to be a central link between obesity and insulin resistance. Therefore, as these animals had an exacerbated metabolic phenotype with no increase in inflammation, this study essentially de-couples adipose tissue inflammation from insulin resistance. This also indicates that the protection from adipose tissue inflammation in obesity as previously observed in the constitutive SPHK1-null mouse arose from SPHK1 in other cell types and not adipocytes. Therefore, the findings suggest that SPHK1 has homeostatic roles in adipocytes in the obese context, an idea that has not been appreciated before.

While molecular mechanisms by which SPHK1 regulates adipocyte function and resulting metabolic homeostasis, some findings from this study may shed light on roles of adipocyte SPHK1 in obesity. First, decreased lipolytic enzymes were observed in $SK1^{fatKO}$ mice, consistent with lower fasting NEFA, lower glycerol release of explants, and larger adipocytes. This suggests a fundamental role for SPHK1 in facilitating lipolysis in obesity; as unrestrained lipolysis elevates NEFA in metabolic disease, and because $SK1^{fatKO}$ animals had reduced NEFA, this might present a strategy for modulation of circulating lipids.

Second, TGF-β1 was much higher in $SK1^{fatKO}$ adipose tissue homogenates on HFD than that of control mice on HFD. TGF-β1 is largely anti-adipogenic and promotes adipocyte de-differentiation (Zamani and Brown, 2011), which could potentially underlie

the hypertrophic adipocyte phenotype. This idea is supported by findings that deletion of SMAD3, a downstream signaling effector of TGF-β1, decreased adipocyte size (Tan, et al., 2011). Numerous studies across a variety of experimental contexts place TGF-β1 upstream of SPHK1, especially in the context of fibrosis (Sato, et al., 2003; Trojanowska, 2009); our results suggest that SPHK1 negatively regulates TGF-β1, which not only presents an additional relationship between the SPHK1 and TGF-β1 axis but also suggests a negative feedback loop that is potentially important in adipocyte regulation.

Third, adipocyte hypertrophy is strongly associated with adipose tissue inflammation, which is thought to contribute to systemic insulin resistance in obesity (Hajer, et al., 2008; Scherer, 2006). However, as previously discussed, $SK1^{fatKO}$ mice had little if any differences in HFD-induced gWAT inflammatory markers which actually trended toward a decrease relative to control mice. This suggests that, though SPHK1 may mediate inflammation downstream of adipocyte hypertrophy, a beneficial role of SPHK1 in regulating adipocyte size and lipolysis is supported by our findings here, suggesting dual and opposing roles for adipocyte SPHK1 in obesity.

Despite lowered trends in lipolysis, mutant mice were still highly glucose intolerant and heavier compared to their control counterparts (Figure 5A, B, D). This finding stands in contrast to other lipolysis-deficient models, such as *Atgl* knockout mice which have vastly different body temperatures and drastic ectopic cardiac lipid deposition compared to control mice, whereas we did not observe such changes (*data not shown*) (Haemmerle, et al., 2006). Furthermore, in a model of pharmacological inhibition of lipolysis, in which mice were treated with the compound Atglistatin, adipocyte size was decreased and body weight was significantly lowered compared to untreated mice, which also contrasts to the greater weight gain and adipocyte hypertrophy observed here in $SK1^{fatKO}$ animals (Figure

5A, B, 7C) (Schweiger, et al., 2017). These apparent discrepancies suggest that, though lowering ATGL may protect from pathology associated with obesity, other effects of SPHK1 depletion outweigh any potential protection. Furthermore, combined with the effects on ABHD5 and FABP4, this may indicate an overall lesser ability to perform lipolysis in adipose tissue from mutant mice (Figure 8C, D). Intriguingly, ATGL-null mice do not exhibit differences in basal adipose glycerol release compared to control, suggesting that other lipases contribute to lipolytic products secreted from the tissue (Haemmerle, et al., 2006). This could include other players such as G0S2, FSP27, HILPDA, and/or PNPLA3 (which were not assessed here) (Schreiber, et al., 2019; Yang and Mottillo, 2020).

In this study we adhered to recent imperatives to study both sexes. In general, data were similar between male and female animals. In some instances, trends were the same and statistically significant within each sex, but combining sexes led to greater variation and therefore higher *p*-values. In cases where data from each sex would lead to different conclusions, data were presented separately for male and female animals. For example, serum levels of adiponectin, an insulin-sensitizing adipokine that is largely beneficial in the metabolic context, were lower in male mice. On the other hand, *Col1a1* expression was higher in male mice. In general, these findings agree with current literature on sex differences in cardiometabolic disease. Additionally, because the major phenotypes described did not differ between sexes (*e.g.*, decreased glucose tolerance, adipocyte hypertrophy, *Tgf-β1* expression on HFD, etc.), parameters that were distinct between sexes do not likely underlie the common phenotypes. For some investigators, however, these differences may be of interest.

While inter-organ crosstalk in obesity is of increasing interest, the mechanism(s) by which *Sphk1* depletion in adipocytes causes NAFLD symptoms are not understood. Normally, the liver serves as a short-term reservoir for excess circulating lipid from the diet and adipose tissue lipolysis, along with lipids generated by the liver through *de novo* lipogenesis. NAFLD progresses as lipid supply exceeds the rate at which the liver can utilize or export it. Impairments of glucose signaling and adipose tissue expansion, along with adipose inflammation and toxic lipid overload all contribute to the development of steatosis. NAFLD progression is multifaceted and it is increasingly evident that adipose tissue impairment is directly involved, but these mechanisms are not fully defined (Azzu, et al., 2020). We show elevation of machinery for *de novo* lipogenesis, which may explain simple steatosis in the liver; however, mechanisms by which this could occur from ablation of SPHK1 in adipocytes will require further study to uncover. A recent study suggested that extracellular vesicles from adipocytes could deliver TGF-β1 to hepatocytes, where it is pro-fibrotic (Koeck, et al., 2014). Indeed, we observed increased *Tgf-β1* in adipocytes and increased expression of *Col1a1* in liver in $SK1^{fatKO}$ animals on HFD. While reduced glucose tolerance and adipose expandability are likely contributors to the steatosis observed in high fat diet-fed $SK1^{fatKO}$ mice, further studies will be required to determine mechanisms mediating SPHK1-dependent adipocyte-liver crosstalk.

In conclusion, as SPHK1 generates sphingosine-1-phosphate, a pro-inflammatory lipid mediator, and its global depletion protected from numerous metabolic phenotypes in diet-induced obesity in mice, we hypothesized that its depletion in adipocytes would also protect from pathological outcomes associated with high fat feeding. However, we found that adipocyte-specific depletion of SPHK1 led to exacerbated glucose intolerance, adipocyte hypertrophy, and impaired lipolysis, supporting a beneficial role for SPHK1 in

adipocytes in the obese context. In addition to revealing novel functions of SPHK1 in adipocytes, our findings may have implications for targeting the SPHK/S1P axis for therapeutic advantage in multiple contexts.

3.4. Experimental Methods

Generation of Adipocyte-Specific Sphk1 Knockout ("SK1^{fatKO}") Mouse

Adipocyte-specific *Sphk1* knockout mice (SK1^{fatKO}) were generated by crossing B6; FVB-Tg(Adipoq-cre)1Evdr/J (Jackson Laboratory strain 010803) and B6N.129S6-Sphk1^{tm2Cgh}/J (Jackson Laboratory strain 019095) (Pappu, et al., 2007). Heterozygous mice were crossed to generate homozygous *flox/flox* or +/+ breeding pairs. Genotype was confirmed using primers for the floxed *Sphk1* and *Adipoq-Cre*. Cre-mediated homologous recombination removes exons 3-6 from the *Sphk1* gene (Supplemental Figure 1A). WT mice were all Cre carriers. Primers used for genotyping were as follows:

Cre1 5' ACGGACAGAAGCATTTTCCA 3'

Cre2 5' GGAGTGCCATGTGAGTCTG 3'

Cre3 5' CTAGGCCACAGAATTGAAAGATCT 3'

Cre4 5' GTAGGTGGAAATTCTAGCATCATCC 3'

Flox F 5' GGAACCTGGCTATGGAACC 3'

Flox R1 5' ATGTTTCTTTCGAGTGACCC 3'

Flox R2 5' AATGCCTACTGCTTACAATACC 3'.

Gene depletion was confirmed by PCR amplification of a shortened fragment of the *Sphk1* gene in adipocyte genomic DNA from flox/flox:CRE/CRE mice, further described below and shown in Supplemental Figure 1.

Animal Model

All animal experiments conformed to the Guide for the Care and Use of Laboratory Animals and were in accordance with Public Health Service/National Institutes of Health guidelines for laboratory animal usage. The experimental groups consisted of male and

female WT and SK1^{fatKO} C57BL/6 mice. Mice were housed in the animal facility at the Medical University of South Carolina (*in vivo* studies), and Virginia Commonwealth University (*ex vivo* studies). Food and water were provided ad libitum, except when fasting was required (*e.g.*, glucose tolerance testing). Animals were maintained on a 12h:12h light:dark cycle and ambient temperature was steadily 21° Celsius (C). Animals were randomized to a high saturated fat diet (HFD) (Envigo, TD.09766) (60% kcal provided by milkfat) or an isocaloric low fat diet (CD) (Envigo, TD.120455) (17% kcal provided by lard) at 6 weeks of age, and diets were administered for 18 weeks (*n* = 8-10 per group). On the day of sacrifice, mice were fasted for 6 hours, and mice were euthanized humanely by isoflurane (Hospira, Inc., Lake Forest, IL) followed by cardiac puncture. Cardiac blood was prepared for non-hemolyzed serum, aliquoted, and stored at -80° C until further analysis. Tissues were collected accordingly as fresh fixed in 10% neutral buffered formalin or fresh snap frozen in liquid nitrogen and stored at -80° C until further processing. All experiments were performed under clean conditions, were approved by the Medical University of South Carolina Institutional Animal Care and Use Committee, the Virginia Commonwealth University Institutional Animal Care and Use Committee, the Ralph H. Johnson Veterans Affairs Medical Center, and the Hunter Holmes McGuire Veterans Affairs Medical Center.

Glucose Tolerance Test

Intraperitoneal glucose tolerance tests were performed on mice after 8 weeks of diet feeding (*i.e.*, 14 weeks of age). Mice were fasted for 6 hours, before conducting a glucose tolerance test, generally 0830 hr to 1430 hr. Blood was collected through a nick in the tail and analyzed neat using a One Touch UltraSmart Blood Glucose Monitoring System at fasting for baseline blood glucose concentration. Mice received a sterile 2 mg/kg D-

glucose injection. Blood glucose was then assessed 15, 30, 60, and 120 minutes after glucose injection.

Bioplex

Serum cytokines (insulin, leptin) were measured using a multiplex adipokine assay service, akin to an ELISA method (Eve Biotechnologies).

Triglyceride Assay

Liver tissue homogenates were prepared according to the manufacturer's instructions with modifications (StanBio, 2200-225). Approximately 50 mg of liver tissue was homogenized in 300 µL of solution of 2:1 100% EtOH and 30% KOH, respectively. This was vortexed and allowed to incubate in a 60° C water bath for 5 hours until the solution turned a translucent yellow with a visible pellet at the bottom. Then, 1.08 volumes of 1 M $MgCl_2$ was added to the tube and vortexed to reach a milky consistency and left on ice for 10 minutes. Following this, tubes were vortexed and centrifuged for thirty minutes at 18,500 × g at ambient temperature. The supernatant was collected, diluted 1:10 with 1x PBS, and subjected to the triglyceride assay according to the manufacturer's instructions. In order to normalize to protein concentration by BCA, an aliquot was taken from the homogenate prior to water bath incubation, dried down, and resuspended in 1x PBS. 10 µL of sample and standards were assayed with 250 µL of the triglyceride reagent. Water was used as a blank. Absorbances were read after 5 minutes' incubation at 37° C at 500 nm.

qPCR

Total RNA was isolated from gonadal adipose tissue and liver tissue homogenized in Trizol (Invitrogen, 15596026) followed by RNeasy mini kit (Qiagen, 74106) extraction and column purification. RNA integrity in tissue was assessed using the Agilent 2100 Bioanalyzer by the MUSC Proteogenomics Facility. All RNA samples had RIN > 7. cDNA was synthesized from 1 µg of total RNA using iScript Advanced cDNA Synthesis Kit (Bio-Rad, 1708890). Real time PCR was performed using a CFX96 Real-Time System (Bio-Rad) and SSoAdvanced Sybr (Bio-Rad, 172-5272). The following primers were used: *Tbp* (Qiagen, PPM03560F), *Ppia* (Qiagen, PPM03717B), *Tnfα* (Qiagen, PPM03113G). Mean normalized expression was calculated by normalizing to the geometric mean of reference genes *Ppia* and *Tbp* in gonadal adipose tissue (*i.e.*, $root_2[C_q$ gene 1 × C_q gene 2]) using the $2^{-\Delta\Delta Ct}$ method. Mean normalized expression was calculated by normalizing to the expression of *Hmbs1* in liver tissue. Other primers are listed below:

Gene	Forward (5' to 3')	Reverse (5' to 3')
Tbp	AAGGGAGAATCATGGACCAG	CCGTAAGGCATCATTGGACT
Ppia	GAGCTGTTTGCAGACAAAGTTC	CCCTGGCACATGAATCCTGG
Hmbs1	ATGAGGGTGATTCGAGTGGG	TTGTCTCCCGTGGTGGACATA
Adipoq	TGTTCCTCTTAATCCTGCCCA	CCAACCTGCACAAGTTCCCTT
Arg1	TGGCTTGCGAGACGTAGAC	GCTCAGGTGAATCGGCCTTTT
Dgat2	GAGGGGTCTGGGCGATGGGGCAC	CGACGGTGGTGATGGGCTTGGAGT
Fasn	GACTCGGCTACTGACACGAC	CGAGTTGAGCTGGGTTAGGG
F4/80	TCATGGCATACCTGTTCACC	GAATGGGAGCTAAGGTCAGTC
Il-6	TAGTCCTTCCTACCCCAATTTCC	TTGGTCCTTAGCCACTCCTTC
iNOS	TTCCATGCTAATGCGAAAGG	GCTCCTCTTCCAAGGTGCTT
Mcp1	TTAAAAACCTGGATCGGAACCAA	GCATTAGCTTCAGATTTACGGGT
Sphk1	GAGTGCTGGTGCTGCTGAA	AGGTTATCTCTGCCTCCTCCA
Sphk2	CACGGCGAGTTTGGTTCCTA	CTTCTGGCTTTGGGCGTAGT
Tgf-β1	TGGCGTTACCTTGGTAACC	GGTGTTGAGCCCTTTCCAG

Basal Lipolysis Assay for Non-esterified Fatty Acids

Sera from mice and cell culture media containing only fatty acid-free bovine serum albumin were prepared for non-esterified fatty acid assay according to the manufacturer's instructions (Wako Diagnostics, 999-34691, 995-34791, 991-34891, 993-35191, 276-76491). Briefly, 5 µL of sample (neat or diluted 1:10), calibrators, and blank were added in duplicate to a 96-well plate. 200 µL of Color Reagent A solution was added and incubated at 37° C for 5 minutes. Absorbance at 550 nm was acquired. Next, 100 µL of Color Reagent B solution was added and incubated at 37° C for 5 minutes. Absorbance was read once more at 550 nm. After subtracting the blanks, the first reading was subtracted from the second reading to obtain the final absorbance, and concentrations were determined by standard curve normalization.

Glycerol Assay

Protocol was adapted from Sigma. 25 µL cell culture media was assayed in duplicate in a 96-well plate. 100 µL of free glycerol reagent (Sigma, F6428) was added per well and incubated for 5 minutes at 37° C. Absorbance at 540 nM was measured on a spectrophotometer. Relative concentrations of glycerol were determined by normalization to a standard curve. Tissue explants glycerol release was normalized to tissue weight.

Lipolysis in Adipose Tissue Explants (ex vivo)

Gonadal adipose tissue was harvested from WT and SK1^{fatKO} mice at 4-6 weeks of age. Tissue was cut into ~12 mg pieces. Two pieces were added to each well of a 12-well plate in 1 mL of DMEM/F12 (Corning, 10-090-CV) + 1% FAF BSA (Thermo Fisher Scientific, 9704100) and 1% penicillin streptomycin antimycotic solution (Sigma, A5955-100ML).

Explants "rested" in the incubator overnight at 37° C and 10% CO_2. The next day, explants were transferred using clean forceps to new 12-well plates containing fresh media. Media was collected after 24 hours for glycerol measurement.

Histology and Immunohistochemistry

Fresh liver tissue was snap frozen in liquid nitrogen. 10-µm frozen sections were prepared for measurement of hepatic neutral lipid accumulation by Oil Red O staining. Sections were counterstained with hematoxylin. Paraffin sections were prepared with adipose and liver tissue fixed in 10% neutral buffered formalin (1 hour). Adipose sections were stained with hematoxylin and eosin (H&E) for adipocyte size analysis. Slides were imaged on a light microscope (Leica DMI1 microscope, Leica MC170 HD camera), and only for the adipose H&E was a fluorescence microscope utilized for better contrast with a 555 laser. For immunofluorescence histology, sections were subjected to antigen retrieval overnight at 60° C in 10 mM sodium citrate, 0.05% Tween 20 pH 6.0 buffer. Slides were blocked using 5% donkey serum (host secondary antibody species). Slides were imaged on a Zeiss FV10i fluorescent microscope for myeloperoxidase (R&D Systems, AF3667, goat anti-mouse MPO, 15 µg/mL), a marker of infiltrating inflammatory immune cells. Secondary detection antibodies were from Life Technologies: Alexa 488 (Invitrogen, A-11055, donkey anti-goat, 1:2000) and ToPro3 to stain nuclei (Thermo Fisher Scientific, T3605, 1:2000). Ten representative images per slide were analyzed by fluorescence intensity of puncta using ImageJ software.

Lipid Measurements

Sphingolipids were measured using liquid chromatography/tandem mass spectrometry at the Virginia Commonwealth University Lipidomics and Metabolomics Core and performed using previously published methods (Haynes, et al., 2009; Shaner, et al., 2009).

Western Blotting

Gonadal adipose tissue was homogenized in RIPA buffer with protease and phosphatase inhibitors (Thermo Fisher Scientific, 78446) using a Dounce homogenizer for at least 30 strokes, or until visibly homogenized. Homogenates were vortexed well and centrifuged at 10,000 × *g* for 10 minutes at 4° C. The resulting infranatant (below fat cake, and above cell debris pellet) was transferred to a new tube with an insulin syringe (28.5G). Protein content was quantified using a BCA protein determination assay (Thermo Fisher Scientific, 23225). Homogenates were diluted 1:10 in RIPA with 2% SDS to minimize lipid interference in the BCA assay. 10 µg protein was used for western blotting. Non-hemolyzed mouse sera was diluted in PBS 1:20, and isovolumetric amounts of diluted sera plus loading buffer was loaded for western blotting. gWAT proteins and sera proteins were separated by SDS-PAGE (Bio-Rad Criterion TGX Stain-Free precast gels), and transferred to nitrocellulose membranes, and sera proteins were transferred to PVDF membranes. The membranes were blocked for 1 hour in 5% BSA. Proteins were detected using (gWAT) HRP-linked anti rabbit secondary (1:5000; Cell Signaling Technology, 7074) or (sera) StarBright-700-linked anti rabbit secondary (1:2,500; Bio-Rad, 12004161), Clarity ECL Western Blotting Substrate (Bio-Rad, 1705061) for HRP, and a ChemiDoc Imaging System (Bio-Rad, 17001401, 17001402). Blots were assessed for protein expression of adiponectin (1:2000; Cell Signaling Technology, 2789), adipose triglyceride lipase (ATGL)

(1:2000, Cell Signaling Technology, 2439), ABHD5 (CGI-58) (1:1000, Novus Biologicals, NB100-5-7850), and FABP4 (1:2000, Cell Signaling Technology, 2120). Vinculin (1:2,000; Cell Signaling Technology, 4650) and stain-free total protein were used to determine even loading. Band intensity was quantified using ImageJ.

Statistical Analysis

All values are presented as mean ± SEM. For single pairwise comparisons of normally distributed data sets, a Student's t-test was performed. For multiple comparisons of means, a one-way ANOVA with Tukey-Kramer post hoc test was performed. $p < 0.05$ was considered statistically significant. All hypothesis tests were conducted using Graphpad Prism 8 software. Experiments were performed in both male and female mice; data are shown by sex only where there were statistically significant differences between male and female experimental groups.

CHAPTER 4

ADIPOCYTE SPHINGOSINE KINASE 1 REGULATES HISTONE MODIFIERS TO DISRUPT CIRCADIAN FUNCTION

(ANDERSON, et al., 2020)

Primary Research Manuscript

4.1. Introduction

Biology abounds with compensatory and reversible mechanisms. Indeed, organismal fitness arises from the ability to rebound from stimuli and return to basal homeostasis. One such example of rebounding is the apparent *de novo* biosynthesis of sphingolipids, a class of lipids specialized in signaling functions that range from cell survival, apoptosis, growth, proliferation, differentiation, and others (Hannun and Obeid, 2018; Harrison, et al., 2018; Ogretmen, 2018). To “rebound” from nutrient overload, the free fatty acid palmitate (or other fatty acid species, such as myristate) may be shunted to the sphingolipid biosynthesis pathway to condense with an amino acid such as serine to generate sphingolipids (*see Figure 3*) (Russo, et al., 2012). Ultimately, a delicate balance is achieved among the levels of these lipid structural and signaling metabolites in the cell, including: sphingomyelin, ceramide, glycosphingolipids, ceramide-1-phosphate, sphingosine, and sphingosine-1-phosphate (S1P) (Breslow and Weissman, 2010; Harrison, et al., 2018; Snider, et al., 2019). The subject of this work is sphingosine kinase 1, responsible for the catalysis of sphingosine phosphorylation, thereby generating a bioactive signaling sphingolipid, S1P, capable of a wide variety of functions, ranging from intracellular to autocrine and paracrine signaling (Hannun and Obeid, 2018; Ogretmen, 2018; Takabe, et al., 2008). Sphingosine kinase 1 (SPHK1) is widely studied for its role as an oncogenic kinase, highly stimulated by most growth factors, including the growth factor cocktail used to synchronize cultured cells for circadian analysis (Hatoum, et al., 2017; Kapitonov, et al., 2009; Kleuser, et al., 2001).

Circadian rhythm research, the study of biological patterns that follow the day, is gaining greater traction due to the Nobel Prize awarded in Medicine or Physiology in 2017 to circadian researchers, thus boosting interest and popularity. Circadian rhythm evolved

to compensate for and anticipate the day and night phenomena generated by the rotation of the Earth on its axis as it revolves around the sun (Dunlap and Loros, 2017; Gerhart-Hines and Lazar, 2015). Fitness and viability of many organisms depended on seeking food during the hours of sunlight and resting by shelter in the hours of darkness (Egli, 2017). Humans experience a highly disruptive circadian pattern in today's 24/7 artificially-lit society (Brown, et al., 2019; James, et al., 2017; Pilorz, et al., 2018). This disruption is far too great to be compensated and has therefore wrought itself in pathological manifestations including but not limited to obesity, cardiovascular disease, organ failure, cancer, metabolic syndrome, thyroid dysfunction, and compromised immune function (Asher and Schibler, 2011; Ikegami, et al., 2019; Johnston, et al., 2016; Truong, et al., 2016).

The circadian clock oscillator is understood at the molecular level as a transcriptional translational feedback loop that has an intrinsic, free-running periodicity of approximately 24 hours. The positive limb of the core loop is comprised of BMAL1 and CLOCK which heterodimerize as transactivators to enhance the expression, by binding E-box elements, of their targets the PERIODs (1, 2, 3) and CRYPTOCHROMEs (1, 2), of the negative core loop; REV-ERBs (α, β), of the negative accessory loop; and RORs (α, β, γ), of the positive accessory loop (*see Figure 2*). As PERIOD and CRYPTCHROME build up, these protein products heterodimerize in a large complex to translocate to the nucleus to repress BMAL1:CLOCK activity, thereby leading to net decreases in their (PER:CRY) levels due to this lack of transcription as well as coordinated ubiquitination-mediated degradation. Once PER:CRY complexes are degraded, BMAL1:CLOCK may-reinitiate another cycle of transcription (*reviewed in* Hardin and Panda, 2013).

Interestingly, findings in the last decade point to circadian oscillations in the sphingolipid biosynthetic system (Brunkhorst, et al., 2019; Druzd, et al., 2017; Hogenesch, et al., 2013-2018; Loizides-Mangold, et al., 2017). The Cowart lab was previously interested in the role of SPHK1 in the adipocyte, which is also a strongly circadian-governed cell type (Bray and Young, 2007; Shostak, et al., 2013; 2013a; van der Spek, et al., 2012). Moreover, the Cowart lab previously identified a role for adipocyte SPHK1 in the maintenance of liver homeostasis, highlighting the impact of adipose:liver crosstalk (Anderson, et al., 2020; Cai, et al., 2018; Rosso, et al., 2019; Ye, et al., 2017). Furthermore, many investigators have shown that histone modifications and their circadian regulation are highly coordinated in the liver to affect numerous metabolic outcomes, such as cholesterol synthesis and secretion (Cox and Takahashi, 2019; Ferrell, et al., 2015; Kovář, et al., 2010; Sobel, et al., 2017). Precedence also existed for S1P influencing the activity of histone-modifying enzymes (Hait, et al., 2009, 2020). Therefore, the hypothesis was that SPHK1 was a circadian-controlled gene in adipocytes and that lack of SPHK1 may influence the circadian features of the adipocyte. This hypothesis was tested by subjecting wildtype and SPHK1-depleted primary adipocytes to standard circadian synchronization procedures in culture and tested the effects of synchronization on *Sphk1* and, conversely, the effects of SPHK1 depletion on circadian gene and protein expression as well as adipocyte functional processes such as circadian histone modifications.

4.2. Results

The Cowart lab and others have empirically highlighted the multifaceted roles of sphingosine kinase 1 (SPHK1) in metabolic disorders and obesity (Anderson, et al., 2020; Geng, et al., 2015; Ross, et al., 2013; Wang, et al., 2014). Specifically, in high fat diet-induced obesity, adipocyte sphingosine kinase 1 contributes to maintenance of lipolysis and adipocyte size (protection from hypertrophy) as well as protection from liver steatosis (Anderson, et al., 2020). Since metabolism and adipocyte processes like lipolysis are tightly coupled with the circadian clock, we wondered if sphingosine kinase 1 may be regulated by the clock (Chaix et al., 2019; Lemmer and Oster, 2018; Shetty, et al., 2018; Zimmet, et al., 2019). Even more intriguing were the mRNA Sequencing findings from the gWAT of control diet-fed WT and $SK1^{fatKO}$ mice from that study in which several circadian transcripts were either elevated or depleted (Supplemental Figure 4). All animals for the dataset were sacrificed at Zeitgeiber Time (ZT) 9 (meaning 9 hours after the light stimulus turns on in the animal housing facility, where 6 a.m. is “lights-on” and ZT0; *i.e.*, 6 a.m + 9 hours = ZT9) and fasted for 6 hours prior to sacrifice.

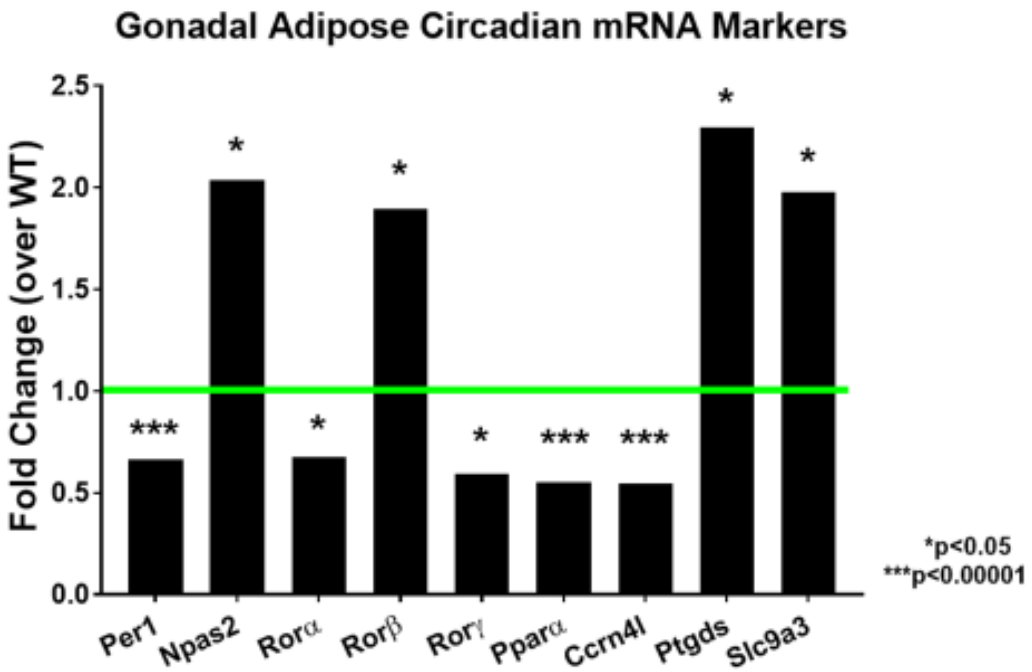

Supplemental Figure 4. SK1^{fatKO} gWAT mRNA Sequencing analysis. gWAT from pooled samples of male and female C57/bl6J mice (WT or SK1^{fatKO}) harvested at ZT9 was analyzed by paired-end fragments per kilobase million mRNA Sequencing and expressed as fold change over wildtype. *Ccrn4l, carbon catabolite repression 4-like protein (also known as nocturnin); Npas2, neuronal PAS containing 2; Per1, period 1; Ptgds, prostaglandin D2 synthase; Pparα, peroxisome proliferator activated receptor alpha; Rorα, β, γ, retinoic acid related orphan receptor alpha, beta, and gamma; Slc9a3, solute carrier family 9 member A3.*

It is already known that AP-1 and PPARα binding elements exist in the sphingosine kinase 1 promoter (Huang, et al., 2014; Lan, et al., 2011; Paugh, et al., 2009; Ross, et al., 2013). A genomic database search for the canonical 5'-CACGTG-3' E-box element in the *Sphk1* gene/promoter proved to be present almost 2 kilobases from the transcriptional start site (TSS) as well as another E-box immediately proximal to the TSS, about 300 base pairs upstream (Figure 10A). In an *in vitro* primary adipocyte model, we found that *Sphk1* did have a circadian oscillation over 24 hours, with a cosinor R^2 value of 0.76 (Figure 10B, D). The canonical negative accessory *Reverbα* (*Nr1d1*) message was measured to demonstrate a proof of principle for the circadian cell culture assay (Figure 10C, D). In the mouse primary adipocyte model, measuring SPHK1 protein was not possible due to lack of a commercially-available, reliably specific antibody for the mouse SPHK1 protein, as every antibody tested yielded a predicted SPHK1 band in SPHK1$^{-/-}$ cells (Anderson, *data not shown*).

Next, chromatin immunoprecipitation (ChIP) analysis of the same regions of the *Sphk1* promoter were assayed for the presence of the transactivator complex BMAL1 and CLOCK. Moreover, concomitant pulldowns for acetylated histone 3 lysine 27 (H3K27ac) were performed as positive controls for transcriptional activation marks. Cell synchronization was accomplished by administering a serum-shock (50% horse serum and 50% DMEM) to growth-arrested matured primary adipocytes for 2 hours, followed by a gentle wash and incubation for the next 46 hours in serum-depleted media. The time at which serum shock commenced was considered "circadian time 0" (CT0). Performing these pulldowns over a time course of 24 hours demonstrated a rhythmic signal of BMAL1, CLOCK, and H3K27ac at the *Sphk1* promoter regions of interest (Figure 10D, E). At some points over this time course, signal for the core clock transactivator was not detectable

over background, which suggested to us that indeed BMAL1 and CLOCK may contribute to the regulation of *Sphk1* expression, in part by time-dependent physical occupancy of the *Sphk1* E-boxes by the clock enhancer complex. In other words, BMAL1 and CLOCK vacate the *Sphk1* locus for some portion of the circadian period. According to the data presented, it appears that activators occupy the *Sphk1* promoter most from CT16-24 (Figure 10D, E).

To understand better the implications of these data, a lipidomics flux assay assessed whether SPHK1 exhibits time-of-day-dependent efficiency in enzymatic activity. First, cells were assessed at baseline, with only a synchronization stimulus to assess the levels of endogenous S1P (Figure 10F). Thus, cells were treated with a bolus of ^{17}C-sphingosine substrate to determine turnover to ^{17}C-sphingosine-1-phosphate (^{17}C-S1P) product. Consistent with the pulsatile expression of *Sphk1*, the generation of ^{17}C-S1P, as measured in cell culture and the cell lysates, showed time-dependent fluctuations (Figure 10G). Moreover, the values of ^{17}C-S1P produced in cells and media were combined as a single value to illustrate ^{17}C-S1P production *in toto* (Figure 10H). As analyzed by goodness of fit to a cosine curve, the production of 17C-S1P does not follow a circadian pattern as strongly as the mRNA of *Sphk1*. This is suggestive that the enzyme could have time-dependent enzymatic efficacy, or that there is time-dependent buildup of the enzyme to handle a larger substrate-to-product turnover, or perhaps other mechanisms relating to the S1P phosphatases (1 and 2) or lyase, but were not explored here.

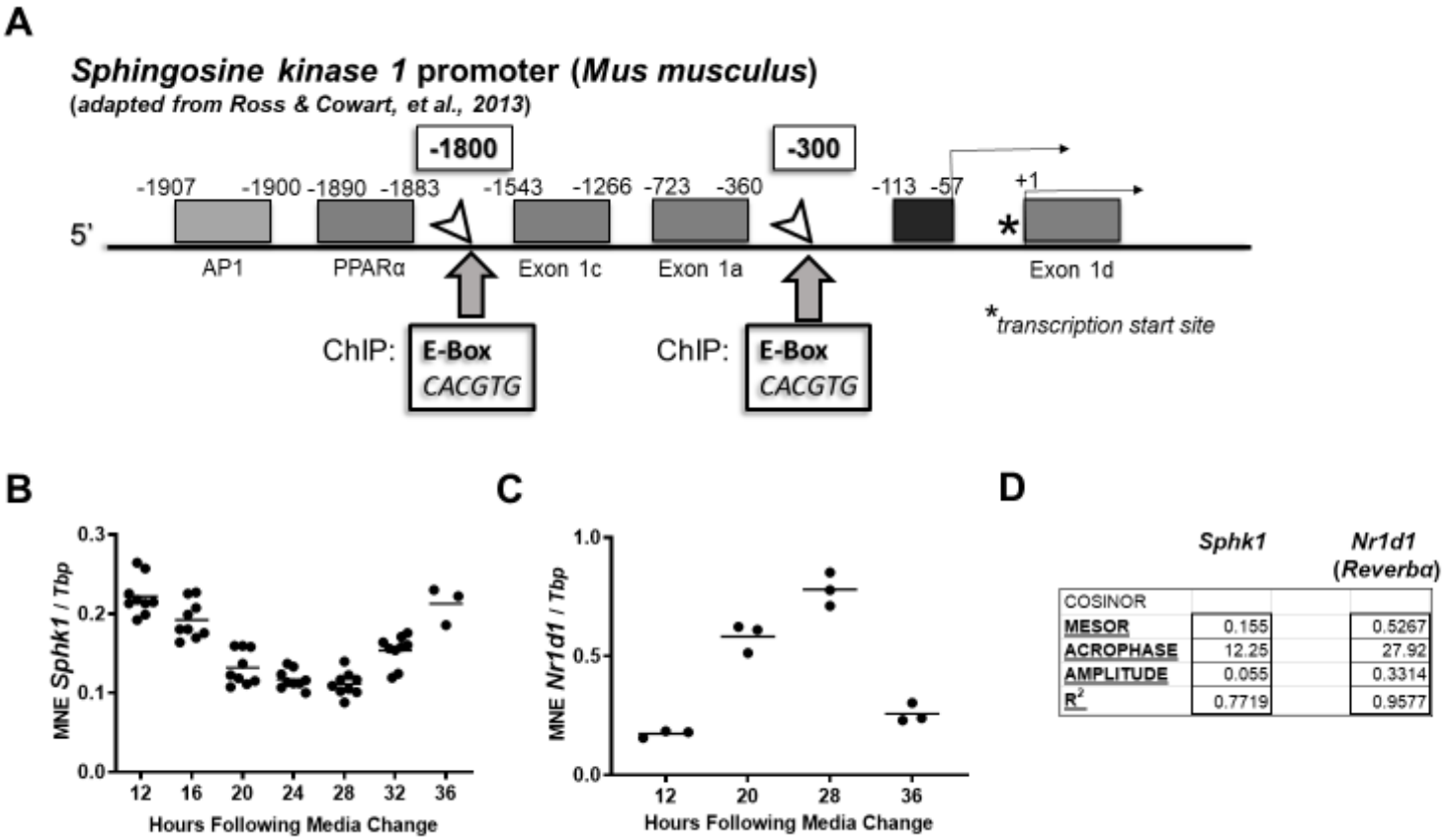

	Sphk1	Nr1d1 (Reverbα)
COSINOR		
MESOR	0.155	0.5267
ACROPHASE	12.25	27.92
AMPLITUDE	0.055	0.3314
R^2	0.7719	0.9577

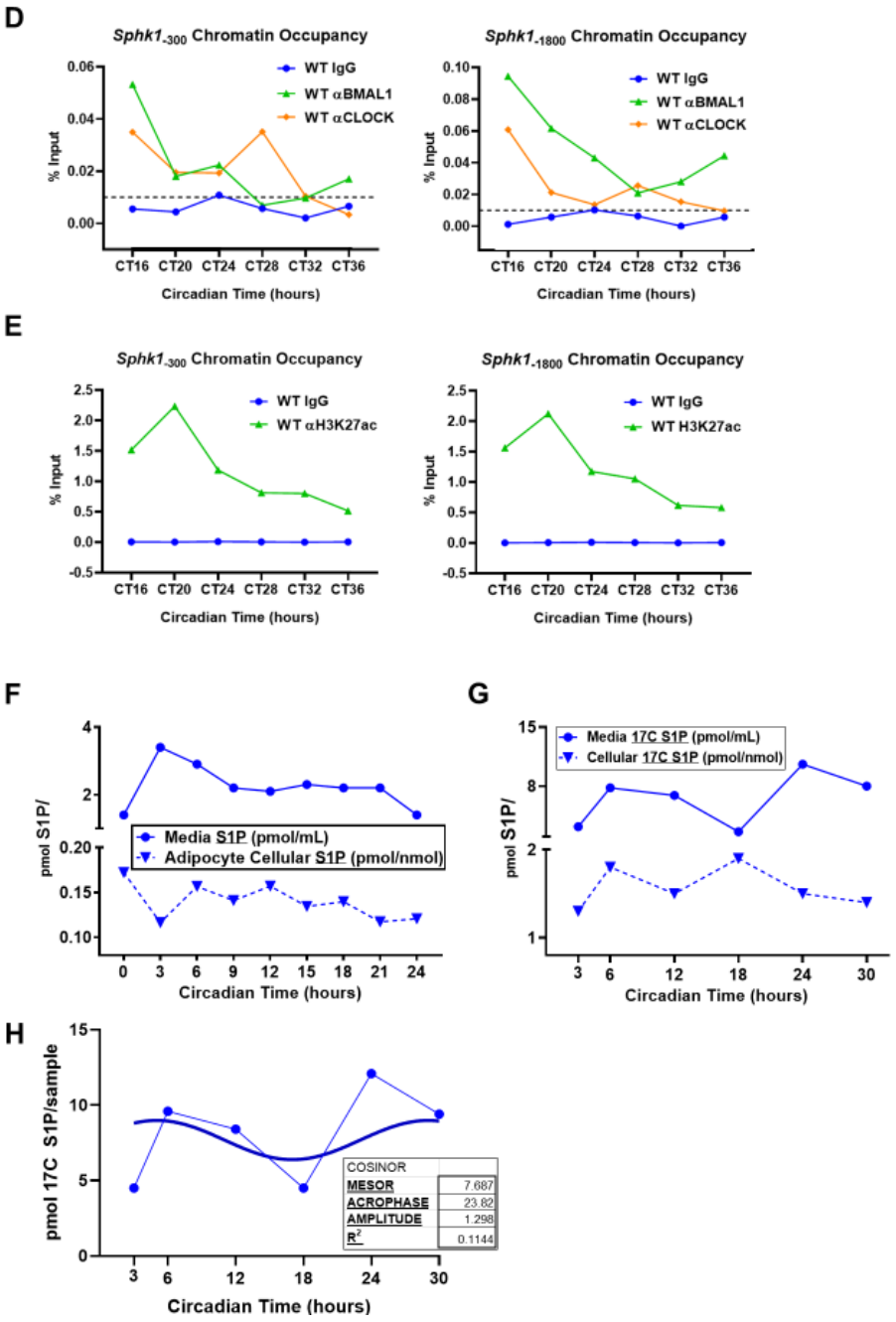

Figure 10. *Sphk1* is a circadian gene in adipocytes. A. Pictorial representation of the *Sphk1* promoter, in which multiple E-boxes reside, including positions -1800 and -300 base pairs from the transcription start site (TSS) (adapted from

(Figure 10 legend, continued.)

Ross and Cowart, et al., 2013). **B.** *Sphk1* mRNA expression in primary adipocytes over 24 hours. **C.** mRNA expression of *Reverbα (Nr1d1)* over 24 hours in the same primary adipocytes. **D.** Cosinor analysis (as described in *Methods*) of mRNA expression of *Sphk1* and *Nr1d1*. **E.** Presence of BMAL1 and CLOCK at the promoter E-box loci in *Sphk1* DNA. Anti BMAL1 and CLOCK antibodies were used to immunoprecipitate chromatin at the specified promoter locations of *Sphk1* DNA. **F.** H3K27ac is a mark of active transcription and was immunoprecipitated side-by-side with (*E.*) at the indicated *Sphk1* DNA promoter loci. **F.** Wildtype adipocytes were synchronized, and cells and media were collected at the indicated timepoints and assessed by LC:MS/MS for native endogenous S1P. **G.** Following synchronization, wildtype adipocytes ^{17}C-S1P production as measured by LC:MS/MS over a circadian time course when fed 5 μM ^{17}C-sphingosine for exactly 30 minutes prior to each harvest. **H.** From (*G.*), total levels of ^{17}C-S1P from cells and media combined were graphed over time and subjected to a cosinor analysis to show overall generation of ^{17}C-S1P. The raw data points are the thin blue line and the cosinor fit is the thick darker line. For (*D., E., F., G.*), the data shown is one representative example of three independent experiments. *CT, circadian time (CT0 is the time at which synchronization serum shock media is administered); MESOR, midline estimating statistic of rhythm ZT, Zeitgeber time*

Over the last couple years, precedence has emerged in the literature for circadian regulation of sphingolipid-associated genes. For example, the circaDB database curated by the Hogenesch group demonstrates a vast array of sphingolipid genes that fluctuate in various tissue types (Hogenesch, et al., 2013-2018). Indeed, of approximately 35,000 circadian genetic hits in mouse and 15,000 in human, *Sphk1* was found to oscillate in two mouse systems, a 3T3 cell line and the lung (Supplemental Figure 5A) (Hogenesch, et al., 2013-2018; Hughes, et al., 2009; Zhang, et al., 2014). As measured by mRNA in mouse gonadal white adipose tissue (gWAT), sphingosine kinase 1 (*Sphk1*) message had a non-constant expression profile (Supplemental Figure 5B). Moreover, it was found that patient plasma had oscillating S1P levels (Brunkhorst, et al., 2019). In addition, Scheiermann, Oster, and colleagues convincingly demonstrated the oscillation of S1P receptor 1 (*S1Pr1*), and that this oscillation specifically drove the fluctuating presence of immune cells in the bloodstream over the circadian day (Druzd, et al., 2017).

It is also already known that fatty acids oscillate in the bloodstream, and fatty acids have been shown in numerous contexts to induce the sphingolipid *de novo* biosynthetic pathway and some of its enzymatic genes, thus providing one mechanistic explanation for the observed daytime-dependent changes in sphingolipids (Bray and Young, 2007; Geng, et al., 2015; Gooley and Chua, 2014; Ross, et al., 2013; Russo, et al., 2012; Shostak, et al., 2013; van der Spek, et al., 2012; Wang, et al., 2014; Wigger, et al., 2019). Sphingolipidomics data in human skeletal muscle biopsies obtained over 24 hours were highly suggestive of diurnal regulation of various sphingolipid species (Loizides-Mangold, et al., 2017). The sphingolipid biosynthetic pathway represents a novel avenue for manipulation by therapeutics coupled with strictly scheduled dosing, or, stated differently, administration of sphingolipid-modifying drugs coupled with chronotherapy.

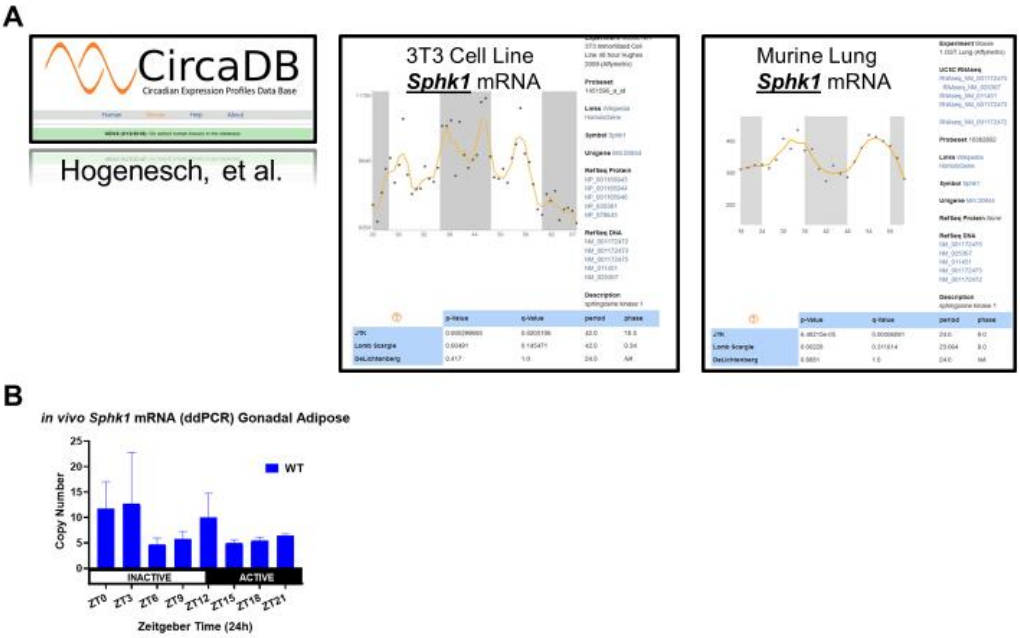

Supplemental Figure 5. *Sphk1* oscillates in 3T3 cells and murine lung tissue. A. *Sphk1* is a fluctuating gene in 3T3 cells and a bona fide circadian gene in mouse lung tissue. These data are searchable at: http://circadb.hogeneschlab.org/, and were accessed on 2020 February 2 for reproduction in this figure (Hogenesch, et al., 2013-2018; Hughes, et al., 2009; Zhang, et al., 2014). **B.** *Sphk1* mRNA expression in gWAT over time in 12hr-light:12hr-dark-entrained wildtype C57bl/6J mice.

Considering the mRNA-Seq and *in silico* findings, the next step was to utilize a controlled *in vitro* system for comparing the core clock transcripts in WT and SPHK1$^{-/-}$ adipocytes. Due to previous work in the Cowart lab characterizing the metabolic phenotype of mice lacking SPHK1 constitutively (SPHK1$^{-/-}$), a model system was readily available to dissect the consequences of SPHK1 depletion on the adipocyte circadian clock and utilize primary cells from a genetic knockout animal. After a horse serum shock synchronization, it was found that negative clock regulators, the *Per*s display a higher amplitude in mutant cells compared to control (Figure 11A, B). Furthermore, the spike in *Bmal1* mRNA in the first 4 hours is the result of the serum shock synchronization protocol (Figure 11A). For cosinor analyses of these data, the first 8 hours of data was not considered since the system was re-equilibrating after the serum shock. Moreover, the typical readout for BMAL1 transcriptional activity (but is not primarily engaged in the core clock mechanism), *Dbp (D-site of albumin promoter binding protein)*, also demonstrated a higher amplitude in mutant cells compared to control (Figure 11A, B). Interestingly, the positive regulator of *Bmal*, *Rorγ* maintained a stronger gene expression over 48 hours compared to the mutant (Figure 11A, B). The corresponding cosinor analyses for the mRNA expression profiles are shown in Figure 11C, which indicated across all genes that SK1$^{-/-}$ adipocytes have stronger baseline levels of these transcripts and generally greater amplitudes.

The protein levels for BMAL1 revealed lower expression levels in SPHK1$^{-/-}$ adipocytes, while still oscillating (Figure 11D). Despite these findings, the amplitude for BMAL1 expression oscillation was greater in SK1$^{-/-}$ adipocytes compared to control, suggesting that the total levels of BMAL1 may not necessarily dictate the transcription of its targets, but rather a larger change from peak to trough may be a larger driving factor

(Figure 11E, F). These results were obtained after normalizing both densitometry datasets to the “trough” value, which in both cases occurred at CT3. Therefore, the relative values of the oscillating BMAL1 protein could be easily compared between $SK1^{-/-}$ and WT cells for rhythmicity (Figure 11E). These values were plotted and analyzed for cosinor goodness of fit (Figure 11F). At the nuclear level, the binding partner for BMAL1, CLOCK protein expression within the nucleus increased with SPHK1 depletion (Figure 11G). This may suggest that CLOCK protein is readily poised in $SK1^{-/-}$ cells to heterodimerize with BMAL1 or that CLOCK nuclear export is compromised or another mechanism. These findings led to the overall conclusion that the adipocyte molecular circadian clock was compromised without a functional sphingosine kinase 1.

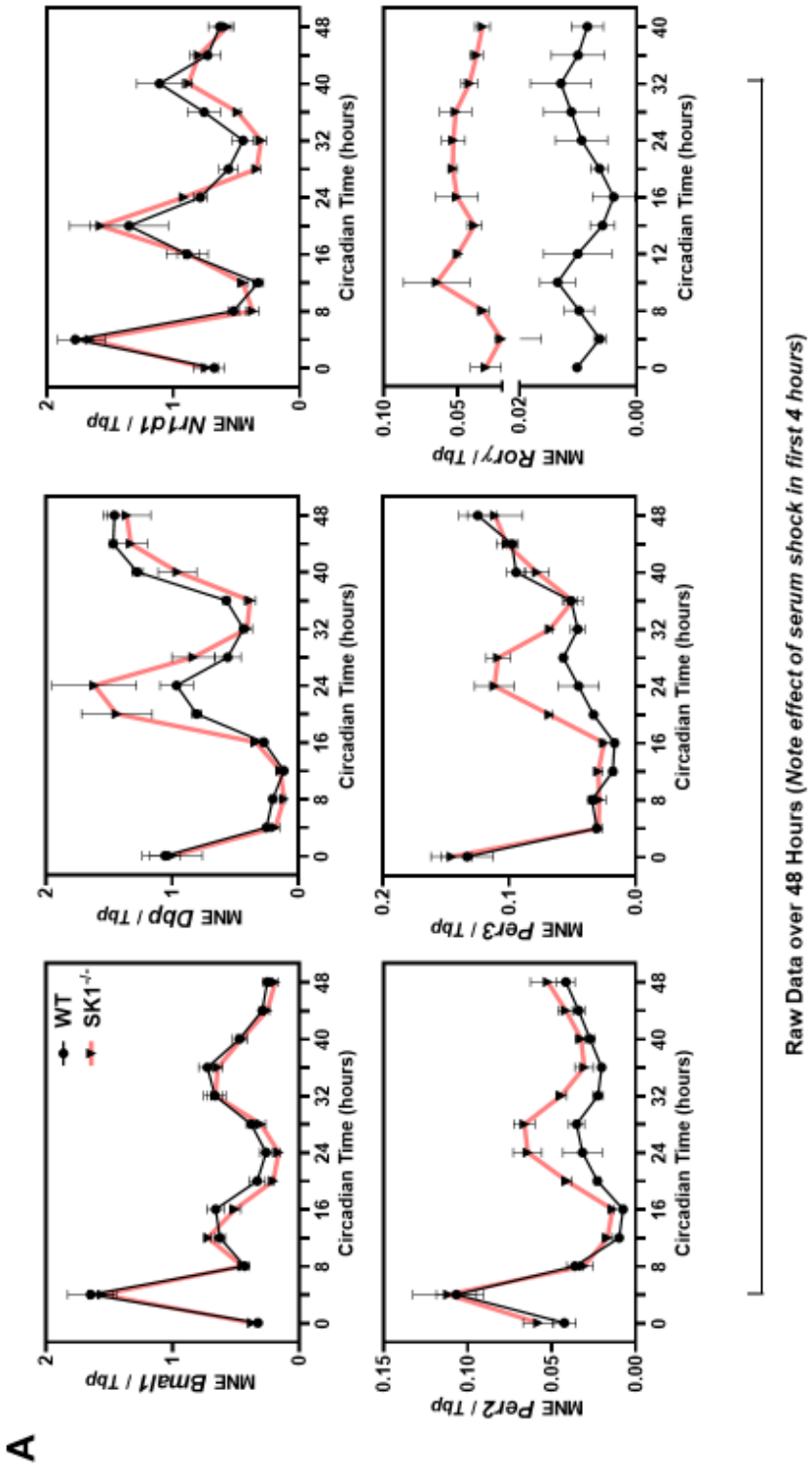

Figure 11. *(Legend on following pages.)*

B

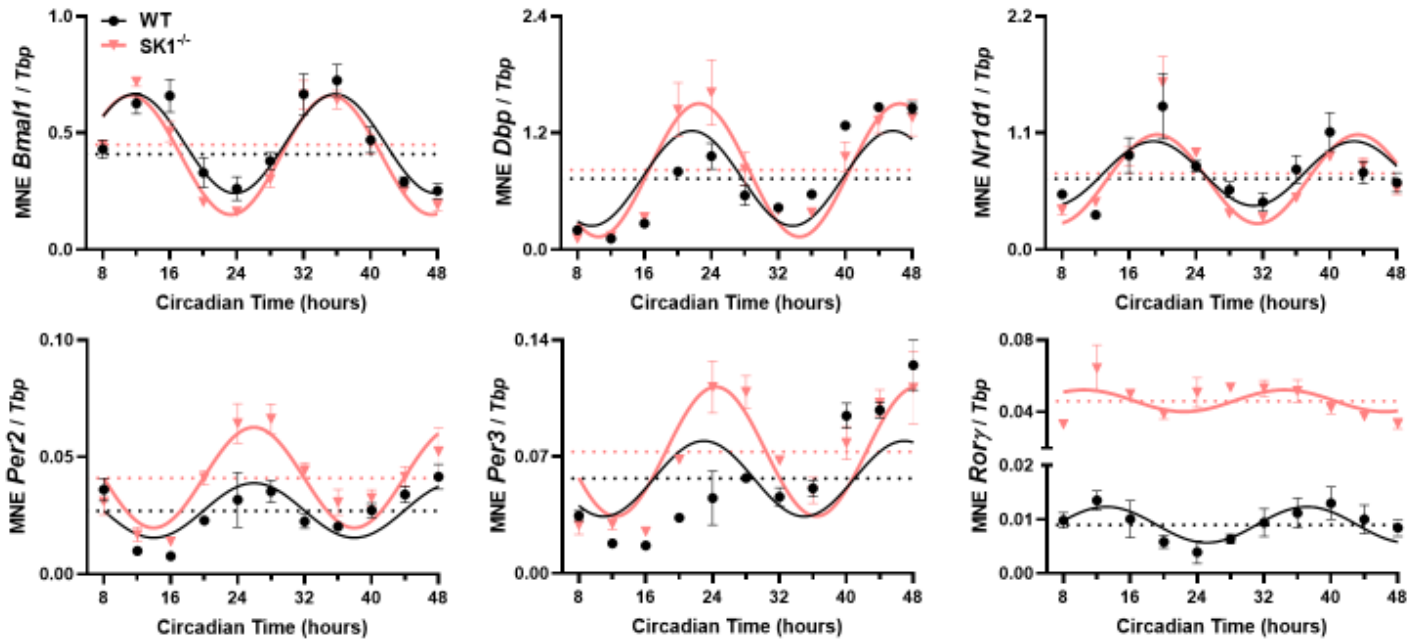

Nonlinear Regression Single-Component Cosinor Goodness-of-Fit of (A) (*Excluding first 2 timepoints*)

C

	Bmal1		***Dbp***		***Nr1d1***		***Per2***		***Per3***		***Rory***	
COSINOR	WT	SK1$^{-/-}$	WT	SK1$^{-/-}$	WT	SK1$^{-/-}$	WT	SK1$^{-/-}$	WT	SK1$^{-/-}$	WT	SK1$^{-/-}$
MESOR	0.45	0.41	0.73	0.82	0.72	0.67	0.03	0.04	0.06	0.07	0.01	0.05
ACROPHASE	34.61	12.75	44.59	31.80	20.19	20.06	43.47	27.77	47.40	25.03	12.27	12.97
AMPLITUDE	0.236	0.278	0.676	0.751	0.511	0.635	0.014	0.026	0.015	0.043	0.005	0.016
R^2	0.68	0.87	0.57	0.75	0.38	0.62	0.42	0.67	0.23	0.60	0.30	0.13

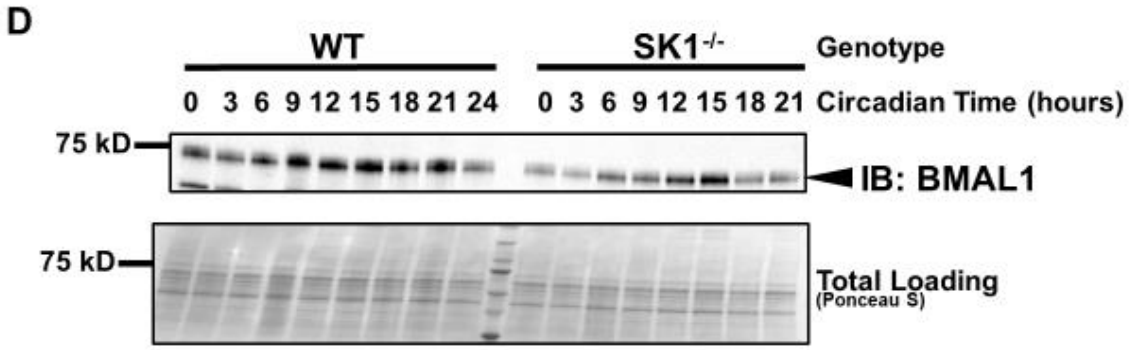

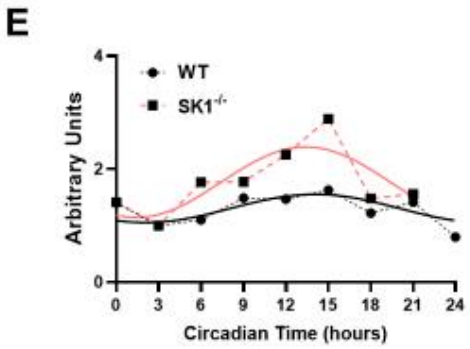

F

COSINOR	WT	SK1$^{-/-}$
MESOR	1.304	1.768
ACROPHASE	15.17	15.34
AMPLITUDE	0.2489	0.624
R^2	0.4971	0.6667

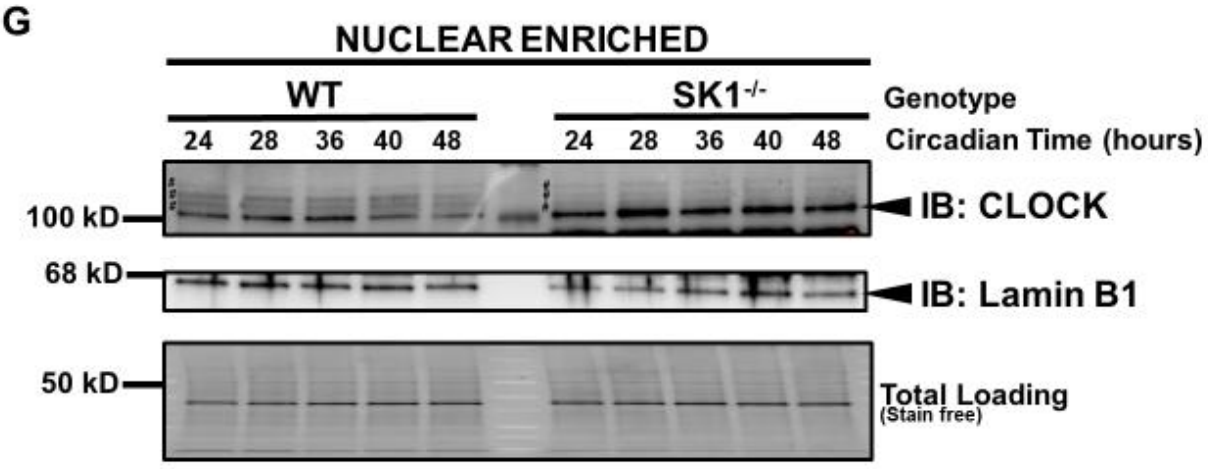

(continued from previous pages)

Figure 11. SPHK1$^{-/-}$ adipocytes have a dysfunctional circadian clock. A. mRNA rhythms of *Bmal1* (positive core loop gene), *Dbp* (canonical clock-controlled gene (ccg)), *Nr1d1* (also known as *Rev-erbα;* negative accessory loop gene), *Per2* (negative core loop gene), *Per3*, and *Rorγ* (positive accessory loop gene) in synchronized primary matured WT and SPHK1$^{-/-}$ adipocytes over a 48-hour time course. *Refer to Figure 2 on page 13 for the molecular circadian clock*. **B.** Cosinor fit curves of raw data presented in (*A.*). **C.** Corresponding cosinor analysis values for MESOR (midline estimating statistic of rhythm), amplitude, acrophase, and R^2. **D.** Western blot of BMAL1 protein expression in primary WT and SPHK1$^{-/-}$ matured adipocytes whole cell lysates across the circadian time course. **E.** Cosinor fit curve for the densitometry normalized to the trough densitometry value for each genotype in (*D.*). Solid lines indicate the cosinor curve, while black dashes are WT and pink dashes are SK1$^{-/-}$. **F.** Corresponding cosinor analysis of BMAL1 protein expression. **G.** Nuclei of primary WT and SPHK1$^{-/-}$ matured adipocytes were isolated, and CLOCK protein expression over 24 hours was measured by Western blot. # *denotes posttranslational modifications*. Experiments were performed 3 times in 3 separate preparations of primary cells for culture, and representative blots are shown for the trends that were observed. *Bmal1, brain and muscle ARNT-like protein 1; Dbp, D-site of albumin promoter binding protein; Nr1d1, nuclear receptor subfamily 1 group D member 1; Per2, 3, period 2, 3; Rorγ, retinoic acid receptor-related orphan receptor gamma; SK1$^{-/-}$, sphingosine kinase 1 knockout (for brevity in figures).*

Having established that SPHK1 is circadian-regulated and that loss of this gene and its functional protein product result in the loss of circadian functionality, the next question to address was the consequence upon circadian clock-mediated transcriptional function. Therefore, the expression patterns of common BMAL1:CLOCK targets were assessed by immunoprecipitating the components of the transactivator complex at the chromatin E-box regions of *Per1*, *Reverbα*, *Dbp*, and *Pparγ* to assay a gamut of targets that span the negative regulators (*Per1* and *Reverbα*) as well as the typical clock-controlled target, *Dbp*, and *peroxisome proliferator γ* for its role in adipocyte function, as a marker of mature adipocytes and of anabolic lipogenic capacity (Figure 12A). In synchronized, naïve (non-transfected) adipocytes, BMAL1 and CLOCK were detected at CT20 (20 hours after synchronization) at all promoters tested, with CLOCK occupancy at the *Reverbα* (also known as *Nr1d1*) promoter being significantly lower in the mutant compared to control, and downward trends in CLOCK occupancy in all other targets (Figure 12A). On the other hand, BMAL1 occupancy at these loci was apparently unchanged between genotypes, suggesting that the differences in transcriptional clock output observed were not due to BMAL1 occupancy of the promoter.

Moreover, the histone marks associated with active chromatin (H3K9ac, H3K27ac) are known to be circadian, and this led to assessing acetylated histone chromatin marks as well (Baerenfaller, et al., 2016; Cox and Takahashi, 2019; Feng, et al., 2011; Kim, et al., 2018; Sato, et al., 2017). In addition, a more abundant epigenetic marker, such as H3K27ac, was a suitable positive control for the success of each ChIP batch, when assessing in parallel the ChIP signals from natively low-expressed clock transcription factors, such as BMAL1 and CLOCK (Figure 12A). Furthermore, S1P has been reported to be a histone deacetylase (HDAC) inhibitor, which lent a novel hypothetical target for

SPHK1-S1P action, in which cytosolic SPHK1 may generate S1P to be carried by HDAC into the nucleus (Hait, et al., 2009). Intriguingly, both H3K9ac and H3K27ac occupancy signal at the promoters of *Dbp*, *Reverbα*, *Per1*, and *Pparγ$_2$* were lower in mutant compared to control in 3 out of 4 promoters for both acetylated histone H3 molecules (Figure 12B). H327ac and H3K9 ac are thought to be marks of transcriptional activation, but they do not seem to follow the transcriptional mRNA data. This could be explained possibly by other histone modifications that have a stronger effect than the acetylated ones studied here, such as H3K4me3, H4K12ac, H4K5ac, and H2BK12ac (Cox & Takahashi, 2019; Nagahashi, et al., 2015; Zhang, et al., 2012). This finding led to the interest in the protein expression of acetylated histones, so H3K27ac protein expression was assessed at the same timepoint as the chromatin immunoprecipitations, CT28. It was observed that H3K27ac protein expression was strongly diminished in SPHK1$^{-/-}$ adipocytes compared to control (Figure 12C, D). This finding was in line with the decreased acetylated histones at clock targets in SPHK1$^{-/-}$ cells. Given the histone findings, it was decided to assess the acetylation pattern on H3K9 and H3K27 over a circadian time course. Strikingly, the acetylation pattern on H3K9 was nearly absent in SPHK1$^{-/-}$ adipocytes compared to control, and the expression pattern of H3K27ac was reversed in SPHK1$^{-/-}$ adipocytes (Figure 12E). The loss of SPHK1, which is known to reside in the cytosol, has effects on nuclear transcriptional and epigenetic regulation (Nishino, et al., 2019).

Given past findings that S1P affects nuclear chromatin-associated histones, the product of SPHK1, S1P was added to adipocytes and chromatin immunoprecipitation of H3K27ac was performed, and qPCR analysis of several clock targets as well as adipocyte functional targets were carried out (Hait, et al., 2009). At lipolysis genes *Atgl* and *Lipe* (also known as *Hsl*), lipogenic genes *Pparγ$_2$* and *Pgc1α*, and circadian clock genes *Cry2*,

Dbp, *Per2*, and *Per3*, acetylated histone H3 signals tended to be increased with S1P treatment compared to the albumin carrier alone (Figure 12F). At the very least, these observations suggest that S1P (a pro-mitogenic bioactive lipid) is facilitating a chromatin disposition that is poised for transcriptional activation.

To follow up further on S1P effects on chromatin modifiers, the temporal profile for the proposed S1P-binding HDACs was characterized in WT adipocytes and adipocytes lacking the S1P-generating kinase SPHK1 (Hait, et al., 2009). Important to this experiment, cells were fractionated into cytosolic-enriched and nuclear-enriched fractions to assess genetic the effects of depletion of SPHK1 on temporal-spatial dynamics of HDAC expression. SPHK1$^{-/-}$ cells had increased expression of HDAC1 protein over time in the cytosol compared to control, and this was paired with a decrease in the nuclear expression of HDAC1 compared to control (Figure 12G). Little changes were observed between cytosolic HDAC2 expression between cell genotypes, however nuclear HDAC2 in SPHK1$^{-/-}$ adipocytes was decreased compared to control, thus implicating a role for SPHK1 in the nuclear/cytoplasmic localization of Class I HDACs, which could potentially impact enzyme activity. Moreover, nuclear accumulation of HDAC3, another Class I HDAC, was depleted in the nuclei of SPHK1$^{-/-}$ adipocytes compared to control (Figure 12H). Intuitively, less histone acetylation in SPHK1$^{-/-}$ adipocytes from the earlier ChIP experiments would have suggested higher HDAC activity in SPHK1$^{-/-}$ cell or perhaps higher protein expression, but the former has yet to be tested and the latter was not found here within the nucleus. In addition, it has been shown by others that HDAC1 and HDAC2 can localize to the cytoplasm, not just the nucleus as canonically thought (Figure 12I). Since Class I HDACs are known to bind S1P (Hait, et al., 2009), we were curious which proportion of HDAC-bound S1P could be found in the cytosol and the nucleus, and it was

found that HDAC1 and 2 can bind S1P, quite strongly in the nucleus, but there is residual S1P bound to these proteins in the cytoplasm (Figure 12J). These data suggest, but do not confirm, the possibility that HDAC1 and 2 could be loaded with S1P prior to exerting effects within the nucleus.

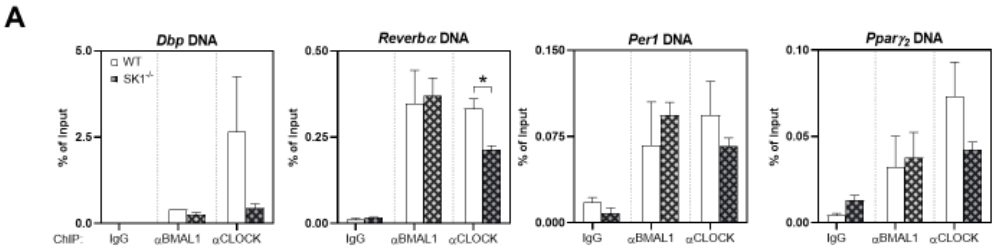
A
Dbp DNA
Reverbα DNA
Per1 DNA
Pparγ2 DNA
WT
SK1-/-
% of Input
ChIP:
IgG
αBMAL1
αCLOCK

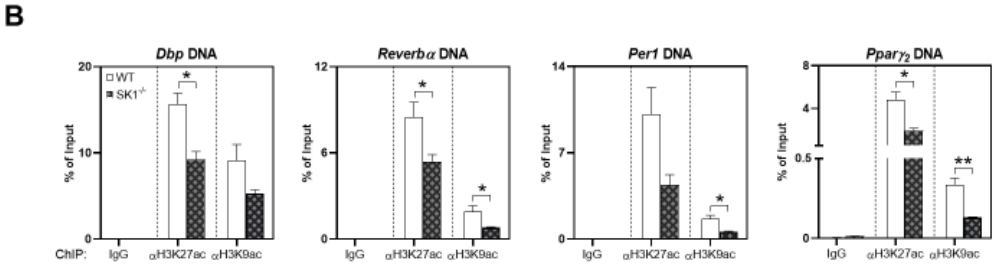
B
Dbp DNA
Reverbα DNA
Per1 DNA
Pparγ2 DNA
WT
SK1-/-
% of Input
ChIP:
IgG
αH3K27ac
αH3K9ac

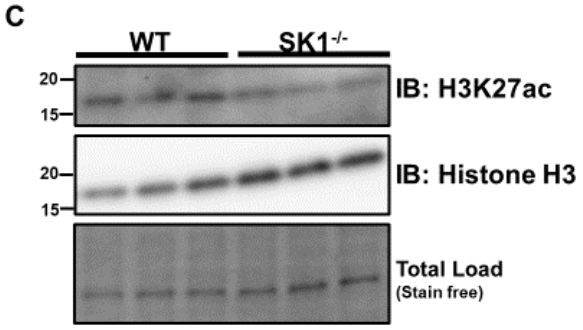
C
WT
SK1-/-
IB: H3K27ac
IB: Histone H3
Total Load
(Stain free)

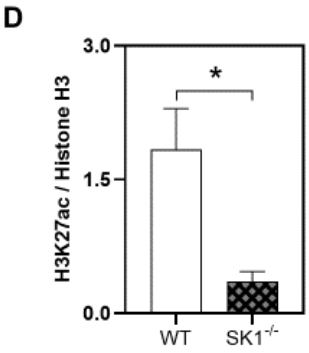
D
H3K27ac / Histone H3
WT
SK1-/-

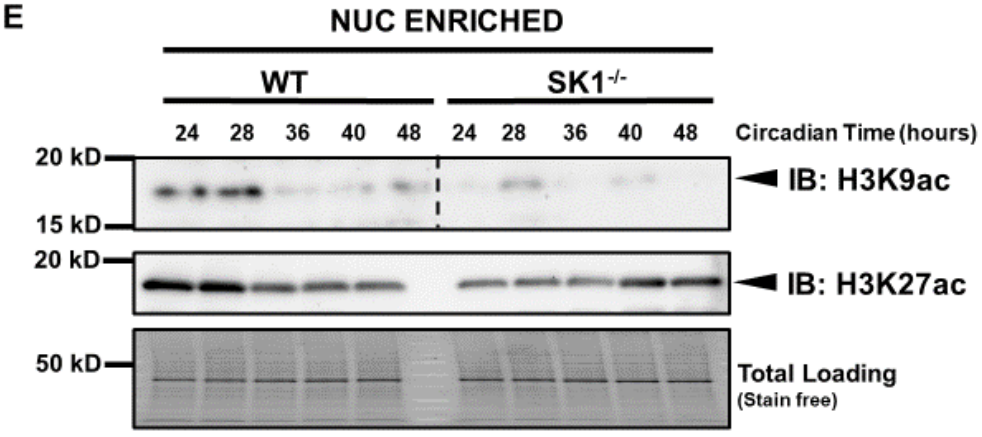
E
NUC ENRICHED
WT
SK1-/-
24 28 36 40 48 24 28 36 40 48
Circadian Time (hours)
20 kD
15 kD
IB: H3K9ac
20 kD
IB: H3K27ac
50 kD
Total Loading
(Stain free)

F

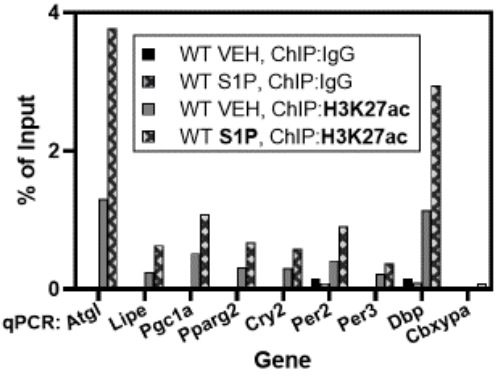
WT VEH, ChIP:IgG
WT S1P, ChIP:IgG
WT VEH, ChIP:H3K27ac
WT S1P, ChIP:H3K27ac
% of Input
4
2
0
qPCR: Atgl
Lipe
Pgc1a
Pparg2
Cry2
Per2
Per3
Dbp
Cbxypa
Gene

G

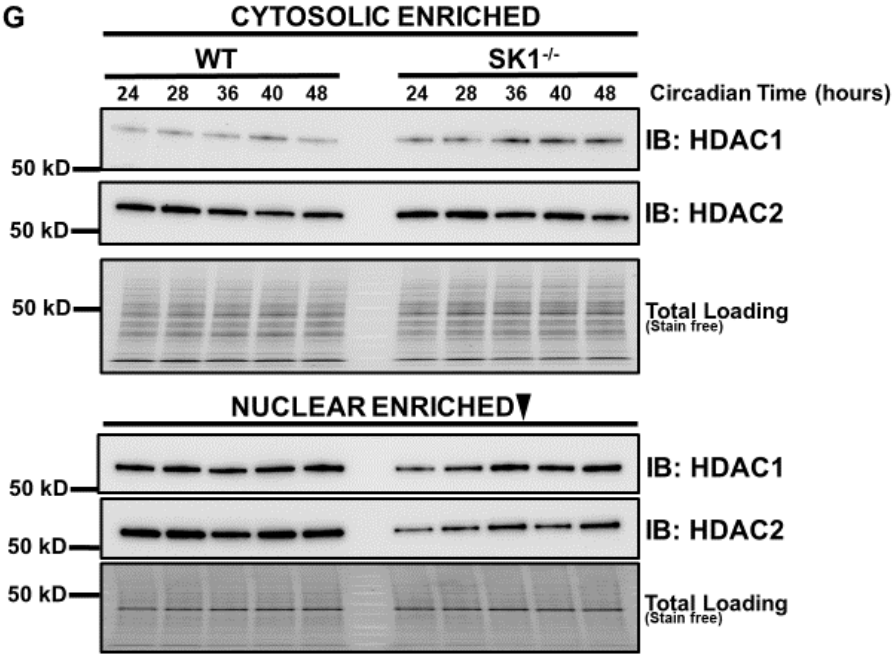
CYTOSOLIC ENRICHED
WT
SK1-/-
24 28 36 40 48 24 28 36 40 48
Circadian Time (hours)
IB: HDAC1
50 kD
IB: HDAC2
50 kD
Total Loading
(Stain free)
50 kD
NUCLEAR ENRICHED
IB: HDAC1
50 kD
IB: HDAC2
50 kD
Total Loading
(Stain free)
50 kD

H

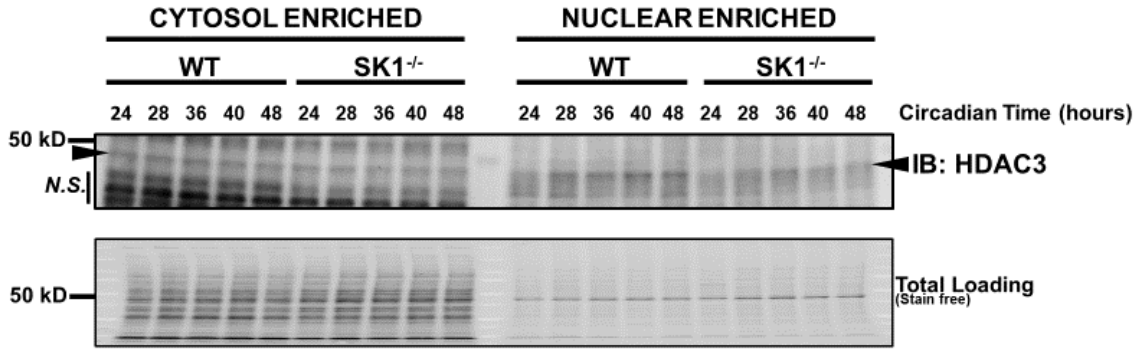
CYTOSOL ENRICHED
NUCLEAR ENRICHED
WT
SK1-/-
WT
SK1-/-
24 28 36 40 48 24 28 36 40 48 24 28 36 40 48 24 28 36 40 48
Circadian Time (hours)
50 kD
N.S.
IB: HDAC3
50 kD
Total Loading
(Stain free)

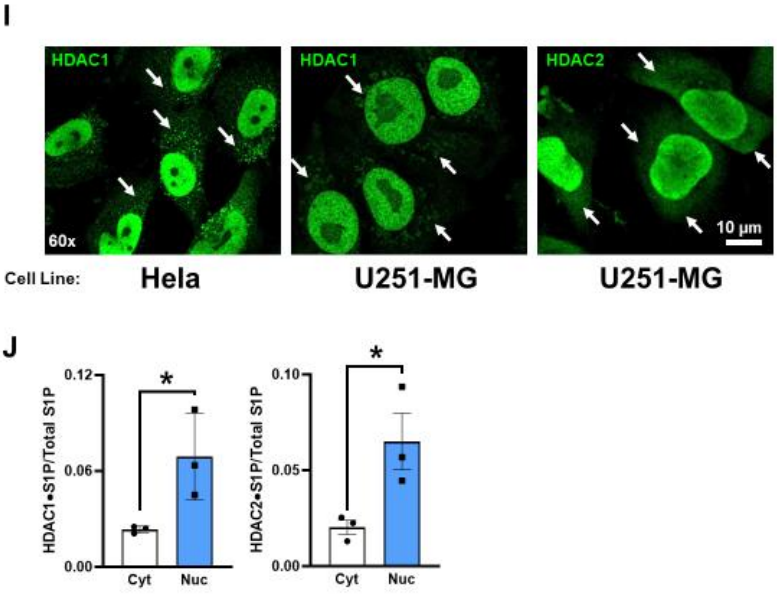

(continued from previous pages)

Figure 12. Loss of actively transcribing chromatin and CLOCK occupancy in SPHK1$^{-/-}$ adipocytes and disruption of chromatin modifiers. **A.** WT and SPHK1$^{-/-}$ primary adipocytes were synchronized and harvested at CT28 for ChIP of BMAL1 and CLOCK at the promoters of *Per1* (negative core loop target), *Reverbα* (negative accessory loop target), *Dbp* (canonical/traditional, non-core-clock-mechanism BMAL1 target), and *Pparγ* (known circadian transcription factor, involved in anabolic adipocyte lipogenesis, BMAL1 target). (*See Figure 2, page 13.*) **B.** A mark of active transcription, acetylated histone 3 at lysines 9 and 27 (H3K9ac and H3K27ac) was immunoprecipitated at the DNA loci of *Per1*, *Reverbα*, *Dbp*, and *Pparγ* in synchronized WT and SPHK1$^{-/-}$ primary matured adipocytes at CT28. **C.** Western blot analysis of H3K27ac in matured primary adipocytes from sWAT of WT and SPHK1$^{-/-}$ mice. **D.** Quantification of the Western blot in (*C.*), displayed as relative acetylated histone3 K27 densitometry over total histone H3. **E.** Nuclear-enriched fraction of synchronized matured

primary WT and SPHK1$^{-/-}$ adipocytes showing acetylated H3K9 and H3K27 expression over 24 hours. **F.** WT synchronized primary matured adipocytes were treated with 150 nM S1P for 30 minutes and cells were subjected to ChIP of H3K27ac at the promoters for *Atgl*, *Lipe*, *Pgc1α*, *Pparγ2*, *Cry2*, *Per2*, *Per3*, *Dbp*, and at negative control *Cbxypa* (a marker present in pancreas tissue, but not adipose tissue)**. G.** Cytosolic- and nuclear-enriched fractions of synchronized primary WT and SPHK1$^{-/-}$ adipocytes and Western analysis of HDAC1 and HDAC2 proteins over 24 hours. **H.** Cytosolic- and nuclear-enriched fractions of synchronized primary WT and SPHK1$^{-/-}$ adipocytes and Western analysis of HDAC3 over 24 hours. **I.** From the Human Protein Atlas database online, HDAC1- and HDAC2-positive staining in Hela and U251-MG cells is in the nucleus and the cytoplasm. White arrows indicate positive staining in the cytoplasm. **J.** Immunoprecipitations of HDAC1 and HDAC2 in fractionated WT cells followed up with lipidomics analysis for S1P binding. Experiments were performed 3 times in 3 separate preparations of primary cells for culture, and representative blots and ChIP batches are shown for the trends that were observed. *$p < 0.05$. *Atgl, adipose triglyceride lipase; Cbxypa, carboxypeptidase A; Cry2, cryptochrome 2; Dbp, D-site of albumin promoter binding protein); Lipe, hormone sensitive lipase; Pgc1α, peroxisome proliferator-activated receptor gamma coactivator 1 alpha; Pparγ2, peroxisome proliferator-activated receptor gamma 2; Per2, period 2; Per3, period 3*.

Finally, these adipocyte cellular effects demonstrated a role for SK1 in the maintenance of the molecular circadian clock. Typical circadian transcripts were increased, suggesting that SK1 and perhaps S1P may be involved in negative feedback regulation of the clock. Furthermore, histone modifications, which are known to be circadian, followed alternative patterns over time compared to control when assessing protein expression. Could these changes at the cellular level be involved in maintaining metabolic homeostasis?

We utilized WT mice and SK1^{fatKO} (mice with an adipocyte-specific depletion of SK1) to determine some overall metabolic parameters (Anderson, et al., 2020). Mice were not fasted and serum was collected for analysis of lipids over a circadian time course. Strikingly, it was found that serum cholesterol was significantly elevated compared to control, and serum triacylglycerols also increased at early time points in the circadian period (Figure 13A, B). These data suggested that the contribution of adipocyte SK1 is critical for maintenance of liver functional homeostasis. In addition, animals were subjected to noninvasive comprehensive monitoring, in which the respiratory exchange ratio (RER), energy expenditure, physical activity, and food intake were measured. It was found that the first half of the day (inactive period) tended to have the most differences, with SK1^{fatKO} mice demonstrating significantly increased RER, indicating more carbohydrate energy utilization compared to control (Figure 13C, D).

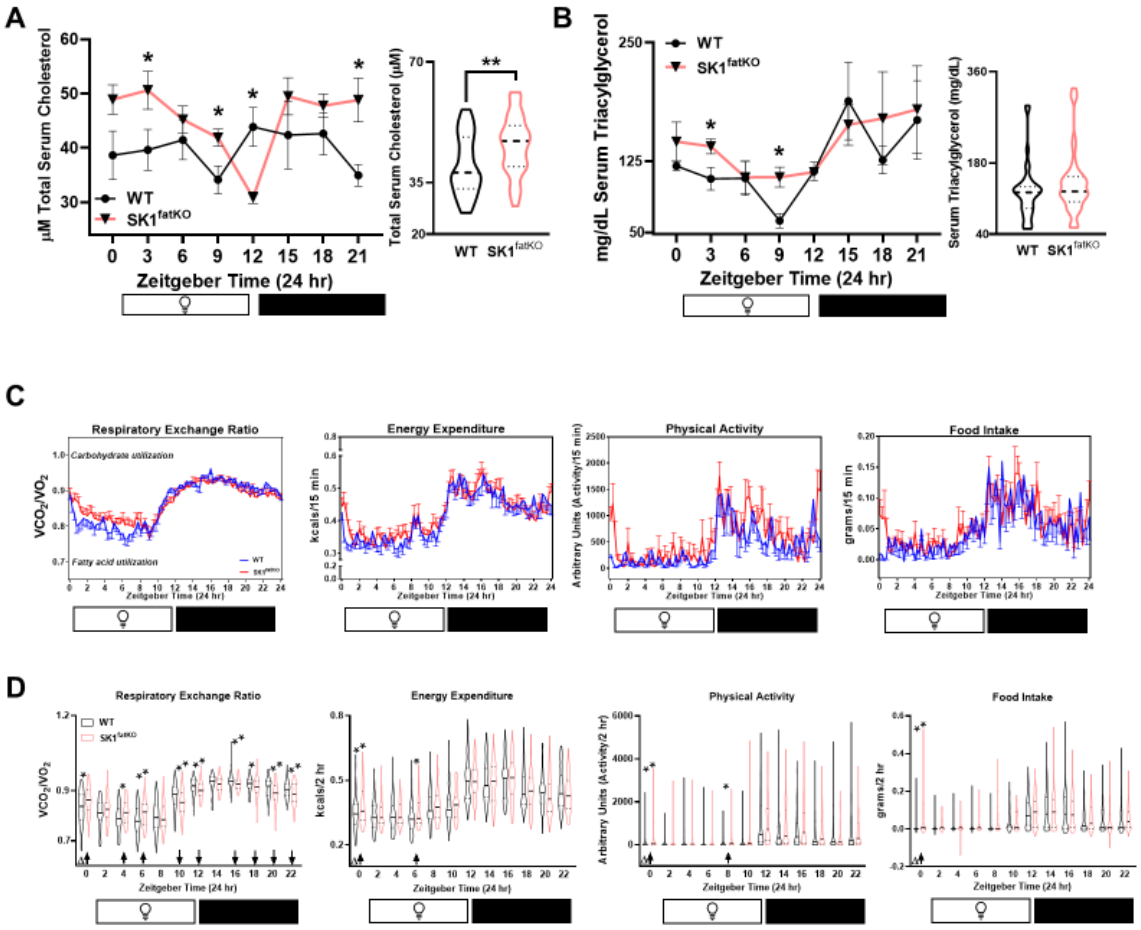

Figure 13. Energy homeostasis and liver metabolism are perturbed in SK1^{fatKO}. A. Serum cholesterol was measured in non-fasted male WT and SK1^{fatKO} mice at the indicated timepoints. ZT0 is 6 a.m. A white bar with a lightbulb and a black bar indicate the lights' status in the mouse room. **B.** Serum cholesterol was measured in non-fasted male WT and SK1^{fatKO} mice at the indicated timepoints. **C.** Comprehensive lab animal monitoring of 6 WT and 6 SK1^{fatKO} male mice measured respiratory exchange ratio as VCO2 over VO2, energy expenditure as kilocalories per 15-minute intervals, physical activity as measured by beam breaks and reported as arbitrary units, and food intake measured by grams per 15-minute intervals. WT in blue, SK1^{fatKO} in red. **D.** Same data as

(*C.*), but displayed as binned 2-hour intervals and shown as violin plots, with the median bolded in a solid line, and the upper and lower quartiles in thinner, dashed lines. WT in black, $SK1^{fatKO}$ in salmon.

4.3. Conclusion

In conclusion, the work here demonstrated that genetic depletion of SPHK1 led to defects in the adipocyte circadian clock with concomitant perturbations to the behavior of histones at key adipocyte and circadian genetic loci (Figure 11, Figure 12). Moreover, it is proposed that *Sphk1* is a circadian gene in adipocytes, due to the expression profile of *Sphk1* mRNA over a circadian time course in wildtype primary adipocytes, the presence of E-boxes in its promoter, as well as the presence of clock transcription factors BMAL1:CLOCK at the promoter E-box sites in *Sphk1* (Figure 10A, D, E). All in all, animals lacking SK1 specifically in the adipocyte also showed enhancements in the respiratory exchange ratio in the beginning of the day, along with increased serum levels of cholesterol and triacylglycerol. Further investigation is needed to comprehensively decipher the role of SPHK1/S1P as well as other sphingolipids in nuclear events such as homeostatic circadian transcription.

4.4. Discussion

With respect to the cyclical nature of reversible or counterregulatory mechanisms, histone modifications (acetylation and deacetylation) and their modifiers are disrupted due to loss of SPHK1. Consistent with the previously established notion that S1P is an inhibitor of HDAC, we found that treatment with S1P could increase the acetylated histone H3 signal at several key adipocyte functional and circadian regulatory genes (Figure 12F) (Hait, et al., 2009). It was expected that an SPHK1-null system would therefore be rampant with HDAC activity with subsequently transcriptionally inactive chromatin. This was demonstrated by decreased acetylated protein at two histone residues (K9 and K27) in SPHK1$^{-/-}$ cells and decreased DNA qPCR signal from immunoprecipitated histones at important adipocyte circadian loci (Figure 12C, E; A, B, respectively). Thus, SPHK1$^{-/-}$ cells had lower overall acetylated histone signal at several circadian target genes, which is in line with evidence that S1P, the product of SPHK1, is a histone deacetylase inhibitor (Hait, et al., 2009). Future studies delineating a role for SPHK1 and S1P in chromatin modifications should include ChIP-Sequencing as a method for a more comprehensive analysis. Despite the ChIP findings, circadian clock transcripts had higher baseline expression values and amplitudes in SK1$^{-/-}$ compared to control. This suggests that the findings from amplified mRNA expression and decreased ChIP signal of H3K9ac and H3K27ac may arise from activity at other histones or histone residues.

Nuclear/cytoplasmic localization of HDAC, on the other hand, was aberrant but not suggestive, by mere protein expression, that HDAC1, 2, and 3-based deacetylation were to blame for the observations made by ChIP of decreased acetylated histone in SPHK1$^{-/-}$ adipocytes (Figure 12A, B, G, H, respectively). Another possibility is a differential effect of SPHK1 on histone acetyltransferases (HATs). For example, CLOCK itself is a histone

acetyltransferase, and the nuclear levels of which were found to be increased in SPHK1$^{-/-}$ adipocytes compared to control (Figure 11G) (Doi, et al., 2006; Hirayama, et al., 2007). Despite this, CLOCK occupancy at several key promoters for which it is known to bind, trended towards decreases for several clock target genes involved in adipocyte homeostasis (Figure 12A, B). Histone deacetylase and acetyltransferase enzymatic activity assays should be utilized to determine the global effect of SPHK1 and S1P on their activity. Moreover, other HDACs (for which there are several isoforms), may be more active or overexpressed, besides HDAC 1, 2, 3, which could explain the decreased acetylated histones found at the circadian and adipocyte gene promoters (Bagchi and Weeks, 2019).

Figure 14 highlights a potential model by which SPHK1 and its product S1P may influence the circadian clock. Histone modifications are known to be circadian and these modifications influence whether genes are enhanced or repressed (Baerenfaller, et al., 2016; Cox and Takahashi, 2019). S1P is known and has been shown here to influence the modification status of histones (Hait, et al., 2009). *Sphk1* mRNA expression and the variations in the production of ^{17}C-S1P demonstrate the cyclical nature of this lipid and its kinase. Thus, a model to encompass these aspects shows that S1P may impart a layer of control upon the circadian clockwork mechanism at the epigenetic level. Importantly, this study highlights for the first time a novel loop by which a cycling bioactive lipid exerts some control over the periodic oscillations of core clock genes and epigenetic machinery.

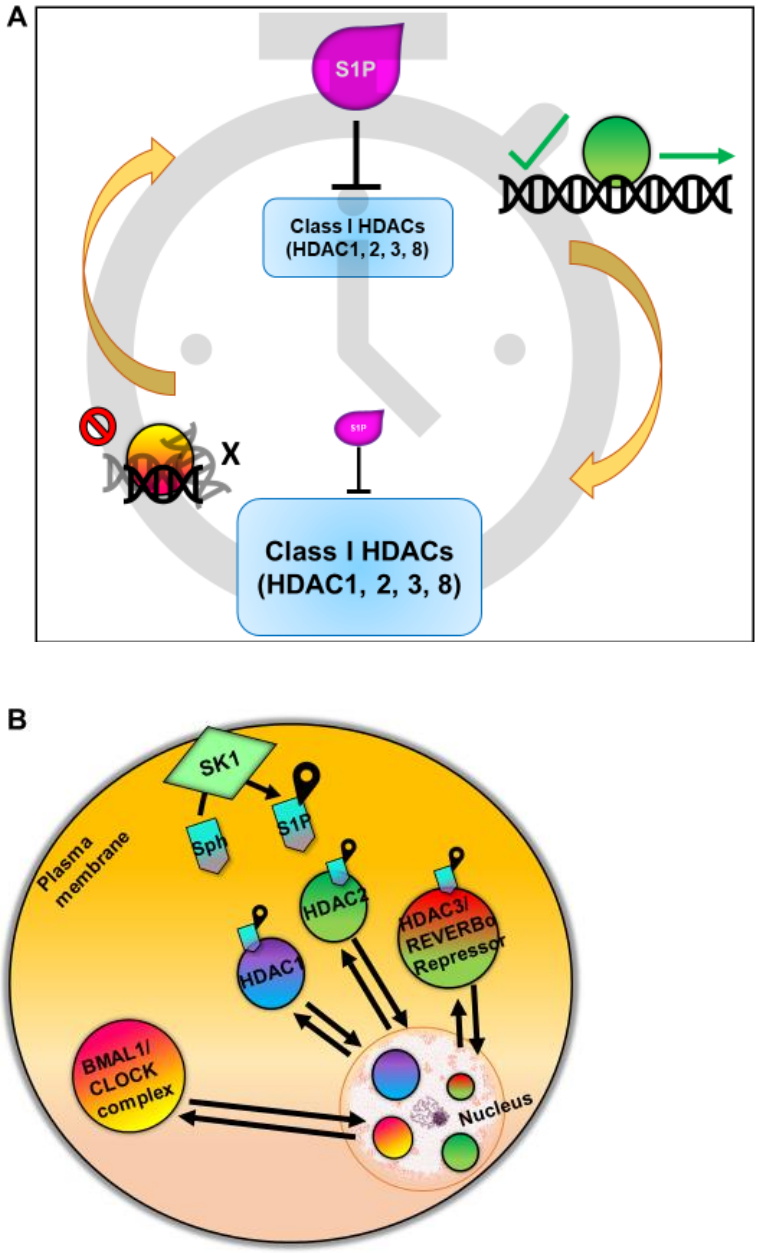

Figure 14. Proposed model of SPHK1/S1P regulation of adipocyte circadian rhythm. A. SPHK1 and S1P levels fluctuate over time, giving rise to a temporally-controlled inhibition on Class I HDAC activity. Temporal control of HDACs gives rise to chromatin conformations that enhance or repress transcription. **B.** Could

HDACs be an intracellular S1P vehicle? This could provide one hypothetical explanation for how cytosolic SK1 and S1P may influence HACDAC-dependent processes in the nucleus.

4.5. Experimental Methods

Cell Culture, Isolation of Stromal Vascular Fraction (SVF) and Differentiation to Mature Adipocytes

Primary adipose-derived stem cells (ADSCs) were isolated from inguinal adipose tissue of 3-8-week-old WT and SPHK1$^{-/-}$ mice (Allende, et al., 2004). Subcutaneous adipose tissue was digested using 0.1% collagenase (Sigma, C6885) in digestion buffer (100 mM HEPES, 120 mM NaCl, 50 mM KCl, 5 mM glucose, 1 mM $CaCl_2$, 1.5% BSA) in a 37º C shaking incubator (New Brunswick Scientific) (150 rpm) for 40 minutes. The digest was filtered through a 100-µM cell strainer and centrifuged at 500 × *g* for 5 minutes. The SVF pellet was re-suspended in media, filtered through a 40-µM cell strainer and plated. Media was changed after two hours to remove non-adherent cells. Cells were grown to confluency in proliferation media (DMEM/F12 50:50 (Corning, 10-090-CV), 10% fetal bovine serum (FBS) (Atlanta Biologicals), 1% penicillin streptomycin antimycotic cocktail (MilliporeSigma, A5955). 48 hours post-confluency, differentiation was induced using 10 µg/mL insulin (Santa Cruz Biotechnology, sc-360248), 1 µM dexamethasone (MilliporeSigma, D4902), 0.5 mM IBMX (Enzo Life Sciences, BMLPD1401000), and 1 µM rosiglitazone (Cayman Chemical, 71740) for two days. Differentiation was maintained with insulin for days 3-4 and proliferation media days 5-8. Mature adipocytes were visualized under a brightfield microscope to assess lipid droplet formation, and plates with large lipid droplets and >90% differentiation were used for experiments (Figure 15).

in vitro Circadian Rhythm

Unless otherwise noted, the *in vitro* circadian experiments are all performed in the same manner, in which primary WT and SPHK1$^{-/-}$ ADSCs were brought to maturity, and on the

day of the experiment, the cells were synchronized with 50% horse serum (Gibco, 26050-070) and 50% DMEM/F12 for 2 hours. Following the horse serum shock, the cell monolayer was gently rinsed once with warm 1x PBS and 2% fatty-acid-free BSA in DMEM/F12 was kept on the cells for the duration of the experiment, which generally lasted 48 hours *in toto*.

S1P Treatment

WT primary matured, synchronized adipocytes were allowed to cycle for 24 hours, after which, cells were treated with a final concentration 150 nM S1P (Avanti Polar Lipids, 860492) complexed to 4 mg/mL FAF BSA or 4 mg/mL FAF BSA without S1P and assayed by ChIP for acetylated histone H3 signal at various adipocyte and circadian gene loci.

^{17}C-Sphingosine Treatment

WT primary matured, synchronized adipocytes were allowed to cycle for 24 hours, after which, cells were treated with a final concentration 5 μM ^{17}C-sphingosine (Avanti Polar Lipids, 860640) (dissolved in 100% ethanol) for exactly 30 minutes, collected immediately with addition of phosphatase inhibitors, for an exact volume of media in a 5-mL borosilicate glass tube and for a cell pellet in minimal PBS in a separate 5-mL borosilicate glass tube, capped, and stored at -80° C until analysis by tandem liquid chromatography and mass spectrometry lipidomics. This 30-minute procedure was repeated every 4 hours over a 24-hour period to assay *in situ* the enzymatic turnover of ^{17}C-sphingosine to ^{17}C-S1P (Spassieva, et al., 2007).

Nuclear Extracts for Immunoprecipitation followed by Lipid Measurements

This method was developed in Hait, et al., 2009. WT primary matured, synchronized adipocytes were allowed to cycle for 24 hours, after which, cells were harvested over a time course. Cells were washed with cold PBS and re-suspended in buffer containing 10 mM HEPES (pH 7.8), 10 mM KCl, 0.1 mM EDTA, 1 mM Na_3VO_4, 1 mM DTT, 1:500 protease inhibitors (Sigma) and 0.2 mM PMSF, and incubated on ice for 15 min. NP-40 was added (0.75%) and cells were vortexed for 10 sec. Nuclei and supernatant ("cytoplasm") were separated by centrifugation at 1000 × *g* for 3 min at 4˚ C. Nuclei were resuspended in buffer containing 20 mM HEPES (pH 7.8), 0.4 M NaCl, 1 mM EDTA, 1 mM Na_3VO_4, 1 mM DTT and 1:500 protease inhibitors and incubated on ice for 15 min. Nuclear extracts were cleared by centrifugation at 14,000 × *g* for 5 min at 4˚ C. Equal milligrams protein from each fraction was immunoprecipitated overnight at 4˚ C (rotating) with 1 µg BMAL1, HDAC1, and HDAC2 antibodies, and the next day immunocomplexes were captured with Protein A/G magnetic beads (Thermo Fisher Scientific, 88802) for an additional 2 hours at 4˚ C, then washed extensively. Immunocomplexes were eluted in 100% methanol and tested by LC:MS/MS at the Virginia Commonwealth University Lipidomics and Metabolomics Core facility for sphingolipids.

Lipid Measurements

Sphingolipids were measured using liquid chromatography/tandem mass spectrometry at the Virginia Commonwealth University Lipidomics and Metabolomics Core and performed using previously published methods (Haynes, et al., 2009; Shaner, et al., 2009). ^{17}C sphingolipids were measured at the Medical University of South Carolina Shared

Lipidomics Resource according to previously published methods (Bielawski, et al., 2010; Spassieva, et al., 2007).

Chromatin Immunoprecipitation (ChIP)

Primary WT and SPHK1$^{-/-}$ matured, synchronized adipocytes were plated on 15-cm plates per 2 ChIPs. Briefly, cells were washed twice with room temperature 1x PBS and the dishes were then placed on an orbital rocker (Sigma, Z768502) in a measured volume of freshly-made PBS solution containing 2 mM disuccinimidyl glutarate (DSG) (ProteoChem, c1104) for 10 minutes. After 10 minutes, fresh 37% formaldehyde (Fisher, BP531-500) was added directly to the solution to a final concentration of 1% and continued swirling gently for another 12 minutes. Finally, the crosslinking reactions were quenched with glycine at a final concentration of 125 mM for 5 additional minutes. Following, the solution was discarded as hazardous waste and the cells were washed twice with cold 1x PBS. The PBS was aspirated, and the cells were scraped into 1.8 mLs adipocyte hypotonic lysis buffer (5mM PIPES pH 7.8, 10 mM KCl, 1% Igepal, plus protease/phosphatase inhibitors and PMSF immediately before use) per 15-cm plate. The cells were collected in a Dounce homogenizer and were sheared with 10 strokes of the Dounce until visibly dissociated. The cells were also passed through a 22G needle to ensure disruption of the monolayer but preservation of the nuclei. The resulting slurry was vortexed and kept on ice for 10 minutes. Next, the tubes were centrifuged at 8,500 × *g* at 4° C for 8 minutes to remove a significant fat cake at the top as well as the cytoplasmic infranatant and to leave the nuclear pellet intact and undisturbed. The pellets were resuspended in the same lysis buffer to wash excess adipocyte lipid from the nuclear pellet and vortexed. They were re spun, and the pellets were saved. Next, the pellets were suspended in 600 µL sonication

lysis buffer (50 mM Tris-HCl, pH 8.0, 10 mM EDTA, 1% SDS, and protease/phosphatase inhibitors and PMSF fresh) per 15-cm plate. The 600 µL was split into two 1.5-mL Eppendorf tubes of 300 µL, and then were sonicated (Branson 150, Branson Ultrasonics, Danbury, CT) for 8 rounds of 30 seconds on, 30 seconds off in a 4° C water bath. The resulting sonicate was then subjected to centrifugation at 18,000 × *g* at 4° C to clarify the chromatin. The chromatin supernatant was collected and split to two chromatin immunoprecipitations as well as the 10% input control. Thus, approximately 500 µL of recovered sonicate was split to 200 µL per ChIP plus a 20-µL 10% input. The ChIP samples were diluted 1:10 with Dilution/Low Salt buffer (20 mM Tris-HCl pH 8.0, 150 mM NaCl, 2 mM EDTA, 1% Triton X-100, 0.1% SDS), pre-cleared with ChIP-grade Protein A/G magnetic beads (Thermo Fisher Scientific, 26162) for one hour, and immunoprecipitated with 1 µg of antibody overnight at 4° C while rocking. The following day, pre-equilibrated magnetic ChIP-grade Protein A/G beads were added to the samples for 2 hours. They were then subjected to extensive washing on the magnetic rack, performing two washes in Low Salt Buffer, 2 subsequent washes in high salt buffer (20 mM Tris-HCl pH 8.0, 500 mM NaCl, 2 mM EDTA, 1% Triton X-100, 0.1% SDS), 2 subsequent washes in LiCl Buffer (10 mM Tris-HCl pH 8.0, 500 mM NaCl, 1 mM EDTA, 1% deoxycholate, 1% NP-40, 0.25 M LiCl), and finally 2 washes in TE buffer (10 mM Tris-HCl pH 8.0, 1 mM EDTA). After these 8 washes, 100 µL of ChIP elution buffer (0.1 M $NaHCO_3$, 1% SDS) was added to the beads, in addition to the reverse crosslinking reagent, 4 µL of 5 M NaCl, and these were incubated overnight at 65° C. The next morning, the samples were treated with RNase A (Thermo Fisher Scientific, EN0531) for 1 hour at 37° C, and after that, treated with Proteinase K (Thermo Fisher Scientific, EO0491) for 1 hour at 60° C. After this, the samples were subjected to DNA isolation and purification with

a column-based washing approach (Zymo Research, D5205). The samples were eluted from the column in 120 µL and 2 µL per well, assayed in triplicate, were used for real time qPCR of the DNA.

Primers used for ChIP are shown below:

Method	*Gene*	Forward (5' to 3')	Reverse (5' to 3')
ChIP	*Cbxypa1*	CATGGTCAAGGGTGAAAG	CTGAGGTCTGAGGCCTTTTT
ChIP	*Atgl*	CGGCGGAGGCGGAGACGCT	TCCCTGCTTGATCCAGTTGGAT
ChIP	*Dbp*	AATGACCTTTGAACCTGATCCCGCT	GCTCCAGTACTTCTCATCCTTCTGT
ChIP	*Lipe*	GCTGCCCTGGGAGGATTAAGCC	CAAAAGCCTGAGAGGTTTCTCCGAG
ChIP	*Nr1d1 (Reverbα)*	ACGACCCTGGACTCCAATAA	CCATTGGAGCTGTCACTGTAGA
ChIP	*Per2*	CAACACAGACGACAGCATCA	TCCTGGTCCTCCTTCAACAC
ChIP	*Per3*	CTGCTCCAACTCAGCTTCCTTT	TTAGACAGCAAGGCTCTGGTTCT
ChIP	*Pgc1α*	GCAATTCAATTCGGGTCCATCTCACC	GGACTTCAGCGTGTTTGCATTCAGTAC
ChIP	*Pparγ*	CTGTACAGTTCACGCCCCTC	TCACACTGGTGTTTTGTCTATG
ChIP	*Sphk1 -1800*	TACACCGGGGCACGTGTGCATT	TCTTTCCCCCCAGGGAACACTA
ChIP	*Sphk1 -300*	ACTTTGTCCCACGTGCATGGA	TCCCGCTGACAAGGGGCCA

Antibodies for ChIP are shown below:

Application	Target	Antibody	Host	Supplier	Catalog #	Concentration or Dilution
ChIP	Mouse	H3K9ac	Rabbit	Thermo	710293	1 µg per IP
ChIP	Mouse	H3K27ac	Rabbit	Thermo	MA5-24671	1 µg per IP
ChIP		Normal IgG	Rabbit	Bethyl	P120-101	1 µg per IP
W.B. and ChIP	Mouse	BMAL1	Rabbit	Bethyl	A302-616A	1 µg per IP
W.B. and ChIP	Mouse	CLOCK	Rabbit	Bethyl	A302-618A	1 µg per IP

qPCR

Total RNA was isolated from cultured primary adipocytes or gonadal adipose tissue homogenized in Trizol (Invitrogen, 15596026) followed by RNeasy mini kit (Qiagen, 74106) extraction and column purification. cDNA was synthesized from 1 µg of total RNA using iScript Advanced cDNA Synthesis Kit (Bio-Rad, 1708890). Real time PCR was performed using a CFX96 Real-Time System (Bio-Rad) and SSoAdvanced Sybr (Bio-Rad,

172-5272). The primers used for cDNA qPCR and DNA CHIP-qPCR are shown in the following tables. Mean normalized expression was calculated by normalizing to the geometric mean of reference genes *Ppia* and *Tbp* in gonadal adipose tissue (*i.e.*, $root_2[C_q$ gene 1 × C_q gene 2]) using the $2^{-\Delta\Delta Ct}$ method. ChIP normalization was carried out with a 10% input control. Primers for ChIP were tabulated in the *ChIP* section.

Method	*Gene*	Forward (5' to 3')	Reverse (5' to 3')
qPCR	*Ppia*	GAGCTGTTTGCAGACAAAGTTC	CCCTGGCACATGAATCCTGG
qPCR	*Tbp*	AAGGGAGAATCATGGACCAG	CCGTAAGGCATCATTGGACT
qPCR	*Bmal1 (Arntl)*	TGACCCTCATGGAAGGTTAGAA	GGACATTGCATTGCATGTTGG
qPCR	*Dbp*	CGTGGAGGTGCTTAATGACCTTT	CATGGCCTGGAATGCTTGA
qPCR	*Nr1d1 (Reverbα)*	TACATTGGCTCTAGTGGCTCC	CAGTAGGTGATGGTGGGAAGTA
qPCR	*Per2*	CCATCCACAAGAAGATCCTAC	GCTCCACGGGTTGATGAAGC
qPCR	*Per3*	CCCTACGGTTGCTATCTTCAG	CTTTCGTTTGTGCTTCTGCC
qPCR	*Rorγ*	GACTGGAGGACCTTCTACG	TCCCACATTGACTTCCTCTG
qPCR	*Sphk1*	GAGTGCTGGTGCTGCTGAA	AGGTTATCTCTGCCTCCTCCA

Cellular Fractionation for Nuclear and Cytoplasmic Enrichment

The Thermo NE-PER Kit (Thermo Fisher Scientific, 78835) was utilized to separate cytoplasmic (post-nuclear) and nuclear fractions from matured primary white adipocytes, with modifications. In a 10-cm dish, adherent mature adipocytes were gently rinsed twice with 1x PBS on the dish, and excess was aspirated with a 200-µL plastic pipet tip from the tilted dish. Next, ~400 µL of CER I solution was added to the monolayer, and adipocytes were scraped into the solution. Importantly, the collected cells were then passed through a 22G syringe 5 times to disperse the cell conglomerate but keep the nuclei intact. These were vortexed and placed on ice for 10 minutes. Next, per the NE-PER protocol, 22 µL of CER II solution was added and tube was vortexed vigorously and placed on ice for 2 minutes. The tube was centrifuged at 500 × *g* for 5 minutes at 4° C. The fat cake and infranatant were collected to a separate tube (as the cytoplasmic/post-nuclear and fat cake

components) while not disturbing the pellet at the bottom. The cytoplasmic tube was spun again in the same manner so that the fat cake and cytoplasmic-enriched infranatant could be separated. The cytoplasmic/post-nuclear infranatant was collected with a 28.5G insulin syringe, avoiding as much lipid as possible, at which point this sample was ready for BCA protein concentration determination. The tube with the pellet was cleaned of excess lipid on the sides of the tube by wicking carefully with a Kimwipe (Kimberly-Clark Professional, 34120), and the pellet was resuspended in 200 µL of NER, passed 5 times through a 28.5 gauge insulin syringe to break up the pellet, sonicated for 20 seconds in a sonicator bath, vortexed vigorously for 30 seconds, and placed on ice for 40 minutes. Finally, the nuclear natant was collected as the nuclear-enriched fraction after a 20-minute spin at 4° C at 18,000 × *g*. Cytoplasmic and nuclear fractions were assessed by Western blot after normalization by BCA. Nuclear fractions tended to be at least 5-fold lower in protein concentration.

Western Blotting

Gonadal adipose tissue was homogenized in RIPA buffer with protease and phosphatase inhibitors (Thermo Fisher Scientific, 78446) using a Dounce homogenizer for at least 30 pulses, or until visibly homogenized. Homogenates were vortexed well and centrifuged at 10,000 × g for 10 minutes at 4° C. The resulting infranatant (below fat cake, and above cell debris pellet) was transferred to a new tube with an insulin syringe (28.5G). Cultured adipocyte whole-cell homogenates were homogenized in RIPA buffer with 1 mM PMSF, and protease and phosphatase inhibitors (Thermo Fisher Scientific, 78446). Cultured adipocyte cell fractions were collected as described in *Cellular Fractionation for Nuclear and Cytoplasmic Enrichment*. Protein content was quantified using a BCA protein

determination assay (Thermo Fisher Scientific, 23225). 5-10 µg protein was used for western blotting. gWAT whole-cell homogenates, cultured adipocyte whole-cell homogenates, and fractionated adipocyte proteins were separated by SDS-PAGE, and transferred to PVDF membranes. The membranes were blocked for 1 hour in 5% BSA. Proteins were detected using HRP-linked anti rabbit secondary (1:5000; Cell Signaling Technology, 7074), Clarity ECL Western Blotting Substrate (Bio-Rad, 1705061) for HRP, and a ChemiDoc Imaging System (Bio-Rad, 17001401, 17001402). Blots were assessed for protein expression of proteins shown in the table on the following page. Vinculin (1:2,000; Cell Signaling Technology, 4650), Ponceau S, and stain-free total protein were used to determine even loading. Band intensity was quantified using ImageJ.

Application	Target	Antibody	Host	Supplier	Catalog #	Concentration or Dilution
Western blot	Mouse	HDAC1	Rabbit	Bethyl	A300-713A	1:2,000
Western blot	Mouse	HDAC2	Rabbit	Bethyl	A300-705A	1:2,000
Western blot	Mouse	HDAC3	Rabbit	Bethyl	A300-464A	1:5,000
Western blot	Mouse	Histone H3	Rabbit	Cell Signaling Technology	4499	1:2,000
Western blot	Mouse	Lamin B1	Rabbit	Cell Signaling Technology	13435	1:1,000
Western blot	Mouse	Vinculin	Rabbit	Cell Signaling Technology	4650	1:1,000
Western blot	Rabbit	HRP-anti-Rabbit IgG	Goat	Cell Signaling Technology	7074	1:5,000
W.B. and ChIP	Mouse	BMAL1	Rabbit	Bethyl	A302-616A	1 µg per IP
W.B. and ChIP	Mouse	CLOCK	Rabbit	Bethyl	A302-618A	1 µg per IP

Antibodies used for Western blotting analysis.

Mice

Adipocyte-specific *Sphk1* knockout ($SK1^{fatKO}$) and WT C57BL/6 mice were utilized for *in vivo* studies (Anderson, et al., 2020). WT and $SPHK1^{-/-}$ C57BL/6 mice were utilized for primary cell culture preparations for adipocytes (Allende, et al., 2004; Pappu, et al., 2007).

Animal Model

All animal experiments conformed to the Guide for the Care and Use of Laboratory Animals and were in accordance with Public Health Service/National Institutes of Health guidelines for laboratory animal usage. The experimental groups consisted of male WT and $SK1^{fatKO}$ C57BL/6 mice. Mice were housed in the animal facility at the Medical University of South Carolina. Standard chow and water were provided *ad libitum*, except when fasting was required (*e.g.*, glucose tolerance testing). Animals were maintained on a 12h:12h light:dark cycle and ambient temperature was steadily 21° C. For diurnal experiments, unfasted WT and $SK1^{fatKO}$ mice were sacrificed at ZT0, 3, 6, 9, 12, 15, 18, and 21, which corresponds to 6 a.m., 9 a.m., 12 p.m., 3 p.m., 6 p.m., 9 p.m., 12 a.m., and 3 a.m. At the time of sacrifice, mice were humanely euthanized by isoflurane (Hospira, Inc., Lake Forest, IL) followed by cardiac puncture. Cardiac blood was prepared for non-hemolyzed serum, aliquoted, and stored at -80° C until further analysis. Tissues were collected accordingly as fresh snap frozen in liquid nitrogen and stored at -80° C until further processing. All experiments were performed under clean conditions, were approved by the Medical University of South Carolina Institutional Animal Care and Use Committee, the Virginia Commonwealth University Institutional Animal Care and Use Committee, the Ralph H. Johnson Veterans Affairs Medical Center, and the Hunter Holmes McGuire Veterans Affairs Medical Center.

Serum Cholesterol and Triacylglycerol Measurements

Non-hemolyzed serum was tested for levels of total cholesterol (total free and total cholesterol esters) and total triacylglycerol with commercially available kits (Cayman Chemical, 10007640, 10010303). For the cholesterol assay, sera were diluted 1:300 using a kit-provided buffer, and for the triacylglycerol assay, the sera were tested undiluted/"neat."

Noninvasive Comprehensive Lab Animal Monitoring System (CLAMS)

Male WT and $SK1^{fatKO}$ C57BL/6 mice, 12-16-weeks old, were housed at the Center for Comparative Medicine at the University of Alabama at Birmingham under controlled conditions (28 ± 1°C and 12-h:12-h LD cycle enforced by environmental chambers) within a Comprehensive Laboratory Animal Monitoring System (CLAMS; Columbus Instruments Inc., Columbus, OH). These studies were approved by the Medical University of South Carolina Institutional Animal Care and Use Committee, the University of Alabama at Birmingham Institutional Animal Care and Use Committee, and the Ralph H. Johnson Veterans Affairs Medical Center. All mice were housed singly (n=6 per genotype), and allowed to acclimatize to the CLAMS for 7 days prior to initiation of the experimental protocol; during acclimatization, mice received standard rodent chow *ad libitum*. Throughout all studies, water was provided in an *ad libitum* fashion. The chow provided in all studies was Harlan NIH-31 Irradiated Open formula Mouse/Rat Diet (4.7% fat). Continuous 24-hour monitoring of behavioral and physiological parameters was performed using the CLAMS. Twenty-four-hour patterns of energy expenditure (indirect calorimetry), physical activity (beam breaks), and food intake were measured.

Cosinor Statistical Analysis

A single component cosinor nonlinear regression goodness of fit analysis was performed in Graphpad Prism 8 according to definitions from accepted literature (Cornelissen, 2014; Halberg, 1969; Halberg & Johnson, 1967; Morelli, et al., 2019; Refinetti, et al., 2007). The equation used for this analysis was : $f(t) = MESOR + A * Cos[(2 \pi t/T) + Acrophase]$. MESOR is the "midline estimating statistic of rhythm" and this value corresponds with the rhythm adjusted mean of the dataset or "baseline" value. Amplitude (A) is calculated as half the difference between the minimum and maximum, as defined by the cosinor fitted curve. The acrophase is the measure of the time at which overall high values recur in each cycle. R^2 corresponds to how well the dataset fit the standard cosinor curve, with 1 being a perfect fit. In other words, R^2 is the resulting statistic that measures the percent variance accounted for by the 24 h approximating waveform (Bray, et al., 2013). Time (t) is presented in hours, where .5 hour is equivalent to 30 minutes. The constants in this equation are $2 \times \pi \times 1/T$, where T is assumed to be a period of 24 hours. Thus, $1/12 \pi = 0.2618$.

General Statistical Analysis

All values are presented as mean ± SEM. For comprehensive lab animal monitoring system, values are also presented as violin plots, showing the median in bold solid lines, and the upper and lower quartiles in dashed black lines. For single pairwise comparisons of normally distributed data sets, a Student's *t*-test was performed. For multiple comparisons of means, a one-way ANOVA with Tukey-Kramer post hoc test was

performed. $p<0.05$ was considered statistically significant. All hypothesis tests were conducted using Graphpad Prism 8 software.

CHAPTER 5

SUMMARY AND PERSPECTIVE

Although the subject matter of sphingolipids, the adipocyte, and the circadian clock are esoteric entities to bring together, there exists the rationale to pay attention to their interplay. We have described here functions for SPHK1 and S1P in adipocyte circadian processes like lipolysis, organismal metabolic processes like glucose utilization and clearance, and novel circadian histone modification.

Many lipid and nutrient species in the circulation are known to have circadian expression patterns (Bailey, et al., 2014; Brunkhorst, et al., 2019; Gooley, 2016; Gooley and Chua, 2014; Kessler, et al., 2018; Shostak, et al., 2013; van den Berg, et al., 2018). Moreover, the adipocyte is poised to influence these circulating species due to its extraordinary secretory capacity (Scherer, 2006; Sulaieva, et al., 2018). In addition, a sprinkling of reports in the literature implicated sphingolipids as possibly being regulated by circadian rhythm (Brunkhorst, et al., 2019; Druzd, et al., 2017; Loizides-Mangold, et al., 2017). Quite importantly, it was emphasized that fatty acids directly impact sphingolipid biosynthesis; that is, palmitate is the most common free fatty acid substrate utilized in *de novo* sphingolipid biosynthesis, and palmitate (palmitic acid) is the most commonly found free fatty acid in mammals, with 16 carbons in its acyl chain (Geng, et al., 2015; Ross, et al., 2013; Russo, et al., 2012; Wang, et al., 2014). Therefore, the adipocyte, which specializes in metabolizing and storing circadian fatty acids, would most likely influence local adipocyte sphingolipid biosynthetic pathways.

At the beginning of the project, it was hypothesized that cycling fatty acids could be eliciting a cyclic transcriptional activation signal for *Sphk1*. This possibility was not ruled out, but instead the project focused on the E-boxes that were present in the *Sphk1* promoter and found that BMAL1 and CLOCK transcription factors were detectable over background at some time points but not all time points over 24 hours (Figure 10). To test

the effect of fatty acids would have introduced a step further upstream from the disrupted clock components being studied. *Sphk1* is not particularly abundant in the healthy adipocyte, so attempting to modify *Sphk1* by fatty acids to then probe further downstream circadian markers would have been murky at best. That would truly be a project in itself, perhaps visualizing a labeled fatty acid as well as a transfected fluorescently-tagged SPHK1 and further subjecting that to a circadian time course protocol.

The emphasis of adipocyte biology was strong because the Cowart lab specialized in metabolic disease, and many questions about the roles of sphingolipids in adipocytes were left to be answered. Adipocytes are one of the lynchpins of metabolic homeostasis, by acting like a sponge to take up excess circulating lipid. In other words, the membranes of adipocytes are highly plastic and dynamic, able to quickly take on increases and decreases in cell surface area and morphology while storing neutral lipids in its large droplet. This emphasizes the importance of sphingolipids in the adipocyte, for they are membrane structural molecules themselves, but also peculiar bioactive signaling molecules that impact cell function from autophagy to inflammation.

The hypothesis that, the adipocyte sphingolipids and the adipocyte circadian clock interact, grew from the known metabolic facts that fatty acids and lipids in circulation are not constant and that fatty acids directly affect sphingolipids. Moreover, obesity is highly characterized by the derangement of adipocytes, and it is well-established that misaligned circadian clocks (*e.g.*, due to shift-working) elicit deleterious effects upon the human body, and this has been demonstrated in a variety of laboratory animal models (Chaix, et al., 2019; Esquirol, et al., 2009; Karlsson, et al., 2009; Ramin, et al., 2015). Obesity is also known to increase SK1 expression and S1P levels, in rodents and in patients in the clinic (Anderson, et al., 2020; Kowalski, et al., 2013; Nagahashi, et al., 2018)

Sphingosine kinase 1, responsible for the phosphorylation of sphingosine to sphingosine-1-phosphate, is integral to maintaining the balance of sphingolipid metabolites. Between cells, tissues, and circulating fluids, S1P gradients are tightly controlled to elicit important responses, such as the gradient of S1P necessary to bring thymocytes out of the lymphoid organs and into the lymphatic fluid (Druzd, et al., 2017; Obinata and Hla, 2019). Evolutionarily speaking, segregating the action of S1P to a particular time of the day is advantageous for the fitness of the organism so that pro-inflammatory and pro-mitogenic signaling are concerted with other physiological processes. Since S1P is a bioactive lipid and has strong effects on the liver, it further corroborates the evolutionary necessity for S1P to be cyclically stimulating a robustly circadian organ (Geng, et al., 2015). Moreover, fatty acids are known to oscillate in the circulation, which may contribute then to potential cyclical activation of the sphingolipid biosynthetic pathway. It remains to be seen the true extent to which the circadian clock and sphingolipids may cross-regulate one another.

CHAPTER 6

SOLUTIONS TO BE FOUND

This project could have benefitted from a commercially available anti-SPHK1 (SPHK1 of mouse origin) antibody that detects native SPHK1 but not the truncated protein lacking exons 3-6 in the Cowart lab's model (Allende, et al., 2011). Future endeavors with SPHK1 might involve in-house generation of a suitable antibody. Moreover, primary culture of adipocytes is cumbersome due to the 7-day grow-up period and the ~10-day differentiation period. This makes transfection of these cells difficult since plating occurs approximately 10 days before the cells are mature, lipid-filled adipocytes for harvest (Figure 15). Moreover, this severely hampers turnaround time and continuity for experimental processing and interpretation.

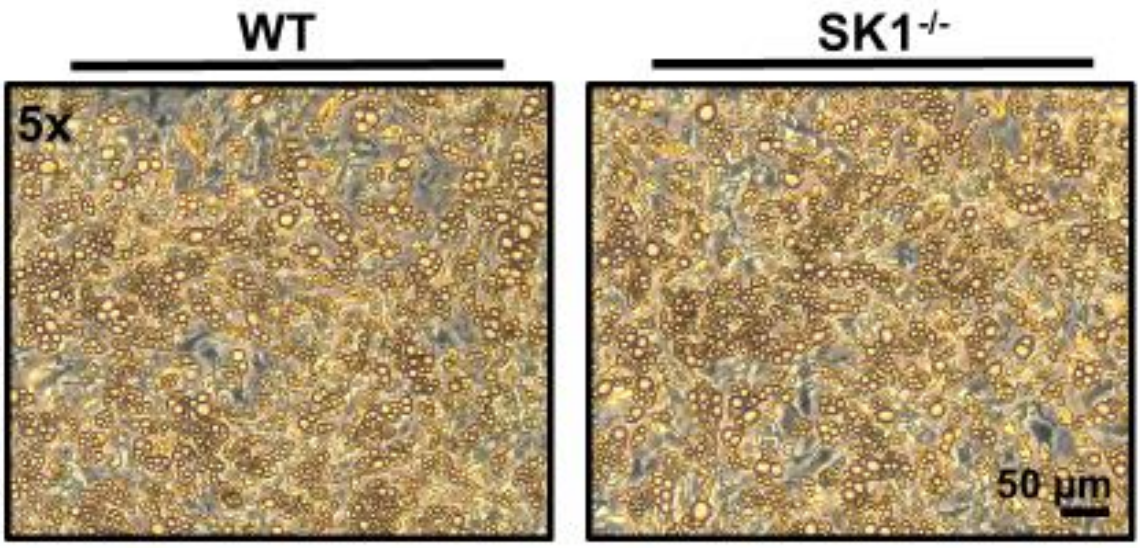

Figure 15. Matured primary adipocytes in culture. Under bright light, mature adipocytes are visualized as the golden cells with circular lipid droplets. The slight blue color pictured beneath the mature rounded adipocytes is barely visible, indicating that the culture achieved >90% differentiation. However, some preadipogenic precursors and stromal stem cells remain below, which is typical in a semi-purified primary culture system as this one. *$SK1^{-/-}$ is $SPHK1^{-/-}$.*

It is believed that the significance of circadian regulation of SPHK1 conveys to other cellular systems, especially considering the pulsatile *Sphk1* message levels in a circadian mouse lung dataset (Supplemental Figure 5). Therefore, further studies into *Sphk1* and circadian regulatory mechanisms may be explored more deeply and comprehensively in a simpler cell line model, perhaps of human origin. Some experiments of particular interest would be to transfect cells with circadian clock components (as control, overexpression, and/or knockout vectors, with or without fluorescent tags) and assess several aspects described in this work, but at an -omics level. For example, under conditions of *Bmal1* overexpression and depletion, to answer whether SPHK1 (and sphingolipids in general) become disrupted, assess by transcriptomics the expression of sphingolipid genes, analyze by proteomics the same, perform ChIP-Sequencing in BMAL1- and CLOCK-based immunoprecipitations, and determine by lipidomics/tandem mass spectrometry the effect on sphingolipid species levels in cells and media. These experiments could also be doubled-up with side-by-side fumonisin B1 treatments, to inhibit the *de novo* biosynthesis pathway and instead probe the circadian nature of the recycling pathways.

A troublesome aspect for the project was the apparent non-response of the clock to exogenously added S1P. For example, various experiments were performed to determine if S1P addition and/or antagonism of the 5 S1P receptors influenced core clock transcripts and proteins, but nothing notable transpired from such treatments according to the readouts measured, which was typically BMAL1 protein expression (Anderson, *data not shown*). Moreover, antagonists of the S1P receptors were utilized in the absence and presence of S1P to also determine if an S1P/S1P-receptor-based mechanism was at play; and similar to before, treatments with S1Pr antagonists and subsequent protein

expression assessment of core clock proteins revealed no differences among treatments and control (Anderson, *data not shown*). This led the logic down the path that SPHK1 is acting in a manner independent of its enzymatic product or that S1P was acting through an intracellular mechanism that could not properly be assessed simply by adding exogenous S1P to the cell culture media.

Another probable and tantalizing reason for the lack of response to exogenous S1P treatment could be the identity of the experimental carrier/vehicle used in the Cowart lab model, which is fatty acid-free BSA, since albumin is a known carrier of S1P in the bloodstream (Kharel, et al., 2020). This is a tantalizing idea because perhaps albumin-bound S1P is well-suited to act on hepatocytes, where a clear response to S1P/albumin is noted in various experiments in the Cowart lab, such as phosphorylation of AKT at serine 473 (Montefusco and Jamil, *unreported*). The same experiment in primary adipocytes does not yield an increase in pAKT (Anderson, *data not shown)*. Insulin treatment in HEK293 cells stimulated pAKT at serine 473, but S1P treatment side-by-side did not induce such phosphorylation of AKT (Zaslavsky, et al., 2005). Perhaps the adipocyte would rather take in S1P from a lipoprotein particle rather than albumin, a hypothesis worth further testing in the future. Moreover, many other labs studying S1P utilize the albumin carrier to conduct S1P signaling analyses. It was always important that the albumin was especially prepared without fatty acids in order to reduce the confounding effects of other signaling lipids as well as to facilitate efficient S1P complexing to albumin. The other known prominent S1P carrier in the circulation is high density lipoprotein (HDL), specifically the ApoM moieties (Blaho, et al., 2015; Kurano, et al., 2020). It was also shown recently that S1P can be transported by ApoA4 (Obinata, et al., 2019). Perhaps

experiments in the future may utilize HDL-like carriers for S1P exogenous treatments in cell culture, as long as HDL carriers are readily available as reagents.

Secretory extracellular vesicles from hepatocytes were shown to carry S1P in a SK1- and SK2-dependent fashion, in which S1P promoted a deleterious pro-inflammatory phenotype in neighboring immune cells which responded to the vesicles of S1P (Liao, et al., 2018). Moreover, it is well-known that S1P undergoes “inside-out” autocrine signaling, meaning that it is readily export out of the cell once it’s generated by intracellular kinase action (Nagahashi, et al., 2018; Takabe, et al., 2008). This would highly suggest that any cell type other than lipoprotein-excreting-capable cells (*i.e.*, hepatocytes) must be secreting S1P in a fashion independent of these known HDL-associated apolipoproteins. Thus, it is hypothesized that S1P leaving the adipocyte and re-entering the adipocyte is either free, albumin-bound, or unidentified other carrier-bound. These notions are worth further investigation in the future. It was stated in a biophysical study of S1P that “two important differences between S1P and ceramide are that S1P stabilizes the lipid bilayer structure, and physiologically relevant concentrations of S1P can exist dispersed in the cytosol” (García-Pacios, et al., 2009).

S1P was also discovered to travel throughout the circulation on HDL through apolipoprotein M, and it was found that the identity of the carrier for S1P generally had effects on its signaling and degradation kinetics (Christoffersen, et al., 2011; Kurano, et al., 2013; Mishima, et al., 2018). S1P and ApoM were shown to ameliorate insulin resistance by enhanced phospho-AKT signaling in livers of mice overexpressing ApoM (Kurano, et al., 2020). Moreover, ApoM-bound S1P (but not albumin-bound) led to decreases in lymphopoiesis, thereby maintaining physiological levels of circulating immune cells and gating against autoreactive autoimmune responses (Blaho, et al., 2015).

In mice lacking both ApoM and albumin, S1P was still detectable and identified on another HDL carrier, ApoA4 (Obinata, et al., 2019). In humans, it was found that single nucleotide polymorphisms in ApoA4 and other triacylglycerol-modulating genes were correlated with worse atherosclerosis-based clinical outcomes in a population samples from China (Fu, et al., 2015). Additionally, Yu and coworkers found that liposomal-S1P versus non-liposomal S1P had differential migratory effects on various cell lines in culture (Yu, et al., 2009). In another study utilizing liposomes (consisting of egg phosphatidylcholine and cholesterol) as a drug delivery vehicle, N,N,N-trimethylsphingosine (TMS) was efficiently delivered to cancer cells while having lower toxicity to healthy tissue (especially blood) compared to delivery of free TMS (Park, et al., 1994). Liposomes are widely used in the cancer field and medicine to better deliver drugs, with liposomes conferring such properties as better efficacy, targeted release, longer half-life, and better tolerability.

These studies seriously suggest that the cargo, carrier, chaperone, or other vehicle for S1P is crucial to its downstream signaling and physiological effects. Thus, future studies should aim to clearly associate findings not just with S1P itself but the carrier to which S1P was complexed for any experiments. This further suggests that cell types are specialized to receive S1P in a specific context and not just on any carrier in order to elicit effects.

Studies from this project utilized S1P on fatty-acid-free bovine serum albumin, which is typical for much of the current literature. It is well-accepted that S1P binds albumin as well as HDL, owing to the amphipathic/zwitterionic properties of the phosphorylated long chain amino alcohol (Camerer, et al., 2009; Sposito, et al., 2019). However, findings from others and anecdotal evidence from this project would suggest that adipocytes may not respond readily to albumin-bound S1P. Thus, further studies in the future may aim to

characterize the role of S1P in physiology by testing treatments that specify albumin, exosome/extracellular vesicle/liposome, ApoM, ApoA4, or simply HDL.

Similar to work of others, we observed that SPHK1$^{-/-}$ adipocytes accumulated the substrate for SPHK1, sphingosine (*data not shown*). Wilkerson et al. demonstrated that the retinas of SPHK1$^{-/-}$ mice also accumulated approximately double the amount of sphingosine compared to WT (Wilkerson, et al., 2019). Moreover, we observed in the SPHK1$^{-/-}$ animals no overt phenotypic consequences of genetic depletion, just as others did (Lima, et al., 2017; Wilkerson, et al., 2019). Besides the mostly unchanged gross phenotypic examination, important processes became disrupted with SPHK1 depletion, such as endocytosis and the adhesion among retinal cells (Lima, et al., 2017; Wilkerson, et al., 2019). In agreement with the overall findings by Wilkerson et al, Terao and colleagues found that light stimulus can induce the release of S1P from retinal cells, implicating a light-responsive property of SK1 (Terao, et al., 2019). These data indicate that further exploration of SK1 regulation is critical.

In the studies carried out in the Cowart lab, it was found in SPHK1$^{-/-}$ primary adipocytes that histone acetylation and circadian timing were defective due to depletion of SPHK1$^{-/-}$. Hinting that the sphingosine kinases are not as straightforward as might be expected, Ravichandran et al. assessed metabolic parameters in SPHK2$^{-/-}$ mice, such as circulating insulin, glucose, and triglycerides (insulin and TAGs were lower, in contrast to the Cowart SK1^{fatKO} model), and they also showed that adipose of these mutant mice were not as heavy as control adipose tissue; however, they did not assess anywhere in the study the concentration of S1P in the blood or tissues (Ravichandran, et al., 2019). It is worth noting that it is well accepted in the sphingolipid field that SPHK2$^{-/-}$ mice have higher circulating S1P, which still has yet to fully be explained, although now is thought to rely on

the lipid phosphate phosphatase 3 transporter (Kharel, et al., 2012, 2020). In another model, Qin and colleagues showed that SPHK1 depletion in human fibroblasts resulted in an increase in the substrate sphingosine compared to control, and they reported an increase in S1P in the SPHK1$^{-/-}$ condition, but did not offer a dedicated discussion for this particular finding (Qin, et al., 2018). These somewhat perplexing findings illustrate that the regulation of SPHKs is complex.

The deconvolution of the actions of Sphk1, Sphk2, and S1P (as well as the S1P-degrading and -transporting enzymes) is critical for a lucid comprehensive understanding of these special lipid kinases and their bioactive lipid product. Genetic ablation of either of the isoenzymes has reliably produced conflicting results with supposedly specific pharmacological inhibitors of the SK isoenzymes (Pyne, et al., 2017). Similar to our findings that serum S1P and adipose S1P did not decrease in SK1^{fatKO} mice, it was found that circulating levels of S1P were increased in global *Sphk2*$^{-/-}$ mice (Anderson, et al., 2020; Nagahashi, et al., 2016). Moreover, treatment with the SPHK2 inhibitor SRL080811 also paradoxically increased serum levels of S1P (Kharel, et al., 2011). Seemingly contradictory findings such as these prompt the speculation that SPHK1 and SPHK2 actions are quite complicated and modification of the enzymes alone does not necessarily predict a logical product outcome for S1P. Therefore, one other possibility or explanation worth further investigation in the future is that genetic downregulation of *Sphk1* with concomitant unchanged S1P might suggest a dearth of export of intracellular S1P, as a mechanism to hold on to what is needed inside the cell and perhaps mitigate the outward transport for other (lower-priority) processes. That is, the intracellular actions of S1P in the adipocyte are more precious than the expendable extracellular actions in the face of *Sphk1* depletion, therefore, total S1P levels as measured by sphingolipidomics do not

yield a net change. Intuitively, however, evidence does indeed point to the substrate long chain base sphingosine building up in SK1$^{-/-}$ adipocytes *in vitro* (*data not shown*).

In closing, the circadian clock is a complex system requiring special cell culture conditions to properly study. As described previously, the regulation of SKs also is not clean-cut. Here, it was shown that adipocyte SK1 impacts adipocyte cell morphology and functional processes, such as lipolysis and circadian rhythm. Surprisingly, adipocyte SK1 deficiency also had measurable effects upon the liver, as demonstrated by histological accumulation of lipid (steatosis) as well as deranged secretion of cholesterol and triacylglycerol over time. More studies are needed to delineate the effects on the liver, such as a circadian study of the tissue for transcriptional and histone status readouts. These effects were observed despite not showing decreases in S1P. This could suggest that specific pools of S1P generated by either kinase may act within the cell in a specific manner depending on its source kinase. Again, these questions remain to be answered, and could potentially direct the development of therapeutics in the future, especially whether sphingolipid-based therapeutics are more effective when administered at a particular time of the day.

CHAPTER 7

MATERIALS AND METHODS

Generation of Adipocyte-Specific *Sphk1* Knockout ("SK1^{fatKO}") Mouse

Adipocyte-specific *Sphk1* knockout mice (SK1^{fatKO}) were generated by crossing B6; FVB-Tg(Adipoq-cre)1Evdr/J (Jackson Laboratory strain 010803) and B6N.129S6-Sphk1^{tm2Cgh}/J (Jackson Laboratory strain 019095) (Pappu, et al., 2007). Heterozygous mice were crossed to generate homozygous *flox/flox* or +/+ breeding pairs. Genotype was confirmed using primers for the floxed *Sphk1* and *Adipoq-Cre*. Cre-mediated homologous recombination removes exons 3-6 from the *Sphk1* gene (Supplemental Figure 1A). WT mice were all Cre carriers. Primers used for genotyping were as follows:

Cre1 5' ACGGACAGAAGCATTTTCCA 3'

Cre2 5' GGAGTGCCATGTGAGTCTG 3'

Cre3 5' CTAGGCCACAGAATTGAAAGATCT 3'

Cre4 5' GTAGGTGGAAATTCTAGCATCATCC 3'

Flox F 5' GGAACCTGGCTATGGAACC 3'

Flox R1 5' ATGTTTCTTTCGAGTGACCC 3'

Flox R2 5' AATGCCTACTGCTTACAATACC 3'.

Gene depletion was confirmed by PCR amplification of a shortened fragment of the *Sphk1* gene in adipocyte genomic DNA from flox/flox:CRE/CRE mice, further described and shown in Supplemental Figure 1.

Animal Model

All animal experiments conformed to the Guide for the Care and Use of Laboratory Animals and were in accordance with Public Health Service/National Institutes of Health guidelines for laboratory animal usage. For Chapter 3, the experimental groups consisted

of male and female WT and SK1^{fatKO} C57BL/6 mice. Mice were housed in the animal facility at the Medical University of South Carolina (*in vivo* studies), and Virginia Commonwealth University (*ex vivo* studies). Food and water were provided *ad libitum*, except when fasting was required (*e.g.*, glucose tolerance testing). Animals were maintained on a 12h:12h light:dark cycle and ambient temperature was steadily 21° C. For Chapter 3, animals were randomized to a high saturated fat diet (HFD) (Envigo, TD.09766) (60% kcal provided by milkfat) or an isocaloric low fat diet (CD) (Envigo, TD.120455) (17% kcal provided by lard) at 6 weeks of age, and diets were administered for 18 weeks (*n* = 8-10 per group). On the day of sacrifice, mice were fasted for 6 hours, and mice were euthanized humanely by isoflurane (Hospira, Inc., Lake Forest, IL) followed by cardiac puncture. Cardiac blood was prepared for non-hemolyzed serum, aliquoted, and stored at -80° C until further analysis. Tissues were collected accordingly as fresh fixed in 10% neutral buffered formalin or fresh snap frozen in liquid nitrogen and stored at -80° C until further processing. For Chapter 4, the experimental groups consisted of male WT and SK1^{fatKO} C57BL/6 mice. Mice were housed in the animal facility at the Medical University of South Carolina. Standard chow and water were provided *ad libitum*, except when fasting was required (*e.g.*, glucose tolerance testing). Animals were maintained on a 12h:12h light:dark cycle and ambient temperature was steadily 21° C. For diurnal experiments, unfasted WT and SK1^{fatKO} mice were sacrificed at ZT0, 3, 6, 9, 12, 15, 18, and 21, which corresponds to 6 a.m., 9 a.m., 12 p.m., 3 p.m., 6 p.m., 9 p.m., 12 a.m., and 3 a.m. At the time of sacrifice, mice were humanely euthanized by isoflurane (Hospira, Inc., Lake Forest, IL) followed by cardiac puncture. Cardiac blood was prepared for non-hemolyzed serum, aliquoted, and stored at -80° C until further analysis. Tissues were collected accordingly as fresh snap frozen in liquid nitrogen and stored at -80° C until further processing. All experiments were

performed under clean conditions, were approved by the Medical University of South Carolina Institutional Animal Care and Use Committee, the Virginia Commonwealth University Institutional Animal Care and Use Committee, the Ralph H. Johnson Veterans Affairs Medical Center, and the Hunter Holmes McGuire Veterans Affairs Medical Center.

Noninvasive Comprehensive Lab Animal Monitoring System (CLAMS)

For Chapter 4, male WT and $SK1^{fatKO}$ C57BL/6 mice, 12-16-weeks old, were housed at the Center for Comparative Medicine at the University of Alabama at Birmingham under controlled conditions (28 ± 1°C and 12-h:12-h LD cycle enforced by environmental chambers) within a Comprehensive Laboratory Animal Monitoring System (CLAMS; Columbus Instruments Inc., Columbus, OH). These studies were approved by the Medical University of South Carolina Institutional Animal Care and Use Committee, the University of Alabama at Birmingham Institutional Animal Care and Use Committee, and the Ralph H. Johnson Veterans Affairs Medical Center. All mice were housed singly (n=6 per genotype), and allowed to acclimatize to the CLAMS for 7 days prior to initiation of the experimental protocol; during acclimatization, mice received standard rodent chow *ad libitum*. Throughout all studies, water was provided in an *ad libitum* fashion. The chow provided in all studies was Harlan NIH-31 Irradiated Open formula Mouse/Rat Diet (4.7% fat). Continuous 24-hour monitoring of behavioral and physiological parameters was performed using the CLAMS. Twenty-four-hour patterns of energy expenditure (indirect calorimetry), physical activity (beam breaks), and food intake were measured.

Glucose Tolerance Test

Intraperitoneal glucose tolerance tests were performed on mice after 8 weeks of diet feeding (*i.e.*, 14 weeks of age). Mice were fasted for 6 hours, before conducting a glucose tolerance test, generally 0830 hr to 1430 hr. Blood was collected through a nick in the tail and analyzed neat using a One Touch UltraSmart Blood Glucose Monitoring System at fasting for baseline blood glucose concentration. Mice received a sterile 2 mg/kg D-glucose injection. Blood glucose was then assessed 15, 30, 60, and 120 minutes after glucose injection.

Bioplex

Serum cytokines (insulin, leptin) were measured using a multiplex adipokine assay service, akin to an ELISA method (Eve Biotechnologies).

Triglyceride Assay

Liver tissue homogenates were prepared according to the manufacturer's instructions with modifications (StanBio, 2200-225). Approximately 50 mg of liver tissue was homogenized in 300 µL of solution of 2:1 100% EtOH and 30% KOH, respectively. This was vortexed and allowed to incubate in a 60° C water bath for 5 hours until the solution turned a translucent yellow with a visible pellet at the bottom. Then, 1.08 volumes of 1 M $MgCl_2$ was added to the tube and vortexed to reach a milky consistency and left on ice for 10 minutes. Following this, tubes were vortexed and centrifuged for thirty minutes at 18,500 × g at ambient temperature. The supernatant was collected, diluted 1:10 with 1x PBS, and subjected to the triglyceride assay according to the manufacturer's instructions. In order to normalize to protein concentration by BCA, an aliquot was taken from the homogenate

prior to water bath incubation, dried down, and resuspended in 1x PBS. 10 µL of sample and standards were assayed with 250 µL of the triglyceride reagent. Water was used as a blank. Absorbances were read after 5 minutes' incubation at 37° C at 500 nm.

qPCR

For Chapter 3, total RNA was isolated from gonadal adipose tissue and liver tissue homogenized in Trizol (Invitrogen, 15596026) followed by RNeasy mini kit (Qiagen, 74106) extraction and column purification. RNA integrity in tissue was assessed using the Agilent 2100 Bioanalyzer by the MUSC Proteogenomics Facility. All RNA samples had RIN > 7. cDNA was synthesized from 1 µg of total RNA using iScript Advanced cDNA Synthesis Kit (Bio-Rad, 1708890). Real time PCR was performed using a CFX96 Real-Time System (Bio-Rad) and SSoAdvanced Sybr (Bio-Rad, 172-5272). The following primers were used: *Tbp* (Qiagen, PPM03560F), *Ppia* (Qiagen, PPM03717B), *Tnfα* (Qiagen, PPM03113G-200). Mean normalized expression was calculated by normalizing to the geometric mean of reference genes *Ppia* and *Tbp* in gonadal adipose tissue (*i.e.*, $root_2[C_q$ gene 1 × C_q gene 2]) using the $2^{-\Delta\Delta Ct}$ method. Mean normalized expression was calculated by normalizing to the expression of *Hmbs1* in liver tissue. Other primers are listed next:

Gene	Forward (5' to 3')	Reverse (5' to 3')
Tbp	AAGGGAGAATCATGGACCAG	CCGTAAGGCATCATTGGACT
Ppia	GAGCTGTTTGCAGACAAAGTTC	CCCTGGCACATGAATCCTGG
Hmbs1	ATGAGGGTGATTCGAGTGGG	TTGTCTCCCGTGGTGGACATA
Adipoq	TGTTCCTCTTAATCCTGCCCA	CCAACCTGCACAAGTTCCCTT
Arg1	TGGCTTGCGAGACGTAGAC	GCTCAGGTGAATCGGCCTTTT
Dgat2	GAGGGGTCTGGGCGATGGGGCAC	CGACGGTGGTGATGGGCTTGGAGT
Fasn	GACTCGGCTACTGACACGAC	CGAGTTGAGCTGGGTTAGGG
F4/80	TCATGGCATACCTGTTCACC	GAATGGGAGCTAAGGTCAGTC
Il-6	TAGTCCTTCCTACCCCAATTTCC	TTGGTCCTTAGCCACTCCTTC
iNOS	TTCCATGCTAATGCGAAAGG	GCTCCTCTTCCAAGGTGCTT
Mcp1	TTAAAAACCTGGATCGGAACCAA	GCATTAGCTTCAGATTTACGGGT
Sphk1	GAGTGCTGGTGCTGCTGAA	AGGTTATCTCTGCCTCCTCCA
Sphk2	CACGGCGAGTTTGGTTCCTA	CTTCTGGCTTTGGGCGTAGT
Tgf-β1	TGGCGTTACCTTGGTAACC	GGTGTTGAGCCCTTTCCAG

Primers used for qPCR analysis.

For Chapter 4, total RNA was isolated from cultured primary adipocytes or gonadal adipose tissue homogenized in Trizol (Invitrogen, 15596026) followed by RNeasy mini kit (Qiagen, 74106) extraction and column purification. cDNA was synthesized from 1 µg of total RNA using iScript Advanced cDNA Synthesis Kit (Bio-Rad, 1708890). Real time PCR was performed using a CFX96 Real-Time System (Bio-Rad) and SSoAdvanced Sybr (Bio-Rad, 172-5272). The primers used for cDNA qPCR and DNA CHIP-qPCR are shown in the following table. Mean normalized expression was calculated by normalizing to the geometric mean of reference genes *Ppia* and *Tbp* in gonadal adipose tissue (*i.e.*, $root_2[C_q$ gene 1 × C_q gene 2]) using the $2^{-\Delta\Delta Ct}$ method. ChIP normalization was carried out with a 10% input control.

Method	*Gene*	Forward (5' to 3')	Reverse (5' to 3')
ChIP	*Cbxypa1*	CATGGTCAAGGGTGAAAG	CTGAGGTCTGAGGCCTTTTT
ChIP	*Atgl*	CGGCGGAGGCGGAGACGCT	TCCCTGCTTGATCCAGTTGGAT
ChIP	*Dbp*	AATGACCTTTGAACCTGATCCCGCT	GCTCCAGTACTTCTCATCCTTCTGT
ChIP	*Lipe*	GCTGCCCTGGGAGGATTAAGCC	CAAAAGCCTGAGAGGTTTCTCCGAG
ChIP	*Nr1d1 (Reverbα)*	ACGACCCTGGACTCCAATAA	CCATTGGAGCTGTCACTGTAGA
ChIP	*Per2*	CAACACAGACGACAGCATCA	TCCTGGTCCTCCTTCAACAC
ChIP	*Per3*	CTGCTCCAACTCAGCTTCCTTT	TTAGACAGCAAGGCTCTGGTTCT
ChIP	*Pgc1α*	GCAATTCAATTCGGGTCCATCTCACC	GGACTTCAGCGTGTTTGCATTCAGTAC
ChIP	*Pparγ*	CTGTACAGTTCACGCCCCTC	TCACACTGGTGTTTTGTCTATG
ChIP	*Sphk1 -1800*	TACACCGGGGCACGTGTGCATT	TCTTTCCCCCCAGGGAACACTA
ChIP	*Sphk1 -300*	ACTTTGTCCCACGTGCATGGA	TCCCGCTGACAAGGGGCCA
qPCR	*Ppia*	GAGCTGTTTGCAGACAAAGTTC	CCCTGGCACATGAATCCTGG
qPCR	*Tbp*	AAGGGAGAATCATGGACCAG	CCGTAAGGCATCATTGGACT
qPCR	*Bmal1 (Arntl)*	TGACCCTCATGGAAGGTTAGAA	GGACATTGCATTGCATGTTGG
qPCR	*Dbp*	CGTGGAGGTGCTTAATGACCTTT	CATGGCCTGGAATGCTTGA
qPCR	*Nr1d1 (Reverbα)*	TACATTGGCTCTAGTGGCTCC	CAGTAGGTGATGGTGGGAAGTA
qPCR	*Per2*	CCATCCACAAGAAGATCCTAC	GCTCCACGGGTTGATGAAGC
qPCR	*Per3*	CCCTACGGTTGCTATCTTCAG	CTTTCGTTTGTGCTTCTGCC
qPCR	*Rorγ*	GACTGGAGGACCTTCTACG	TCCCACATTGACTTCCTCTG
qPCR	*Sphk1*	GAGTGCTGGTGCTGCTGAA	AGGTTATCTCTGCCTCCTCCA

Primers used for ChIP/qPCR and qPCR analysis.

Chromatin Immunoprecipitation

Primary WT and SPHK1$^{-/-}$ matured, synchronized adipocytes were plated on 15-cm plates per 2 ChIPs. Briefly, cells were washed twice with room temperature 1x PBS and the dishes were then placed on an orbital rocker (Sigma, Z768502) in a measured volume of freshly-made PBS solution containing 2 mM disuccinimidyl glutarate (DSG) (ProteoChem, c1104) for 10 minutes. After 10 minutes, fresh 37% formaldehyde (Fisher, BP531-500) was added directly to the solution to a final concentration of 1% and continued swirling gently for another 12 minutes. Finally, the crosslinking reactions were quenched with glycine at a final concentration of 125 mM for 5 additional minutes. Following, the solution was discarded as hazardous waste and the cells were washed twice with cold 1x PBS.

The PBS was aspirated, and the cells were scraped into 1.8 mLs adipocyte hypotonic lysis buffer (5mM PIPES pH 7.8, 10 mM KCl, 1% Igepal, plus protease/phosphatase inhibitors and PMSF immediately before use) per 15-cm plate. The cells were collected in a Dounce homogenizer and were sheared with 10 strokes of the Dounce until visibly dissociated. The cells were also passed through a 22G needle to ensure disruption of the monolayer but preservation of the nuclei. The resulting slurry was vortexed and kept on ice for 10 minutes. Next, the tubes were centrifuged at 8,500 × *g* at 4° C for 8 minutes to remove a significant fat cake at the top as well as the cytoplasmic infranatant and to leave the nuclear pellet intact and undisturbed. The pellets were resuspended in the same lysis buffer to wash excess adipocyte lipid from the nuclear pellet and vortexed. They were re spun, and the pellets were saved. Next, the pellets were suspended in 600 µL sonication lysis buffer (50 mM Tris-HCl, pH 8.0, 10 mM EDTA, 1% SDS, and protease/phosphatase inhibitors and PMSF fresh) per 15-cm plate. The 600 µL was split into two 1.5-mL Eppendorf tubes of 300 µL, and then were sonicated (Branson 150, Branson Ultrasonics, Danbury, CT) for 8 rounds of 30 seconds on, 30 seconds off in a 4° C water bath. The resulting sonicate was then subjected to centrifugation at 18,000 × *g* at 4° C to clarify the chromatin. The chromatin supernatant was collected and split to two chromatin immunoprecipitations as well as the 10% input control. Thus, approximately 500 µL of recovered sonicate was split to 200 µL per ChIP plus a 20-µL 10% input. The ChIP samples were diluted 1:10 with Dilution/Low Salt buffer (20 mM Tris-HCl pH 8.0, 150 mM NaCl, 2 mM EDTA, 1% Triton X-100, 0.1% SDS), pre-cleared with ChIP-grade Protein A/G magnetic beads (Thermo Fisher Scientific, 26162) for one hour, and immunoprecipitated with 1 µg of antibody overnight at 4° C while rocking. The following day, pre-equilibrated magnetic ChIP-grade Protein A/G beads were added to the samples

for 2 hours. They were then subjected to extensive washing on the magnetic rack, performing two washes in Low Salt Buffer, 2 subsequent washes in high salt buffer (20 mM Tris-HCl pH 8.0, 500 mM NaCl, 2 mM EDTA, 1% Triton X-100, 0.1% SDS), 2 subsequent washes in LiCl Buffer (10 mM Tris-HCl pH 8.0, 500 mM NaCl, 1 mM EDTA, 1% deoxycholate, 1% NP-40, 0.25 M LiCl), and finally 2 washes in TE buffer (10 mM Tris-HCl pH 8.0, 1 mM EDTA). After these 8 washes, 100 µL of ChIP elution buffer (0.1 M $NaHCO_3$, 1% SDS) was added to the beads, in addition to the reverse crosslinking reagent, 4 µL of 5 M NaCl, and these were incubated overnight at 65° C. The next morning, the samples were treated with RNase A (Thermo Fisher Scientific, EN0531) for 1 hour at 37° C, and after that, treated with Proteinase K (Thermo Fisher Scientific, EO0491) for 1 hour at 60° C. After this, the samples were subjected to DNA isolation and purification with a column-based washing approach (Zymo Research, D5205). The samples were eluted from the column in 120 µL and 2 µL per well, assayed in triplicate, were used for real time qPCR of the DNA. Primers used for ChIP are shown in the previous section *qPCR*. Antibodies used for ChIP are as follows:

Application	Target	Antibody	Host	Supplier	Catalog #	Concentration or Dilution
ChIP	Mouse	H3K9ac	Rabbit	Thermo	710293	1 µg per IP
ChIP	Mouse	H3K27ac	Rabbit	Thermo	MA5-24671	1 µg per IP
ChIP		Normal IgG	Rabbit	Bethyl	P120-101	1 µg per IP
W.B. and ChIP	Mouse	BMAL1	Rabbit	Bethyl	A302-616A	1 µg per IP
W.B. and ChIP	Mouse	CLOCK	Rabbit	Bethyl	A302-618A	1 µg per IP

Antibodies used for ChIP analysis.

Basal Lipolysis Assay for Non-esterified Fatty Acids

Sera from mice and cell culture media containing only fatty acid-free bovine serum albumin were prepared for non-esterified fatty acid assay according to the manufacturer's instructions (Wako Diagnostics, 999-34691, 995-34791, 991-34891, 993-35191, 276-76491). Briefly, 5 µL of sample (neat or diluted 1:10), calibrators, and blank were added in duplicate to a 96-well plate. 200 µL of Color Reagent A solution was added and incubated at 37° C for 5 minutes. Absorbance at 550 nm was acquired. Next, 100 µL of Color Reagent B solution was added and incubated at 37° C for 5 minutes. Absorbance was read once more at 550 nm. After subtracting the blanks, the first reading was subtracted from the second reading to obtain the final absorbance, and concentrations were determined by standard curve normalization.

Glycerol Assay

Protocol was adapted from Sigma. 25 µL cell culture media was assayed in duplicate in a 96-well plate. 100 µL of free glycerol reagent (Sigma, F6428) was added per well and incubated for 5 minutes at 37° C. Absorbance at 540 nM was measured on a spectrophotometer. Relative concentrations of glycerol were determined by normalization to a standard curve. Tissue explants glycerol release was normalized to tissue weight.

Lipolysis in Adipose Tissue Explants (*ex vivo*)

Gonadal adipose tissue was harvested from WT and $SK1^{fatKO}$ mice at 4-6 weeks of age. Tissue was cut into ~12 mg pieces. Two pieces were added to each well of a 12-well plate in 1 mL of DMEM/F12 (Corning, 10-090-CV) + 1% FAF BSA (Thermo Fisher Scientific, 9704100) and 1% penicillin streptomycin antimycotic solution (Sigma, A5955-100ML).

Explants "rested" in the incubator overnight at 37° C and 10% CO_2. The next day, explants were transferred using clean forceps to new 12-well plates containing fresh media. Media was collected after 24 hours for glycerol measurement.

Histology and Immunohistochemistry

Fresh liver tissue was snap frozen in liquid nitrogen. 10-µm frozen sections were prepared for measurement of hepatic neutral lipid accumulation by Oil Red O staining. Sections were counterstained with hematoxylin. Paraffin sections were prepared with adipose and liver tissue fixed in 10% neutral buffered formalin (1 hour). Adipose sections were stained with hematoxylin and eosin (H&E) for adipocyte size analysis. Slides were imaged on a light microscope (Leica DMI1 microscope, Leica MC170 HD camera), and only for the adipose H&E was a fluorescence microscope utilized for better contrast with a 555 laser. For immunofluorescence histology, sections were subjected to antigen retrieval overnight at 60° C in 10 mM sodium citrate, 0.05% Tween 20 pH 6.0 buffer. Slides were blocked using 5% donkey serum (host secondary antibody species). Slides were imaged on a Zeiss FV10i fluorescent microscope for myeloperoxidase (R&D Systems, AF3667, goat anti-mouse MPO, 15 µg/mL), a marker of infiltrating inflammatory immune cells. Secondary detection antibodies were from Life Technologies: Alexa 488 (Invitrogen, A-11055, donkey anti-goat, 1:2000) and ToPro3 to stain nuclei (Thermo Fisher Scientific, T3605, 1:2000). Ten representative images per slide were analyzed by fluorescence intensity of puncta using ImageJ software.

Serum Cholesterol and Triacylglycerol Measurements

Non-hemolyzed serum was tested for levels of total cholesterol (total free and total cholesterol esters) and total triacylglycerol with commercially available kits (Cayman Chemical, 10007640, 10010303). For the cholesterol assay, sera were diluted 1:300 using a kit-provided buffer, and for the triacylglycerol assay, the sera were tested undiluted/"neat."

Cell Culture, Isolation of Stromal Vascular Fraction (SVF) and Differentiation to Mature Adipocytes

Primary adipose-derived stem cells (ADSCs) were isolated from inguinal adipose tissue of 3-8-week-old WT, $SPHK1^{-/-}$, or $SK1^{fatKO}$ mice. Subcutaneous adipose tissue was digested using 0.1% collagenase (Sigma, C6885) in digestion buffer (100 mM HEPES, 120 mM NaCl, 50 mM KCl, 5 mM glucose, 1 mM $CaCl_2$, 1.5% BSA) in a 37º C shaking incubator (New Brunswick Scientific) (150 rpm) for 40 minutes. The digest was filtered through a 100-µM cell strainer and centrifuged at 500 × *g* for 5 minutes. The SVF pellet was re-suspended in media, filtered through a 40-µM cell strainer and plated. Media was changed after two hours to remove non-adherent cells. Cells were grown to confluency in proliferation media (DMEM/12 50:50 (Corning, 10-090-CV), 10% fetal bovine serum (FBS) (Atlanta Biologicals), 1% penicillin streptomycin antimycotic cocktail (MilliporeSigma, A5955). 48 hours post-confluency, differentiation was induced using 10 µg/mL insulin (Santa Cruz Biotechnology, sc-360248), 1 µM dexamethasone (MilliporeSigma, D4902), 0.5 mM IBMX (Enzo Life Sciences, BMLPD1401000), and 1 µM rosiglitazone (Cayman Chemical, 71740) for two days. Differentiation was maintained with insulin for days 3-4

and proliferation media days 5-8. Mature adipocytes were visualized under a brightfield microscope to assess lipid droplet formation, and plates with large lipid droplets and >90% differentiation were used for experiments (Figure 15).

in vitro Circadian Rhythm

Unless otherwise noted, the *in vitro* circadian experiments are all performed in the same manner, in which primary WT and SPHK1$^{-/-}$ ADSCs were brought to maturity, and on the day of the experiment, the cells were synchronized with 50% horse serum (Gibco, 26050-070) and 50% DMEM/F12 for 2 hours. Following the horse serum shock, the cell monolayer was gently rinsed once with warm 1x PBS and 2% fatty-acid-free BSA in DMEM/F12 was kept on the cells for the duration of the experiment, which generally lasted 48 hours *in toto*.

S1P Treatment

WT primary matured, synchronized adipocytes were allowed to cycle for 24 hours, after which, cells were treated with a final concentration 150 nM S1P (Avanti Polar Lipids, 860492) complexed to 4 mg/mL FAF BSA or 4 mg/mL FAF BSA without S1P and assayed by ChIP for acetylated histone H3 signal at various adipocyte and circadian gene loci.

^{17}C-Sphingosine Treatment

WT primary matured, synchronized adipocytes were allowed to cycle for 24 hours, after which, cells were treated with a final concentration 5 μM ^{17}C-sphingosine (Avanti Polar Lipids, 860640) (dissolved in 100% ethanol) for exactly 30 minutes, collected immediately with addition of phosphatase inhibitors, for an exact volume of media in a 5-mL borosilicate

glass tube and for a cell pellet in minimal PBS in a separate 5-mL borosilicate glass tube, capped, and stored at -80° C until analysis by tandem liquid chromatography and mass spectrometry lipidomics. This 30-minute procedure was repeated every 4 hours over a 24-hour period to assay *in situ* the enzymatic turnover of ^{17}C-sphingosine to ^{17}C-S1P (Spassieva, et al., 2007).

Lipid Measurements

For Chapters 3 and 4, sphingolipids were measured using liquid chromatography/tandem mass spectrometry at the Virginia Commonwealth University Lipidomics and Metabolomics Core and performed using previously published methods (Haynes, et al., 2009; Shaner, et al., 2009). For Chapter 4, sphingolipids were also measured at the Medical University of South Carolina Shared Lipidomics Resource according to previously published methods (Bielawski, et al., 2010; Spassieva, et al., 2007).

Cellular Fractionation for Nuclear and Cytoplasmic Enrichment

The Thermo NE-PER Kit (Thermo Fisher Scientific, 78835) was utilized to separate cytoplasmic (post-nuclear) and nuclear fractions from matured primary white adipocytes, with modifications. In a 10-cm dish, adherent mature adipocytes were gently rinsed twice with 1x PBS on the dish, and excess was aspirated with a 200-µL plastic pipet tip from the tilted dish. Next, ~400 µL of CER I solution was added to the monolayer, and adipocytes were scraped into the solution. Importantly, the collected cells were then passed through a 22G syringe 5 times to disperse the cell conglomerate but keep the nuclei intact. These were vortexed and placed on ice for 10 minutes. Next, per the NE-PER protocol, 22 µL of CER II solution was added and tube was vortexed vigorously and placed on ice for 2

minutes. The tube was centrifuged at 500 × *g* for 5 minutes at 4° C. The fat cake and infranatant were collected to a separate tube (as the cytoplasmic/post-nuclear and fat cake components) while not disturbing the pellet at the bottom. The cytoplasmic tube was spun again in the same manner so that the fat cake and cytoplasmic-enriched infranatant could be separated. The cytoplasmic/post-nuclear infranatant was collected with a 28.5G insulin syringe, avoiding as much lipid as possible, at which point this sample was ready for BCA protein concentration determination. The tube with the pellet was cleaned of excess lipid on the sides of the tube by wicking carefully with a Kimwipe (Kimberly-Clark Professional, 34120), and the pellet was resuspended in 200 µL of NER, passed 5 times through a 28.5 gauge insulin syringe to break up the pellet, sonicated for 20 seconds in a sonicator bath, vortexed vigorously for 30 seconds, and placed on ice for 40 minutes. Finally, the nuclear natant was collected as the nuclear-enriched fraction after a 20-minute spin at 4° C at 18,000 × *g*. Cytoplasmic and nuclear fractions were assessed by Western blot after normalization by BCA. Nuclear fractions tended to be at least 5-fold lower in protein concentration.

Nuclear Extracts for Immunoprecipitation followed by Lipid Measurements

This method was developed in Hait, et al., 2009. WT primary matured, synchronized adipocytes were allowed to cycle for 24 hours, after which, cells were harvested over a time course. Cells were washed with cold PBS and re-suspended in buffer containing 10 mM HEPES (pH 7.8), 10 mM KCl, 0.1 mM EDTA, 1 mM Na_3VO_4, 1 mM DTT, 1:500 protease inhibitors (Sigma) and 0.2 mM PMSF, and incubated on ice for 15 min. NP-40 was added (0.75%) and cells were vortexed for 10 sec. Nuclei and supernatant ("cytoplasm") were separated by centrifugation at 1000 × *g* for 3 min at 4˚ C. Nuclei were

resuspended in buffer containing 20 mM HEPES (pH 7.8), 0.4 M NaCl, 1 mM EDTA, 1 mM Na_3VO_4, 1 mM DTT and 1:500 protease inhibitors and incubated on ice for 15 min. Nuclear extracts were cleared by centrifugation at 14,000 × *g* for 5 min at 4˚ C. Equal milligrams protein from each fraction was immunoprecipitated overnight at 4˚ C (rotating) with 1 µg BMAL1, HDAC1, and HDAC2 antibodies, and the next day immunocomplexes were captured with Protein A/G magnetic beads (Thermo Fisher Scientific, 88802) for an additional 2 hours at 4˚ C, then washed extensively. Immunocomplexes were eluted in 100% methanol and tested by LC:MS/MS at the Virginia Commonwealth University Lipidomics and Metabolomics Core facility for sphingolipids.

Western Blotting

For Chapter 3, gonadal adipose tissue was homogenized in RIPA buffer with protease and phosphatase inhibitors (Thermo Fisher Scientific, 78446) using a Dounce homogenizer for at least 30 strokes, or until visibly homogenized. Homogenates were vortexed well and centrifuged at 10,000 × *g* for 10 minutes at 4° C. The resulting infranatant (below fat cake, and above cell debris pellet) was transferred to a new tube with an insulin syringe (28.5G). Protein content was quantified using a BCA protein determination assay (Thermo Fisher Scientific, 23225). 10 µg protein was used for western blotting. Non-hemolyzed mouse sera was diluted in PBS 1:20, and isovolumetric amounts of diluted sera plus loading buffer was loaded for western blotting. gWAT proteins and sera proteins were separated by SDS-PAGE (Bio-Rad Criterion TGX Stain-Free precast gels), and transferred to nitrocellulose membranes, and sera proteins were transferred to PVDF membranes. The membranes were blocked for 1 hour in 5% BSA. Proteins were detected using (gWAT) HRP-linked anti rabbit secondary (1:5000; Cell

Signaling Technology, 7074) or (sera) StarBright-700-linked anti rabbit secondary (1:2,500; Bio-Rad, 12004161), Clarity ECL Western Blotting Substrate (Bio-Rad, 1705061) for HRP, and a ChemiDoc Imaging System (Bio-Rad, 17001401, 17001402). Blots were assessed for protein expression of adiponectin (1:2000; Cell Signaling Technology, 2789), adipose triglyceride lipase (ATGL) (1:2000, Cell Signaling Technology, 2439), ABHD5 (CGI-58) (1:1000, Novus Biologicals, NB100-5-7850), and FABP4 (1:2000, Cell Signaling Technology, 2120). Vinculin (1:2,000; Cell Signaling Technology, 4650) and stain-free total protein were used to determine even loading. Band intensity was quantified using ImageJ. For Chapter 4, gonadal adipose tissue was homogenized in RIPA buffer with protease and phosphatase inhibitors (Thermo Fisher Scientific, 78446) using a Dounce homogenizer for at least 30 pulses, or until visibly homogenized. Homogenates were vortexed well and centrifuged at 10,000 × g for 10 minutes at 4° C. The resulting infranatant (below fat cake, and above cell debris pellet) was transferred to a new tube with an insulin syringe (28.5G). Cultured adipocyte whole-cell homogenates were homogenized in RIPA buffer with 1 mM PMSF, and protease and phosphatase inhibitors (Thermo Fisher Scientific, 78446). Cultured adipocyte cell fractions were collected as described in *Cellular Fractionation for Nuclear and Cytoplasmic Enrichment*. Protein content was quantified using a BCA protein determination assay (Thermo Fisher Scientific, 23225). 5-10 µg protein was used for western blotting. gWAT whole-cell homogenates, cultured adipocyte whole-cell homogenates, and fractionated adipocyte proteins were separated by SDS-PAGE, and transferred to PVDF membranes. The membranes were blocked for 1 hour in 5% BSA. Proteins were detected using HRP-linked anti rabbit secondary (1:5000; Cell Signaling Technology, 7074), Clarity ECL Western Blotting Substrate (Bio-Rad, 1705061) for HRP, and a ChemiDoc Imaging

System (Bio-Rad, 17001401, 17001402). Blots were assessed for protein expression of proteins shown in the table below. Vinculin (1:2,000; Cell Signaling Technology, 4650), Ponceau S, and stain-free total protein were used to determine even loading. Band intensity was quantified using ImageJ.

Application	Target	Antibody	Host	Supplier	Catalog #	Concentration or Dilution
Western blot	Mouse	HDAC1	Rabbit	Bethyl	A300-713A	1:2,000
Western blot	Mouse	HDAC2	Rabbit	Bethyl	A300-705A	1:2,000
Western blot	Mouse	HDAC3	Rabbit	Bethyl	A300-464A	1:5,000
Western blot	Mouse	Histone H3	Rabbit	Cell Signaling Technology	4499	1:2,000
Western blot	Mouse	Lamin B1	Rabbit	Cell Signaling Technology	13435	1:1,000
Western blot	Mouse	Vinculin	Rabbit	Cell Signaling Technology	4650	1:1,000
Western blot	Rabbit	HRP-anti-Rabbit IgG	Goat	Cell Signaling Technology	7074	1:5,000
W.B. and ChIP	Mouse	BMAL1	Rabbit	Bethyl	A302-616A	1 µg per IP
W.B. and ChIP	Mouse	CLOCK	Rabbit	Bethyl	A302-618A	1 µg per IP

Antibodies used for Western blotting analysis.

Cosinor Statistical Analysis

A single component cosinor nonlinear regression goodness of fit analysis was performed in Graphpad Prism 8 according to definitions from accepted literature (Cornelissen, 2014; Halberg, 1969; Halberg & Johnson, 1967; Morelli, et al., 2019; Refinetti, et al., 2007). The equation used for this analysis was : $f(t) = MESOR + A * Cos[(2 \pi t/T) + Acrophase]$.

MESOR is the “midline estimating statistic of rhythm” and this value corresponds with the rhythm adjusted mean of the dataset or “baseline” value. Amplitude (A) is calculated as

half the difference between the minimum and maximum, as defined by the cosinor fitted curve. The acrophase is the measure of the time at which overall high values recur in each cycle. R^2 corresponds to how well the dataset fit the standard cosinor curve, with 1 being a perfect fit. In other words, R^2 is the resulting statistic that measures the percent variance accounted for by the 24 h approximating waveform (Bray, et al., 2013). Time (t) is presented in hours, where .5 hour is equivalent to 30 minutes. The constants in this equation are $2 \times \pi \times 1/T$, where T is assumed to be a period of 24 hours. Thus, $1/12\ \pi = 0.2618$.

Statistical Analysis

All values are presented as mean ± SEM. For single pairwise comparisons of normally distributed data sets, a Student's *t*-test was performed. For multiple comparisons of means, a one-way ANOVA with Tukey-Kramer post hoc test was performed. $p<0.05$ was considered statistically significant. All hypothesis tests were conducted using Graphpad Prism 8 software.

CHAPTER 8

REFERENCES

Adada, M., Canals, D., Hannun, Y.A., Obeid, L.M. (2013) Sphingosine-1-phosphate receptor 2. The FEBS Journal 280 (24): 6354-6366.

Adamovich, Y., Ladeuix, B., Golik, M., Koeners, M.P., Asher, G. (2016) Rhythmic oxygen levels reset circadian clocks through HIF1α. Cell Metabolism 25 (1): 93-101.

Adams, J.M., Pratipanawatr, T., Berria, R., Wang, E., DeFronzo, R.A., Sullards, M.C., Mandarino, L.J. (2004) Ceramide content is increased in skeletal muscle from obese insulin-resistant humans. Diabetes 53 (1): 25-31.

Aguilar-Arnal, L., Sassone-Corsi, P. (2015) Chromatin landscape and circadian dynamics: spatial and temporal organization of clock transcription. Proceedings of the National Academy of Sciences of the United States of America 112 (22): 6863-6870. PMC4460512

Aguilar-Salinas, C. A., Viveros-Ruiz, T. (2019) Recent advances in managing/understanding the metabolic syndrome. F1000Research 8.

Alexaki, A., Clarke, B.A., Gavrilova, O., Ma, Y., Zhu, H., Ma, X., Xu, L., Tuymetova, G., Larman, B.C., Allende, M.L. (2017) De novo sphingolipid biosynthesis is required for adipocyte survival and metabolic homeostasis. The Journal of Biological Chemistry 292 (9): 3929-3939.

Allende, M.L., Bektas, M., Lee, B.G., Bonifacino, E., Kang, J., Tuymetova, G., Chen, W., Saba, J.D., Proia, R.L. (2011) Sphingosine-1-phosphate lyase deficiency produces a pro-inflammatory response while impairing neutrophil trafficking. The Journal of Biological Chemistry 286 (9): 7348-7358. PMC3044991

Allende, M.L., Sasaki, T., Kawai, H., Olivera, A., Mi, Y., van Echten-Deckert, G., Hajdu, R., Rosenbach, M., Keohane, C.A., Mandala, S., Spiegel, S., Proia, R.L. (2004) Mice deficient in sphingosine kinase 1 are rendered lymphopenic by FTY720. The Journal of Biological Chemistry 279 (50): 52487-92.

Alvarez, S.E., Harikumar, K.B., Hait, N.C., Allegood, J., Strub, G.M., Kim, E., Maceyka, M., Jiang, H., Luo, C., Kordula, T., Milstien, S., Spiegel, S. (2010) Sphingosine-1-phosphate: a missing cofactor for the E3 ubiquitin ligase TRAF2. Nature 465 (7391): 1084-1088. PMC2946785

Anderson, A.K., Lambert, J.M., Montefusco, D.J., Ngan Tran, B., Roddy, P., Holland, W.L., Cowart, L.A. (2020) Depletion of adipocyte sphingosine kinase 1 leads to cell hypertrophy, impaired lipolysis, and non-alcoholic fatty liver disease. Journal of Lipid Research jlr.RA120000875. *Advance online publication*. https://doi.org/10.1194.

Andersson, C. X., Gustafson, B., Hammarstedt, A., Hedjazifar, S., Smith, U. (2008) Inflamed adipose tissue, insulin resistance and vascular injury. Diabetes/Metabolism Research and Reviews 24: 595-603.

Aryal R.P., Kwak, P.B., Tamayo, A.G., Gebert, M., Chiu, P-L., Walz, T., Weitz, C.J. (2017) Macromolecular assemblies of the mammalian circadian clock. Molecular Cell 67: 770-782.

Asher, G., Schibler, U. (2011) Crosstalk between components of circadian and metabolic cycles in mammals. Cell Metabolism 13 (2): 125-137.

Atkinson, G., Reilly, T. (1996) Circadian variation in sports performance. Sports Medicine 21: 292-312.

Aviram, R., Manella, G., Kopelman, N., Neufeld-Cohen, A., Zwighaft, Z., Elimelech, M., Adamovich, Y., Golik, M., Wang, C., Han, X., Asher, G. (2016) Lipidomics analyses reveal temporal and spatial lipid organization and uncover daily oscillations in intracellular organelles. Molecular Cell 62 (4): 636-648.

Azzu, V., Vacca, M., Virtue, S., Allison, M., Vidal-Puig, A. (2020) Adipose tissue-liver cross talk in the control of whole-body metabolism: implications in non-alcoholic fatty liver disease. Gastroenterology 158 (7): 1899-1912.

Baerenfaller K., Shu H., Hirsch-Hoffmann M., Fütterer, J., Opitz L., Rehrauer, H., Hennig L., Gruissem, W. (2016) Diurnal changes in the histone H3 signature H3K9ac|H3K27ac|H3S28p are associated with diurnal gene expression in Arabidopsis. Plant, Cell and Environment 39 (11): 2557-2569.

Bagchi, R.A., Weeks, K.L. (2019) Histone deacetylases in cardiovascular and metabolic diseases. Journal of Molecular and Cellular Cardiology 130: 151-159.

Bailey, S.M., Udoh, U.S., Young, M.E. (2014) Circadian regulation of metabolism. The Journal of Endocrinology 222 (2): R75-R96. PMC4109003

Ballestri, S., Nascimbeni, F., Baldelli, E., Marrazzo, A., Romagnoli, D., Lonardo, A. (2017) NAFLD as a sexual dimorphic disease: role of gender and reproductive status in the development and progression of nonalcoholic fatty liver disease and inherent cardiovascular risk. Advances in Therapy 34: 1291-1326.

Barbarroja, N., Rodriguez-Cuenca, S., Nygren, H., Camargo, A., Pirraco, A., Relat, J., Cuadrado, I., Pellegrinelli, V., Medina-Gomez, G., Lopez-Pedrera, C. (2014) Increased dihydroceramide/ceramide ratio mediated by defective expression of DEGS1 impairs adipocyte differentiation and function. Diabetes 64 (4): 1180-1192.

Bektas, M., Allende, M.L., Lee, B.G., Chen, W., Amar, M.J., Remaley, A.T., Saba, J.D., Proia, R.L. (2010) Sphingosine 1-phosphate lyase deficiency disrupts lipid homeostasis in liver. The Journal of Biological Chemistry 285 (14): 10880-10889.

Berg, A.H., Scherer, P.E. (2005) Adipose tissue, inflammation, and cardiovascular disease. Circulation Research 96: 939-949.

Berry, D.C., Jiang, Y., Graff, J.M. (2016) Emerging roles of adipose progenitor cells in tissue development, homeostasis, expansion and thermogenesis. Trends in Endocrinology and Metabolism 27 (8): 574-585.

Bezaire, V., Mairal, A., Ribet, C., Lefort, C., Girousse, A., Jocken, J., Laurencikiene, J., Anesia, R., Rodriguez, A-M., Ryden, M., Stenson, B.M., Dani, C., Ailhaud, G., Arner, P.,

Langin, D. (2009) Contribution of adipose triglyceride lipase and hormone-sensitive lipase to lipolysis in hMADS adipocytes. The Journal of Biological Chemistry 284: 18282-18291.

Bielawski, J., Pierce, J.S., Snider, J., Rembiesa, B., Szulc, Z.M., Bielawska, A. (2010) Sphingolipid analysis by high performance liquid chromatography-tandem mass spectrometry (HPLC-MS/MS). Advances in Experimental Medicine and Biology 688: 46-59.

Billich A, Bornancin F, Devay P, Mechtcheriakova D, Urtz N, Baumruker T. Phosphorylation of the immunomodulatory drug FTY720 by sphingosine kinases. (2003) The Journal of Biological Chemistry 278: 47408-47415.

Blachnio-Zabielska, A.U., Pułka, M., Baranowski, M., Nikołajuk, A., Zabielski, P., Górska, M., Górski, J. (2012) Ceramide metabolism is affected by obesity and diabetes in human adipose tissue. Journal of Cellular Physiology 227 (2): 550-557.

Blachnio-Zabielska, A.U., Koutsari, C., Tchkonia, T., Jensen, M.D. (2012a) Sphingolipid content of human adipose tissue: relationship to adiponectin and insulin resistance. Obesity 20 (12): 2341-2347.

Blaho, V.A., Galvani, S., Engelbrecht, E., Liu, C., Swendeman, S.L., Kono, M., Proia, R.L., Steinman, L., Han, M.H., Hla, T. (2015) HDL-bound sphingosine-1-phosphate restrains lymphopoiesis and neuroinflammation. Nature 523 (7560): 342-346. PMC4506268

Brabant, G., Prank, K., Ranft, U., Schuermeyer, T., Wagner, T.O.F., Hauser, H., Kummer, B., Feistner, H., Hesch, R.D., von sur Mühlen, A. (1990) Physiological regulation of circadian and pulsatile thyrotropin secretion in normal man and woman. Journal of Clinical Endocrinology and Metabolism 70: 403-409.

Bray, M.S., Ratcliffe, W.F., Grenett, M.H., Brewer, R.A., Gamble, K.L., Young, M.E. (2013) Quantitative analysis of light-phase restricted feeding reveals metabolic dyssynchrony in mice. International Journal of Obesity (2005) 37 (6): 843-852. PMC3505273

Bray, M.S., Young, M.E. (2007) Circadian rhythms in the development of obesity: potential role for the circadian clock within the adipocyte. Obesity Reviews : An Official Journal of the International Association for the Study of Obesity 8 (2): 169-181.

Bréart, B., Ramos-Perez, W.D., Mendoza, A., Salous, A.K., Gobert, M., Huang, Y., Adams, R.H., Lafaille, J. J., Escalante-Alcalde, D., Morris, A.J., Schwab, S.R. (2011) Lipid phosphate phosphatase 3 enables efficient thymic egress. The Journal of Experimental Medicine 208 (6): 1267-1278. PMC3173249

Breathnach, C.S. (2001) Johann Ludwig Wilhelm Thudichum 1829-1901, bane of the protagonisers. Historical Psychiatry 12 (47 Pt 3): 283-296.

Breslow, D.K., Weissman, J.S. (2010) Membranes in balance: mechanisms of sphingolipid homeostasis. Molecular Cell 40 (2): 267-279. PMC2987644

Brown, L.A., Fisk, A.S., Pothecary, C.A., Peirson, S.N. (2019) Telling the time with a broken clock: quantifying circadian disruption in animal models. Biology 8 (1): 18. PMC6466320

Brugger, B., Graham, C., Leibrecht, I., Mombelli, E., Jen, A., Wieland, F., Morris, R. (2004) The membrane domains occupied by glycosylphosphatidylinositol-anchored prion protein and Thy-1 differ in lipid composition. The Journal of Biological Chemistry 279: 7530-7536.

Brunkhorst, R., Pfeilschifter, W., Rajkovic, N., Pfeffer, M., Fischer, C., Korf, H.W., Christoffersen, C., Trautmann, S., Thomas, D., Pfeilschifter, J., Koch, A. (2019) Diurnal regulation of sphingolipids in blood. Biochimica et Biophysica Acta. Molecular and Cell Biology of Lipids 1864 (3): 304-311.

Bryan, L., Kordula, T., Spiegel, S., Milstien, S. (2008) Regulation and functions of sphingosine kinases in the brain. Biochimica et Biophysica Acta 1781 (9): 459-466. PMC2712649

Cai, J., Pires, K.M., Ferhat, M., Chaurasia, B., Buffolo, M.A., Smalling, R., Sargsyan, A., Atkinson, D.L., Summers, S.A., Graham, T.E., Boudina, S. (2018) Autophagy ablation in adipocytes induces insulin resistance and reveals roles for lipid peroxide and Nrf2 signaling in adipose-liver crosstalk. Cell Reports 25 (7): 1708-1717. PMC6802939

Camell, C.D., Nguyen, K.Y., Jurczak, M.J., Christian, B.E., Shulman, G.I., Shadel, G.S., Dixit, V.D. (2015) Macrophage-specific de novo synthesis of ceramide is dispensable for inflammasome-driven inflammation and insulin resistance in obesity. The Journal of Biological Chemistry 290 (49): 29402-29413.

Camerer, E., Regard, J.B., Cornelissen, I., Srinivasan, Y., Duong, D.N., Palmer, D., Pham, T.H., Wong, J.S., Pappu, R., Coughlin, S.R. (2009) Sphingosine-1-phosphate in the plasma compartment regulates basal and inflammation-induced vascular leak in mice. The Journal of Clinical Investigation 119 (7): 1871-1879. PMC2701879

Candi, E., Tesauro, M., Cardillo, C., Lena, A.M., Schinzari, F., Rodia, G., Sica, G., Gentileschi, P., Rovella, V., Annicchiarico-Petruzzelli, M., Di Daniele, N., Melino, G. (2018) Metabolic profiling of visceral adipose tissue from obese subjects with or without metabolic syndrome. Biochemical Journal 475: 1019-1035.

Cannon, B., Nedergaard, J. (2004) Brown adipose tissue: function and physiological significance. Physiological Reviews 84 (1): 277-359.

Cantrell Stanford, J., Morris, A.J., Sunkara, M., Popa, G.J., Larson, K.L., Özcan, S. (2012) Sphingosine 1-Phosphate (S1P) regulates glucose-stimulated insulin secretion in pancreatic beta cells. The Journal of Biological Chemistry 287 (16): 13457-13464.

Cardone, L., Hirayama, J., Giordano, F., Tamaru, T., Palvimo, J.J., Sassone-Corsi, P. (2005) Circadian clock control of SUMOylation of BMAL1. Science 309 (5739): 1390-1394.

Castillo, R.I., Rojo, L.E., Henríquez-Henríquez, M., Silva, H., Maturana, A., Villar, M.J., Fuentes, M., Gaspar, P.A. (2016) From molecules to the clinic: linking schizophrenia and metabolic syndrome through sphingolipids metabolism. Frontiers in Neuroscience 10 (488): doi: 10.3389.

Cawthorn, W.P., Scheller, E.L., MacDougald, O.A. (2012) Adipose tissue stem cells meet preadipocyte commitment: going back to the future. Journal of Lipid Research 53 (2): 227-246.

Chaix, A., Lin, T., Le, H.D., Chang, M.W., Panda, S. (2019) Time-restricted feeding prevents obesity and metabolic syndrome in mice lacking a circadian clock. Cell Metabolism 29 (2): 303-319.

Chaurasia, B., Kaddai, V.A., Lancaster, G.I., Henstridge, D.C., Sriram, S., Galam, D.L.A., Gopalan, V., Prakash, K.N.B., Velan, S.S., Bulchand, S., Tsong, T.J., Wang, M., Siddique, M.M., Yuguang, G., Sigmundsson, K., Mellet, N.A., Weir, J.M., Meikle, P.J., Bin, M., Yassin, M.S., Shabbir, A., Shayman, J.A., Hirabayashi, Y., Shiow, S.T., Sugii, S., Summers, S.A. (2016) Adipocyte ceramides regulate subcutaneous adipose browning, inflammation, and metabolism. Cell Metabolism 24 (6): 820-834.

Chavez, J.A., Summers, S.A. (2012) A ceramide-centric view of insulin resistance. Cell Metabolism 15 (5): 585-594.

Chavez, J.A., Knotts, T.A., Wang, L.P., Li, G., Dobrowsky, R.T., Florant, G.L., and Summers, S.A. (2003) A role for ceramide, but not diacylglycerol, in the antagonism of insulin signal transduction by saturated fatty acids. The Journal of Biological Chemistry 278: 10297-10303.

Chavez, J.A., Summers, S.A. (2003) Characterizing the effects of saturated fatty acids on insulin signaling and ceramide and diacylglycerol accumulation in 3T3-L1 adipocytes and C2C12 myotubes. Archives of Biochemistry and Biophysics 419 (2): 101-109.

Chimin, P., Andrade, M.L., Belchior, T., Paschoal, V.A., Magdalon, J., Yamashita, A.S., Castro, É., Castoldi, A., Chaves-Filho, A.B., Yoshinaga, M.Y. (2017) Adipocyte mTORC1 deficiency promotes adipose tissue inflammation and NLRP3 inflammasome activation via oxidative stress and de novo ceramide synthesis. Journal of Lipid Research 58 (9): 1797-1807.

Choi, K.-M., Lee, Y.-S., Choi, M.-H., Sin, D.-M., Lee, S., Ji, S.-Y., Lee, M.K., Lee, Y.-M., Yun, Y.-P., Hong, J.-T. (2011) Inverse relationship between adipocyte differentiation and ceramide level in 3T3-L1 cells. Biological and Pharmaceutical Bulletin 34 (6): 912-916.

Christensen, P.M., Liu, C.H., Swendeman, S.L., Obinata, H., Qvortrup, K., Nielsen, L.B., Hla, T., Di Lorenzo, A., Christoffersen, C. (2016) Impaired endothelial barrier function in apolipoprotein M-deficient mice is dependent on sphingosine-1-phosphate receptor 1. The FASEB Journal 30: 2351-2359.

Christoffersen, C., Obinata, H., Kumaraswamy, S.B., Galvani, S., Ahnström, J., Sevvana, M., Egerer-Sieber, C., Muller, Y.A., Hla, T., Nielsen, L.B., Dahlbäck, B. (2011) Endothelium-protective sphingosine-1-phosphate provided by HDL-associated

apolipoprotein M. Proceedings of the National Academy of Sciences of the United States of America 108: 9613-9618.

Christoffersen, C., Federspiel, C.K., Borup, A., Christensen, P.M., Madsen, A.N., Heine, M., Nielsen, C.H., Kjaer, A., Holst, B., Heeren, J., Nielsen, L.B. (2018) The apolipoprotein M/S1P axis controls triglyceride metabolism and brown fat activity. Cell Reports 22 (1): 175-188.

Clark, G., Magoun, H.W., Ranson, S.W. (1939) Hypothalamic regulation of body temperature. Journal of Neurophysiology 2: 61-80.

Conroy, R.T.W.L., O'Brien, M. (1974) Diurnal variation in athletic performance. The Journal of Physiology 236: 51.

Cooper, D.M. (2003) Regulation and organization of adenylyl cyclases and cAMP. Biochemical Journal 375 (3): 517-529.

Cornelissen G. (2014) Cosinor-based rhythmometry. Theoretical Biology & Medical Modelling 11: 16. PMC3991883

Cowart, L.A. (2009) Sphingolipids: players in the pathology of metabolic disease. Trends in Endocrinology and Metabolism 20 (1): 34-42.

Cox, K.H., Takahashi, J.S. Circadian clock genes and the transcriptional architecture of the clock mechanism. (2019) Journal of Molecular Endocrinology 63 (4): R93-R102.

Crewe, C., An, Y.A., Scherer, P.E. (2017) The ominous triad of adipose tissue dysfunction: inflammation, fibrosis, and impaired angiogenesis. The Journal of Clinical Investigation 127 (1): 74-82.

Dal Canto, E., Ceriello, A., Ryden, L., Ferrini, M., Hansen, T.B., Schnell, O., Standl, E., Beulens, J.W. (2019) Diabetes as a cardiovascular risk factor: an overview of global trends of macro and micro vascular complications. European Journal of Preventive Cardiology 26: 25-32.

Daval, M., Foufelle, F., Ferré, P. (2006) Functions of AMP-activated protein kinase in adipose tissue. The Journal of Physiology 574(Pt 1): 55-62. PMC1817807

Davidson, A.J., London, B., Block, G.D., Menaker, M. (2005) Cardiovascular tissues contain independent circadian clocks. Clinical and Experimental Hypertension 27 (2-3): 307-311.

Dodd, A.N., Salathia, N., Hall, A., Kevel, E., Toth, R., Nagy, F., Hibberd, J.M., Millar, A.J., Webb, A.A.R. (2005) Plant circadian clocks increase photosynthesis, growth, survival, and competitive advantage. Science 309: 630-633.

Doi, M., Hirayama, J., Sassone-Corsi, P. (2006) Circadian regulator CLOCK is a histone acetyltransferase. Cell 125 (3): 497-508.

Donoviel, M.S., Hait, N.C., Ramachandran, S., Maceyka, M., Takabe, K., Milstien, S., Oravecz, T., Spiegel, S. (2015) Spinster 2, a sphingosine-1-phosphate transporter plays a critical role in inflammatory and autoimmune diseases. The FASEB Journal 29 (12): 5018-5028.

Druzd, D., Matveeva, O., Ince, L., Harrison, U., He, W., Schmal, C., Herzel, H., Tsang, A.H., Kawakami, N., Leliavski, A., Uhl, O., Yao, L., Sander, L.E., Chen, C-S., Kraus, K., de Juan, A., Hergenhan, S.M., Ehlers, M., Koletzko, B., Haas, R., Solbach, W., Oster, H., Scheiermann, C. (2017) Lymphocyte circadian clocks control lymph node trafficking and adaptive immune responses. Immunity 46 (1): 120-132.

Duncan, R.E., Ahmadian, M., Jaworski, K., Sarkadi-Nagy, E., Sul, H.S. (2007) Regulation of lipolysis in adipocytes. Annual Review of Nutrition 27: 79-101.

Dunlap, J.C., Loros, J.J. (2017) Making time: conservation of biological clocks from fungi to animals. Microbiology Spectrum 5 (3): 10. PMC5446046

Durgan, D.J., Young, M.E. (2010) The cardiomyocyte circadian clock: emerging roles in health and disease. Circulation Research 106 (4): 647-658. PMC3223121

Dyar, K.A., Eckel-Mahan, K.L. (2017) Circadian metabolomics in time and space. Frontiers in Neuroscience 11: 369. PMC5504240

Egli M. (2017) Architecture and mechanism of the central gear in an ancient molecular timer. Journal of the Royal Society, Interface 14 (128): 20161065. PMC5378140

Elgazar-Carmon, V., Rudich, A., Hadad, N., Levy, R. Neutrophils transiently infiltrate intra-abdominal fat early in the course of high-fat feeding. (2008) Journal of Lipid Research 49: 1894-1903.

Esquirol, Y., Bongard, V., Mabile, L., Jonnier, B., Soulat, J.M., Perret, B. (2009) Shift work and metabolic syndrome: respective impacts of job strain, physical activity, and dietary rhythms. Chronobiology International 26: 544-559.

Feng, D., Liu, T., Sun, Z., Bugge, A., Mullican, S.E., Alenghat, T., Liu, X.S., Lazar, M.A. (2011) A circadian rhythm orchestrated by histone deacetylase 3 controls hepatic lipid metabolism. Science 331 (6022): 1315-9. PMC3389392

Ferreira, G.N., Rossi-Valentim, R., Buzelle, S.L., Paula-Gomes, S., Zanon, N.M., Garofalo, M.A.R., Frasson, D., Navegantes, L.C.C., Chaves, V.E., Kettelhut, I.D.C. (2017) Differential regulation of glyceroneogenesis by glucocorticoids in epididymal and retroperitoneal white adipose tissue from rats. Endocrine 57 (2): 287–297.

Ferrell, J.M., Chiang, J.Y. (2015) Circadian rhythms in liver metabolism and disease. Acta Pharmaceutica Sinica. B 5 (2): 113-122. PMC4629216

Franckhauser, S., Munoz, S., Pujol, A., Casellas, A., Riu, E., Otaegui, P., Su, B., Bosch, F. (2002) Increased fatty acid re-esterification by PEPCK overexpression in adipose tissue leads to obesity without insulin resistance. Diabetes 51 (3): 624–630.

Fruhbeck, G., Mendez-Gimenez, L., Fernandez-Formoso, J.A., Fernandez, S., Rodriguez, A. (2014) Regulation of adipocyte lipolysis. Nutrition Research Reviews 27: 63-93.

Fu, P., Ebenezer, D.L., Ha, A.W., Suryadevara, A.H., Natarajan, V. (2018) Nuclear lipid mediators: role of nuclear sphingolipids and sphingosine-1-phosphate signaling in epigenetic regulation of inflammation and gene expression. Journal of Cellular Biochemistry 119: 6337-6353.

Fu, Q., Tang, X., Chen, J., Su, L., Zhang, M., Wang, L., Jing, J., Zhou, L. (2015) Effects of polymorphisms in APOA4-APOA5-ZNF259-BUD13 gene cluster on plasma levels of triglycerides and risk of coronary heart disease in a Chinese Han population. PloS One 10 (9): e0138652. PMC4580433

Fukuhara, S., Simmons, S., Kawamura, S., Inoue, A., Orba, Y., Tokudome, T., Sunden, Y., Arai, Y., Moriwaki, K., Ishida, J., Uemura, A., Kiyonari, H., Abe, T., Fukamizu, A., Hirashima, M., Sawa, H., Aoki, J., Ishii, M., Mochizuki, N. (2012) The sphingosine-1-phosphate transporter Spns2 expressed on endothelial cells regulates lymphocyte trafficking in mice. Journal of Clinical Investigation 122 (4): 1416-1426.

Gable, K., Gupta, S.D., Han, G., Niranjanakumari S., Harmon, J.M., Dunn, T.M. (2010) A disease-causing mutation in the active site of serine palmitoyltransferase causes catalytic promiscuity. The Journal of Biological Chemistry 285 (30): 22846-22852. PMC2906276

Gabriel, T.L., Mirzaian, M., Hooibrink, B., Ottenhoff, R., van Roomen, C., Aerts, J.M., van Eijk, M. (2017) Induction of Sphk1 activity in obese adipose tissue macrophages promotes survival. PLoS One 12 (7): e0182075.

Gates, L.A., Shi, J., Rohira, A.D., Feng, Q., Zhu, B., Bedford, M.T., Sagum, C.A., Jung, S.Y., Qin, J., Tsai, M.-J., Tsai, S.Y., Li, W., Foulds, C.E., O'Malley, B.W. (2017) Acetylation on histone H3 lysine 9 mediates a switch from transcription initiation to elongation. The Journal of Biological Chemistry 292 (35): 14456.

Geerling, J.J., Boon, M.R., Kooijman, S., Parlevliet, E.T., Havekes, L.M., Romijn, J.A., Meurs, I.M., Rensen, P.C. (2014) Sympathetic nervous system control of triglyceride metabolism: novel concepts derived from recent studies. Journal of Lipid Research 55 (2): 180-189. PMC3886657

Geng, T., Sutter, A., Harland, M.D., Law, B.A., Ross, J.S., Lewin, D., Palanisamy, A., Russo, S.B., Chavin, K.D., Cowart, L.A. (2015) SphK1 mediates hepatic inflammation in a mouse model of NASH induced by high saturated fat feeding and initiates proinflammatory signaling in hepatocytes. Journal of Lipid Research 52 (12): 2359-2371.

Gerhart-Hines, Z., Lazar, M.A. (2015) Circadian metabolism in the light of evolution. Endocrine Reviews 36 (3): 289-304. PMC4446517

Gifford, L.S. (1987) Circadian variation in human flexibility and grip strength. Australian Journal of Physiotherapy 33: 3-9.

Giralt, M., Martin, I., Iglesias, R., Viñas, O., Villarroya, F., Mampel, T. (1990) Ontogeny and perinatal modulation of gene expression in rat brown adipose tissue. Unaltered iodothyronine 5'-deiodinase activity is necessary for the response to environmental temperature at birth. European Journal of Biochemistry 193 (1): 297-302.

Gosejacob, D., Jäger, P.S., vom Dorp, K., Frejno, M., Carstensen, A.C., Köhnke, M., Degen, J., Dörmann, P., Hoch, M. (2016) Ceramide synthase 5 is essential to maintain C16:0-ceramide pools and contributes to the development of diet-induced obesity. The Journal of Biological Chemistry 291 (13): 6989-7003.

Gooley, J.J. (2016) Circadian regulation of lipid metabolism. The Proceedings of the Nutrition Society 75 (4): 440-450.

Gooley, J.J., Chua, E.C. (2014) Diurnal regulation of lipid metabolism and applications of circadian lipidomics. Journal of Genetics and Genomics 41 (5): 231-250.

Greenberg, A.S., Shen, W.J., Muliro, K., Patel, S., Souza, S.C., Roth, R.A., Kraemer, F.B. (2001) Stimulation of lipolysis and hormone-sensitive lipase via the extra-cellular signal-regulated kinase pathway. The Journal of Biological Chemistry 276 (48): 45456-45461.

Guilherme, A., Virbasius, J.V., Puri, V., Czech, M.P. (2008) Adipocyte dysfunctions linking obesity to insulin resistance and type II diabetes. Nature Reviews: Molecular and Cellular Biology 9 (5): 367-377.

Gulbins, E., Kolesnick, R. (2003) Raft ceramide in molecular medicine. Oncogene 22: 7070-7077.

Gustafson, B., Gogg, S. Hedjazifar, S., Jenndahl, L., Hammarstedt, A., Smith, U. (2009) Inflammation and impaired adipogenesis in hypertrophic obesity in man. American Journal of Physiology: Endocrinology and Metabolism 297: E999-E1003.

Gustafson, B., Hammarstedt, A., Andersson, C.X., Smith, U. (2007) Inflamed adipose tissue: a culprit underlying the metabolic syndrome and atherosclerosis. Arteriosclerosis, Thrombosis, and Vascular Biology 27: 2276-2283.

Haczeyni, F., Bell-Anderson, K.S., Farrell, G.C. (2018) Causes and mechanisms of adipocyte enlargement and adipose expansion. Obesity Reviews 19: 406-420.

Haemmerle, G., Lass, A., Zimmermann, R., Gorkiewicz, G., Meyer, C., Rozman, J., Heldmaier, G., Maier, R., Theussl, C., Eder, S. (2006) Defective lipolysis and altered energy metabolism in mice lacking adipose triglyceride lipase. Science 312: 734-737.

Hait, N.C., Allegood, J., Maceyka, M., Strub, G.M., Harikumar, K.B., Singh, S.K., Luo, C., Marmorstein, R., Kordula, T., Milstien, S., Spiegel, S. (2009) Regulation of histone acetylation in the nucleus by sphingosine-1-phosphate. Science 325 (5945): 1254-1257. PMC2850596

Hait, N.C., Maiti, A., Xu, P., Qi, Q., Kawaguchi, T., Okano, M., Takabe, K., Yan, L., Luo, C. (2020) regulation of hypoxia-inducible factor functions in the nucleus by sphingosine-1-phosphate. The FASEB Journal 34 (3): 4293-4310.

Hajer, G.R., von Haeften, T.W., Visseren, F.L. (2008) Adipose tissue dysfunction in obesity, diabetes, and vascular disease. European Heart Journal 29: 2959-2971.

Halaas, J.L., Gajiwala, K.S., Maffei, M., Cohen, S.L., Chait, B.T., Rabinowitz, D., Lallone, R.L., Burley, S.K., Friedman, J.M. (1995) Weight-reducing effects of the plasma-protein encoded by the obese gene. Science 269: 543-546.

Halberg, F. (1969) Chronobiology. Annual Reviews of Physiology. 31: 675-725.

Halberg, F.T.Y., Johnson, E.A. Circadian system phase- an aspect of temporal morphology; procedures and illustrative examples. (1967) HV Mayersbach, ed. Proceedings of the International Congress of Anatomists: The Cellular Aspects of Biorhythms, Symposium on Biorhythms. Edited by New York: Springer-Verlag; 1967: 20-48.

Hammad, S.M., Crellin, H.G., Wu, B.X., Melton, J., Anelli, V., Obeid, L.M. (2008) Dual and distinct roles for sphingosine kinase 1 and sphingosine 1 phosphate in the response to inflammatory stimuli in RAW macrophages. Prostaglandins and Other Lipid Mediators 85 (3–4): 107-114.

Han G., Gupta S.D., Gable K., Niranjanakumari S., Moitra P., Eichler F., Brown R.H., Jr., Harmon J.M., Dunn T.M. (2009) Identification of small subunits of mammalian serine palmitoyltransferase that confer distinct acyl-CoA substrate specificities. Proceedings of the National Academy of Sciences of the United States of America 106: 8186–8191. PMC2688822

Hannun, Y.A. (1996) Functions of ceramide in coordinating cellular responses to stress. Science 274 (5294): 1855-1859.

Hannun, Y.A., Obeid, L.M. (2002) The ceramide-centric universe of lipid-mediated cell regulation: stress encounters of the lipid kind. The Journal of Biological Chemistry 277: 25847-25850.

Hannun, Y. A., Obeid, L.M. (2018) Sphingolipids and their metabolism in physiology and disease. Nature Reviews Molecular and Cellular Biology 19: 175-191.

Hardin, P.E., Panda, S. (2013) Circadian timekeeping and output mechanisms in animals. Current Opinion in Neurobiology 23: 724-731.

Hardy, O. T., Czech, M.P., Corvera, S. (2012) What causes the insulin resistance underlying obesity? Current Opinion in Endocrinology, Diabetes and Obesity 19: 81-87.

Harper, J. W., Adami, G., Wei, N., Keyomarsi, K., and Elledge, S. (1993) The p21 cdk-interacting protein Cip1 is a potent inhibitor of G1 cyclin-dependent kinases. Cell 75: 805-816.

Harper, J. W., Elledge, S. J., Keyomarsi, K., Dynlacht, B., Tsai, L., Zhang, P., Dobtowolski, S., Bai, C., Connell-Crowley, L., Swindell, E., Fox, M. P., and Wei, N. (1995) Inhibition of cyclin dependent kinases by p21. Molecular Biology of the Cell 6: 387-400.

Harrison, P.J., Dunn, T.M., Campopiano, D.J. (2018) Sphingolipid biosynthesis in man and microbes. Natural Product Reports 35 (9): 921-954. PMC6148460

Hashimoto, T., Igarashi, J., Kosaka, H. (2009) Sphingosine kinase is induced in mouse 3T3-L1 cells and promotes adipogenesis. Journal of Lipid Research 50 (4): 602-610.

Hashimoto, Y., Matsuzaki, E., Higashi, K., Takahashi-Yanaga, F., Takano, A., Hirata, M., Nishimura, F. (2015) Sphingosine-1-phosphate inhibits differentiation of C3H10T1/2 cells into adipocyte. Molecular and Cellular Biochemistry 401 (1-2), 39-47.

Hatori, M., Vollmers, C., Zarrinpar, A., DiTacchio, L., Bushong, E.A., Gill, S., Leblanc, M., Chaix, A., Joens, M., Fitzpatrick, J.A.J., Ellisman, M.H., Panda, S. (2012) Time restricted feeding without reducing caloric intake prevents metabolic diseases in mice fed a high fat diet. Cell Metabolism 15 (6): 848-860.

Hatoum, D., Haddadi, N., Lin, Y., Nassif, N.T., McGowan, E.M. (2017) Mammalian sphingosine kinase (SphK) isoenzymes and isoform expression: challenges for SphK as an oncotarget. Oncotarget 8 (22): 36898–36929. PMC5482707

Haynes, C. A., Allegood, J.C., Park, H., Sullards, M.C. (2009) Sphingolipidomics: methods for the comprehensive analysis of sphingolipids. Journal of Chromatography B. Analytical Technologies in the Biomedical and Life Sciences 877: 2696-2708.

Heinecke, J.W., Goldberg, I.J. Myeloperoxidase: a therapeutic target for preventing insulin resistance and the metabolic sequelae of obesity? (2014) Diabetes 63 (12): 4001-4003. PMC4238000

Heintzman, N. D., Stuart, R. K., Hon, G., Fu, Y., Ching, C. W., Hawkins, R. D., Barrera, L. O., Van Calcar, S., Qu, C., Ching, K. A., Wang, W., Weng, Z., Green, R. D., Crawford, G. E., and Ren, B. (2007) Distinct and predictive chromatin signatures of transcriptional promoters and enhancers in the human genome. Nature Genetics 39: 311–318.

Hennessy, T.L., Field, C.B. (1991) Circadian rhythms in photosynthesis: oscillations in carbon assimilation and stomatal conductance under constant conditions. Plant Physiology 96 (3): 831-836. PMC1080851

Hernández, A., Obregón, M.J. (2000) Triiodothyronine amplifies the adrenergic stimulation of uncoupling protein expression in rat brown adipocytes. American journal of physiology. Endocrinology and Metabolism 278 (5): E769-E777.

Hirayama, J., Sahar, S., Grimaldi, B., Tamaru, T., Takamatsu, K., Nakahata, Y., Sassone-Corsi, P. (2007) CLOCK-mediated acetylation of BMAL1 control circadian function. Nature 450: 1086-1090.

Hisano, Y., Kobayashi, N., Kawahara, A., Yamaguchi, A., Nishi, T. (2011) The sphingosine 1-phosphate transporter, SPNS2, functions as a transporter of the phosphorylated form of the immunomodulating agent FTY720. The Journal of Biological Chemistry 286 (3): 1758–1766.

Hodson, L., Humphreys, S.M., Karpe, F., Frayn, K.N. (2013) Metabolic signatures of human adipose tissue hypoxia in obesity. Diabetes 62 (5): 1417–1425.

Hogenesch, et al. (*Find 15 references contained therein, from which transcript sequencing data was accepted for deposition and use in this free circadian data bank.*) (2013-2018) github.com/circadb ; http://circadb.hogeneschlab.org/ (Accessed 2020 February 2.)

Hojjati, M. R., Li, Z., Jiang, X.C. (2005) Serine palmitoyl-CoA transferase (SPT) deficiency and sphingolipid levels in mice. Biochimica et Biophysica Acta 1737 (1): 44-51.

Holland, W.L., Brozinick, J.T., Wang, L.P., Hawkins, E.D., Sargent, K.M., Liu, Y., Narra, K., Hoehn, K.L., Knotts, T.A., Siesky, A., Nelson, D.H., Karathanasis, S.K., Fontenot, G.K., Birnbaum, M.J., Summers, S.A. (2007) Inhibition of ceramide synthesis ameliorates glucocorticoid-, saturated-fat-, and obesity-induced insulin resistance. Cell Metabolism. 5: 167-179.

Holland, W.L., Miller, R.A., Wang, Z.V., Sun, K., Barth, B.M., Bui, H.H., Davis, K.E., Bikman, B.T., Halberg, N., Rutkowski, J.M. (2011) Receptor-mediated activation of ceramidase activity initiates the pleiotropic actions of adiponectin. Nature Medicine 17 (1): 55-63.

Hong, S., Zhou, W., Fang, B., Lu, W., Loro, E., Damle, M., Ding, G., Jager, J., Zhang, S., Zhang, Y., Feng, D., Chu, Q., Dill, B.D., Molina, H., Khurana, T.S., Rabinowitz, J.D., Lazar, M.A., Sun, Z. (2017) Dissociation of muscle insulin sensitivity from exercise endurance in mice by HDAC3 depletion. Nature Medicine 23 (2): 223–34.

Hornemann T., Penno A., Rütti M. F., Ernst D., Kivrak-Pfiffner F., Rohrer L., von Eckardstein, A. (2009) The SPTLC3 subunit of serine palmitoytransferase generates short chain sphingoid bases. The Journal of Biological Chemistry 284: 26322–26330. PMC2785320

Hosogai, N., Fukuhara, A., Oshima, K., Miyata, Y., Tanaka, S., Segawa, K., Furukawa, S., Tochino, Y., Komuro, R., Matsuda, M., Shimomura, I. (2007) Adipose tissue hypoxia in obesity and its impact on adipocytokine dysregulation. Diabetes 56 (4): 901-911.

Huang, K.P. (1989) The mechanism of protein kinase C activation. Trends in Neurosciences 12 (11): 425-32.

Huang, K., Huang, J., Chen, C., Hao, J., Wang, S., Huang, J., Liu, P., Huang, H. (2014) AP-1 regulates sphingosine kinase 1 expression in a positive feedback manner in glomerular mesangial cells exposed to high glucose. Cellular Signalling 26 (3): 629-638.

Huang, H., Kasumov, T., Gatmaitan, P., Heneghan, H.M., Kashyap, S.R., Schauer, P.R., Brethauer, S.A., Kirwan, J.P. (2011) Gastric bypass surgery reduces plasma ceramide subspecies and improves insulin sensitivity in severely obese patients. Obesity 19 (11): 2235–2240.

Hudak, C.S., Sul, H.S. (2013) Pref-1, a gatekeeper of adipogenesis. Frontiers in Endocrinology 4: 79.

Hughes, M.E., DiTacchio, L., Hayes, K.R., Vollmers, C., Pulivarthy, S., Baggs, J.E., Panda, S., Hogenesch, J.B. (2009) Harmonics of circadian gene transcription in mammals. PLoS Genetics 5 (4): e1000442. PMC2654964

Hunt, S.R., Lu, Y., Fustin, J-M., Okamura, H., Partch, C.L., Forger, D.B., Kim, J.K., Virshup, D.M. (2018) CK1δ/ε protein kinase primes the PER2 circadian phosphoswitch. Proceedings of the National Academy of Sciences of the United States of America 115: 5986–5991.

Igarashi, N., Okada, T., Hayashi, S., Fujita, T., Jahangeer, S., Nakamura, S. (2003) Sphingosine kinase 2 is a nuclear protein and inhibits DNA synthesis. The Journal of Biological Chemistry 278 (47): 46832-46839.

Ihlefeld, K., Vienken, H., Claas, R.F., Blankenbach, K., Rudowski, A., ter Braak, M., Koch, A., Van Veldhoven, P.P., Pfeilschifter, J., Meyer zu Heringdorf, D. (2015) Upregulation of ABC transporters contributes to chemoresistance of sphingosine 1-phosphate lyase-deficient fibroblasts. Journal of Lipid Research 56 (1): 60-69. PMC4274072

Ikegami, K., Refetoff, S., Van Cauter, E., Yoshimura, T. (2019) Interconnection between circadian clocks and thyroid function. Nature Reviews Endocrinology 15 (10): 590-600.

Ishii, I., Ye, X., Friedman, B., Kawamura, S., Contos, J.J., Kingsbury, M.A., Yang, A.H., Zhang, G., Brown, J.H., Chun, J. (2002) Marked perinatal lethality and cellular signaling deficits in mice null for the two sphingosine 1-phosphate (S1P) receptors, S1P(2)/LP(B2)/EDG-5 and S1P(3)/LP(B3)/EDG-3. The Journal of Biological Chemistry 277 (28): 25152–25159.

James, S.M., Honn, K.A., Gaddameedhi, S., Van Dongen, H. (2017) Shift work: disrupted circadian rhythms and sleep-implications for health and well-being. Current Sleep Medicine Reports 3 (2): 104-112. PMC5647832

Japtok, L., Schmitz, E.I., Fayyaz, S., Kramer, S., Hsu, L.J., Kleuser, B. (2015) Sphingosine 1-phosphate counteracts insulin signaling in pancreatic beta-cells via the sphingosine 1-phosphate receptor subtype 2. The FASEB Journal 29 (8): 3357-3369.

Jeong, J.K., Moon, M.H., Park, S.Y. (2015) Modulation of the expression of sphingosine 1-phosphate 2 receptors regulates the differentiation of pre-adipocytes. Molecular Medicine Reports 12 (5): 7496-7502.

Jo, J., Gavrilova, O., Pack, S., Jou, W., Mullen, S., Sumner, A.E., Cushman, S.W., Periwal, V. (2009) Hypertrophy and/or hyperplasia: dynamics of adipose tissue growth. PLoS Computational Biology 5 (3): e1000324. PMC2653640

Johnson, K.R., Becker, K.P., Facchinetti, M.M., Hannun, Y.A., Obeid, L.M. (2002) PKC-dependent activation of sphingosine kinase 1 and translocation to the plasma membrane. Extracellular release of sphingosine-1-phosphate induced by phorbol 12-myristate 13-acetate (PMA). The Journal of Biological Chemistry 277 (38): 35257-35262.

Johnston, J.D., Ordovás, J.M., Scheer, F.A., Turek, F.W. (2016) Circadian rhythms, metabolism, and chrononutrition in rodents and humans. Advances in Nutrition (Bethesda, Md.) 7 (2): 399-406. PMC4785478

Jonnalagadda, D., Sunkara, M., Morris, A.J., Whiteheart, S.W. (2014) Granule-mediated release of sphingosine-1-phosphate by activated platelets. Biochimica et Biophysica Acta 1841 (11): 1581-1589. PMC4223867

Jordan, S.D., Lamia, K.A. (2013) AMPK at the crossroads of circadian clocks and metabolism. Molecular and Cellular Endocrinology 366 (2): 163-169. PMC3502724

Jun, D.-J., Lee, J.-H., Choi, B.-H., Koh, T.-K., Ha, D.-C., Jeong, M.-W., Kim, K.-T. (2006) Sphingosine-1-phosphate modulates both lipolysis and leptin production in differentiated rat white adipocytes. Endocrinology 147 (12): 5835-5844.

Kabayama, K., Sato, T., Saito, K., Loberto, N., Prinetti, A., Sonnino, S., Kinjo, M., Igarashi, Y., Inokuchi, J.-I. (2007) Dissociation of the insulin receptor and caveolin-1 complex by ganglioside GM3 in the state of insulin resistance. Proceedings of the National Academy of Sciences of the United States of America 104 (34): 13678-13683.

Kajimoto, T., Caliman, A.D., Tobias, I.S., Okada, T., Pilo, C.A., Van, A.N., Andrew McCammon, J., Nakamura S.I., Newton, A.C. (2019) Activation of atypical protein kinase C by sphingosine 1-phosphate revealed by an aPKC-specific activity reporter. Science Signaling 12 (562). PMC6657501

Kapitonov, D., Allegood, J.C., Mitchell, C., Hait, N.C., Almenara, J.A., Adams, J.K., Zipkin, R.E., Dent, P., Kordula, T., Milstien, S., Spiegel, S. (2009) Targeting sphingosine kinase 1 inhibits Akt signaling, induces apoptosis, and suppresses growth of human glioblastoma cells and xenografts. Cancer Research 69 (17): 6915-6923. PMC2752891

Karlsson, B., Knutsson, A., Lindahl, B. (2001) Is there an association between shift work and having a metabolic syndrome? Results from a population based study of 27,485 people. Occupational and Environmental Medicine 58: 747-752.

Karlsson, B.H., Knutsson, A.K., Lindahl, B.O., Alfredsson, L.S. (2003) Metabolic disturbances in male workers with rotating three-shift work. Results of the WOLF study. Occupational and Environmental Health 76: 424-430.

Kersten, S. (2001) Mechanisms of nutritional and hormonal regulation of lipogenesis. EMBO Reports 2 (4): 282-286.

Kessler, K., Hornemann, S., Petzke, K.J., Kemper, M., Markova, M., Rudovich, N., Grune, T., Kramer, A., Pfeiffer, A., Pivovarova-Ramich, O. (2018) Diurnal distribution of carbohydrates and fat affects substrate oxidation and adipokine secretion in humans. The American Journal of Clinical Nutrition 108 (6): 1209-1219.

Kharel, Y., Raje, M., Gao, M., Gellett, A.M., Tomsig, J.L., Lynch, K.R., Santos, W.L. (2012) Sphingosine kinase type 2 inhibition elevates circulating sphingosine 1-phosphate. The Biochemical Journal 447 (1): 149-157. PMC3443596

Kharel, Y., Huang, T., Salamon, A., Harris, T.E., Santos, W.L., Lynch, K.R. (2020) Mechanism of sphingosine 1-phosphate clearance from blood. The Biochemical Journal 477 (5): 925-935. PMC7059866

Kim, Y., Han, S., Yeom, M., Kim, H., Lim, J., Cha, J.Y., Kim, W.Y., Somers, D.E., Putterill, J., Nam, H.G., Hwang, D. (2013) Balanced nucleocytosolic partitioning defines a spatial network to coordinate circadian physiology in plants. Developmental Cell 26 (1): 73-85.

Kim, Y.H., Marhon, S.A., Zhang, Y., Steger, D.J., Won, K.J., Lazar, M.A. (2018) Rev-erbα dynamically modulates chromatin looping to control circadian gene transcription. Science (New York, N.Y.), 359 (6381) 1274-1277. PMC5995144

Kitatani, K., Idkowiak-Baldys, J., Hannun, Y.A. (2008) The sphingolipid salvage pathway in ceramide metabolism and signaling. Cellular Signaling 20(6): 1010-1018. PMC2422835

Kleuser, B. (2018) The enigma of sphingolipids in health and disease. International Journal of Molecular Sciences 19 (10): 3126. PMC6213595

Kleuser, B., Maceyka, M., Milstien, S., Spiegel, S. (2001) Stimulation of nuclear sphingosine kinase activity by platelet-derived growth factor. FEBS Letters 503 (1): 85-90.

Koeck, E. S., Iordanskaia, T., Sevilla, S., Ferrante, S.C., Hubal, M.J., Freishtat, R.J., Nadler, E.P. (2014) Adipocyte exosomes induce transforming growth factor beta pathway dysregulation in hepatocytes: a novel paradigm for obesity-related liver disease. Journal of Surgical Research 192: 268-275.

Kolak, M., Westerbacka, J., Velagapudi, V.R., Wågsäter, D., Yetukuri, L., Makkonen, J., Rissanen, A., Häkkinen, A.-M., Lindell, M., Bergholm, R., Hamsten, A., Eriksson, P., Fisher, R.M., Orešič, M., Yki-Järvinen, H. (2007) Adipose tissue inflammation and increased ceramide content characterize subjects with high liver fat content independent of obesity. Diabetes 56 (8): 1960-1968.

Kolak, M., Gertow, J., Westerbacka, J., Summers, S.A., Liska, J., Franco-Cereceda, A., Orešič, M., Yki-Järvinen, H., Eriksson, P., Fisher, R.M. (2012) Expression of ceramide-metabolising enzymes in subcutaneous and intra-abdominal human adipose tissue. Lipids in Health and Disease 11 (1): 115.

Konturek, P.C., Brzozowski, T., Konturek, S.J. (2011) Gut clock: implication of circadian rhythms in the gastrointestinal tract. Journal of Physiology and Pharmacology 62 (2): 139-150.

Koulouri, O., Moran, C., Halsall, D., Chatterjee, K., Gurnell, M. (2013) Pitfalls in the measurement and interpretation of thyroid function tests. Best Practice and Research: Clinical Endocrinology and Metabolism 27 (6): 745-762. PMC3857600

Kovář, J., Leníček, M., Zimolová, M., Vítek, L., Jirsa, M., Piťha, J. (2010) Regulation of diurnal variation of cholesterol 7α-hydroxylase (CYP7A1) activity in healthy subjects. Physiology Research 59: 233-238.

Kowalski, G.M., Carey, A.L., Selathurai, A., Kingwell, B.A., Bruce, C.R. (2013) Plasma sphingosine-1-phosphate is elevated in obesity. PLoS One 8 (9): e72449.

Kraegen, E.W., Cooney, G.J., Ye, J.M., Thompson, A.L., Furler, S.M. (2001) The role of lipids in the pathogenesis of muscle insulin resistance and beta cell failure in type II diabetes and obesity. Experimental and Clinical Endocrinology and Diabetes 109 (Suppl. 2): S189–S201.

Krycer, J.R., Yugi, K., Hirayama, A., Fazakerley, D.J., Quek, L.E., Scalzo, R., Ohno, S., Hodson, M.P., Ikeda, S., Shoji, F., Suzuki, K., Domanova, W., Parker, B.L., Nelson, M.E., Humphrey, S.J., Turner, N., Hoehn, K.L., Cooney, G.J., Soga, T., Kuroda, S., James, D.E. (2017) Dynamic metabolomics reveals that insulin primes the adipocyte for glucose metabolism. Cell Reports 21 (12): 3536-3547.

Kurano, M., Nishikawa, M., Kuma, H., Jona, M., Yatomi, Y. (2017) Involvement of Band3 in the efflux of sphingosine 1-phosphate from erythrocytes. PloS One 12 (5): e0177543. PMC28494002

Kurano, M., Tsukamoto, K., Ohkawa, R., Hara, M., Iino, J., Kageyama, Y., Ikeda, H., Yatomi, Y. (2013) Liver involvement in sphingosine 1-phosphate dynamism revealed by adenoviral hepatic overexpression of apolipoprotein M. Atherosclerosis 229 (1): 102-109.

Kurano, M., Tsukamoto, K., Shimizu, T., Kassai, H., Nakao, K., Aiba, A., Hara, M., Yatomi, Y. (2020) Protection against insulin resistance by apolipoprotein M/sphingosine-1-phosphate. Diabetes 69 (5): 867-881.

Kusminski, C.M., Bickel, P.E., Scherer, P.E. (2016) Targeting adipose tissue in the treatment of obesity-associated diabetes. Nature Reviews Drug Discovery 15: 639-660.

Kwon, I., Lee, J., Chang, S.H., Jung, N.C., Lee, B.J., Son, G.H., Kim, K., Lee, K.H. (2006) BMAL1 shuttling controls transactivation and degradation of the CLOCK/BMAL1 heterodimer. Molecular and Cellular Biology 26 (19): 7318-7330. PMC1592876

Laaksonen, R., Ekroos, K., Sysi-Aho, M., Hilvo, M., Vihervaara, T., Kauhanen, D., Suoniemi, M., Hurme, R., Marz, W., Scharnagl, H., Stojakovic, T., Vlachopoulou, E., Lokki, M.L., Nieminen, M.S., Klingenberg, R., Matter, C.M., Hornemann, T., Juni, P., Rodondi, N., Raber, L., Windecker, S., Gencer, B., Pedersen, E.R., Tell, G.S., Nygard, O., Mach, F., Sinisalo, J., Luscher, T.F. (2016) Plasma ceramides predict cardiovascular

death in patients with stable coronary artery disease and acute coronary syndromes beyond LDL-cholesterol. European Heart Journal 37: 1967-1976.

Lambert, J.M., Anderson, A.K., Cowart, L.A. (2018) Sphingolipids in Adipose Tissue: What's Tipping the Scale? Advances in Biological Regulation 70: 19-30.

Lamia, K.A., Sachdeva, U.M., DiTacchio, L., Williams, E.C., Alvarez, J.G., Egan, D.F., Vasquez, D.S., Juguilon, H., Panda, S., Shaw, R.J., Thompson, C.B., Evans, R.M. (2009) AMPK regulates the circadian clock by cryptochrome phosphorylation and degradation. Science 326: 437-40.

Lan, T., Liu, W., Xie, X., Xu, S., Huang, K., Peng, J., Shen, X., Liu, P., Wang, L., Xia, P., Huang, H. (2011) Sphingosine kinase-1 pathway mediates high glucose-induced fibronectin expression in glomerular mesangial cells. Molecular Endocrinology 25 (12): 2094-2105. PMC3231833

Langin, D., Dicker, A., Tavernier, G., Hoffstedt, J., Mairal, A., Rydén, Arner, E., Sicard, A., Jenkins, C.M., Viguerie, N., van Harmelen, V., Gross, R.W., Holm, C., Arner, P. (2005) Adipocyte lipases and defect of lipolysis in human obesity. Diabetes 190-3197.

Larsen, P.J., Tennagels, N. (2014) On ceramides, other sphingolipids and impaired glucose homeostasis. Molecular Metabolism 3 (3): 252-260.

Layer, P., Singer, M.V., Eysselein, V.E. (1987) Effect of circadian rhythm on gastrointestinal motility. Zeitschrift für Gastroenterologie 25 (3): 69-73.

Lee, K.J., Mwongela, S.M., Kottegoda, S., Borland, L., Nelson, A.R., Sims, C.E., Allbritton, N.L. (2008) Determination of sphingosine kinase activity for cellular signaling studies. Analytical Chemistry 80 (5): 1620-1627.

Lee, S.Y., Hong, I.K., Kim, B.R., Shim, S.M., Sung Lee, J., Lee, H.Y., Soo Choi, C., Kim, B.K., Park T.S. (2015) Activation of sphingosine kinase 2 by endoplasmic reticulum stress ameliorates hepatic steatosis and insulin resistance in mice. Hepatology 62 (1): 135-146.

Lee, S.-Y., Lee, H.-Y., Song, J.-H., Kim, G.-T., Jeon, S., Song, Y.-J., Lee, J.S., Hur, J.-H., OH, H.H., Park, S.-Y. (2017) Adipocyte-specific deficiency of de novo sphingolipid biosynthesis leads to lipodystrophy and insulin resistance. Diabetes 66 (10): 2596-2609.

Lemmer, B., Oster, H. (2018) The role of circadian rhythms in the hypertension of diabetes mellitus and the metabolic syndrome. Current Hypertension Reports 20 (5): 43.

Leso, V., Vetrani, I., Sicignano, A., Romano, R., Iavicoli, I. (2020) The impact of shift-work and night shift-work on thyroid: a systematic review. International Journal of Environmental Research and Public Health 17 (5): 1527. PMC7084223

Levy, M., Futerman, A.H. (2010) Mammalian ceramide synthases. IUBMB Life 62 (5): 347-356.

Lewis, C.S., Voelkel-Johnson, C., Smith, C.D. (2018) Targeting sphingosine kinases for the treatment of cancer. Advances in Cancer Research 140: 295-325. PMC6447312

Li, C.M., Park, J.H., Simonaro, C.M., He, X., Gordon, R.E., Friedman, A.H., Ehleiter, D., Paris, F., Manova, K., Hepbildikler, S., Fuks, Z., Sandhoff, K., Kolesnick, R., Schuchman, E.H. (2002) Insertional mutagenesis of the mouse acid ceramidase gene leads to early embryonic lethality in homozygotes and progressive lipid storage disease in heterozygotes. Genomics 79 (2): 218-224.

Lima, S., Milstien, S., Spiegel, S. (2017).Sphingosine and sphingosine kinase 1 involvement in endocytic membrane trafficking. The Journal of Biological Chemistry 292 (8): 3074-3088. PMC5336145

Lindsay, M.E., Holaska, J.M., Welch, K., Paschal, B.M., Macara, I.G. (2001) Ran-binding protein 3 is a cofactor for Crm1-mediated nuclear protein export. Journal of Cell Biology 153: 1391-1402. PMC2150735

Liu. Y., Wada, R., Yamashita, T., Mi, Y., Deng, C.X., Hobson, J.P., Rosenfeldt, H.M., Nava, V.E., Chae S.S., Lee, M.J., Liu, C.H., Hla, T., Spiegel, S., Proia, R.L. (2000) Edg-1, the G protein-coupled receptor for sphingosine-1-phosphate, is essential for vascular maturation. Journal of Clinical Investigation 106: 951-961.

Loizides-Mangold, U., Perrin, L., Vandereycken, B., Betts, J.A., Walhin, J.P., Templeman, I., Chanon, S., Weger, B.D., Durand, C., Robert, M., Paz Montoya, J., Moniatte, M., Karagounis, L.G., Johnston, J.D., Gachon, F., Lefai, E., Riezman, H., Dibner, C. (2017) Lipidomics reveals diurnal lipid oscillations in human skeletal muscle persisting in cellular myotubes cultured in vitro. Proceedings of the National Academy of Sciences of the United States of America 114 (41): E8565–E8574. PMC5642690

López-Juárez, A., Morales-Lázaro, S., Sánchez-Sánchez, R., Sunkara, M., Lomelí, H., Velasco, I., Morris, A. J., Escalante-Alcalde, D. (2011) Expression of LPP3 in Bergmann glia is required for proper cerebellar sphingosine-1-phosphate metabolism/signaling and development. Glia 59 (4): 577-589. PMC3196773

Maggio, C.A., Greenwood, M.R. (1982) Adipose tissue lipoprotein lipase (LPL) and triglyceride uptake in Zucker rats. Physiology and Behavior 29 (6): 1147-1152.

Manfredini, R., Fabbian, F., Cappadona, R., De Giorgi, A., Bravi, F., Carradori, T., Flacco, M.E., Manzoli, L. (2019) Daylight saving time and acute myocardial infarction: a meta-analysis. Journal of Clinical Medicine 8 (3): 404. PMC6463000

Mastrandrea, L.D. (2013) Role of sphingosine kinases and sphingosine 1-phosphate in mediating adipogenesis. Journal of Diabetes 3 (2): 52-61.

Mathias, S., Kolesnick, R. (1993) Ceramide: a novel second messenger. Advances in Lipid Research 25: 65-90.

Meikle, P.J., Summers, S.A. (2017) Sphingolipids and phospholipids in insulin resistance and related metabolic disorders. Nature Reviews Endocrinology 13 (2): 79.

Merrill Jr., A.H., Wang, E., Mullins, R.E. (1988) Kinetics of long-chain (sphingoid) base biosynthesis in intact LM cells: effects of varying the extracellular concentrations of serine and fatty acid precursors of this pathway. Biochemistry 27: 340-345.

Merrill Jr., A.H., Schmelz, E.M., Dillehay, D.L., Spiegel, S., Shayman, J.A., Schroeder, J.J., Riley, R.T., Voss, K.A., Wang, E. (1997) Sphingolipids–the enigmatic lipid class: biochemistry, physiology, and pathophysiology. Toxicology and Applied Pharmacology 142 (1): 208-225.

Merrill Jr., A.H. (2002) De novo sphingolipid biosynthesis: a necessary, but dangerous, pathway. The Journal of Biological Chemistry 277 (29): 25843-25846.

Miller, C.N., Yang, J.-Y., England, E., Yin, A., Baile, C.A., Rayalam, S. (2015) Isoproterenol increases uncoupling, glycolysis, and markers of beiging in mature 3T3-L1 adipocytes. PLoS One 10 (9): e0138344.

Mishima, Y., Kurano, M., Kobayashi, T., Nishikawa, M., Ohkawa, R., Tozuka, M., Yatomi, Y. (2018) Dihydro-sphingosine 1-phosphate interacts with carrier proteins in a manner distinct from that of sphingosine 1-phosphate. Bioscience Reports 38 (5): BSR20181288.

Mitra, P., Oskeritzian, C.A., Payne, S.G., Beaven, M.A., Milstien, S., Spiegel, S. (2006) Role of ABCC1 in export of sphingosine-1-phosphate from mast cells. Proceedings of the National Academy of Sciences of the United States of America 103 (44): 16394-16399. PMC1637593

Mitsutake, S., Zama, K., Yokota, H., Yoshida, T., Tanaka, M., Mitsui, M., Ikawa, M., Okabe, M., Tanaka, Y., Yamashita, T., Takemoto, H., Okazaki, T., Watanabe, K., Igarashi, Y. (2011) Dynamic modification of sphingomyelin in lipid microdomains controls development of obesity, fatty liver, and type 2 diabetes. The Journal of Biological Chemistry 286 (32): 28544-28555.

Mizugishi, K., Yamashita, T., Olivera, A., Miller, G.F., Spiegel, S., Proia, R.L. Essential role for sphingosine kinases in neural and vascular development. (2005) Molecular and Cellular Biology 25 (24): 11113-11121. PMC1316977

Mohawk, J.A., Green, C.B., Takahashi, J.S. (2012) Central and peripheral circadian clocks in mammals. Annual Review of Neuroscience 35: 445-462. PMC3710582

Montefusco, D.J., Allegood, J.C., Spiegel, S., Cowart, L.A. (2018) Non-alcoholic fatty liver disease: insights from sphingolipidomics. Biochemical and Biophysical Research Communications 504 (3): 608-616.

Moon, M.H., Jeong, J.K., Lee, J.H., Park, Y.G., Lee, Y.J., Seol, J.W., Park, S.Y. (2012) Antiobesity activity of a sphingosine 1-phosphate analogue FTY720 observed in adipocytes and obese mouse model. Experimental and Molecular Medicine 44 (10): 603-614.

Morelli, D., Bartoloni, L., Rossi, A., & Clifton, D. A. (2019) A computationally efficient algorithm to obtain an accurate and interpretable model of the effect of circadian rhythm on resting heart rate. Physiological Measurement 40 (9): 095001.

Morgan, J.I., Curran, T. (1989) Stimulus-transcription coupling in neurons: role of cellular immediate-early genes. Trends in Neuroscience 12: 459-462.

Morigny, P., Houssier, M., Mouisel, E., Langin, D. (2016) Adipocyte lipolysis and insulin resistance. Biochimie 125: 259-266.

Morrison, S.F., Madden, C.J., Tupone, D. (2014) Central neural regulation of brown adipose tissue thermogenesis and energy expenditure. Cell Metabolism 19 (5): 741-756.

Muir, L.A., Neeley, C.K., Meyer, K.A., Baker, N.A., Brosius, A.M., Washabaugh, A.R., Varban, O.A., Finks, J.F., Zamarron, B.F., Flesher, C.G., Chang, J.S., DelProposto, J.B., Geletka, L., Martinez-Santibanez, G., Kaciroti, N., Lumeng, C.N., O'Rourke, R.W. (2016) Adipose tissue fibrosis, hypertrophy, and hyperplasia: correlations with diabetes in human obesity. Obesity (Silver Spring) 24 (3): 597-605. PMC4920141

Nagafuku, M., Sato, T., Sato, S., Shimizu, K., Taira, T., Inokuchi, J. (2015) Control of homeostatic and pathogenic balance in adipose tissue by ganglioside GM3. Glycobiology 25 (3): 303-318.

Nagahashi, M., Kim, E.Y., Yamada, A., Ramachandran, S., Allegood, J.C., Hait, N.C., Maceyka, M., Milstien, S., Takabe, K., Spiegel, S. (2013) Spns2, a transporter of phosphorylated sphingoid bases, regulates their blood and lymph levels, and the lymphatic network. FASEB Journal 27 (3): 1001-1011. PMC3574288

Nagahashi, M., Takabe, K., Liu, R., Peng, K., Wang, X., Wang, Y., Hait, N.C., Wang, X., Allegood, J.C., Yamada, A., Aoyagi, T., Liang, J., Pandak, W.M., Spiegel, S., Hylemon, P.B., Zhou, H. (2015) Conjugated bile acid-activated S1P receptor 2 is a key regulator of sphingosine kinase 2 and hepatic gene expression. Hepatology (Baltimore, Md.) 61 (4): 1216-1226. PMC4376566

Nagahashi, M., Yamada, A., Aoyagi, T., Allegood, J., Wakai, T., Spiegel, S., Takabe, K. (2016) Sphingosine-1-phosphate in the lymphatic fluid determined by novel methods. Heliyon 2 (12): e00219. PMC5198727

Nagahashi, M., Yamada, A., Katsuta, E., Aoyagi, T., Huang, W.C., Terracina, K.P., Hait, N.C., Allegood, J.C., Tsuchida, J., Yuza, K., Nakajima, M., Abe, M., Sakimura, K., Milstien, S., Wakai, T., Spiegel, S., Takabe, K. (2018) Targeting the SphK1/S1P/S1PR1 axis that links obesity, chronic inflammation, and breast cancer metastasis. Cancer Research 78 (7): 1713-1725. PMC6945803

Nieuwenhuis, B., Lüth, A., Chun, J., Huwiler, A., Pfeilschifter, J., Schäfer-Korting, M., Kleuser, B. (2009) Involvement of the ABC-transporter ABCC1 and the sphingosine 1-phosphate receptor subtype S1P(3) in the cytoprotection of human fibroblasts by the glucocorticoid dexamethasone. Journal of Molecular Medicine (Berlin, Germany) 87 (6): 645-657.

Nishino, S., Yamashita, H., Tamori, M., Mashimo, M., Yamagata, K., Nakamura, H., Murayama, T. (2019) Translocation and activation of sphingosine kinase 1 by ceramide-1-phosphate. Journal of Cellular Biochemistry 120 (4): 5396-5408.

Ntambi, J.M., Miyazaki, M., Stoehr, J.P., Lan, H., Kendziorski, C.M., Yandell, B.S., Song, Y., Cohen, P., Friedman, J.M., Attie, A.D. (2002) Loss of stearoyl-CoA desaturase-1

function protects mice against adiposity. Proceedings of the National Academy of Sciences of the United States of America 99 (17): 11482-11486. PMC123282

Obinata, H., Hla, T. (2019) Sphingosine 1-phosphate and inflammation. International Immunology 31 (9): 617-625. PMC6939830

Obinata, H., Kuo, A., Wada, Y., Swendeman, S., Liu, C.H., Blaho, V.A., Nagumo, R., Satoh, K., Izumi, T., Hla, T. (2019) Identification of ApoA4 as a sphingosine 1-phosphate chaperone in ApoM- and albumin-deficient mice. Journal of Lipid Research 60 (11): 1912-1921. PMC6824498

Obregón M.J. (2008) Thyroid hormone and adipocyte differentiation. Thyroid : Official Journal of the American Thyroid Association 18 (2): 185-195.

Obregón, M.J., Pitamber, R., Jacobsson, A., Nedergaard, J., Cannon, B. (1987) Euthyroid status is essential for the perinatal increase in thermogenin mRNA in brown adipose tissue of rat pups. Biochemical and Biophysical Research Communications 148 (1): 9-14.

Ogretmen B. (2018) Sphingolipid metabolism in cancer signalling and therapy. Nature reviews. Cancer 18 (1): 33-50. PMC5818153

Ohotski, J., Edwards, J., Elsberger, B., Watson, C., Orange, C., Mallon, E., Pyne, S., Pyne, N.J. (2013) Identification of novel functional and spatial associations between sphingosine kinase 1, sphingosine 1-phosphate receptors and other signaling proteins that affect prognostic outcome in estrogen receptor-positive breast cancer. International Journal of Cancer 132 (3): 605-616.

Osuga, J., Ishibashi, S., Oka, T., Yagyu, H., Tozawa, R., Fujimoto, A., Shionoiri, F., Yahagi, N., Kraemer, F.B., Tsutsumi, O., Yamada, N. Targeted disruption of hormone-sensitive lipase results in male sterility and adipocyte hypertrophy, but not in obesity. (2000) Proceedings of the National Academy of Sciences of the United States of America 97 (2): 787-792.

Orr, J.W., Newton, A.C. (1992) Interaction of protein kinase C with phosphatidylserine. 2. Specificity and regulation. Biochemistry 31 (19): 4667-4673.

Panza, J.A., Epstein, S.E., Quyyumi, A.A. (1991) Circadian variation in vascular tone and its relation to alpha-sympathetic vasoconstrictor activity. New England Journal of Medicine 325 (14): 986-990.

Pappu, R., Schwab, S.R., Cornelissen, I., Pereira, J.P., Regard, J.B., Xu, Y., Camerer, E., Zheng, Y., Huang, Y., Cyster, J.G., Coughlin, S.R. (2007) Promotion of lymphocyte egress into blood and lymph by distinct sources of sphingosine-1-phosphate. Science 316 (5822): 295-308.

Park, Y.S., Hakomori, S., Kawa, S., Ruan, F., Igarashi, Y. (1994) Liposomal N,N,N-trimethylsphingosine (TMS) as an inhibitor of B16 melanoma cell growth and metastasis with reduced toxicity and enhanced drug efficacy compared to free TMS: cell membrane signaling as a target in cancer therapy III. Cancer Research 54 (8): 2213-2217.

Parrill, A.L., Lima, S., Spiegel, S. (2012) Structure of the first sphingosine 1-phosphate receptor. Science Signaling 5 (225): pe23-pe23.

Parsons, M.J., Lester, K.J., Barclay, N.L., Archer, S.N., Nolan, P.M., Eley, T.C., Gregory, A.M. (2014) Polymorphisms in the circadian expressed genes PER3 and ARNTL2 are associated with diurnal preference and GNβ3 with sleep measures. Journal of Sleep Research 23: 595-604.

Paschos, G.K., Ibrahim, S., Song, W.L., Kunieda, T., Grant, G., Reyes, T.M., Bradfield, C.A., Vaughan, C.H., Eiden, M., Masoodi, M., Griffin, J.L., Wang, F., Lawson, J.A., Fitzgerald, G.A. (2012) Obesity in mice with adipocyte-specific deletion of clock component Arntl. Nature Medicine 18: 1768-1777.

Paugh, B.S., Bryan, L., Paugh, S.W., Wilczynska, K.M., Alvarez, S.M., Singh, S.K., Kapitonov, D., Rokita, H., Wright, S., Griswold-Prenner, I., Milstien, S., Spiegel, S., Kordula, T. (2009) Interleukin-1 regulates the expression of sphingosine kinase 1 in glioblastoma cells. The Journal of Biological Chemistry 284 (6): 3408-3417. PMC2635028

Peek, C.B., Levine, D.C., Cedernaes, J., Taguchi, A., Kobayashi, Y., Tsai, S.J., Bonar, N.A., McNulty, M.R., Ramsey, K.M., Bass, J. (2017) Circadian clock interaction with HIF1α mediates oxygenic metabolism and anaerobic glycolysis in skeletal muscle. Cell Metabolism 25 (1): 86-92.

Pelletier, D., Hafler, D.A. (2012) Fingolimod for multiple sclerosis. The New England Journal of Medicine 366: 339-347.

Peterson, L.R., Xanthakis, V., Duncan, M.S., Gross, S., Friedrich, N., Völzke, H., Felix, S.B., Jiang, H., Sidhu, R., Nauck, M., Jiang, X., Ory, D.S., Dörr, M., Vasan, R.S., Schaffer, J.E. (2018) Ceramide remodeling and risk of cardiovascular events and mortality. Journal of the American Heart Association 7 (10): e007931. PMC6015315

Pilorget, A., Demeule, M., Barakat, S., Marvaldi, J., Luis, J., Béliveau, R. (2007) Modulation of P-glycoprotein function by sphingosine kinase-1 in brain endothelial cells. Journal of Neurochemistry 100 (5): 1203-1210.

Pilorz, V., Helfrich-Förster, C., Oster, H. (2018) The role of the circadian clock system in physiology. Pflugers Archives: European Journal of Physiology 470 (2): 227-239.

Pitson, S.M. (2011) Regulation of sphingosine kinase and sphingolipid signaling. Trends in Biochemical Sciences 36 (2): 97-107.

Pitson, S.M., Xia, P., Leclercq, T.M., Moretti, P.A.B., Zebol, J.R., Lynn, H.E., Wattenberg, B.W., Vadas, M.A. (2005) Phosphorylation-dependent translocation of sphingosine kinase to the plasma membrane drives its oncogenic signaling. Journal of Experimental Medicine 201 (1): 49-54.

Ponnusamy, S., Meyers-Needham, M., Senkal, C., Saddoughi, S.A., Sentelle, D., Selvam, S.P., Salas, A., Ogretmen, B. (2010) Sphingolipids and cancer: ceramide and sphingosine-1-phosphate in the regulation of cell death and drug resistance. Future Oncology 6 (10): 1603-1624.

Pruett, S.T., Bushnev, A., Hagedorn, K., Adiga, M., Haynes, C.A., Sullards, M.C., Liotta, D.C., Merrill Jr., A.H. (2008) Biodiversity of sphingoid bases ("sphingosines") and related amino alcohols. Journal of Lipid Research 49 (8): 1621-1639.

Pyne, N.J., Adams, D.R., Pyne, S. (2017) Sphingosine kinase 2 in autoimmune/inflammatory disease and the development of sphingosine kinase 2 inhibitors. Trends in Pharmacological Sciences 38 (7): 581-591.

Pyne, N.J., Pyne, S. (2017) Sphingosine 1-phosphate receptor 1 signaling in mammalian cells. Molecules 22 (3).

Qi, Y., Chen, J., Lay, A., Don, A., Vadas, M., Xia, P. (2013) Loss of sphingosine kinase 1 predisposes to the onset of diabetes via promoting pancreatic beta-cell death in diet-induced obese mice. The FASEB Journal 27: 4294-4304.

Qin, J., Kilkus, J.P., Dawson, G. (2018) The cross roles of sphingosine kinase 1/2 and ceramide glucosyltransferase in cell growth and death. Biochemical and Biophysical Research Communications 500 (3): 597-602.

Qu, M., Duffy, T., Hirota, T., Kay, S.A. (2018) Nuclear receptor HNF4A transrepresses CLOCK:BMAL1 and modulates tissue-specific circadian networks. Proceedings of the National Academy of Sciences of the United States of America 115 (52): E12305-E12312. PMC6310821

Raichur, S., Wang, S.T., Chan, P.W., Li, Y., Ching, J., Chaurasia, B., Dogra, S., Öhman, M.K., Takeda, K., Sugii, S. 2014. CerS2 haploinsufficiency inhibits β-oxidation and confers susceptibility to diet-induced steatohepatitis and insulin resistance. Cell Metabolism 20 (4): 687-695.

Ramin, C., Devore, E.E., Wang, W., Pireer-Paul, J., Wegrzyn, L.R., Schernhammer, E.S. (2015) Night shift work at specific age ranges and chronic disease risk factors. Occupational and Environmental Medicine 72 (2): 100-107.

Ranieri, D., Cucina, A., Bizzarri, M., Alimandi, M., Torrisi, M.R. (2015) Microgravity influences circadian clock oscillation in human keratinocytes. FEBS Open Bio 5: 717-723.

Ravichandran, S., Finlin, B.S., Kern, P.A., Özcan, S. (2019) Sphk2$^{-/-}$ mice are protected from obesity and insulin resistance. Biochimica et Biophysica Acta. Molecular Basis of Disease 1865 (3): 570-576. PMC6368224

Refinetti, R., Lissen, G.C., Halberg, F. (2007) Procedures for numerical analysis of circadian rhythms. Biological Rhythm Research 38 (4): 275-325. PMC3663600

Rensing, L., Ruoff, P. (2002) Temperature effect on entrainment, phase shifting, and amplitude of circadian clocks and its molecular bases. Chronobiology International 19 (5): 807-864.

Roenneberg, T., Wirz-Justice, A., Skene, D.J., Ancoli-Israel, S., Wright, K.P., Dijk, D.J., Zee, P., Gorman, M. R., Winnebeck, E.C., Klerman, E.B. (2019) Why should we abolish daylight saving time? Journal of Biological Rhythms 34 (3): 227-230. PMC7205184

Romero, M.d.M., Sabater, D., Fernández-López, J.A., Remesar, X., Alemany, M. (2015) Glycerol production from glucose and fructose by 3T3-L1 cells: a mechanism of adipocyte defense from excess substrate. PLoS One 10 (10): e0139502.

Rosen, Evan D., Spiegelman, Bruce M. (2014) What we talk about when we talk about fat. Cell 156 (1-2): 20-44.

Ross, J.S., Hu, W., Rosen, B., Snider, A.J., Obeid, L.M., Cowart, L.A. (2013) Sphingosine kinase 1 is regulated by peroxisome proliferator-activated receptor alpha in response to free fatty acids and is essential for skeletal muscle interleukin-6 production and signaling in diet-induced obesity. The Journal of Biological Chemistry 288 (31): 22193-22206.

Ross, J.S., Russo, S.B., Chavis, G.C., Cowart, L.A., 2014. Sphingolipid regulators of cellular dysfunction in Type 2 diabetes mellitus: a systems overview. Clinical Lipidology 9 (5): 553-569.

Rosso, C., Kazankov, K., Younes, R., Esmaili, S., Marietti, M., Sacco, M., Carli, F., Gaggini, M., Salomone, F., Møller, H.J., Abate, M.L., Vilstrup, H., Gastaldelli, A., George, J., Grønbæk, H., Bugianesi, E. (2019) Crosstalk between adipose tissue insulin resistance and liver macrophages in non-alcoholic fatty liver disease. Journal of Hepatology 71 (5): 1012-1021.

Rotondo, F., Ho-Palma, A.C., Remesar, X., Fernández-López, J.A., Romero, M.d.M., Alemany, M. (2017) Glycerol is synthesized and secreted by adipocytes to dispose of excess glucose, via glycerogenesis and increased acyl-glycerol turnover. Science Reports 7: 8983.

Russo, S.B., Baicu, C.F., Van Laer, A., Geng, T., Kasiganesan, H., Zile, M.R., Cowart, L.A. (2012) Ceramide synthase 5 mediates lipid-induced autophagy and hypertrophy in cardiomyocytes. The Journal of Clinical Investigation 122 (11): 3919-3930.

Ruvolo, P.P., Clark, W., Mumby, M., Gao, F., May, W.S. (2002) A functional role for the B56 alpha-subunit of protein phosphatase 2A in ceramide-mediated regulation of Bcl2 phosphorylation status and function. The Journal of Biological Chemistry 277: 22847-22852.

Ryzhikov, M., Ehlers, A., Haspel, J.A. (2019). Adventures in spacetime: circadian rhythms and the dynamics of protein catabolism. Autophagy 15 (6):1115-1116. PMC6526858

Ryzhikov, M., Ehlers, A., Steinberg, D., Xie, W., Oberlander, E., Brown, S., Gilmore, P.E., Townsend, R.R., Lane, W.S., Dolinay, T., Nakahira, K., Choi, A., Haspel, J.A. (2019a) Diurnal rhythms spatially and temporally organize autophagy. Cell Reports 26 (7): 1880-1892. PMC6442472

Saba, J.D., Hla, T. (2004) Point-counterpoint of sphingosine 1-phosphate metabolism. Circulation Research 94 (6): 724-734.

Sachs, C.W., Ballas, L.M., Mascarella, S.W., Safa, A.R., Lewin, A.H., Loomis, C., Carroll, F.I., Bell, R.M., Fine, R.L. (1996) Effects of sphingosine stereoisomers on P-glycoprotein phosphorylation and vinblastine accumulation in multidrug-resistant MCF-7 cells. Biochemical Pharmacology 52 (4): 603-612.

Sahar, S., Zocchi, L., Kinoshita, C., Borrelli, E., Sassone-Corsi, P. (2010) Regulation of BMAL1 protein stability and circadian function by GSK3β-mediated phosphorylation. PLoS One 5 (1): e8561. PMC2797305

Salinas, M., López-Valdaliso, R., Martín, D., Alvarez, A., Cuadrado, A. (2000) Inhibition of PKB/Akt1 by C2-ceramide involves activation of ceramide-activated protein phosphatase in PC12 cells. Molecular and Cellular Neuroscience 15 (2): 156-169.

Samad, F., Hester, K.D., Yang, G., Hannun, Y.A., Bielawski, J. (2006) Altered adipose and plasma sphingolipid metabolism in obesity: a potential mechanism for cardiovascular and metabolic risk. Diabetes 55 (9): 2579-2587.

Samocha-Bonet, D., Dixit, V.D., Kahn, C.R., Leibel, R.L., Lin, X., Nieuwdorp, M., Pietilainen, K.H., Rabasa-Lhoret, R., Roden, M., Scherer, P.E., Klein, S., Ravussin, E. (2014) Metabolically healthy and unhealthy obese--the 2013 Stock Conference report. Obesity Reviews 15: 697-708.

Sanada, K., Okano, T., Fukada, Y. (2002) Mitogen-activated protein kinase phosphorylates and negatively regulates basic helix-loop-helix-PAS transcription factor BMAL1. The Journal of Biological Chemistry 200277 (1): 267-71.

Sanchez, T., Estrada-Hernandez, T., Paik, J.H., Wu, M.T., Venkataraman, K., Brinkmann, V., Claffey, K., Hla, T. (2003) Phosphorylation and action of the immunomodulator FTY720 inhibits VEGF-induced vascular permeability. The Journal of Biological Chemistry 278: 47281-47290.

Sato, M., Markiewicz, M. Yamanaka, M., Bielawska, A., Mao, C., Obeid, L.M., Hannun, Y.A., Trojanowska, M. (2003) Modulation of transforming growth factor-beta (TGF-beta) signaling by endogenous sphingolipid mediators. The Journal of Biological Chemistry 278: 9276-9282.

Sato, S., Solanas, G., Peixoto, F.O., Bee, L., Symeonidi, A., Schmidt, M.S., Brenner, C., Masri, S., Benitah, S.A., Sassone-Corsi, P. (2017) Circadian reprogramming in the liver identifies metabolic pathways of aging. Cell 170 (4): 664-677.

Scherer, P.E. (2006) Adipose tissue: from lipid storage compartment to endocrine organ. Diabetes 55: 1537-1545.

Schreiber, R., Xie, H., Schweiger, M. (2019) Of mice and men: The physiological role

of adipose triglyceride lipase (ATGL). Biochimica et Biophysica Acta: Molecular and Cell Biology of Lipids 1864: 880-899.

Schubert, K.M., Scheid, M.P., Duronio, V. (2000) Ceramide inhibits protein kinase B/Akt by promoting dephosphorylation of serine 473. The Journal of Biological Chemistry 275 (18): 13330-13335.

Schweiger, M., Romauch, M., Schreiber, R., Grabner, G.F., Hütter, S., Kotzbeck, P., Benedikt, P., Eichmann, T.O., Yamada, S., Knittelfelder, O. (2017) Pharmacological inhibition of adipose triglyceride lipase corrects high-fat diet-induced insulin resistance and hepatosteatosis in mice. Nature Communications 8: 1-15.

Selvam, S.P., De Palma, R.M., Oaks, J.J., Oleinik, N., Peterson, Y.K., Stahelin, R.V., Skordalakes, E., Ponnusamy, S., Garrett-Mayer, E., Smith, C.D., Ogretmen, B. (2015) Binding of the sphingolipid S1P to hTERT stabilizes telomerase at the nuclear periphery by allosterically mimicking protein phosphorylation. Science Signaling 16 (8): 381. PMC4492107

Sensken, S.C., Bode, C., Nagarajan, M., Peest, U., Pabst, O., Gräler, M.H. (2010) Redistribution of sphingosine 1-phosphate by sphingosine kinase 2 contributes to lymphopenia. Journal of Immunology (Baltimore, Md. : 1950) 184 (8): 4133-4142.

Seo, Y.J., Blake, C., Alexander, S., Hahm, B. (2010) Sphingosine 1-phosphate-metabolizing enzymes control influenza virus propagation and viral cytopathogenicity. Journal of Virology 84: 8124-8131.

Seo, Y-J., Pritzl, C.J., Vijayan, M., Bomb, K., McClain, M.E., Alexander, S., Hahm, B. (2013) Sphingosine kinase 1 serves as a pro-viral factor by regulating viral RNA synthesis and nuclear export of viral ribonucleoprotein complex upon influenza virus infection. PLoS One 8 (8): e75005.

Shaner, R.L., Allegood, J.C., Park, H., Wang, E., Kelly, S., Haynes, C.A., Sullards, M.C., Merrill, Jr., A.H. (2009) Quantitative analysis of sphingolipids for lipidomics using triple quadrupole and quadrupole linear ion trap mass spectrometers. Journal of Lipid Research 50: 1692-1707.

Shetty, A., Hsu, J.W., Manka, P.P., Syn, W.K. (2018) Role of the circadian clock in the metabolic syndrome and nonalcoholic fatty liver disease. Digestive Diseases and Sciences 63 (12): 3187-3206.

Shostak, A., Meyer-Kovac, J., Oster, H. (2013) Circadian regulation of lipid mobilization in white adipose tissues. Diabetes 62 (7): 2195-2203.

Shostak, A., Husse, J., Oster, H. (2013a) Circadian regulation of adipose function. Adipocyte 2 (4): 201-206.

Siow, D.L., Anderson, C.D., Berdyshev, E.V., Skobeleva, A., Natarajan, V., Pitson, S.M., Wattenberg, B.W. (2011) Sphingosine kinase localization in the control of sphingolipid metabolism. Advances in Enzyme Regulation 51 (1): 229-244.

Skurk, T., Alberti-Huber, C., Herder, C., Hauner, H. (2007) Relationship between adipocyte size and adipokine expression and secretion. The Journal of Clinical Endocrinology & Metabolism 92: 1023-1033.

Snider, J.M., Luberto, C., Hannun, Y.A. (2019) Approaches for probing and evaluating mammalian sphingolipid metabolism. Analytical Biochemistry 575: 70-86. PMC6498843

Sobel, J.A., Krier, I., Andersin, T., Raghav, S., Canella, D., Gilardi, F., Kalantzi, A.S., Rey, G., Weger, B., Gachon, F., Dal Peraro, M., Hernandez, N., Schibler, U., Deplancke, B., Naef, F. (2017) Transcriptional regulatory logic of the diurnal cycle in the mouse liver. 2017. PLoS Biology 15 (4): e2001069. PMC5393560

Sonnino, S., Mauri, L., Chigorno, V., Prinetti, A. Gangliosides as components of lipid membrane domains (2006) Glycobiology 17: 1R-13R.

Spassieva, S., Bielawski, J., Anelli, V., Obeid, L.M. (2007) Combination of C(17) sphingoid base homologues and mass spectrometry analysis as a new approach to study sphingolipid metabolism. Methods in Enzymology 434: 233-241.

Spengler, C.M., Shea, S.A. (2000) Endogenous circadian rhythm of pulmonary function in healthy humans. American Journal Respiratory and Critical Care Medicine 162 (3-1): 1038-1046.

Spiegel, K., Leproult, R., Van Cauter, E. (1999) Impact of sleep debt on metabolic and endocrine function. Lancet 354 (9188): 1435-1439.

Spiegel, S., Maczis, M.A., Maceyka, M., Milstien, S. (2019) New insights into functions of the sphingosine-1-phosphate transporter SPNS2. Journal of Lipid Research 60 (3): 484-489. PMC6399492

Spiegel, S., Milstien, S. (2003) Sphingosine-1-phosphate: an enigmatic signalling lipid. Nature Reviews Molecular Cell Biology 4 (5): 397-407.

Sposito, A.C., de Lima-Junior, J.C., Moura, F.A., Barreto, J., Bonilha, I., Santana, M., Virginio, V.W., Sun, L., Carvalho, L., Soares, A., Nadruz, W., Feinstein, S.B., Nofer, J.R., Zanotti, I., Kontush, A., Remaley, A.T. (2019) Reciprocal multifaceted interaction between HDL (high-density lipoprotein) and myocardial infarction. Arteriosclerosis, Thrombosis, and Vascular Biology 39 (8): 1550-1564.

Storch, K.F., Lipan, O., Leykin, I., Viswanathan, N., Davis, F.C., Wong, W.H., Weitz, C.J. (2002) Extensive and divergent circadian gene expression in liver and heart. Nature 417 (6884): 78-83.

Stratford, S., Hoehn, K.L., Liu, F., Summers, S.A. (2004) Regulation of insulin action by ceramide: dual mechanisms linking ceramide accumulation to the inhibition of Akt/protein kinase B. The Journal of Biological Chemistry 279 (35): 36608-36615.

Sulaieva, O., Chereshneva, Y., Kartashkina, N., Ivanova, M., Tsomartova, D. (2018) Secretory function of white adipose tissue and adipokines: biological effects and clinical significance (review). Georgian Medical News 274: 116-124.

Summers, S.A., Garza, L.A., Zhou, H., Birnbaum, M.J. (1998) Regulation of insulin-stimulated glucose transporter GLUT4 translocation and Akt kinase activity by ceramide. Molecular and Cellular Biology 18 (9): 5457-5464.

Tabarean, I. Morrison, B., Marcondes, M.C., Bartfai, T., Conti, B. (2010) Hypothalamic and dietary control of temperature-mediated longevity. Ageing Research Reviews 9 (1): 41.

Tagami, S., Inokuchi, J.-I., Kabayama, K., Yoshimura, H., Kitamura, F., Uemura, S., Ogawa, C., Ishii, A., Saito, M., Ohtsuka, Y., Sakaue, S., Igarashi, Y. (2002) Ganglioside GM3 participates in the pathological conditions of insulin resistance. The Journal of Biological Chemistry 277 (5): 3085-3092.

Takabe, K., Paugh, S.W., Milstien, S., Spiegel, S. (2008) “Inside-out ”signaling of sphingosine-1-phosphate: therapeutic targets. Pharmacological Reviews 60 (2): 181-195. PMC2695666

Takahashi, J.S. (2017) Transcriptional architecture of the mammalian circadian clock. Nature Reviews Genetics 18 (3): 164-179.

Tamaru, T., Hirayama, J., Isojima, Y., Nagai, K., Noroika, S., Takamatsu, K., Sassone-Corsi, P. CK2 phosphorylates BMAL1 to regulate the mammalian clock. (2009) Nature Structural and Molecular Biology 16: 446-448.

Tan, S.F., Dunton, W., Liu, X., Fox, T.E., Morad, S., Desai, D., Doi, K., Conaway, M.R., Amin, S., Claxton, D.F., Wang, H.G., Kester, M., Cabot, M. C., Feith, D.J., Loughran, T.P., Jr. (2019) Acid ceramidase promotes drug resistance in acute myeloid leukemia through NF-κB-dependent P-glycoprotein upregulation. Journal of Lipid Research 60 (6): 1078-1086.

Tan, C. K., Leuenberger, N., Tan, M.J., Yan, Y.W., Chen, Y., Kambadur, R., Wahli, W., Tan, N.S. (2011) Smad3 deficiency in mice protects against insulin resistance and obesity induced by a high-fat diet. Diabetes 60: 464-476.

Tang, Q.Q., Lane, M.D. (2012) Adipogenesis: from stem cell to adipocyte. Annual Review of Biochemistry 81: 715-736.

Tang, X., Benesch, M.G., Brindley, D.N. (2015) Lipid phosphate phosphatases and their roles in mammalian physiology and pathology. Journal of Lipid Research 56 (11): 2048-2060. PMC4617392

Tao, C., Huang, S., Wang, Y., Wei, G., Zhang, Y., Qi, D., Wang, Y., Li, K. (2015) Changes in white and brown adipose tissue microRNA expression in cold-induced mice. Biochemical and Biophysical Research Communications 463 (3): 193-199.

Terao, R., Honjo, M., Ueta, T., Obinata, H., Izumi, T., Kurano, M., Yatomi, Y., Koso, H., Watanabe, S., Aihara, M. (2019) Light stress-induced increase of sphingosine 1-phosphate in photoreceptors and its relevance to retinal degeneration. International Journal of Molecular Sciences 20 (15): 3670. PMC6696268

Thiede, M.A., Strittmatter, P. (1985) The induction and characterization of rat stearoyl-CoA desaturase mRNA. The Journal of Biological Chemistry 260: 14459-14463.

Thudichum, J.L.W. A Treatise on the Chemical Constitution of the Brain. Archon Books; North Haven, CT, USA: 1962.

Toh, K.L., Jones, C.R., He, Y., Eide, E.J., Hinz, W.A., Virsup, D.M., Ptacek, L.J., Fu, Y.H. (2001) An hPer2 phosphorylation site mutation in familial advanced sleep phase syndrome. Science 291: 1040-1043.

Tous, M., Ferrer-Lorente, R., Badimon, L. (2014) Selective inhibition of sphingosine kinase-1 protects adipose tissue against LPS-induced inflammatory response in Zucker diabetic fatty rats. The American Journal of Physiology: Endocrinology and Metabolism 307 (5): E437-E446.

Trojanowska, M. 2009. Noncanonical transforming growth factor beta signaling in scleroderma fibrosis. Current Opinion in Rheumatology 21: 623-629.

Truong, K.K., Lam, M.T., Grandner, M.A., Sassoon, C.S., Malhotra, A. (2016) Timing matters: circadian rhythm in sepsis, obstructive lung disease, obstructive sleep apnea, and cancer. Annals of the American Thoracic Society 13 (7): 1144-1154. PMC5015754

Turpin, S.M., Nicholls, H.T., Willmes, D.M., Mourier, A., Brodesser, S., Wunderlich, C.M., Mauer, J., Xu, E., Hammerschmidt, P., Brönneke, H.S., Trifunovic, A., LoSasso, G., Wunderlich, F.T., Kornfeld, J.W., Bluher, M., Kronke, M., Bruning, J.C. (2014) Obesity-induced CerS6-dependent C16:0 ceramide production promotes weight gain and glucose intolerance. Cell Metabolism 20: 678-686.

Unger, R.H., Scherer, P.E., Holland, W.L. (2013) Dichotomous roles of leptin and adiponectin as enforcers against lipotoxicity during feast and famine. Molecular Biology of the Cell 24 (19): 3011-3015.

Van Brocklyn, J.R., Williams, J.B. (2012) The control of the balance between ceramide and sphingosine-1-phosphate by sphingosine kinase: oxidative stress and the seesaw of cell survival and death. Comparative Biochemistry and Physiology - Part B: Biochemistry and Molecular Biology 163 (1): 26-36.

van den Berg, R., Kooijman, S., Noordam, R., Ramkisoensing, A., Abreu-Vieira, G., Tambyrajah, L.L., Dijk, W., Ruppert, P., Mol, I.M., Kramar, B., Caputo, R., Puig, L.S., de Ruiter, E.M., Kroon, J., Hoekstra, M., van der Sluis, R.J., Meijer, O.C., Willems van Dijk, K., van Kerkhof, L., Christodoulides, C., Karpe, F., Gerhart-Hines, Z., Kersten, S., Meijer, H.M., Coomans, C.P., van Heemst, D., Biermasz, N.R., Rensen, P.C.N. (2018) A diurnal rhythm in brown adipose tissue causes rapid clearance and combustion of plasma lipids at wakening. Cell Reports 22 (13): 3521-3533.

van der Spek, R., Kreier, F., Fliers, E., Kalsbeek, A. (2012) Circadian rhythms in white adipose tissue. Progress in Brain Research 199: 183-201.

van Eijk, M., Aten, J., Bijl, N., Ottenhoff, R., van Roomen, C.P., Dubbelhuis, P.F., Seeman, I., Ghauharali-van der Vlugt, K., Overkleeft, H.S., Arbeeny, C. (2009) Reducing glycosphingolipid content in adipose tissue of obese mice restores insulin sensitivity, adipogenesis and reduces inflammation. PLoS One 4 (3): e4723.

van Meer, G., Halter, D., Sprong, H., Somerharju, P., Egmond, M.R. (2006) ABC lipid transporters: extruders, flippases, or flopless activators? FEBS Letters 580 (4): 1171-1177.

Vasiliauskaité-Brooks, I., Sounier, R., Rochaix, P., Bellot, G., Fortier, M., Hoh, F., De Colibus, L., Bechara, C., Saied, E.M., Arenz, C., Leyrat, C., Granier, S. (2017) Structural insights into adiponectin receptors suggest ceramidase activity. Nature 544 (7648): 120-123. PMC5595237

Vishvanath, L., Gupta, R.K. (2019) Contribution of adipogenesis to healthy adipose tissue expansion in obesity. Journal of Clinical Investigation 129: 4022-4031.

Walton, Z.E., Patel, C.H., Brooks, R.C., Yu, Y., Ibrahim-Hashim, A., Riddle, M., Porcu, A., Jiang, T., Ecker, B.L., Tameire, F., Koumenis, C., Weeraratna, A.T., Welsh, D.K., Gillies, R., Alwine, J.C., Zhang, L., Powell, J.D., Dang, C.V. (2018) Acid suspends the circadian clock in hypoxia though inhibition of mTOR. Cell 174 (1): 72-87.

Wang, J., Badeanlou, L., Bielawski, J., Ciaraldi, T.P., Samad, F. (2014) Sphingosine kinase 1 regulates adipose proinflammatory responses and insulin resistance. The American Journal of Physiology: Endocrinology and Metabolism 306 (7): E756-E768.

Wang, Q., Xie, Z., Zhang, W., Zhou, J., Wu, Y., Zhang, M., Zhu, H., Zou, M.H. (2014) Myeloperoxidase deletion prevents high-fat diet-induced obesity and insulin resistance. Diabetes 63 (12): 4172-85.

Wattenberg, B.W. (2010) Role of sphingosine kinase localization in sphingolipid signaling. World Journal of Biological Chemistry 1 (12): 362-368.

Wei, L.N. (2012) Chromatin remodeling and epigenetic regulation of the CrabpI gene in adipocyte differentiation. Biochimica et Biophysica Acta 1821 (1): 206-212. PMC3151335

Wigger, D., Gulbins, E., Kleuser, B., Schumacher, F. (2019) Monitoring the sphingolipid de novo synthesis by stable-isotope labeling and liquid chromatography-mass spectrometry. Frontiers in Cell and Developmental Biology 7: 210. PMC6779703

Wilkerson, J.L., Stiles, M.A., Gurley, J.M., Grambergs, R.C., Gu, X., Elliott, M.H., Proia, R.L., Mandal, N.A. (2019) Sphingosine kinase-1 Is essential for maintaining external/outer limiting membrane and associated adherens junctions in the aging retina. Molecular Neurobiology 56 (10): 7188-7207.

Wu, Y., Tang, D., Liu, N., Xiong, W., Huang, H., Li, Y., Ma, Z., Zhao, H., Chen, P., Qi, X., Zhang, E.E. (2017) Reciprocal regulation between the circadian clock and hypoxia signaling at the genome level in mammals. Cell Metabolism 25 (1): 73-85.

Wyatt, J.K., Ritz-De Cecco, A., Czeisler, C.A., Dijk, D.J. (1999) Circadian temperature and melatonin rhythms, sleep, and neurobehavioral function in humans living on a 20-h day. The American Journal of Physiology 277 (4 Pt 2): R1152-R1163.

Xia, J.Y., Holland, W.L., Kusminski, C.M., Sun, K., Sharma, A.X., Pearson, M.J., Sifuentes, A.J., McDonald, J.G., Gordillo, R., Scherer, P.E. (2015) Targeted induction of ceramide degradation leads to improved systemic metabolism and reduced hepatic steatosis. Cell Metabolism 22 (2): 266-278.

Xia, J.Y., Sun, K., Hepler, C., Ghaben, A.L., Gupta, R.K., An, Y.A., Holland, W.L., Morley, T.S., Adams, A.C., Gordillo, R., Kusminski, C.M., Scherer, P.E. (2018) Acute loss of adipose tissue-derived adiponectin triggers immediate metabolic deterioration in mice. Diabetologia 61 (4): 932-941.

Xiong, Y., Lee, H.J., Mariko, B., Lu, Y.-C., Dannenberg, A.J., Haka, A.S., Maxfield, F.R., Camerer, E., Proia, R.L., Hla, T. (2013) Sphingosine kinases are not required for inflammatory responses in macrophages. The Journal of Biological Chemistry 288 (45): 32563-32573.

Xu, Y., Padiath, Q.S., Shapiro, R.E., Jones, C.R., Wu, S.C., Saigoh, N., Saigoh, K., Ptacek, L.J., Fu, Y.H. (2005) Functional consequences of a CKIdelta mutation causing familial advanced sleep phase syndrome. Nature 434: 640-644.

Xu, Y., Toh, K.L., Jones, C.R., Shin, J.Y., Fu, Y.H., Ptacek, L.J. (2007) Modeling of a human circadian mutation yields insights into clock regulation by PER2. Cell 128: 59-70.

Yamada, A., Nagahashi, M., Aoyagi, T., Huang, W.C., Lima, S., Hait, N.C., Maiti, A., Kida, K., Terracina, K.P., Miyazaki, H., Ishikawa, T., Endo, I., Waters, M.R., Qi, Q.,Yan, L., Milstien, S., Spiegel, S., Takabe, K. (2018) ABCC1-exported sphingosine-1-phosphate, produced by sphingosine kinase 1, shortens survival of mice and patients with breast cancer. Molecular Cancer Research 16 (6): 1059-1070.

Yamashita, T., Hashiramoto, A., Haluzik, M., Mizukami, H., Beck, S., Norton, A., Kono, M., Tsuji, S., Daniotti, J.L., Werth, N., Sandhoff, R., Sandhoff, K., Proia, R.L. (2003) Enhanced insulin sensitivity in mice lacking ganglioside GM3. Proceedings of the National Academy of Sciences of the United States of America 100 (6): 3445-3449.

Yamashita, T., Wada, R., Proia, R.L. (2002) Early developmental expression of the gene encoding glucosylceramide synthase, the enzyme controlling the first committed step of glycosphingolipid synthesis. Biochimica et Biophysica Acta 1573 (3): 236-240.

Yang, A., Mottillo, E.P. (2020) Adipocyte lipolysis: from molecular mechanisms of regulation to disease and therapeutics. The Biochemical Journal 477: 985-1008.

Yano, M., Yamamoto, T., Nishimura, N., Gotoh, T., Watanabe, K., Ikeda, K., Garan, Y., Taguchi, R., Node, K., Okazaki, T. (2013) Increased oxidative stress impairs adipose tissue function in sphingomyelin synthase 1 null mice. PLoS One 8 (4): e61380.

Yatomi, Y., Igarashi, Y., Yang, L., Hisano, N., Qi, R., Asazuma, N., Satoh, K., Ozaki, Y., Kume, S. (1997) Sphingosine 1-phosphate, a bioactive sphingolipid abundantly stored in Platelets, is a normal constituent of human plasma and serum. The Journal of Biochemistry 121: 969-973.

Ye, D.W., Rong, X.L., Xu, A.M., Guo, J. (2017) Liver-adipose tissue crosstalk: a key player in the pathogenesis of glucolipid metabolic disease. Chinese Journal of Integrative Medicine 23 (6): 410-414.

Yu, H., Okada, T., Kobayashi, M., Abo-Elmatty, D.M., Jahangeer, S., Nakamura, S. (2009) Roles of extracellular and intracellular sphingosine 1-phosphate in cell migration. Genes to Cells : Devoted to Molecular & Cellular Mechanisms 14 (5): 597-605.

Zamani, N., and C. W. Brown. 2011. Emerging roles for the transforming growth factor-β superfamily in regulating adiposity and energy expenditure. Endocrinology Reviews 32: 387-403.

Zaslavsky, A., Li, S., Xu, Y. (2005) Sphingosine-1-phosphate induces a PDGFR-dependent cell detachment via inhibiting beta1 integrin in HEK293 cells. FEBS Letters 579 (18): 3899-3906.

Zelnik, I.D., Ventura, A.E., Kim, J.L., Silva, L.C., Futerman, A.H. (2020) The role of ceramide in regulating endoplasmic reticulum function. Biochimica et Biophysica Acta. Molecular and Cell Biology of Lipids 1865 (1): 158489.

Zhang, Q.-Z., Holland, W.L., Wilson, L., Tanner, J.M., Kearns, D., Cahoon, J.M., Pettey, D., Losee, J., Duncan, B., Gale, D., Kowalski, C.A., Deeter, N., Nichols, A., Deesing, M., Arrant, C., Ruan, T., Boehme, C., McCamey, D.R., Rou, J., Ambal, K., Narra, K.K., Summers, S.A., Abel, E.D., Symons, J.D. (2012) Ceramide mediates vascular dysfunction in diet-induced obesity by PP2A-mediated dephosphorylation of the eNOS-Akt complex. Diabetes 61 (7): 1848-1859.

Zhang, R., Lahens, N.F., Balance, H.I., Hughes, M.E., Hogenesch, J.B. (2014) A circadian gene expression atlas in mammals: implications for biology and medicine. Proceedings of the National Academy of Sciences of the United States of America 111 (45): 16219-16224. PMC4234565

Zhang, Y., Proenca, R., Maffel, M., Barone, M., Leopold, L., Friedman, J.M. (1994) Positional cloning of the mouse obese gene and its human homologue. Nature 372: 425-432.

Zhang, Q., Ramlee, M.K., Brunmeir, R., Villanueva, C.J., Halperin, D., Xu, F. (2012) Dynamic and distinct histone modifications modulate the expression of key adipogenesis regulatory genes. Cell Cycle (Georgetown, Tex.): 11 (23): 4310-4322. PMC3552913

Zhao, Z.-D., Yang, W.Z., Gao, C., Fu, X., Zhang, W., Zhou, Q., Chen, W., Ni, X., Lin, J.-K., Yang, J., Xu, X.-H., Shen, W.L. (2017) A hypothalamic circuit that control body temperature. Proceedings of the National Academy of Sciences of the United States of America 114 (8): 2042-2047.

Zheng, X., Zhao, X., Zhang, Y., Tan, H., Qiu, B., Ma, T., Zeng, J., Tao, D., Liu, Y., Lu, Y., & Ma, Y. (2019) RAE1 promotes BMAL1 shuttling and regulates degradation and activity of CLOCK:BMAL1 heterodimer. Cell Death and Disease 10: 62.

Zhu, Q., Belden, W.J. (2020) Molecular Regulation of Circadian Chromatin. Journal of Molecular Biology 2836 (20): 30039-30045.

Zimmet, P., Alberti, K., Stern, N., Bilu, C., El-Osta, A., Einat, H., Kronfeld-Schor, N. (2019) The circadian syndrome: is the metabolic syndrome and much more! Journal of Internal Medicine 286 (2): 181-191. PMC6851668